BISMUTH BASED THIN FILM SUPERCONDUCTORS

by

Ayhan Guldeste

Pembroke College

A thesis submitted for the degree of Doctor of Philosophy in the University of Oxford.

Hilary Term 1994

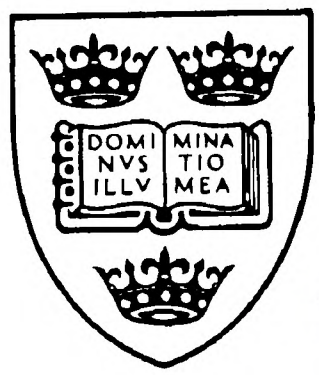

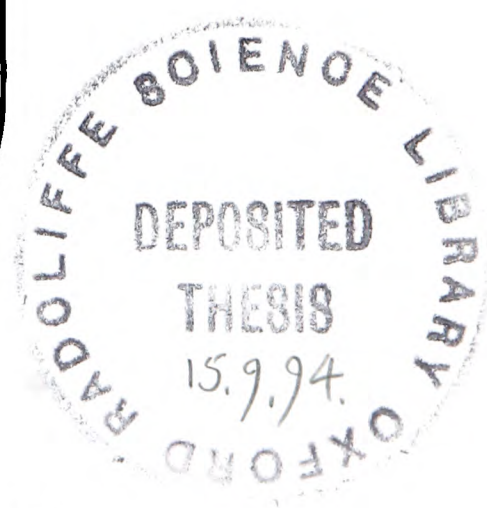

Department of Materials,
Parks Road,
Oxford OX1 3PH

ABSTRACT

BISMUTH BASED THIN FILM SUPERCONDUCTORS

A thesis submitted for the degree of Doctor of Philosophy in the University of Oxford.

A. GULDESTE, Pembroke College, Oxford, Hilary Term 1994.

This thesis describes investigations performed into the growth and characterisation of Bi-based ($Bi_2Sr_2Ca_{n-1}Cu_nO_{2n+4+x}$, $n=2$, 3) ceramic superconducting material in the form of thin films, about 0.5μm thick, grown on single crystal MgO, $LaAlO_3$ and $SrTiO_3$ substrates by r.f. magnetron sputtering. The effect of oxygen content on the Pb doped Bi-2223 ($n=3$) phase was also studied by changing the cooling process and by annealing in different partial pressures of oxygen at ambient pressure.

The films produced have been assessed by considering their initial composition where it is found that Bi/Sr ratios can be between $0.9<Bi/Sr<1$ for the Bi-2212 ($n=2$) phase, while for the Bi-2223 phase the Bi-content should be below 1.9 or lower than the Sr-content, for the films not to peel off the substrate during high temperature annealing. $T_{c\text{-}zero}$ of around 80K is achievable for (Ca + Sr)/Bi ratios between 1.4 and 1.65 while $T_{c\text{-}onset}$ remains above 90K for Bi-2212 films. However, the best superconducting properties can be obtained for a (Ca + Sr)/Bi ratio which is quite close the nominal composition

The use of a heavily Pb doped target is an effective way of Pb doping Bi-2223 thin films. A Bi-content of $1.4<Bi<1.8$ in as deposited films may provide almost single phase Bi-2223 thin films with Tc values running from 105.5K to 109.5K and $Jc>10^4 A/cm^2$ at 77K. The effect of the initial Pb content and annealing conditions on the formation of the Bi-2223 phase was investigated. It was found that high Pb content ($0.9<Pb/Bi<1.5$) lowers the formation temperature appreciably and increases the range of sintering temperature (to at least 10K). The Bi-2223 phase starts to form at 835°C from the initial phases (Bi-2212, CuO and Ca_2PbO_4) formed below 835°C and its fraction increases with increasing sintering temperature up to 862°C, while the fraction of initial phases decreases. An annealing duration of 30 min. has provided highly oriented films with c-axis perpendicular to the substrate surface and sharp superconducting transition (<5K). Although Pb/Bi ratio is not critical in the range studied, when it is above 1.3 slow heating and cooling is necessary to prevent retention of excess Ca_2PbO_4 in the film after sintering. On $LaAlO_3$ and $SrTiO_3$ perovskite substrates, T_c is at least 5K lower than in the case of MgO. Nevertheless, $LaAlO_3$ can provide good microstructure with a critical current density, of $5x10^4 A/cm^2$ at 77K.

The direction and the range of variation of T_c in Bi-2223 films with oxidising process can be related to both the film composition (especially Bi and Pb content) and initial oxygen content. The variation range of T_c with oxidising is controlled by the Pb content. However, the maximum variation is around 4K at ambient pressure.

Radiation response measurements were carried out on films patterned into a 150 μm wide, and 1 cm long meander-type structure using standard photolithography and wet chemical etching in EDTA. The results showed that the optical response using a continuous wave (cw) He-Ne laser is bolometric, while the microwave response using a 34.5 GHz Gunn diode microwave generator contains a non bolometric component.

Such polycrystalline Bi-based high T_c thin films may have interesting applications as sensitive microwave detectors, but they are not particularly good for microwave applications because of their high surface resistance, Rs, at microwave frequencies.

PREFACE

This thesis describes research carried out by the author in the Department of Materials, University of Oxford, between October 1990 and March 1994, under the supervision of Dr. M.J. Goringe. The work was supported by Erciyes University (Turkey).

No part of this work has been previously submitted for a degree at this or any other university. The work of other authors has been freely drawn upon and is duly acknowledged in the text. A list of references is given at the end of each chapter in the order in which they occur.

Some of the work described in this thesis has been presented at the following conferences and published in journals or conference proceedings, respectively:

- ★ The 1992 Applied Superconductivity Conference, Chicago, August 23-28 1992.
- ★ E-MRS 1992 Fall Conference on High T_c Superconductors, Strasbourg, France, November 3-6, 1992.
- ★ European Conference on Applied Superconductivity (EUCAS '93), Gottingen, Germany, October 4-8, 1993.

- ★ IEEE Trans. on Appl. Superconductivity, 3 (1993) 1757.
- ★ IEEE Trans. on Appl. Superconductivity, 3 (1993) 2128.
- ★ Journal of Alloys and Compounds, 195 (1993) 567.
- ★ Journal of Alloys and Compounds, 195 (1993) 591.
- ★ Applied Superconductivity, Edited by H.C. Freyhardt, Vol. 1, pp. 555 (Conference Proceedings of EUCAS '93).

The author is grateful for the financial support of Erciyes University (Turkey). The author would also like to thank the Department of Materials, University of Oxford and Pembroke College for a bursary and funding for attending conferences (E-MRS '92 and EUCAS '93).

ACKNOWLEDGEMENT

I would like to express my sincere thanks to the following people, who have been a great help to me throughout the course of this study:

Professor Sir P.B. Hirsch and Professor R.J. Brook for the provision of laboratory facilities.

Dr. M.J. Goringe, my supervisor, for his interest, advice, encouragement and invaluable guidance.

Dr. C.R.M. Grovenor for his constant supervision, help and encouragement.

Mr. J. Short for his patient and kind help in using the student's Workshop.

The members of the Department of Materials in Oxford, in particular, M.J. Purches, R. Cripps, J. Stead, B. Williams, B. Lloyd, G. Dixon-Brown, R.C. Doole, P. Hambridge, D Pinfold and Bill Bryant, for their helpful and kind technical assistance.

The Archaeology Research Lab., Oxford for the provision of the Cameca SEMPROBE facility and Mr. C.J. Salter for help with the use of this electron microscope.

All the members of the High T_c Group, especially, Mr. J.D. Chern for his collaboration in radiation response measurements and useful discussions and also for his friendship.

Dr. J.C. Gallop in National Physical Laboratory (NPL) and A. Jenkins, Oxford for the surface resistance measurements.

Dr. S.G. Roberts for provision of some computer program used in the writing of this thesis and the key of the computer room during the weekends and over the nights, and for his kind help.

Mr. A. McKnight and Mr. M. Taheri for reproducing the photographs for the thesis.

Dr. S. Ezz for his help in using Laue X-Ray Diffractometer and for his friendship.

Dr. Y.S. Hascicek and Dr. M. Gunduz, whose recommended me to study in Oxford.

Mr. N. Marasli, Mr. U. Sezer, Dr. A. Vahabzade Dr. S. Patat, Dr. A. Kaya, and Dr. K. Yalci for their valuable friendship and help over the years.

Erciyes University for the financial support.

Finally, I would like to thank the mother of Mustafa Talha, Ikbal Vildan and Ekrem Taha, to whom this thesis is dedicated, for her patient understanding, encouragement and constant emotional support throughout the past years.

Ayhan Guldeste

Oxford,

March, 1994

CONTENTS

CHAPTER 2

Thin Film Processing of high-T_c superconductors

CHAPTER 3

Experimental methods used for preparation and characterisation of films

General introduction

Before 1986, superconductivity was a phenomenon restricted to metals, occurring only at very low temperatures and requiring liquid helium as a refrigerant. The highest known critical temperature, T_c, the temperature below which all electrical resistance is lost and the material becomes a superconductor, was 23K for the intermetallic compound Nb_3Ge.

In the early part of 1986, Bednorz and Muller [1] realized that a mixed oxide of lanthanum, barium and copper with the nominal composition $La_{5-x}Ba_xCu_5O_{5(3-z)}$, from which later on $La_{2-x}Ba_xCuO_{4-z}$ was identified as the superconducting phase [2], became superconducting at a critical temperature above 30K.

Within a few months of the announcement of the original discovery another mixed oxide, $YBa_2Cu_3O_7$, (YBCO), was found to have a superconducting critical temperature of 90K [3]. Superconductivity at liquid nitrogen temperature (77K) was at last a reality. The intense research effort thus unleashed has led to the discovery of further compounds: bismuth strontium calcium copper oxides (BSCCO) with values of T_c up to 110K [4] and thallium barium calcium copper oxides (TBCCO) which held the record with $T_c = 125$K [5] until the recent discovery [6] of superconductivity above 130K in a material containing $HgBa_2Ca_2Cu_3O_{1+x}$ (with three CuO layers per unit cell).

A common characteristic of most of these materials is the presence of copper-oxygen planes. Superconductivity is confined to these copper-oxygen planes [7] and T_c depends on the free charge carrier concentration in them. In most of the superconducting compounds which have been discovered so far, holes seem to be the dominant charge carriers [8]. Apart from high T_c, ceramic superconductors have two other fundamental properties: a short Ginzburg-Landau coherence length ξ, and a large anisotropy. The small value of ξ allows the achievement of high critical fields, H_{c2}, but thermal fluctuations in the mixed state in these materials play an important negative role. These fluctuations give rise to creep of the vortex lattice which causes dissipation.

Despite the attractive properties of all of the copper oxide superconductors, it is very difficult to obtain them in suitable form for various interesting applications, even if their superconducting properties are less sensitive to impurities than their metal counterparts, because of their ceramic character, small ξ and anisotropy. In these materials especially, one may expect that due to the small value of ξ, the effect of grain boundaries will be important. In order for them to reach their full potential the problems of processing ceramic superconductors must first be overcome.

Initial research on High-T_c ceramic superconductors in bulk ceramic form revealed potential limitations for engineering applications. The brittle nature of the material and the high reactivity of the constituents make it difficult to synthesize this new family of superconducting compounds into usable form as wires, tapes, rods or composites. Since many of the potential applications of superconductivity lie in the field of electronics, for example in the fabrication of active and passive devices, analog Josephson junctions, SQUID's, analog and digital signal processors and detectors, thin films of various High-T_c superconductors are indispensable.

This thesis describes an investigation of processing and characterisation of Bi-based ceramic superconductors represented by $Bi_2Sr_2Ca_{n-1}Cu_nO_{2n+4+y}$ with $n=2,3$ (denoted Bi-2212 and Bi-2223 for $n=2$ and $n=3$, respectively) in the form of thin films (0.5 to 1 μm thick) on various single crystal substrates. These thin films are grown by the rf-magnetron sputtering technique. The first chapter summarises the underlying principles of superconductivity, the potential of thin films for device application, and finally the properties of high T_c superconducting materials. The literature surveys of processing and characterisation of high T_c superconducting thin films are presented in chapter 2. Chapter 3 describes the experimental techniques used in the work described in this thesis, including patterning of thin films into the preliminary device structures using standard photolithography and wet chemical etching and the results obtained. In the following chapters (4, 5, 6) experimental results are presented. The influence of sputtering parameters on film composition has been investigated mostly on Bi-2212 phase (chapter 4).

The effect of annealing conditions on superconducting properties was also investigated on both phases. The real effort was on Bi-2223 as it is more promising for devices to operate in liquid nitrogen (chapter 5). Device performance of these films have been investigated by measuring their response to electromagnetic radiation and measurement of surface resistance (chapter 6).

In this general introduction, we addressed the aspects of the research subject described in this thesis only very briefly. More extensive introductions can be found in the chapters which follow.

References

1 J.G. Bednorz and K.A. Muller, Z. Phys. B64 (1986) 189.

2 H. Takagi, S. Uchida, K. Kitazawa and S. Tanaka, Jpn. J. Appl. Phys. 23 (1987) L123.

3 M.K.Wu, J.R. Ashburn, C.J. Torng, P.H. Hor, R.L. Meng, L. Gao, Z.J. Huang, Y.Q. Wang, and C.W. Chu, Phys. Rev. Lett. 58 (1987) 908.

4 H. Maeda, Y. Tanaka, M. Fukutomi, and T. Asano, Jpn. J. Appl. Phys. 27 (1988) 209.

5 S.S.P. Parkin, V.Y. Lee, E.M. Engler, A.L. Nazzal, T.C. Huang, G. Gorman, R. Savoy and R Beyers, Phys. Rev. Lett. 60 (1988) 2539.

6 A. Schilling, M. Cantoni, J.D. Guo, and H.R. Ott, Nature 363 (1993) 56.

7 C. Thomsen, M. Cardona, B. Gegenheimer, R. Liu and A. Simon, Phys. Rev. B37 (1988) 9860.

8 H. Takagi, T. Ido, S. Ishibashi, M. Uota, S. Uchida and Y. Tokura, Phys. Rev. B40 (1989) 2254.

CHAPTER 1

Introduction to superconductivity and high T_c superconductors

1.1. Basic phenomenologies describing superconductivity

Superconductivity is usually defined as the complete loss of electrical resistance in a static electric field. Very soon after its initial discovery, experiments also showed that the superconducting state could be destroyed by the application of magnetic induction, B, if the magnitude of B is larger than the value of critical magnetic induction, B_c, which is a function of temperature, rising from zero at T_c to a value $B_c(0)$ at $T=0K$. If the applied magnetic flux density is less than B_c, then it is entirely expelled by "Type I superconductors" (**Fig. 1.1**). This perfect diamagnetism is called the Meissner effect. The exclusion is provided by the generation of shielding currents set up in the surface (or skin) of the superconductor which create a magnetic flux equal and opposite to that outside the material. The passage of an electrical current greater than a critical value, I_c, also destroys superconductivity. I_c is the current which results in the critical magnetic flux being formed at the surface of the superconductor. I_c is therefore a function of temperature, applied magnetic field and conductor size. This exact behaviour is shown only by "type I superconductors" which are generally pure metals. In these materials critical magnetic fluxes, and therefore currents, are low, and their practical utility is limited.

However, many alloy and high T_c materials have much higher critical magnetic flux, but also an incomplete Meissner effect. In these materials which are called "type II

superconductors" magnetic flux can penetrate the body of the superconductor in the form of localised flux lines, each carrying a single quantum of magnetic flux ($\varnothing_0 = h/2e$), but the material remains superconducting up to a maximum value of magnetic flux (B_{c2}) (**Fig. 1.2**) [1]. At B_{c1} the flux begins to penetrate the material and at B_{c2} the material becomes normal. The Meissner effect is usually regarded as a more reliable test of superconductivity than the observation of a sudden drop in resistivity. Even though a superconductor has a complete Meissner effect the applied field does not suddenly fall to zero at the surface, but instead decays exponentially away from the surface. The distance of this flux penetration is called the penetration depth, λ. λ is very large near Tc, becoming smaller at lower temperatures.

In the case of an incomplete Meissner effect, that is when a Type II superconductor is in a magnetic induction, $>B_{c1}$, where a flux line penetrates the surface it consists of a normal core surrounded by circulating supercurrent in a cylinder with radius of the order of the penetration depth (fluxoid). At this stage, if a current of density J_c is passed through the superconductor, flux lines experience a Lorentz force $\mathbf{F_l = JxB}$. Under the action of this force, the flux lines will try to move and if they do so will generate an induced emf and hence an electrical resistance. This phenomenon is known as flux flow. If this happens, the passage of current will be no longer lossless. The motion of flux lines can be prevented if they are pinned, for example if they are able to interact with microstructural defects such as dislocation tangles, grain and sub-grain boundaries and precipitates of a second phase in the superconductor. Since the Lorentz force is proportional to J the critical current density, J_c, is determined by the strength of this interaction. The critical Lorentz force ($F_c = J_c B$) is just equal to the total pinning force per unit volume F_p, which is a function of both temperature and magnetic induction.

1.2. BCS theory of superconductivity

In order to explain the zero resistivity behaviour in low T_c materials, this theory was developed by Bardeen, Cooper and Schrieffer in 1957 [2]. It explains most of the observed

data for conventional metallic superconductors, such as the change in T_c for a change in isotope of a component element of the superconductor and predicts the existence of a critical current density (J_c) which the superconductor can support before turning normal; for high T_c materials some of the basic ideas can still be used. BCS theory shows how the electron-phonon interaction can result in an indirect attractive force between electrons. Electrons and ions that form the lattice are oppositely charged. Any electron in its motion through the lattice polarizes the lattice along its path and the polarization remains for the time required for the phonons making up the ion displacements to disperse. This time for dispersion is sufficiently long to allow another electron to experience the local polarization caused by the first electron. Its potential energy is thereby reduced, so it can be considered that through the intermediacy of the phonons the electrons can have an effective attraction between them at a distance. The average maximum distance at which the phonon coupled attraction can occur is called the coherence length (ξ). This attraction of the two electrons of a pair (called a Cooper pair), which lowers the energy of the pair relative to the mean energy (Fermi energy) of the unpaired electrons, is greatest when they have opposite spins and equal and opposite wave vectors. The exchange of a virtual phonon pairs electrons with opposite wave vectors, so that the pair cannot be scattered without breaking up and increasing the energy of the system. Hence there is no resistance to the flow of electrons.

The decreasing of the energy of the system on electron pairing results in an energy gap of magnitude 2Δ, in the band structure of a superconductor at the Fermi surface, as shown in **Fig. 1.3**. The Cooper pairs lie in a condensed state at the Fermi energy and the excited quasi-particle states lie at an energy Δ above the Fermi energy. BCS theory predicts a value of $2\Delta_0/kT_c = 3.52$ at 0K, which is fairly well obeyed in conventional metallic superconductors. Measurement using superconductor-insulator-superconductor thin film structures have confirmed the value of $2\Delta/kT_c$ to be $3.5(+0.4,-0.6)$ in high T_c materials [3]. The coherence length, ξ, can take values up to $1\mu m$ in low T_c materials, but in high T_c materials it is much smaller (≤ 2.7 nm).

1.3. Electron tunnelling

When two metals are separated by a very thin(~nm) insulating barrier, electrons can tunnel from one to the other by a quantum-mechanical process. If the metals are superconducting, single electrons cannot tunnel through the barrier unless a voltage sufficient to break up the pairs is applied. However, at zero volts, electron pairs can tunnel and give rise to a critical tunnelling current I_0. This is the Josephson effect. The tunnelling device is called a Josephson junction and forms the basis of several electronic devices.

1.3.1. Josephson junctions

A Josephson junction is formed by providing a separating layer thinner than ξ, so that a hole pair(or Cooper pair) may tunnel through the barrier. The separating layer can be regarded as a superconductor with a reduced critical current. Very similar properties to those produced by tunnelling can be obtained by reducing the critical current at, for example, a constriction or "weak link" in the material. A current up to a maximum I_0 can flow across the junction without the application of a voltage, but a phase change $\Delta\psi$ must occur because of the difference in phase coherences of the two superconductors. The I-V characteristic for a junction is shown in **Fig. 1.4.** The critical current of Josephson junctions is very sensitive to magnetic fields, being reduced by them. High T_c Josephson junctions hold the key to the development of numerous superconductor device and circuit applications.

1.4. Superconducting thin film devices

Though currents in electronic devices are small, due to the restricted dimensions, current densities are similar to those in large machines like superconducting magnets. However, magnetic fields are generally small. In thin film form ceramic superconductors can have adequate critical current density ($>10^6$ Acm^{-2} at 77 K). It seems reasonable to suggest that the first applications of ceramic superconductors will be in electronic circuits and devices. The use of superconductors, with high current densities and absence of dissipation, implies the possibility of higher packing density on a circuit board or chip.

Conventional superconductivity is not very attractive in these applications as the associated semiconductor elements do not operate well at liquid helium temperatures. However, nitrogen temperatures are beneficial to semiconductor operation, as carrier mobilities are often maximised in this temperature range. Thus the possible use of ceramic superconductors as passive circuit elements can confer a double advantage. All of the above applications require the production of high current density superconducting films which can be processed in compatibility with the semiconducting components.

The great reduction in size of devices, especially "Superconducting Quantum Interference Devices" (SQUIDs) which are described below, made possible by thin film technology, is a powerful incentive for further development of superconducting circuits. Several applications are only made possible by using thin films, such as Josephson computer elements. By far the most common use of superconducting thin films is in SQUIDs which are very sensitive to small changes in magnetic flux. The application of oxide superconductors to magnetic detectors or microwave detectors [4] has been achieved by utilizing the change of the superconductive properties caused by the application of magnetic flux or microwaves. Since these materials in the form of polycrystals have grain boundaries working as weak links, the superconducting properties (J_c, T_c) are greatly influenced by an applied magnetic field [5-7]. These weak links which are undesirable for high critical current density J_c, are indispensable for magnetic detectors using superconductive films. Device operation at temperatures as high as 104K [5] and energy resolutions of less than 10^{-29} J/Hz at 77K have been achieved [9] using natural grain boundaries as the Josephson element. However, to fabricate reproducibly natural grain boundaries and incorporate them into the more complex structures is difficult. So, many research groups have turned toward fabricating weak link, or microbridge, junctions using techniques such as "Step Edge" [9,10] and "Grain Boundary"[11]. It is expected that a magnetic detector using magneto resistance is much more sensitive than the conventional magnetic detector using semiconductors (In-Sb and others). Other uses include rf. detectors, voltage standards, superconducting bolometers and SIS mixers.

The thin-film-type Josephson junction has many advantages for practical applications because of the reproducibility of junction characteristics and its potential for integration. In the field of high T_c superconducting device research, several preliminary attempts at this type of Josephson junction have been made using hybrid structures constructed by metal [12,13] and oxide superconductors[14,15]. In order to realize such Josephson junctions, the key point is to fabricate a clear interface between the superconducting electrodes and the barrier layer. For example, on conventional sandwich-type Josephson junctions using metal superconductors such as Nb/Al-oxide-Al/Nb [16] and NbN/MgO/NbN [17] junctions, these interfaces can be easily fabricated without a noticeable interdiffusion of the elements because the thin films are deposited at relatively low temperature. These low temperature procedures cannot be used in junction fabrication using a high T_c oxide superconductor because these materials need relatively high temperatures for crystallization. For example, in the sputtering technique the substrates are typically heated to a temperature over 600^{o}C. One possible solution to prevent this interdiffusion may be to use non-superconducting oxide material as a barrier layer. Mizuno et al.[18] used $Bi_2Sr_2Ca_1Cu_2O_x$ films for both superconducting electrodes and $Bi_2Sr_2Cu_1O_y$ for the barrier layer. These S/N/S-type junctions clearly exhibited the ac Josephson effect under irradiation by radio frequency waves of 12GHz.

1.4.1. SQUIDs

If a pair of junctions are connected in parallel, **Fig. 1.5**, the total supercurrent is simply the sum of the individual critical currents, provided there is no magnetic flux inside the circuit. As flux is introduced into the circuit, the current oscillates, the maximum value corresponding to an integral number of flux quanta, $n\varnothing_0$, and falling to zero when the flux is equivalent to $(n+1/2)\varnothing_0$, **Fig. 1.6**. This two junction device is called as a SQUID. It can be used as a sensitive detector and very accurate meter for magnetic flux.

If only one Josephson junction is present in the loop, the voltage response of the SQUID cannot be measured directly, but is obtained by coupling the loop to an r.f. biased

tank circuit. Such a device is known as an r.f. SQUID. If the loop contains two weak links the d.c. V-I characteristic can be observed. This is called a d.c. SQUID. It is more sensitive than an r.f. SQUID, but more complicated to operate.

1.4.2. Superconducting bolometer

This application does not require Josephson technology. If a superconductor is held at the temperature where $\partial R/\partial T$ is a maximum (i.e in the middle of the superconducting transition) and is exposed to electromagnetic radiation, the absorbtion of the radiation will cause a slight increase in temperature of the superconductor. This will cause a much larger increase in its resistance, which can be measured. The increase in resistance can be correlated with the amount of radiation incident on the bolometer. If the voltage change is due to the thermal effect caused by electromagnetic radiation heating, the radiation response is termed bolometric. On the other hand, if it is due to other mechanisms such as the breaking of Cooper pairs [19], it is regarded as a non-bolometric response.

The bolometric detector has many advantages due to the essentially flat energy response and simple absolute calibration. The use of high temperature superconductor thin films is appropriate for this application due to their low noise and high sensitivity to temperature changes, when operating at the superconducting transition temperature. The theoretical possibility of realising a very low-noise bolometer for the far infrared range has been discussed [20] and was shown to be potentially superior to any other existing detection method in the wavelength range $\lambda > 20\mu m$. Some low-T_c ($T_c = 11K$) quantum detectors have already shown excellent performance and wide bandwidth (>1GHz) [21]. High-T_c superconducting films have been tested and show promising bolometric response to near-infrared ($\lambda \approx 1.3\mu m$) visible radiation [21].

The requirements are clearly different for bolometric and non-bolometric detectors: bolometers require sharp transitions indicative of high-quality (preferably epitaxial) films on low heat capacity (or miniature) substrates; non-bolometric detectors using the resistive tail

do not rely on a sharp transition but may depend on increased numbers of granular weak links associated with larger detector areas.

1.4.3. Microwave Properties

Nearly all the applications one can anticipate for high T_c superconducting thin films involve high frequencies, so it is very important that they can be made with low high-frequency loss. Many of the applications depend on the superconductor being greatly superior to normal metals in this respect. There are many reports of high frequency properties of high temperature superconductors.

The microwave surface impedance is an important quantity of high T_c superconductors for microwave and microelectronic applications [22]. For both, the surface resistance R_s determines the power dissipation in a device and therefore the device performance. Experimental data of R_s measured with polycrystalline and single-crystalline samples of high T_c superconductors at frequencies between 0.2 and 150 GHz have been published by a large number of laboratories [23]. Their results show that the lowest R_s (77K) values occur for c-axis oriented in-situ prepared thin films [24, 25] and single crystals of $YBa_2Cu_3O_7$ [26]. The very impressive results of Klein et al. [24] ($R_s < 0.008\Omega$ at 86,76 GHz and 77K) were on a film with a rather rough surface. Recent reports of Rs measurements show that $(Tl_{0.5}Pb_{0.5})Sr_2Ca_2Cu_3O_9$ and $Tl_2B_2CaCu_2O_8$ thin films on $LaAlO_3$ can be as good as $YBa_2Cu_3O_7$ thin films [27, 28]. As the thickness of such films is on the order of the magnetic field penetration depth, the effective values of the surface impedance are enhanced and depend on the film thickness and the dielectric properties of the substrate material. The magnitude of the penetration depth is also important for high-frequency applications as it controls the kinetic inductance of transmission lines. It would seem that the values measured by high- frequency techniques are still very dependent on film quality.

Measurements of the frequency dependence of the surface impedance of superconductors have been extremely valuable in assessing fundamental parameters like the

penetration depth λ, mean free path l, electron density, Fermi velocity V_f, and the superconducting band gap 2Δ.

1.5. High Tc ceramic superconductors

An accepted common feature of copper-oxide based superconductors is their perovskite layered crystal structure consisting of one or more two-dimensional CuO_2 planes (in one unit cell) separated by varying thicknesses of non-superconducting planes containing other cations and oxygen such as SrO, LaO, CuO, PbO, BaO, BiO, and TlO, or planes containing just cations such as Y or Ca [29, 30]. It appears also that both CuO and CuO_2 planes are present. A feature common to these perovskites is their variability in oxygen content and the sensitivity of the properties of interest to the amount of intercalated oxygen. Some of the properties of the new high T_c oxides are quite different from those of the conventional low T_c superconducting metals and alloys. Most prominent is the low critical current density of polycrystalline samples, one of the outstanding problems that need to be solved for large scale applications. There is experimental evidence that grain boundaries, even if free of second phase material, act as weak coupling junctions between grains rather than as pinning centres. On the other hand, very high critical current densities have been achieved in high quality oriented films and single crystals. There are also many indications that the oxides are basically BCS (Bardeen-Cooper-Schrieffer) superconductors, with a gap over the entire Fermi surface. Their unconventional properties are a result of their short coherence length, rather than to a radically different type of superconductivity. This short coherence length renders the superconducting order parameter very sensitive to defects on the atomic scale. The superconducting properties were found to be highly anisotropic, with the superconducting electrons basically confined to the Cu-O planes which lie on the basal plane because of the extremely short coherence length along the c-axis [31].

Another common property of high T_c superconductors is that the temperature coefficient of conductivity $d\sigma/dT$ is nearly zero in the normal state. Namely, they have the intermediate conducting property between metals ($d\sigma/dT < 0$) and semiconductors ($d\sigma/dT > 0$)

[32]. The possibility of varying the number of planes in a group, the metal atom separating the planes and chemistry, thickness and structure of the intercalating layers, gives rise to the large number of superconducting copper oxides now discovered. But most of the research is concentrated on the three systems with the highest transition temperatures (above 77K, the boiling point of liquid nitrogen), YBaCuO, BiSrCaCuO, and TlBaCaCuO. The crystal structure and superconducting properties of Yttrium and Thallium based superconductors will be briefly reviewed, followed by a fuller discussion of the BiSrCaCuO ceramic material.

1.5.1. YBaCuO

The material which has received the most attention to date is $YBa_2Cu_3O_7$, often referred to as the 123 compound. Its crystal structure [33] is orthorhombic,with a≈b and c≈ 3a (only slightly distorted from tetragonal) [34]. This gives rise to extreme anisotropy in the superconducting properties [35]. Yttrium can be replaced by most rare earth elements (e.g. europium, gadolinium and holmium) without affecting the structure significantly, and with negligible effect upon the critical temperature, which remains close to 90K. T_c is very sensitive to the oxygen content and it is also known from neutron diffraction studies that T_c is maximised when the oxygen vacancies are ordered. It has been shown that when fully oxygenated, $T_c = 92K$ and that as the oxygen content is reduced it undergoes an orthorhombic-tetragonal transition. Thin films with critical currents in excess of 10^6 A/cm^2 at 77K and zero field have been made using this material by a number of groups, mostly by in-situ methods [36] but also ex-situ [37].

1.5.2. TlBaCaCuO

In the thallium system there are two series of compounds, $Tl_1Ba_2Ca_{n-1}Cu_nO_{2n+3}$ and $Tl_2Ba_2Ca_{n-1}Cu_nO_{2n+4}$ (n = 1-5) which can be modelled as an interleaving of rock salt and defective perovskite units. The structures of the different phases are very similar. It has been shown that Cu perovskite-like units are sandwiched between Tl-O monolayers [38]. The common feature of these high T_c materials is the existence of the Tl-O layer and the

$(CuO_2)_n$ network, which is likely to be the path of the superconducting electron pairs [39]. The 2223 ($Tl_2Ba_2Ca_2Cu_3O_x$) phase of this system exhibits the highest value of T_c(125K). The 1212 compound is the phase of this family which has the lowest "high temperature" T_c value (of approximately 90K). The thallium compounds are more attractive for some applications than YBaCuO in that they have the highest T_c, are less anisotropic, and are not very sensitive to oxygen content.

1.5.3. BiSrCaCuO

1.5.3.1. Structures and T_c values

The BiSrCaCuO system has a very similar layered crystal structure to some of the thallium containing oxide superconductors. Firstly superconductivity at 20K was reported by Michel et al. [40] for the Bi-Sr-Cu-O system. The addition of Ca to this ternary led Maeda et al. [41] to the discovery of bulk superconductivity at 85K and evidence of superconductivity at 110K in the Bi-Sr-Ca-Cu-O system. It has been demonstrated that three phases of general formula $Bi_2Sr_2Ca_{n-1}Cu_nO_x$ with n=1,2 and 3 exist which are closely related from a structural point of view [42]. Their pseudo tetragonal structures (**Fig. 1.7**) can be described as a stacking of a basic $Bi_2Sr_2CuO_6$ unit with either zero, one, or two $CaCuO_2$ slabs inserted. The observed increase in the c lattice parameter from 2.46 to 3.06 and finally to 3.71 nm in going from the n=1 to n=2 and n=3 phases results from the progressive addition of $CaCuO_2$ layers, each about 0.3 nm thick, to the stacking sequence in the unit cell in the sequence Bi-Sr-Ca-Cu. The phases are generally referred as 2201, 2212 and 2223 with respect to the increasing n values, and each number represents the number of cations of each element in the unit cell. The number of Cu-O planes are closely related to T_c, it increases with the number of Cu-O layers, n (up to n=3). Although a number of investigators have succeeded in obtaining multilayer films (2234 and 2245 structures) with a c-dimension larger than 3.7 nm, the XRD line width from these films is usually broad and the films show poor superconducting behaviour [43].

The 2201 phase is not regarded in the literature as one of the "superconducting phases" as its T_c is only around 14K. The 2212 phase is known as the "low T_c" phase and has a typical T_c of between 80-90K. The low T_c phase is promising for various high current density applications at 4.2K, because its high critical current density ($1.4x10^5 A/cm^2$ around this temperature) can be maintained even at extremely high magnetic fields beyond 20T, being superior to metallic hard superconductors such as Nb_3Sn [44]. An essential feature of 2212 phase is the very high degree of anisotropy. The 2223 phase of BSCCO is known as the "high T_c" phase which has a zero resistance at about 110K.

The weak link grain boundaries lead to a highly magnetic field-dependent critical current, decreasing considerably in a small magnetic field. The critical current density, J_c does not depend only on the field strength but also on the field direction. According to Kes et al. [45], in Bi-2212 the CuO_2 layers completely decouple and the transport properties of this material are independent of magnetic field $B \perp c$ in the 2 dimensional regime, while for a magnetic field inclined by some angle θ with respect to the CuO_2 planes only the field component $B// = B \cos\theta$ influences the transport properties. This model has been shown to apply to the critical current anisotropy $J_c(\theta)$ of epitaxial [46] and polycrystalline [47] Bi-2212 films. Flux creep is particularly a problem in BSCCO, where it is very fast above 30K; below this both flux pinning and $J_c(B)$ are much enhanced [48]. Much effort has concentrated on improving and controlling microstructure and grain orientation.

1.5.3.2. Phase stability

The 2212 phase is reported to be stable over a wide temperature region from 800 to 850^oC in air [49]. At temperatures around 750^oC the 2201 phase, CuO and CaO ($CaCO_3$) coexist stably [50, 51]. The high T_c phase is considered to be produced from reaction of excess Ca and Cu with the low T_c phase which is readily formed by sintering. The transformation from the low T_c to the high T_c phase is accelerated by seeding of the high T_c phase [52]. Furthermore, the high T_c phase is produced by long-term annealing at a temperature just below the melting point. The facts indicate that the high T_c phase is more

stable than the low T_c phase at this temperature, although the low T_c phase is also fairly stable at high temperatures. For producing the high T_c phase, reducing the ambient oxygen partial pressure [53] and also excess Ca and Cu addition [54] are effective and are thought to lower the melting temperature of the low T_c phase; i.e., the low T_c phase melts partially prior to the formation of the high T_c phase, and the high T_c phase grows from the partially melted phase [55].

Certain dopants, particularly Pb, have been found to promote the formation of the 2223 phase. The high T_c phase was produced from a Pb-free amorphous thin film by Pb-vapour doping; the films were annealed for 3 hours with the Pb source pellets in a closed Au capsule. High T_c phase could not be formed in the film by annealing for a relatively short period, if the low T_c phase was formed prior to the Pb treatment [56]. In the case of thin films, long-term annealing causes deviation of chemical composition because almost all of the lead evaporates [57], and short-term annealing is required for producing a high volume fraction of the high T_c phase. It is, therefore, expected that the high T_c phase can be produced by short term annealing directly from amorphous films containing neither the low T_c phase nor the nucleus for the low T_c phase. It has proved very difficult to obtain bulk material with a high proportion of 2223 phase. Since Takano et al. [58] obtained >90% of 2223 phase in a Pb-doped BiSrCaCuO system many scientists have become interested in the preparation and properties of the Pb doped Bi-based superconducting system. The roles of Pb are likely to be: 1, to decrease the melting point of the Bi compound and widen the range of temperature for annealing; and 2, to enhance the formation of 2223 phase from 2212 phase. For the latter role, a slight excess of Ca and Cu from the ideal 2223 composition was reported to be effective [59].

In addition, the Bi-Sr-Ca-Cu-O system is superior to the RE-Ba-Cu-O system (RE = rare-earth) in not only higher T_c but also chemical stability. However, It has been clearly shown that the total variation of T_c extends over 43K in the 2212 phase. This variation which is common to many high T_c systems, is attributed basically to a change of the oxygen content.

1.5.3.3. Effects of reducing and oxidizing

The oxygen stoichiometry is one of the most important crystal chemical parameters governing the physical properties of high-T_c superconducting compounds. All are oxides and the superconducting properties are closely related to the mixed-valency states they contain. Mixed-valency states are controlled by the oxygen stoichiometry. The dependence of hole concentration on the oxygen concentration clearly showed that oxygen supplies holes to the system [60]. Hole doping in cuprates is chemically equivalent to an increase in the formal copper valence above 2+. According to the structure refinement by Yamamoto et al. [61] excess oxygen atoms exist in the Bi dilute region of Bi_2O_2 layers, which is consistent with crystallochemical considerations by Ikeda et al. [62]. Thus, the most dominant origin of the hole reservoir is excess oxygen existing in the Bi_2O_2 layers. In the Bi compounds, several authors reported that the control of the hole concentration is possible by substitution of cations with atoms of different chemical valence [63-66]. Maeda et al. [67], for various samples of the Bi systems, found that the change in oxygen content with increasing temperature is about 0.8 weight% at maximum, and below 600^{o}C there is almost no loss of oxygen.

In general, it is well established that the superconducting transition temperature, T_c, strongly depends on the oxygen concentration. The correlation between carrier concentration and T_c does not extend to the maximum concentration (assuming that the charge carriers are holes), i.e., the superconducting properties are optimised in a range of charge carrier densities [60]. The dependence of the transition temperature on the hole concentration was extensively investigated by several groups specially for Bi-2212 using either cation substitution or redox thermal treatments to vary the oxygen content [68-70]. These studies definitely indicated that in Bi-2212 the optimum hole concentration is 0.2 holes per Cu atom which corresponds to the highest possible value of T_c (about 94K), and the increase in the number of CuO_2 planes per unit cell causes the decrease in the carrier concentration in the CuO_2 plane. A similar relationship between the number of CuO_2 planes and the carrier concentration is reported in the Tl-based superconductors [71].

Most of the results concerning the oxygen content are from bulk BSCCO material. However similar effects have been observed on thin films. For example, Miura et al. [72] have annealed the as-grown 2212 films in various oxygen atmospheres at 400^{o}C for 2 h in order to change the oxygen content, and found that $T_{c\text{-onset}}$ and c-axis lattice constant increased with decreasing oxygen content (**Fig.1.8**). Their result also suggested that the oxygen content could be varied reversibly by low temperature annealing. Oxygen desorption starts even at temperatures as low as 170^{o}C in vacuum and the oxygen content in the film decreases with increasing annealing temperature, but further reduction in oxygen content, in the temperature range above 250^{o}C in vacuum, degrades T_c while the c-axis lattice constant remains almost constant. This result indicated that there is an optimum oxygen content for the 2212 phase. However, the reason for the c-axis lattice constant to be unchanged rather than longer with decreasing oxygen content has not been clarified yet. Balestrino et al. [69] have shown on epitaxial thin films grown by liquid phase epitaxy that the critical temperature of both undoped and lead doped BSCCO 2212 films can be reversibly changed by reducing and oxidizing thermal treatments, and for both kinds of film the maximum range of variation of T_c is 15K. The same group also reported for the first time that reducing treatments, while increasing the transition temperature to 94K, reduce the critical current density relative to the as-grown value. This effect is attributed to a decrease of the anisotropy in the oxygenated Bi-2212 films [73]. The Bi-2212 structure is not stable at low (10^{-5} atm., above 700^{o}C) and high (10^{2} atm., above 500^{o}C) oxygen pressures. These regions do not contain metallic phases. The largest variation of T_c (51.5 to 94.4K) on 2212 bulk materials attributed to the oxygen content has been reported by Triscone et al. [74], while no significant variation of the lattice parameters was observed.

There have been few reports regarding the dependence of Bi-2223 on oxygen content. [60, 75, 76]. The decrease in T_c with increasing oxygen content is small [77, 78] in comparison with the similar effect observed in the Bi-2212 phase, suggesting that the incorporation of the additional CaCuO layer plays a mitigating role. If too much oxygen disintercalates, however, the 2223 phase undergoes a structural collapse with a concomitant

suppression of T_c. The collapse of the 2223 structure with decreasing oxygen content may be related to the stabilisation of the 2223 phase accomplished by partially substituting Pb for Bi. In this picture, the role of Pb is to optimise the oxygen content of the Bi-O slabs for insertion of the third CaCuO layer [76]. The oxygen deficiency of about 1.2 per chemical formula unit on the composition $Bi_{1.8}Pb_{0.2}Sr_2Ca_2Cu_3O_{9.9}$ by vacuum annealing causes decomposition of the superconducting phase into non-superconducting phases such as CaO, Cu_2O and probably $Bi_{1.8}Pb_{0.2}Sr_2CaO_{5.9}$ [79]. On the other hand 2223 decomposes completely to 2201 and other non-superconducting phases at 700 and 800^oC under high [77] or low [60] oxygen pressure.

There have been contrary reports on the directions and variation range of T_c with oxygen content for the n = 3 bulk material. For example, on the 2223 phase coexisting with the 2212 phase in $Bi_{1.6}Pb_{0.4}Sr_2Ca_3Cu_4O_x$ samples a decrease of T_c from 105K to 89K was observed as a result of ≈0.22% weight loss, whereas for the 2212 phase an increase of T_c from 67K to 89K is observed (by Zhao et al. [80]). This opposite tendency is in agreement with previously reported results by Tallon [81] and Buckley [82] et al. for the separate n = 2 and n = 3 materials quenched in liquid nitrogen from different annealing temperature. Li and Li [78] found a small change of 2.3K on T_c for the samples; air-quenched at 860^oC (T_c = 106K) and O_2-annealed at 600^oC for 12 h (T_c = 108.3K). On the other hand, others [75-77] reported that T_c decreases from 110K to 106K with increasing oxygen concentration (annealed in above 100 bar of O_2 at above 600^oC).

Hattori et al. [60]. have reported that with decreasing oxygen partial pressure T_c shifts to lower temperature (from 107K to above 90K, annealed at 600^oC for 30 minutes) and the normal state resistivity increases for films of composition $Bi_{1.7}Pb_{0.3}Sr_{1.3}Ca_{3.3}Cu_{3.4}O_x$, which is quite close to the composition referred to in ref. [80]. This similarity between composition and result may allow us to attribute the contrary results concerning n = 3 material mentioned above to the change of sample composition, precise preparation condition and particularly the post-annealing process. Consequently, it can be said that oxygen excess is not the only factor which contributes to the optimisation of the critical

temperature, and the cationic composition also plays a role. The oxygen stoichiometry may be related to the latter. In general, T_c of the unleaded samples is more sensitive to oxygen stoichiometry than the Pb doped sample.

1.5.3.4. Role of Pb in the promotion of Bi-phases

Since the enhanced effect of Pb addition on the formation of the $Bi_2Sr_2Ca_2Cu_3O_x$ phase has been found [83], much effort has been extended to increase the fraction of the 2223 phase, to shorten the annealing time and to investigate the growth mechanism [84]. When this method is applied to thin films, various problems related to the ease of evaporation of Pb [85], the requirement of a longer annealing time [86] and the formation of impurity phases such as Ca_2PbO_4 were found.

It has been previously shown that lead does not simply act as a flux in the growth of this phase. Chemical analysis [87], crystallographic [88], and electron microscopy experiments [89] have established that lead actually enters the crystal structure of the superconducting phases, and that it is principally substituted for bismuth atoms [90]. The maximum quantity of lead which enters in both $n=2$ [91] and $n=3$ phases is at a value corresponding to the ratio Bi:Pb = 1.65:0.35 [92, 93] (**Fig.1.9**). As lead substitutes for bismuth within the superconducting phases its role is likely to modify the structural properties of these phases. The c parameter decreases with increasing lead concentration (**Fig.1.10**) [81, 92] and twinning of the domains disappears as a consequence of an increase in the strength of bonding between the Bi-O slabs which constitute the building blocks of the compounds. The Pb content is also found to influence T_c. T_c decreases with further increasing of Pb content above 0.2 and then remains constant in Bi-2212 (**Fig.1.11**) [91]. The decrease of T_c is explained in terms of substituting Bi^{3+} by Pb^{2+} and thus increasing hole concentration. Pb substitution tends to remove the resistivity toe at T_c that is characteristic of the Bi based superconductors.

References

1 H.P. Myers, *Introductory to Solid State Physics* (Chapter 13) Taylor & Francis Press, 1990

2 J. Bardeen, L.N. Cooper, and J.R. Schrieffer, Phys. Rev. 108 (1957) 1175.

3 K. Hirata, K. Yamamoto, K. Ijima, J. Tanaka, T. Terashima, Y. Bando, and H. Mazaki, Appl. Phys. Lett. 56 (1990) 683.

4 Y. Yoshisato, A. Takeoka, T. Ikemachi, K. Niki, T. Yokoo, S. Nakano, and Y. Kuwano, Jpn. J. Appl. Phys. 29 (1990) 1080.

5 M. Miura, H. Kumakura, K. Togano, and H. Maeda, Appl. Phys. Lett. 54 (1989) 1582.

6 T. Hikata, T. Nishikawa, H. Mukai, K. Sato, and H. Hitotsuyanagi, Jpn. J. Appl. Phys. 28 (1989) L1204.

7 T. Hikata, K. Sato, and H. Hitotsuyanagi, Jpn. J. Appl. Phys. 28 (1989) L82.

8 R.B. Laibowitz, R.H. Koch, A. Gupta, G. Koren, W.J. Gallagher, V. Foglietti, B. Oh, and J.M. Viggiano, Appl. Phys. Lett. 56 (1990) 686.

9 R.H. Koch, W.J. Gallagher, B. Bumble, and W. Lee, Appl. Phys. Lett. 53 (1989) 951.

10 M.S. Dilorio, S. Yoshizumi, K-Y. Yang, J. Zang, and M. Maung, Appl. Phys. Lett. 58 (1991) 2552.

11 R. Gross, P. Chaudhari, M. Kawasaki, M.B, Ketchen, and A. Gupta, Appl. Phys. Lett. 57 (1990) 727.

12 H. Akoh, F. Shinoki, M. Takahashi, and S. Takada, Jpn. J. Appl. Phys. 27 (1988) L519.

13 A. Nakayama, A. Inoue, K. Takeuchi, and Y. Okabe, Jpn. J. Appl. Phys. 26 (1987) L2055.

14 T. Shiota, K. Takechi, Y. Takai, and H. Hayakawa, in *Advances in Superconductivity, Proceedings of the 1st International Symposium on Superconductivity (ISS'88), 1988,* Nagoya, edited by K. Kitazawa, and T. Ishiguro (Springer, Tokyo, 1989), p.755.

15 C.T. Rogers, A. Inam, M.S. Hegde, B. Dutta, X.D. Wu, and T. Venkatesan, Appl. Phys. Lett. 55 (1989). 2032.

16 M. Gurvitch, M.A. Washington, and H.A. Huggins, Appl. Phys. Lett. 42, (1983) 472

17 A. Shoji, M. Aoyagi, S. Kosaka, F. Shinoki, and H. Hayakawa, Appl. Phys. Lett. 46 (1985) 1098.

18 K. Mizuno, K. Higashino, K, Setsune, and K. Wasa, Appl. Phys. Lett. 56 (1990) 1469.

19 Y. Enomoto, and T. Murakami, J. Appl. Phys. 59 (1986) 3807.

20 P.L. Richards, J. Clarke, R. Leoni, P. Lerch, S. Verghese, M.R. Beasley, T.H. Geballe, R.H. Hammond, P. Rosenthal, and S.R. Spielman, Appl. Phys. Lett. 54 (1989) 283.

21 Y. Enomoto, T. Murakami, and M. Suzuki, Physica C 153-155, (1988) 1592.

22 H. Chaloupka, and H. Piel, in *proceedings of the Third Workshop on RF Superconductivity*, edited by K.W. Shepard, Argonne Nat. Lab. Report No. ANL-PHY-1 (1988), p. 273.

23 For a review see G. Muller, in *proceedings of the Fourth Workshop on RF Superconductivity*, Tsukuba, edited by Y. Kojima KEK Report 80-21 (1990), p. 267.

24 N. Klein, G. Muller, H. Piel, B. Roas, L. Schultz, U. Klein, and M. Peiniger, Appl. Phys. Lett. 54 (1989) 757.

25 L Drabeck, G. Gruner, J.J. Chang, A. Inam, X.D. Wu, L. Nazar, T. Venkatesan, and D.J. Scalapino, Phys. Rev. B40 (1989) 7350.

26 Dong-Ho Wu, W.L. Kennedy, C. Zahapoulos, and S. Sridhar, Appl. Phys. Lett. 55 (1989) 696.

27 A. Lauder, C. Wilker, D.J. Kountz, W.L. Holstein, and D.W. Face, IEEE Trans. on Appl. Superconductivity, 3 (1993) 1683.

28 W.L. Holstein, L.A. Parisi, C.Wilker, and R.B. Flippen , Appl. Phys. Lett. 60 (1992) 2014.

29 I.K. Schuller, J.D. Jorgensen, Mater. Res. Soc. Bull., January 1989, p. 27.

30 R.M. Hazen, in *Physical Properties of High Temperature Superconductors II*, edited by D.M. Ginsberg, World Scientific, Singapore (1990), p. 121.

31 S.W. Tozer, A.W. Kleinasser, T. Penney, D. Kaiser, and F. Holtzberg, Phys. Rev. Lett. 59 (1987) 1768.

32 Y. Idemoto, S. Fujiwara, and K. Fueki, Physica C 176 (1991) 325.

33 M.A. Beno, L. Soderholm, D.W. Caponne II, D.G. Hinks, J.D. Jorgenson, I.K. Schuller, C.A. Segre, K. Zhang, and J.D. Grace, Appl. Phys. Lett. 51, 57 (1987).

34 T. Siegrist, S. Sunshine, D.W. Murphy, R.J. Cava, and S.M. Zahurak, Phys. Rev. B35 (1987) 7137.

35 R.J. Cava, B. Batlog, R.B. van Dower, D.W. Murphy, S. Sunshine, T. Siegrist, J.P. Remeika, E.A. Rietman, S. Zahurak, and G.P. Espinosa, Phys. Rev. Lett. 58 (1987) 1676.

36 D.M. Hwang, T. Venkatesan, C.C. Chang, L. Nazar, X.D. Wu, A. Inam, and M.S. Hegde, Appl. Phys. Lett. 54 (1989) 1702.

37 A. Mogro-Campero, L.G. Tunner, and E.L. Hall, J. Appl. Phys. 65 (1989) 4951.

38 R. Beyers, S.S. P. Parkin, V.Y. Lee, A.L. Nazzal, R. Savoy, G. Gorman, and T.C. Huang, Appl. Phys. Lett. 53 (1988) 432.

39 T. Ttoh, Jpn. Appl. Phys. 28 (1989) 200.

40 C. Michel, M. Hervieu, M.M. Borel, A. Grandin, F. Deslandes, J. Prorost, and B. Raveau, Z. Phys. B68, (1987) 421.

41 H. Maeda, Y. Tanaka, M. Fukutomi, and T. Asano, Jpn. J. Appl. Phys. 27 (1988) 209.

42 J.M. Tarascon, W.R. McKinnon, P. Barboux, D.M. Hwang, B.G. Bagley, L.H. Greene, G.W. Hull, Y. LePage, N. Staffel and M. Giroud, Phys. Rev. B 38 (1988) 8885.

43 K. Nakamuna, J. Sato, and K. Ogawa, Jpn. J. Appl. Phys. 29 (1990) 77.

44 K. Heine, J. Tenbrink, and M. Thoner, Appl. Phys. Lett. 55 (1989) 2441.

45 P.H. Kes, J. Aarts, V.M. Vinokur, and C.J. van der Beek, Phys. Rev.Lett. 64 (1990) 1063.

46 P. Schmitt, P. Kummeth, L. Schultz and G. Saemann-Ischenko, Phys. Rev.Lett. 67 (1991) 267.

47 H. Raffy, S.Labdi, O. Laborde, and P. Monceau, Physica B 165-166 (1990) 1423; H. Raffy, S.Labdi, O. Laborde, and P. Monceau, Supercond. Sci. Technol. 4 (1991) 100.

48 J.W. Burgoyne, Magnetic Flux Instabilities In High Temperature Superconductors, D. Phil. thesis, 1993

49 K. Shulze, P. Majewski, B. Hettich, and G.Petzow, Z. Metall. 81 (1990) 836.

50 G.R. PAZ-Pujaalt, Physica C 166 (1990) 177.

51 S. Yaegashi, H. Murakami, J. Nishino, Y. Shiohara, and S. Tanaka, Jpn. J. Appl. Phys. 30 (1991) 471.

52 Y. Iwai, M. Takata, T. Yamashita, M. Ishii and H. Koinuma, Jpn. J. Appl. Phys. 28 (1989) 1518.

53 U. Endo, S. Koyama, and T. Kawai, Jpn. J. Appl. Phys. 27 (1988) 1476.

54 A. Sumiyama, T. Yoshitomi, H. Endo, J. Tsuchiya, N. Kijima, M. Mizuno and Y. Oguri, Jpn. J. Appl. Phys. 27 (1988) 542.

55 J. Tsuchiya, H. Endo, N. Kijima, A. Sumiyama, M. Muzuno, Y Oguri, Jpn. J. Appl. Phys. 28 (1989) 1918.

56 H. Hayakawa, M. Kaise, K. Nakamura, and K. Ogawa, Jpn. J. Appl. Phys. 28 (1989) 967.

57 S. Nagai, N. Fujimura, and T. Ito, Jpn. Soc. Powder and Powder Metallurgy 37 (1990) 99.

58 M. Takano, J. Takada, K. Oda, H. Kitaguchi, Y. Miura, Y. Ikeda, Y. Tomii, and H. Mazaki, Jpn. J. Appl. Phys. 27 (1988) 1041.

59 Y.H. Wang, L. Li, Y.Z. Zhang, Y.Y. Zhao, and P.Xu, Cryogenics, 31 (1991) 439.

60 H. Hattori, K. Nakamura, and K. Ogawa, Jpn. J. Appl. Phys. 29 (1990) 36.

61 A. Yamamoto, M. Onoda, E. Takayama-Muromachi, F. Izumi, T. Ishigaki, and H. Asano, Phys. Rev. B 42 (1990) 4228.

62 Y. Ikeda, H. Ito, S. Shimomura, Y. Oue, K. Inaba, Z. Hiroi, and M. Takano, Physica C 159 (1989) 93.

63 N. Fukushima, H. Niu, and K. Ando, Jpn. J. Appl. Phys. 27 (1988) L790.

64 Y. Koike, Y. Iwabuchi, S. Hosoya, N. Koboyashi, and T. Fukase, Physica C 159 (1989) 105.

65 J.M. Tarascon, P. Barboux, G.W. Hull, R. Ramesh, H.H. Greene, M. Giroud, M.S. Hedge, and W.R. McKinnon, Phys. Rev. B 39 (1989) 4316.

66 Y. Takemura, M. Hongo, and S. Yamazaki, Jpn. J. Appl. Phys. 28 (1989) L916.

67 A. Maeda, M. Hase, I. Tsukada, K. Noda, S. Takebayashi, and K. Uchinokura, Phys. Rev. B 41 (1990) 6418.

68 P. Strobel, B. Bonnet, C. Mouget, and B. Souletie, Physica C 172 (1990) 193.

69 G. Balestrino, M. Marinelli, E. Milani, M. Montuori, A. Paoletti, and P. Paroli, J. Appl. Phys. 72 (1992) 191.

70 I. Matsubara, H. Tanigawa, T. Ogura, H. Yamashita, M. Kinoshita, and T. Kaway, Physica C 167 (1990) 503.

71 D. Shindo, H. Sato, G.L. Liedl, D. Perry, K. Hiraga, M. Hirabayashi, S. Nakajima, M. Kikuchi, Y. Syono, K. Hojou, and T. Soga, Jpn. J. Appl. Phys. 28 (1989) L955.

72 S. Miura, T. Yoshitake, and N. Shohata, Physica C 165 (1990) 241.

73 G. Balestrino, M. Marinelli, E. Milani, and A. Paoletti, J. Appl. Phys. 73 (1993) 3903.

74 G. Triscone, J.-Y. Genoud, T. Graf, A. Junod, and J. Muller, Physica C 185 (1991) 793.

75 D.E. Morris, C.T. Hultgren, A.M. Markelz, J.Y.T. Wei, N.G. Asmar, and J.H. Nickel, Phys. Rev. B 39 (1989) 6612.

76 S,M. Green, Yu Mei, A.E. Manzi, and H.L. Luo, J. Appl. Phys. 66 (1989) 3703.

77 C.-H Hsu and N.A. Gokcen, Appl. Supercunductivity, 1 (1992) 19.

78 Y. Li, and Y. Li, J. of Superconductivity, 5 (1992) 1.

79 Y. Kimishima, and J. Nakano, Physica C 185-189 (1991) 835.

80 J. Zhao, M. Wu, W. Abdul-Razzaq, and M.S. Seehra, Physica C 165 (1990) 135.

81 J.L. Tallon, R.G. Buckley, P.W. Gilberd, and M.R. Presland, Physica C 158 (1989) 247.

82 R.G. Buckley, J.L. Tallon, I.W.M. Brown, M.R. Pressland, N.E. Flower, P.W. Gilbert, M.Bowden, and N.B. Milestone, Physica C 156 (1988) 629.

83 M. Takano, J. Takada, K. Oda, H. Kitaguchi, Y. Miura, Y. Ikeda, Y. Tomii, and H. Mazaki, Jpn. J. Appl. Phys. 27 (1988) L1041.

84 T. Hatano, K. Aota, S. Ikeda, K. Nakamura, and K. Ogawa, Jpn. J. Appl. Phys. 27 (1988) L2055.

85 Y. Hakuraku, Y. Aridome, and T. Ogushi, Jpn. J. Appl. Phys. 27 (1988) L2091.

86 S.K. Dew, N.R. Osborne, P.J. Mulhern, and R.R. Parsons, Appl. Phys. Lett. 54 (1989) 1929.

87 L. Pierre, D. Morin, J. Schneck, J.C. Toledano, J. Primot, C. Daguet, F. Glas, J. Etrillard, and H. Savary, Solid-State Commun. 69 (1989) 499.

88 J. Schneck, L. Pierre, J.C. Toledano, and C. Daguet, Phys. Rev. B 39 (1989) 9624; L. Pierre, J. Schneck, J.C. Toledano, and C. Daguet, Phys. Rev. B 41 (1990) 766.

89 C.H. Chen, D.J. Werder, S.H. Liou, H.S. Chen, and M. Hong, Phys. Phys. Rev. B 37 (1988) 9834.

90 H. Nobumasa, T. Arima, K. Shimizu, Y. Otsuka, Y. Murata, and T. Kawai, Jpn. J. Appl. Phys. 28 (1989) L57.

91 M. Boekholt, D. Gotz, H. Idink, M. Fleuster, T. Hahn, E. Woermann, G. Guntherodt, Physica C 185-189 (1991) 789.

92 L. Pierre, J. Schneck, D. Morin, J.C. Toledano, J. Primot, C. Daguet, and H. Savary, J. Appl. Phys. 68 (1990) 2296.

93 S.M. Green, Yu Mei, A.E. Manzi, and H.L. Luo, R. Ramesh and G. Thomas, J. Appl. Phys. 66 (1989) 728.

94 D. Dew-Hughes, Ceramics (1988) 741.

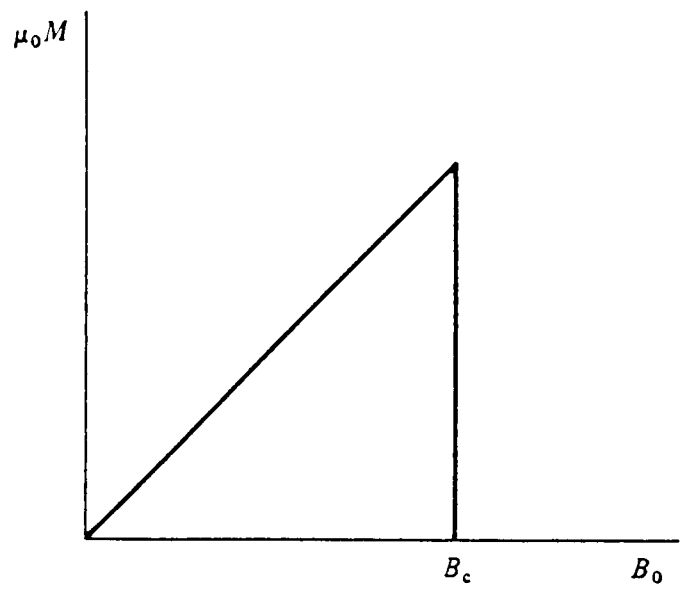

Figure 1.1 For type I superconductors the diamagnetization grows linearly with magnetic field until the critical value is reached. At this point the flux penetrates the sample and the magnetic susceptibility assumes the normal low value. (After [1])

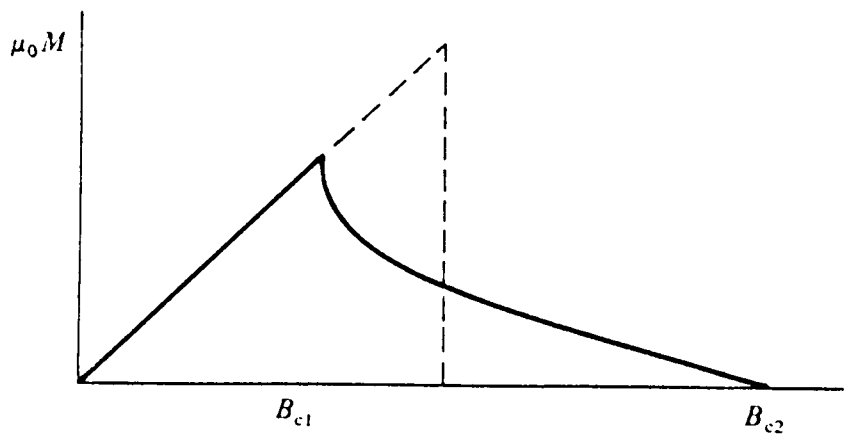

Figure 1.2 For type II superconductors the initial behaviour of the diamagnetization is linear with external field, but at a certain field B_{c1} flux begins to penetrate the sample and the magnetization decreases, initially rapidly, but then slowly, until in a field B_{c2} the sample becomes saturated with lines of flux quanta. (After [1])

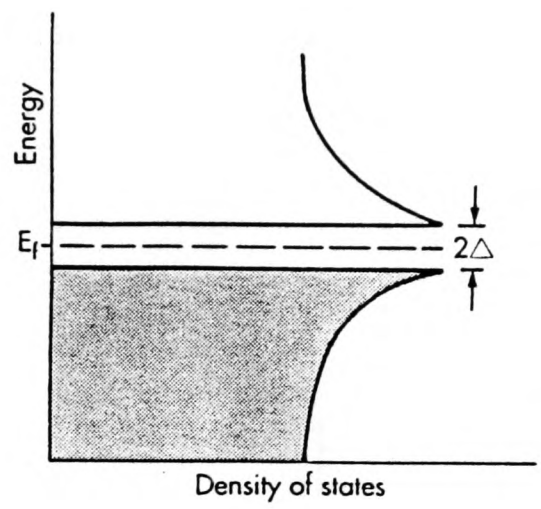

Figure 1.3 Density of electron states close to the Fermi level in a BCS superconductor, showing the energy gap 2Δ. (After [94])

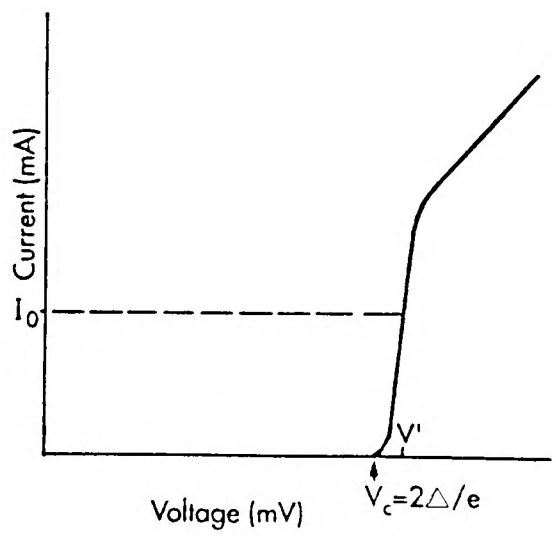

Figure 1.4 Current-voltage characteristic for a Josephson junction between two identical superconductors. If the current exceeds I_c the voltage suddenly jumps from zero to a finite value V'. (After [94])

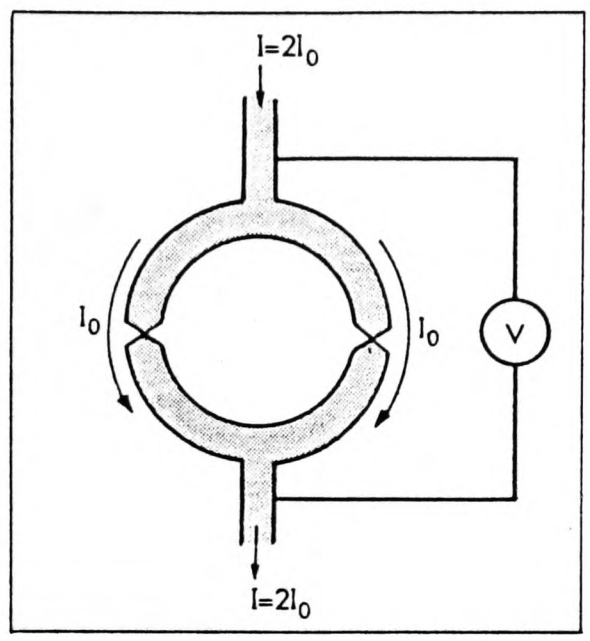

Figure 1.5 Quantum interferometer consisting of two Josephson junctions in parallel. (After [94])

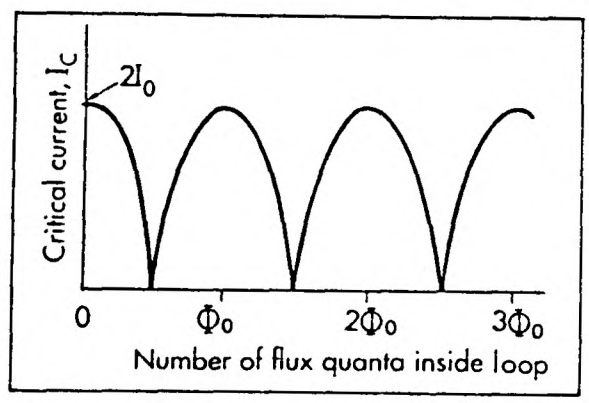

Figure 1.6 Variation in critical current with number of flux quanta inside a quantum interferometer. (After [94])

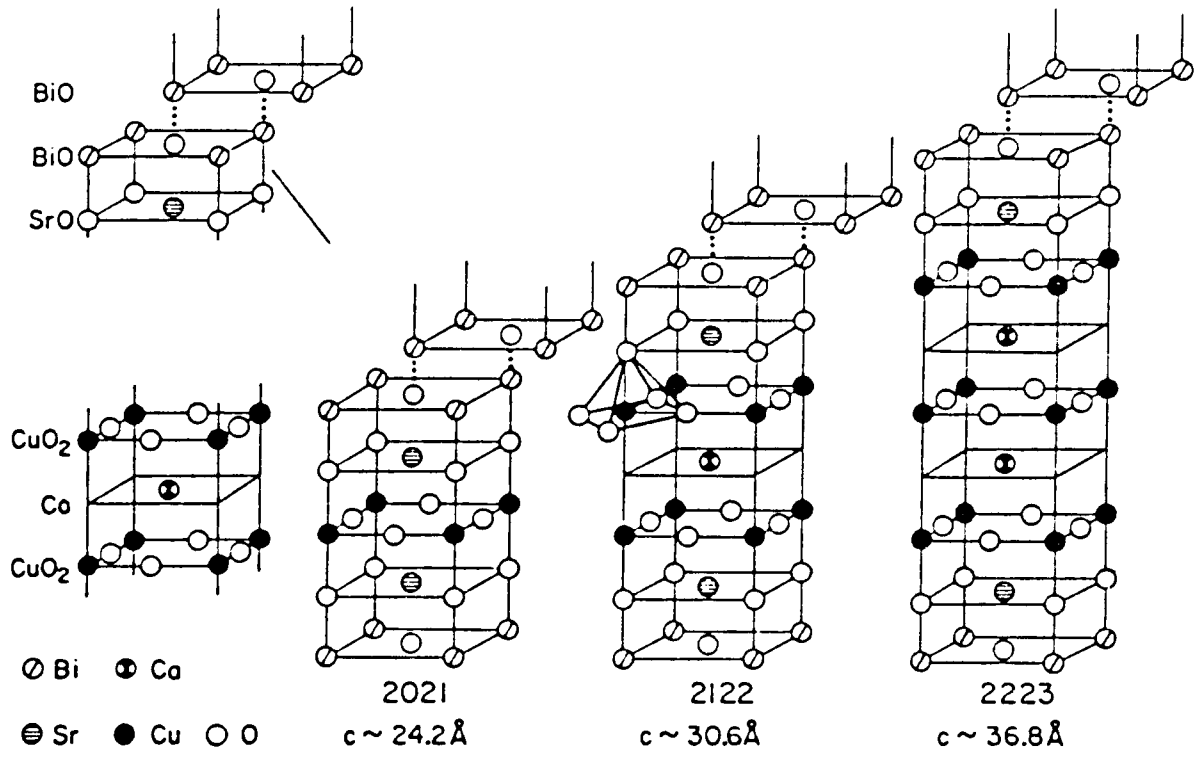

Figure 1.7 Crystal structures for phases in the system $Bi_2Ca_{n-1}Sr_2Cu_nO_{2n+4}$, with $n = 1,2,3$. (After [42])

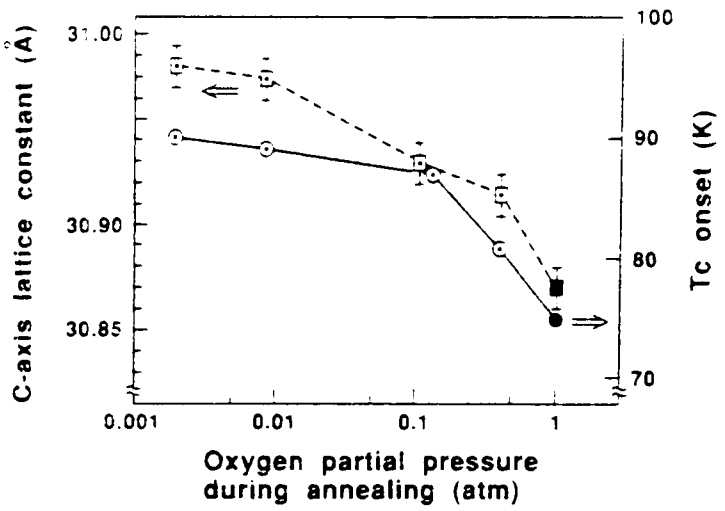

Figure 1.8 The c-axis lattice constant and $T_{c\text{-onset}}$ as a function of the oxygen partial pressure during annealing. Circles indicate the values of $T_{c\text{-onset}}$, whereas squares denote the c-axis lattice constants. Filled circles and squares denote those of the standard film (annealed at 400°C for 3 h in atmospheric pressure oxygen to standardise the oxygen content). (After [72])

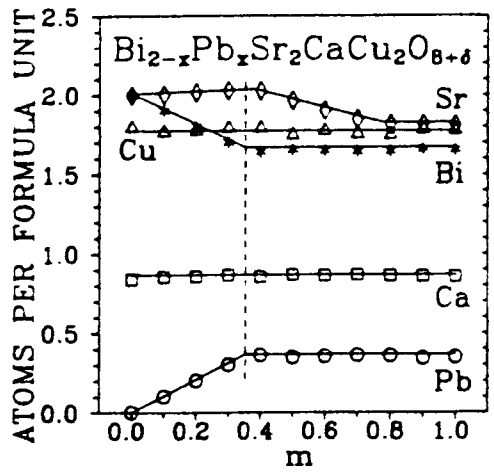

Figure 1.9 Atomic composition of the $Bi_{2-x}Pb_xSr_2CaCu_2O_{8+\delta}$ phase measured by EPMA as a function of Pb ratio, m, in the nominal composition of the sample. Parameter "x " refers to the actual measured composition. The dashed vertical line at m = 0.35 refers to the solubility limit of Pb. (After [91])

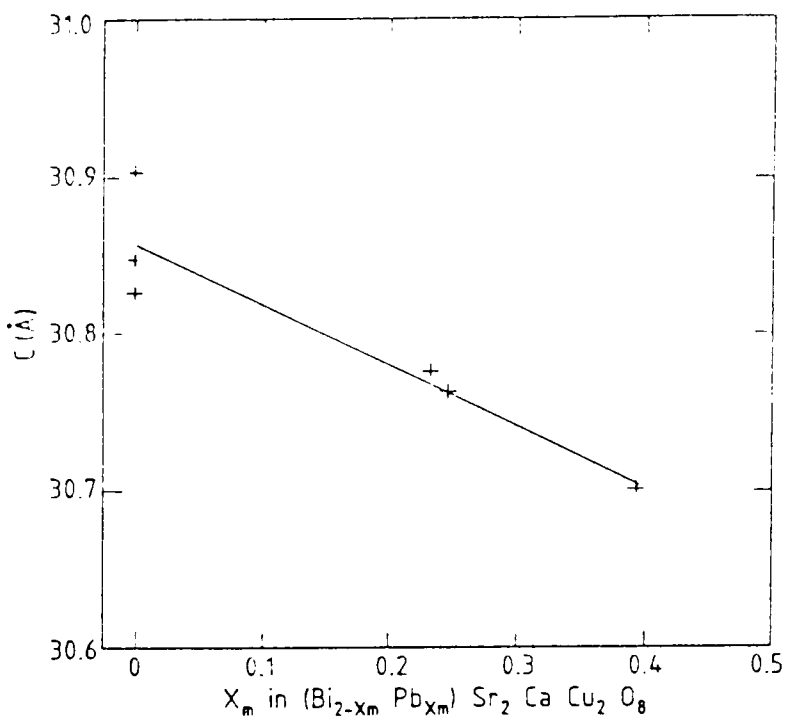

Figure 1.10 Evolution of the c parameter with x_m in single crystals of the Pb containing Bi-2212 phase. (After [92])

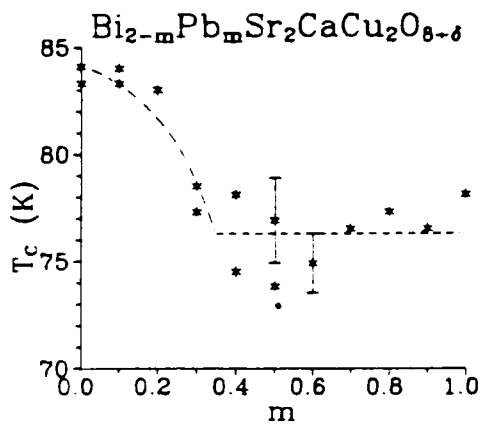

Figure 1.11 T_c of the $Bi_{2-m}Pb_mSr_2CaCu_2O_{8+\delta}$ samples as a function of m. The dashed line is only a guide to the eye. (After [91])

CHAPTER 2

Thin film processing of high T_c superconductors

2.1. Introduction

Since the discovery of high T_c superconductors a great deal of effort world-wide has been put into the development of thin-film technologies. There are many motivations for this intense activity: not only do thin films have superior properties to bulk materials, but they are also required for the success of most device applications. But, producing film for electronics applications must take many factors into consideration, some of which are compositional homogeneity, surface quality, large area deposition, substrate compatibility, etc. The difficulties apparent in the deposition of high T_c materials are related to the fact that they are complex, multicomponent materials, with a delicate sensitivity to film composition that significantly influences the electrical properties of the films.

This chapter briefly reviews processing of high T_c superconducting thin films. The common thin film deposition techniques such as sputtering, laser ablation, evaporation and chemical vapour deposition for controlled deposition of the high T_c superconducting thin films are described and the influence of the processing conditions on the thin film properties summarised for Bi-based superconductors.

2.2. Growth techniques

The processes for growth of thin films of high temperature superconducting compounds generally fall into one of two categories: (a) deposition of the required stoichiometry of metal atoms followed by a high-temperature ex-situ anneal, where the superconducting phase is formed, or (b) in-situ growth of the film crystallised during deposition, usually occurring at a substantially lower temperature.

In preparing films by ex-situ annealing the metallic elements are deposited in approximately the correct composition as an amorphous layer. If they are on a suitable substrate, subsequent annealing in air or partial oxygen pressure at high temperature (about 850^{o}C) will lead to the film crystallising by a solid state regrowth mechanism to form a polycrystalline but locally epitaxial layer. Since the crucial growth step takes place long after deposition, the actual technique used to deposit the layer is of only secondary importance. A very large number of groups have reported ex-situ annealed thin films, and nearly all the known high T_c superconductors have been made in this way. An early detailed description of an ex-situ processes is given by Naito et al. [1].

In in-situ growth the film is deposited in crystalline form and, although it may need some low-temperature annealing to achieve the correct oxygen stoichiometry (especially for YBaCuO films), it requires no substantial rearrangement of the lattice after growth. This has a number of advantages. In particular, the lower temperatures involved minimise contamination from the substrate, single-crystal films can be grown with greatly improved physical properties, and the film surface can be smooth. It also offers reduced processing time and the possibility of growth of multilayers. For many electronic applications it is likely that such in-situ growth will be preferred, especially for layered device structures and for compatibility with other materials processes.

The high-order layer compounds of the Bi-Sr-Ca-Cu-O and Tl-Ba-Ca-Cu-O families have so far proved very difficult to make by in-situ techniques and most of the reported films with $T_c > 100$K [2] have been made by careful ex-situ annealing, while the most widely studied YBaCuO is mainly made by in-situ methods.

2.2.1. Deposition techniques

Three physical vapour deposition techniques (PVD) have been widely used for thin film growth. These are sputtering, laser ablation and evaporation including molecular beam epitaxy (MBE). In addition, chemical vapour deposition (CVD) techniques with thermal and/or plasma assisted decomposition of the precursors have recently become more popular. The different techniques can be divided into three groups: deposition from a single source, simultaneous deposition from multiple sources and sequential deposition from multiple sources.

When choosing a deposition technique the stability and purity of the source materials should be taken into consideration. In some cases the pure metals, for example Ba, Sr and Ca, oxidise or hydrolyse easily. This is why metal alloys are preferred to pure metals for sputter processes, but even better are sintered metal-oxides.

Each of these techniques will be described in more detail in this review followed by its recent achievements. A general comparison of the technological achievements and limitations is also presented.

2.2.1.1. Sputtering

Planar magnetron [3] or ion beam [4] sputter deposition techniques(PMS/IBS) constituted some of the first approaches to depositing thin superconducting films. The principle of sputtering is based on the production of atomic or ionic species from a target material as a consequence of bombardment by high energy particles, usually ions of inert gases such as Ar^+. The argon ions are either produced in a separate ion source (IBS), or in a magnetron-driven discharge (PMS) formed in front of the target plate and accelerated towards the target held at a large negative potential. The PMS technique, which is the technique used in this study for the deposition of films, will be described in detail in the next chapter.

Even though the principle of sputtering is well understood, almost every research team uses their own deposition parameters which are somewhat different from each other.

This indicates that the properties of the films are quite sensitive to the deposition parameters of PMS. Almost all variables are varied, such as deposition mode (RF or DC) [5] gas composition (reactive or nonreactive) [6,7], substrate position (on-axis, off-axis) [8,9], and common process parameters (power, substrate temperature, gas pressure etc.). However, the control of the "global" parameters alone does not lead to a stable and reproducible deposition of high T_c superconductors. Major problems of this technique are spatial inhomogeneities and instabilities of the plasma which lead to inhomogeneous film deposition.

The main problem in the sputtering process is that in most cases it suffers from non-stoichiometric transfer of the elements from the target to the substrate in traditional geometry, where the substrate faces the target for maximum deposition rate. It has been most pronounced for YBaCuO that negative oxygen ions produced in the sputtering plasma cause a backsputtering effect on the substrate that etches the growing film, depleting it of some elements (Cu, Ba) more than others [5, 8] The same effect in BSCCO for the loss of bismuth, when deposited on a hot substrate (700^{o}C), was first reported by Grace et al. [7]. To avoid this problem possible solutions are (1) off-axis sputtering [10], where the substrates do not face the target, (2) placing the substrates facing the target but away from it [8], (3) adjusting the target composition to compensate the losses of certain elements [3], (4) utilising a multi-source set-up with adjusted sputtering rates [11], (5) applying very low or no oxygen partial pressures in the process gas [12, 13], (6) using separate gas feeds (Ar to target, and O_2 to substrate [14]), (7) DC sputtering at very high pressures [13, 15] (8) utilising an unbalanced magnetic field configuration [16].

The choice of deposition mode (RF or DC) depends on whether the target is a conductor or not, because DC sputtering needs a conducting target with a significant oxygen partial pressure during the sputtering process to keep the target sufficiently conductive. In RF sputtering the non-stoichiometric transfer of the elements from the target to the thin film can be compensated by adjusting the target composition and process pressure, and oxygen is not essential in the process gas.

All research groups have produced high-quality superconducting thin films, so there is no obvious preference of one technique over the other, especially when every process usually includes several ways to optimise it. Therefore, it is important to know how the individual process parameters interact with each other, and which are more sensitive than others. In general comparison, it can be said that off-axis techniques are more tolerant to process parameter changes [17], whereas most on axis sputtering techniques are especially sensitive to gas pressure.

2.2.1.2. Evaporation

The basic principle of co-evaporation techniques involves the simultaneous and continuous evaporation of two or more metallic components (usually one source for each element in the film except oxygen) for the high T_c film in an atmosphere of oxygen and/or other reactive gases, resulting in reactive evaporation (RE). In basic RE, the individual elements stemming from the evaporation sources reach the substrate with an arrival energy typically 0.5eV. The low incident energy of the evaporated atoms means that the substrate temperature is very important in controlling the microstructure of the deposited film. In many instances the reactivity of the gas is too low (or the necessary substrate temperature is too high), requiring additional activation (e,g., in a plasma),and this process is described as activated reactive evaporation (ARE). Most commonly used evaporation sources are resistance-heated or electron-beam evaporators.

A major benefit of the multi-source co-evaporation technique (e.g. RE/ARE) is the independence of each evaporation source, allowing individual control of the deposition rate of each component. This allows compensation of possible compositional drift from the required stoichiometry. Usually, the evaporation rate of each source is measured in-situ by quartz crystal rate monitors. It has been found that this technique is capable of keeping the composition of the film within 1%, reproducible from run to run within 3% [18].

Improvements in controlling and enhancing the film formation (particularly oxidation of the film near the substrate) were achieved by using an ARE system, resulting in a reduced

deposition temperature and better large area film homogeneity [19]. Bi and Cu are evaporated as pure elements; CaF_2 and SrF_2 are often used due to the high affinity to oxygen and water vapour when the Ca and Sr sources are pure metals. Fluorine has to be eliminated from the film by annealing in a wet atmosphere [20].

Another technique related to co-evaporation is flash evaporation in which material from a single source is evaporated instantly, and that process is repeated until the desired film thickness is deposited. The chemical and metallurgical quality of the material to be evaporated greatly influences the deposited film quality, due to factors such as purity and outgassing [21].

2.2.1.3. Molecular beam epitaxy (MBE)

Molecular beam epitaxy (MBE) is in several respects similar to the co-evaporation techniques described above, except that the deposition is carried out mostly sequentially rather than simultaneously. A distinct characteristic of MBE is the extremely low background pressure ($1.0x10^{-8}$ Torr) that allows the application of reflective high-energy electron diffraction (RHEED)analysis during growth. The individual components that form the film are evaporated from separate sources. In most instances, activated oxygen or ozone is applied to the substrate to compensate for the low reactive gas pressure permitted [22].

With the possibility of using MBE to form films of precisely controllable atomic layers and without any macroparticles, it is an excellent research tool for investigating problems of interface formation, nucleation, and film growth phenomena. MBE has proven to be very viable for the deposition of multilayer films of only a few unit cells thickness, as required for active device fabrication[22]. Another approach for producing complex superconducting films with the aid of MBE is the multilayers technique, where the individual components or suitable compounds of these are deposited separately and sequentially to form a structure of thin layers that forms the desired homogeneous composition by diffusion in a post-anneal [24]. To facilitate a thorough interdiffusion during annealing to form the superconducting phase, it is necessary that the film thickness for each individual component be sufficiently

small (10-240nm at deposition rate below 0.3nm/s). Low deposition rates are essential to ensure formation of a homogeneous and defect-free film and film thickness ratios for the individual components determine the composition of the film after annealing.

2.2.1.4. Laser ablation

In this technique a high energy laser beam enters the vacuum chamber through a window and is focused on to a target of material to be deposited. The target material vaporised by the laser beam is deposited from the gas phase on to the substrate. The vapour pressures of the different constituents are very different, but the material is transported from the target to the substrate as a cluster of the composite oxides. The emission of large "molecules" (as a cluster) gives an excellent stoichiometry match between target and film, when a single composite target is used with reactive oxygen [25].

The process works in high vacuum as well as in oxygen ambients. A wide variety of lasers of different wavelength are used such as Nd:YAG, CO_2, and excimer lasers (UV) [26]. Nevertheless the excimer laser is considered to be the most suitable laser for the deposition of oxide thin films, due to the short wavelength which, together with short pulse width, produce the best film quality [27].

Epitaxial Bi-2212 films have been grown by Zhu et al. [28] on MgO (001) which have $T_c = 71K$, with $J_c \approx 8x10^5 A/cm^2$ at 50K and $J_c \approx 5x10^6 A/cm^2$ at 4.2K, from a rotating stoichiometric Bi-2212 target with entirely in-situ processing. Multiple target pulsed laser deposition techniques for sequential atomic layer-by-layer deposition have been successfully used by Tabata et al. [29] to investigate substitutions in the BSCCO system.

Some disadvantages of this technique are (1) occasional ejection of molten droplets or semi-molten particulates, which are generated during the local melting of the target by the laser beam, leading to a rough film surface, (2) inability for large area deposition due to the geometrical constriction of the plasma to a small substrate area. However, looking at the complex composition of superconductors and the requirements of exact stoichiometry

regarding the metal components, and high deposition rate, it is a very successful method of depositing thin films of high T_c superconductors.

2.2.1.5. Chemical vapour deposition (CVD)

Chemical vapour deposition (CVD) techniques are widely used as thin film deposition processes and are reasonably economic because they do not require a high vacuum. CVD permits easy alteration of the chemical components. The major advantages are primarily the ability to deposit films homogeneously over large areas having complex shapes, and the capability for large-scale production.

Most CVD processes employ evaporation sources containing the respective precursors, located outside the deposition chamber, with consecutive mixing of the vapours (with or without additional carrier gas). The volatile precursor gases are passed over a heated substrate where they decompose and interact on the substrate surface to form the desired superconducting phase. The substrate is usually heated to provide adequate reaction energy.

Metalorganic (MO) CVD is by far the most widely used technique. Recently, Endo et. al. succeeded in preparing single phase epitaxial films of BSCCO (2223) on $LaAlO_3$ substrates by MOCVD, without post annealing, which have a high critical current density of $\approx 10^5$ A/cm^2 at 77.3K in a magnetic field of 8T [30]. Later, a plasma enhanced metalorganic chemical vapour deposition (PE-MOCVD) process, which substitutes kinetic energy for conventional thermal energy and consequently facilitates low-temperature deposition, has been developed for fabrication of high T_c superconducting oxide films at a greatly reduced temperature [31].

2.2.1.6. Other deposition techniques

The RF plasma deposition process at atmospheric pressure has been successfully used and shown that Bi-2223 thin films with critical temperatures of >100K and critical

current densities of $1x10^5 A/cm^2$ at 77K and zero field can be made in-situ at atmospheric pressure on single crystal MgO (100) [32].

A thermal decomposition method using an organic acid salt is a relatively simple chemical one, and the method is suitable for making larger area and homogeneous films [33].

Another simple and low cost chemical technique is spray pyrolysis. In this technique, a solution is sprayed on a substrate, and then annealed. The process may be repeated several times to build up the film thickness. Other advantages of the technique are that the film is homogeneous, stoichiometric and can produce oriented films [34].

Several attempts have been made to prepare mostly Bi-2212 thin films by liquid phase epitaxy (LPE) using KCl as a flux, and epitaxial films have been successfully grown on several kinds of substrate [35].

The electrodeposition process, which consists of simultaneously depositing the metallic constituents of the superconductor from a single electrolyte, and thermally oxidising the resulting precursor film to form the superconducting phase, has been also developed for the production of superconducting films [36].

Recently, a new, simple fabrication technique for thin-film superconductors by bulk processing has been developed. Approximately 0.3μm thick films of BSCCO, highly textured and weak-link free, have been obtained by heavy cold rolling and partial meltprocessing on a silver substrate ($J_c \approx 10^4$-$10^5 A/cm^2$ at 4.2K-20K, in magnetic fields up to 5T). This technique, which does not require epitaxial growth on single-crystal substrates, may be suitable for high-speed, low-cost production of large area thin films [37].

2.2.2. Comparison of process characteristics

A comparative evaluation of the potential of the deposition techniques is given recently in review paper by Stoessel et al. [38]. It is very difficult to compare process characteristics when we consider the large number of different techniques and the fact that almost all research group use their own modified specific process. All the techniques

mentioned above are able to produce films with quite comparable quality in respect of superconducting properties (critical temperatures and current densities). This illustrates that the critical parameters of the produced thin film depend on the material used rather than on the deposition technique. Nevertheless, there are some other characteristics which can be related to the deposition techniques, such as control of film stoichiometry, film surface quality, large-area coverage and deposition rate; they are summarised in **Table 2.1**.

Single target sputtering, laser ablation, and single source CVD techniques which use a precursor of a fixed composition reducing the number of process variables, can more reliably allow control of the composition and achieve exact stoichiometry. Plasma-assisted reactive evaporation as well as CVD are good at large-area coverage, followed by the sputtering technique. Molecular beam epitaxy (MBE) exceeds the others in exact structural control over the film growth. When we want to compare films in respect of surface quality, which is essential for device application, sputtering, reactive evaporation, MBE and CVD show good performance if the stoichiometry of the metal components can be kept in a close enough range to avoid "copper lumps". Laser ablation and flash evaporation usually emit molten matter that is incorporated into the film if no filtering techniques are applied, However, an in-situ post anneal with its accompanying phase transformation greatly affects the final surface quality of the film.

Although thin films are produced using each of these techniques, magnetron sputtering using a single composite target has become more popular due to its simplicity, the deposition mechanism being relatively complicated in a multi-element oxide target.

2.3. Substrates

The ideal substrate for high T_c superconductors would be chemically non-contaminating, a good lattice and thermal expansion match to the film, cheap large-size single crystals, have low dielectric constant and loss, and be easily cut and polished. Ideally, it would also be a material in which integrated circuits can be made, but the list of these is rather short!

When depositing superconducting films on crystalline substrates, it has been observed that c-axis oriented films form easily (with or without buffer layers), but due to twinning with a random distribution of *a* and *b* axes, multiple weak links form at high-angle grain boundaries within the film and reduce the critical current density by several orders of magnitude. Therefore, epitaxial films with high perfection are crucial to achieve optimum properties in thin film high T_c superconductors, because all high T_c superconductors have very anisotropic properties with the superconducting current flowing almost entirely along the CuO_2 planes perpendicular to the c-axis. A crystal substrate plays an important role in epitaxial growth. It has already been found that epitaxial growth of thin films is possible even if the misfit between the lattice constants of substrate and film is considerable, as in the case of MgO [39].

The most widely and successfully used substrates for all the high T_c superconductors are $LaAlO_3$ and $SrTiO_3$. Unfortunately, $SrTiO_3$ is only available in small sizes, is expensive and often strained. Still worse, it is nearly ferroelectric and both its dielectric constant and loss are very large [40]. The best candidate so far is $LaAlO_3$ for microwave applications and it is available in large sizes, 3 inch diameter. The next most widely used is MgO, which is relatively inert, and a poorer lattice match to the a-b plane of the high T_c phases but nevertheless can give excellent films with a suitably optimised process. It has a dielectric constant suitable for high-frequency applications, an acceptably low loss and is much cheaper than $SrTiO_3$ and $LaAlO_3$. It is not at present available in very large sizes. The ideal materials from these points of view are Si or Al_2O_3. These have proved much more difficult to grow good material on, but steady progress is being made with both oriented growth on Al_2O_3 and epitaxial growth on buffer layers on Si [41]. Since there is a strong requirement regarding dielectric loss and dielectric constant for high frequency applications recently attention has focused on $NdGaO_3$, $CaNdAlO_4$, $LaGaO_3$, $LaSrGaO_4$ and $LaSrAlO_4$, etc. These appear to have a number of desirable properties with small misfit lattice constant if they can be grown reproducibly and cheaply in large sizes. A material which is cheap and available in large sizes, although with rather complicated

dielectric properties, is $LiNbO_3$ and it is worth noting that films of reasonably good quality have been grown epitaxially on this material [42]. In **Table 2.2**. some of the most popular single crystal substrate materials and their properties are listed. Comparing *a,b*-axis lattice constants with that of BSCCO material in **Table 2.3**. shows that *a,b*-axis crystal parameters do not match very well. The percentage mismatch between Bi-based superconductors and substrates at typical temperatures for epitaxial growth (~850^{o}C) is summarised in **Table 2.4**. However, in their favour, most of these substrate materials have very high melting points, and some are also inert to the highly oxidising high T_c superconductors

Attempts to deposit superconducting BSCCO films on Au and Pt substrates have so far been unsuccessful. In regard to potential substrates, metallic Ag appears to be unique because of its excellent compatibility with the high T_c materials, excellent electrical and thermal conductivity, and good bonding properties. Thin superconducting BSCCO films have recently been deposited on Ag substrates by sputtering and organometallic chemical vapour deposition (onset transition at ≈80K, estimated $J_c \approx 3.9 \times 10^5 A/cm^2$ at 5.5K) [43]. Another alternative in finding a suitable substrate for high T_c films might be to use as a substrate one of the related non-superconducting compounds in the same series as the high T_c superconductor [44].

2.4. Effect of the processing conditions on film properties

There are several technical difficulties in depositing high T_c films that have to be addressed regardless of the deposition technique used. The most important one is to get the exact stoichiometry of the film. If the composition of the film is strongly influenced by growth conditions, proper studies of film characteristics as a function of one growth variable are difficult, if not impossible. Off-stoichiometric metallic compositions not only affect superconducting properties of the film but also cause a rough surface morphology.

In the following sections the different parameters are discussed which affect the properties of the Bi-based superconducting thin films, mainly relevant to the sputtering

deposition technique, viz. substrate temperature, annealing for ex-situ process, substrate etc..

2.4.1. Low temperature processing

The exact mechanism by which in-situ crystallisation occurs at significantly low temperature (≈150^{o}C below a typical post-annealing temperature) is not yet well understood, but it is attributed to the idea that substrate heating during film deposition provides energy and atomic mobility to the absorbed surface atoms and molecules, and that the energy required for surface diffusion is much smaller than that for bulk diffusion. Thus the possibility exists that increases in surface energy relative to the underlying film could promote crystal growth at even lower substrate temperatures [45]

In the in-situ process, control of the substrate temperature, Ts, during deposition has been found to be a critical parameter together with deposition rate [46, 47] in affecting the phase formation, initial stoichiometry, initial distribution of the species, the incorporation of oxygen into the film, film orientation and morphology.

Bismuth loss has been a problem in sputtered BSCCO films [45, 48] with increasing substrate temperature, Ts, without a similar loss of Sr, Ca, or Cu. Initially it was not clear that the Bi loss is caused by a resputtering mechanism rather than by its significantly higher volatility compared to the other cations in BSCCO, or possibly a thermaly aggravated resputtering phenomenon. Grace et. al. [7] definitely established that the preferential bismuth loss is a result of resputtering and not a thermal effect. Therefore, Bi-enriched targets have been widely used under relatively high pressure ($4x10^{-1}$mbar) [47] to compensate for possible Bi loss at high Ts.

Although the film surface is very smooth and uniform, some small white second phase particles with a dimension of about 0.2 μm diameter are usually observed even for an optimised substrate temperature. The presence of the these second phase particles on the film surface introduces some roughness to the surface since they are observed to grow out of the smooth matrix.

For the in-situ process the maximum processing temperatures are in the region of 600-800^{o}C depending on sputtering conditions and measurement differences. Immediately after the deposition at high temperature, a soak process for a short time and cooling of the samples under high oxygen pressure (about 1 atm.) have been usually found essential to incorporate enough oxygen into the film structure.

The zero resistivity temperature of the as-grown film with a Bi-2212 phase can reach the same value as for the 80K bulk samples, and critical current density values in the as-grown Bi-2212 films are much higher than those of the ex-situ post annealed films. **Table 2.5** provides a summary of some selected reports on "in-situ" or as-grown Bi-based superconducting thin films prepared by sputtering [47, 49-56].

However, the critical values for the Bi-2223 phase are still lower than that of the 110K bulk samples, even if the X-ray diffraction (XRD) pattern shows c-axis oriented pure single Bi-2223 phase with a very narrow diffraction profile [57]. As yet no group has reported any high quality films by the in-situ process except for Endo et. al. [30] (mentioned before in section 2.2.1.5. with the MOCVD technique). To date Bi-2223 films have always required a high temperature ex-situ anneal to give good superconducting properties with $T_c > 100K$ and $J_c > 10^6 A/cm^2$ at 77K. This contrast with Bi-2212 phase implies that with the increasing c-dimension the ordering of cations and oxygen in the crystal lattice of the BSCCO system becomes more difficult during deposition, mainly due to the lack of Pb in the as-grown film composition.

2.4.2. High temperature processing

Thin films consisting of predominantly Bi-2223 phase have been prepared by high temperature (840-870^{o}C) post annealing of Bi-based thin films deposited on heated or unheated substrates. Itozaki et al. [58, 59] have studied the crystallisation of thin films having a nominal composition Bi:Sr:Ca:Cu = 2:2:2:3, as a function of the substrate temperature and the post-annealing temperature. **Fig. 2.1** shows the diagram of the crystallinity as a function of substrate and post annealing temperatures. The 110K

$Bi_2Sr_2Ca_2Cu_3O_x$ phase was found to nucleate only in a narrow range of substrate temperatures around 700°C. T_c of the film deposited at substrate temperature of 700°C increased from an initial value of 40K to 95K as the post annealing temperature was increased to 890°C. They have prepared single phase Bi-2223 thin films on MgO single crystals by this process. One of their films was found to have a critical current density, J_c of $1.9x10^6$ A/cm^2 at 77K and $2.1x10^7$ A/cm^2 at 40K. Another film showed a J_c of $3.4x10^6$ A/cm^2 at 77K. However, J_c decreased to $2.6x10^5$ A/cm^2 at 77K in a magnetic field of 0.5T. They have also reported that Pb addition is not as essential in the growth of Bi-2223 thin films as it is in the bulk materials. However, the preparation procedure by partial substitution of Pb for Bi has currently been found to be effective in obtaining Bi-2223 phase superconductors under lower temperatures during the post annealing. Thus, many investigators have attempted to incorporate Pb into the structure of the superconducting phase in some way. Mostly, doping of Pb into the film has been carried out by annealing the film with Pb doped BSCCO bulk material placed in different positions with respect to the film. Putting the film facing down on the bulk pellet has been found effective for the desired Pb diffusion in to the film, but it gave rise to roughness on the film surface [60]. In order to minimise evaporation of the Pb and to obtain effective doping, films have also been annealed in a closed novel metal capsule or Al_2O_3 box with bulk material [61, 62]. This doping process usually needed long time annealing of 15 hours or more. As a Pb source, the uncalcined BSCCO bulk material has also been found to be better in controlling the Pb potential than those calcined [60]. The other way of Pb doping is to load a large amount of Pb (the optimum molar ratio of Pb is around 2) during deposition at low temperature by using a Pb-rich or separate PbO [63] target. Because of the much larger surface/volume ratio in films than in bulk materials, Pb evaporated readily from the film during sintering. This process can reduce the annealing time to 1 hour or less.

Hakuraku and Mori [2] have concluded that it was very difficult to deposit the as-grown Bi-2223 thin films having zero resistivity above 90K in their recently puplished report. However, they succeeded in reaching zero resistivity at 105K with critical current density of

about $3x10^6$ A/cm^2 at 77K by annealing the as-grown film together with a Pb doped sintered bulk BSCCO pellet at 840^{o}C for 30 seconds in air. The critical current density of the as-grown film deposited at 724^{o}C was $8x10^4$ A/cm^2 at 77K with zero resistivity at 83K. They have observed a decrease of c-axis lattice constant from 37.26 to 37.17 A^o after annealing. Finally X-ray photoelectron spectroscopy measurements on as-grown and annealed films showed that the valence of the Cu is increased by Pb doping (i.e., hole creation), and so they concluded that the change in hole concentration is responsible for the increase in T_c. Surface smoothness did not change except for an increase of 0.2μm in size of rocklike crystals of Bi-2223 phase scattered on the smooth surface.

Dew and co-workers [64] have deposited films doped with Pb by single target magnetron sputtering on unheated MgO substrates and have found that there is considerably higher Pb loss during post-annealing treatment of thin films than bulk materials. Hence they enriched their targets in Pb and succeeded in obtaining T_c of 106K. A rich Pb doped target (Pb/Bi≥1) has also been used by Kula et al. [65] who deposited the film on different substrates heated to 150^{o}C and annealed for 1 hour in air at 870^{o}C. They recognised that the critical temperature is lower for the Bi-2223 films grown on epitaxial $CaNdAlO_4$ and $SrTiO_3$ substrates (T_c = 99K for $SrTiO_3$, 104K for $CaNdAlO_4$ and 106K for MgO). **Table 2.6** gives a summary of typical experimental results published by other groups, including processing conditions [60, 61, 63, 65-71].

2.5. Film characterisation and properties.

There are several aspects of a superconducting thin film which need to be known as a matter of routine. These are metallic element composition, structure and electrical properties.

2.5.1. Composition determination

The most widely used methods for determining film composition are EDX (energy dispersive X-ray spectrometry), WDX (wavelength dispersive X-ray spectrometry),

inductively coupled plasma (ICP) spectroscopy and Rutherford backscattering spectroscopy (RBS). These are sufficiently fast turnaround techniques to be used on a substantial fraction of the total number of films produced by a process. Except for ICP they are also non-destructive and fairly accurate. Although ICP is a very sensitive technique with good accuracy, the sample is lost because it has to be dissolved for the analysis. EDX and WDX are simply different methods of measuring the wavelengths and intensities of X-rays generated by the electron probe hitting a sample. EDX and WDX are relative techniques and require calibrating with standards, but they are reproducible to higher accuracy than RBS. They can only obtain reproducible results on films with smooth surfaces so routine characterisation of films deposited at low temperature must be done prior to any high temperature annealing. Inevitably, there is some uncertainty about the validity of the absolute calibration of composition: there are many fine effects which could contribute a systematic error of a percent. However, a good test of the correct composition is that it makes a good superconductor. Although not conclusive, the correspondence between the composition and the other properties suggests that the systematic errors of EDX and WDX measurement are small.

RBS has also been widely used for composition analysis. This has the advantage of being capable of giving a depth profile of the composition but being slightly less accurate for the mean film composition than EDX and WDX . The most accurate results are obtained from very thin films (below a few hundred A^{O}) and using high particle energies to obtain separate peaks from the metallic elements, with a corresponding improvement in accuracy [72]. RBS is also widely used to give information on structural quality through channelling measurements [73] which yield quickly and easily information which is difficult to obtain in any other way. The results from electron probe microanalysis (EPMA) and RBS have been compared for BSCCO thin films by Dhere et al. [74].

2.5.2. Structure determination

A high degree of c-axis orientation is of great importance due to the highly anisotropic physical properties of BSCCO materials that are associated with the two-dimensional character of CuO based superconductors. There is ample evidence that the in-plane critical current density increases with an increasing degree of *c*-axis orientation.

The structural assessment routinely done by most groups is limited to X-ray diffraction in the Bragg-Brentano geometry in which the diffracting planes are those parallel to the substrate surface. This gives information about the preferred crystallographic orientation of the films normal to the substrate and lattice parameters in this direction, but it does not demonstrate epitaxy. It is quite common in the literature to find claims that a film is highly textured on the basis of some quite modest enhancement of the intensity of the 00l diffraction peaks. Depending on the geometry of the diffractometer, in a randomly orientated powder only about one grain in 10^3-10^4 contributes to a particular diffraction peak. The rest are incorrectly orientated. In orientated material much of the sample contributes, depending on the diffractometer resolution compared to the rocking curve width. Aligned material thus gives much stronger diffraction peaks than powder and the signature of well aligned material is that the strongest powder lines which do not lie in the texture of the film are not observable.

To prove an epitaxial relationship between the layer and the substrate, it is necessary to investigate the orientation of the crystallographic axes in the layer plane with respect to the axes of the substrate. This can be done using transmission electron microscopy (TEM), reflection high energy electron diffraction (RHEED), glancing incidence X-ray diffraction [75] or diffraction off planes tilted with respect to the substrate [76]. TEM gives a wealth of detailed information. RHEED is unique in that it permits structural assessment during growth, and is an invaluable aid to controlling and understanding the growth process.

2.5.3. Transport measurements

The essential characteristics of superconductors are electrical so it is obviously necessary to characterise the material electrically. There are many different measurement which have been made, but it is not possible to review all of them. The most obvious and widely measured parameters are resistivity and critical current density measured by transport techniques e.g. by the standard four-point probe technique. This requires a means of contacting the sample and most workers use sputtered or evaporated Ag or Au, with some extra heat treatment if a particularly low contact resistance and good adhesion are required [77]. The very low contact resistances which can be obtained may be related to the proximity effect, which has now been reported [78] for noble metal-high T_c superconductor contacts at low temperatures.

The DC critical current density J_c of thin films has become widely adopted as a figure of merit for material quality. It is not clear that the most perfect films will have the highest J_c, or that they will be most useful in applications. Nevertheless there is some connection between material quality and critical current density, and it is a quantity which is easy to measure.

In order to make quantitative measurements it is necessary to pattern the films into structures with a defined geometry by using standard lithography with either wet etching or ion milling. Wet chemical etching and reactive ion etching are not considered optimum for making superconducting structures. Instead, physical removal of material by argon ion milling is used to sputter the structures [79].

The most sensitive magnetic measurements, on both thin films and bulk material, are performed using a SQUID magnetometer, an instrument that is itself an interesting commercial application of superconductors. The magnetisation curves of the materials themselves show large hysteresis, which gives detailed information on flux pinning in the superconducting state [80]. With the aid of relatively simple models the hysteresis can be interpreted in terms of the critical current, so allowing a contactless method of measuring J_c.

For routine characterisation of thin films, the inductive surface coil technique has been mostly used to measure the transition temperature, critical current and to have additional information of the presence of secondary phases in the film. The strength of the shielding currents in the film give a better indication of the amount of superconducting phases in the film than a standard four point probe measurement.

References

1 M. Naito, R.H. Hammond, B. Oh, M.R. Hahn, J.W.P. Hsu, P. Rosenthal, A.F. Marshall, M.R. Beasley, T.H. Geballe, and A. Kapitulnik, Mater. Res. 2 (1987) 713.

2 Y. Hakuraku and Z. Mori, J. Appl. Phys. 73 (1993) 309.

3 K. Setsune, T. Kamada, H. Adachi, and K. Wasa, J. Appl. Phys. 65 (1988) 1318.

4 J. Gao, Y.Z. Zhang, B.R. Zhao, P. Out, C.W. Yuan, and L.Li, Appl. Phys. Lett. 53, (1988) 2675.

5 M. Migliuolo, R.M. Belan, and J.A. Brewer, *Proc.3rd Annual conf. on High-Temperature Superconductivity*, Genova, 13 Feb. 1990.

6 Z. Qi, W. Shi, J. Sun, H. Ke, and L. Liu, J. Phys. D Appl. Phys. 21 (1988) 1040.

7 J.M. Grace, D.B. McDonald, M.T. Reiten, J. Olson, R.T. Kampwirth, and K.E. Gray, J. Appl. Phys. 70 (1991) 3867.

8 T.I. Selinder, G. Larsson, U. Helmersson, and S. Rudner, Supercond. Sci. Technol. 4 (1991) 379.

9 O. Nakamura, E.E. Fullerton, J. Guimpel, and I.K. Schuller, Appl. Phys. Lett. 60 (1992) 120.

10 J. Gao, B. Hauser, and H. Rogalla, J. Appl. Phys. 67 (1990) 2512.

11 V. Matijasevic, R.H. Hammond, P. Rosenthal, K. Shinohara, A.F. Marshall, and M.R. Beasley, Supercond. Sci. Technol. 4 (1991) 376.

12 M. Migliuolo, A.K. Stamper, D.W. Greve, and T.E. Schlesinger, Appl. Phys. Lett. 54 (1989) 859.

13 C. Blue and P. Boolchand, Appl. Phys. Lett. 58 (1991) 2036.

14 G.C. Xiong, and S.Z. Wang, Appl. Phys. Lett. 55 (1989) 902.

15 P. Prieto, M.E. Gomez, L.F. Castro, H. Soltner, U. Poppe, W. Sybertz, and A. Lubig, Surface Science 251/252 (1991) 712.

16 N. Savvides, and A. Katsaros, Appl. Phys. Lett. 62 (1993) 528.

17 C.B. Eom, J.Z. Sun, K. Yamamoto, A.F. Marshall, K.E. Luther, and T.H. Geballe, Appl. Phys. Lett. 55 (1989) 595.

18 F. Baudenbacher, K. Hirata, P. Berberich, H. Kinder, W. Assmann, and H.P. Lang, Physica C 185 (1991) 2177.

19 D. Zhang, D.V. Plant, H.R. Fetterman, K. Chou, S. Prakash, C.V. Deshprandey, and R.F. Bunshah, Appl. Phys. Lett. 58 (1991) 1560.

20 M. Mukaida, K. Kuroda, and S. Miyazawa, Appl. Phys. Lett. 55 (1989) 1129.

21 M.S. Osofsky, P. Lubitz, M.Z. Harford, A.K. Singh, S.B. Qadri, E.F. Skelton, W.T. Elam, R.J. Soulen, Jr., W.L. Lechter, and S.A. Wolf, Appl. Phys. Lett. 53 (1988) 1663.

22 J.N. Eckstein, I. Bozovic, K.E. von Dessonneck, D.G. Schlom, J.S. Harris, Jr., and S.M. Baumann, Appl. Phys. Lett. 57 (1990) 931.

23 R.H. Ono, MRS Bull. 8 (1992) 34.

24 M. Kanai, T. Kawai, and S. Kawai, Jpn. J. Appl. Phys. 31 (1992) L331.

25 S. Komuro, Y. Aoyagi, T. Morikawa,and S. Namba, Jpn. J. Appl. Phys. 27 (1988) L34.

26 J. Cheung and J. Horwitz, MRS Bull. 17 (1992) 30.

27 G. Koran, A. Gupta, R.J. Baserman, M.I. Lutchye, and R.B. Laibowitz, Appl. Phys. Lett. 55 (1989) 2450.

28 S. Zhu, D.H. Lowndes, B.C. Chakoumakos, J.D. Budai, D.K. Christen, X.-Y. Zheng, E. Jones, B. Warmack. Appl. Phys. Lett. 63 (1993) 409.

29 H. Tabata, O. Murata, T. Kawai, and S. Kawai, Appl. Phys. Lett. 56 (1990) 1576.

30 K. Endo, H. Yamasaki, S. Misawa, S. Yoshida, and K. Kajimura, Nature 355 (1992) 327.

31 J. Zhao, D.W. Noh, C. Chern, Y.Q. Li, P. Norris, B. Gallois, and B. Kear, Appl. Phys. Lett. 56 (1990) 2342.

32 A. Shah, S. Patel, E. Narumi, and D.T. Shaw, Appl. Phys. Lett. 62 (1993) 2422.

33 T. Murayama and S. Higashi, Jpn. J. Appl. Phys. 28 (1989) 624.

34 H. Nobumasa, K. Shimizu, Y. Kitano, and T. Kawai, Jpn. J. Appl. Phys. 27 (1988) 1669.

35 G. Balestrino, M. Marinelli, E. Milani, and A. Paoletti, J. Appl. Phys. 73 (1993) 3903.

36 M. Maxfield, H. Eckhardt, Z. Iqbal, F. Reidinger, and R.H. Baughman, Appl. Phys. Lett. 54 (1989) 1932.

37 T.H. Tiefel, S. Jin. G.W. Kammlott, J.E. Graebner, and R.B. van Dover, Appl. Phys. Lett. 58 (1991) 1917.

38 C.H. Stoessel, R.F. Bunshah, S. Prakash, and H.R. Fetterman, Journal of Superconductivity 6 (1993) 1.

39 T. Sugimoto, M. Yoshida, K. Yamaguchi, K. Sugawara, Y. Shiohara, and S. Tanaka, Appl. Phys. Lett. 57 (1990) 928.

40 T. Sakudo and H. Unoki, Phys. Rev. Lett. 26 (1971) 851.

41 X.D. Wu, A. Inam, M.S. Hegde, B. Wilkens, C.C. Chang, D.M. Hwang, L. Nazar, and T. Venkatesan, Appl. Phys. Lett. 54 (1989) 754.

42 A. Hohler, D. Guggi, H. Neeb, and C. Heiden, Appl. Phys. Lett. 54 (1989) 1066.

43 J.M. Zhang, B.W. Wessels, L.M. Tonge, and T.J. Marks, Appl. Phys. Lett. 56 (1990) 976.

44 K. Lee, and G. Park, Appl. Phys. Lett. 58 (1991) 1100.

45 R.T. Kampwirth, J.M. Grace, D.J. Miller, D.B. McDonald, K.E. Gray, M. Reiten, M. Ascolese, and H. Latvakoski, IEEE Trans. on Magn. 27 (1991) 1219.

46 H. Yamasaki,K. Endo, Y. Nakagawa, M. Umeda, S. Kosaka, S. Misawa, and S. Yoshida, Nature 335 (1992) 327.

47 Y. Hakuraku, S. Higo, T. Ogushi, Appl. Phys. Lett. 57 (1990) 925.

48 R.T. Kampwirth, J.M. Grace, D.J. Miller, D.B. McDonald, K.E. Gray, P.H. Anderson, B. Driehuys, M. Reiten, and M. Ascolese, *Proceedings of the Second Colorado Conference on Science and Technology of Thin Film Superconductors* (Plenum, New York, 1990) p.39.

49 S. Miura, T. Yoshitake, and N. Shohata, Physica C 165 (1990) 241.

50 D. Jedamzik, B.R. Barnard, M.R. Harrison, W.G. Freeman, and P.J. Howard, Appl. Phys. Lett. 56 (1990) 1371.

51 Y. Hakuraku, I. Kawano, S. Higo, T. Ogushi, Supercond. Sci. Technol. 3 (1990) 510.

52 T.S. Chin, J.Y. Huang, L.H. Perng, T.W. Huang, S.J. Yang, and S.E. Hsu, Jpn. J. Appl. Phys. 31 (1992) 2092.

53 P. Wagner, H. Adrian, and C. Tome-Rosa, Physica C 195 (1992) 258.

54 J.T. Kucera, L.M. Rubin, K. Uwai, J.D. Perkins, J.M. Graybeal, T.P. Orlando, and J.B. Vander Sande, Physica C 192 (1992) 23.

55 H-C. Yang, M-C. Kim, and H-E. Horng, Jpn. J. Appl. Phys. 31 (1992) 44.

56 J. Fujita, T. Yoshitake, and H. Igarashi, Appl. Phys. Lett. 56 (1990) 295.

57 N. Nakamura, J. Sato, and K. Ogawa, Jpn. J. Appl. Phys. 29 (1990) L77.

58 H. Itozaki, K. Higaki, K. Harada, S. Tanaka, S. Yazu, and K. Tada, Physica C 162-164 (1989) 367.

59 H. Itozaki, K. Higaki, K. Harada, S. Tanaka, N. Fujimori, and S. Yazu, Advances in Superconductivity, Ed. K. Kitazawa, T. Ishiguro. Ch. 151 pp. 599 (1989).

60 M.R. Tseng, J.J. Chu, Y.T. Huang, P.T. Wu, and W.N. Wang, J. Appl. Phys. 67 (1990) 2657.

61 H. Hayakawa, M. Kaise, K. Nakamura and K. Ogawa, Jpn. J. Appl. Phys. 28 (1989) L967.

62 H. Hattori K. Nakamura and K. Ogawa, Jpn. J. Appl. Phys. 29 (1990) L36.

63 A. Tanaka, T. Machi, N. Kamehara, and K. Niwa, Appl. Phys. Lett. 54 (1989) 1362.

64 S.K. Dew, N.R. Osborne, P.J. Mulhern, and R.R. Parsons, Appl. Phys. Lett. 54 (1989) 1929.

65 W. Kula, R. Sobolewski, J. Gorecka, and S.J. Lewandowski, J. Appl. Phys. 70 (1991) 3171.

66 A. Marino, T. Yasuda, E. Holguin and L. Rinderer, Physica C 210 (1993) 16.

67 T.S. Chin, S.L. Lin, C, Tien, T.W. Huang and M.P. Hung, Supercond. Sci. Technol. 3 (1990) 302.

68 M.R. Tseng, J.J. Chu, Y.T. Huang, W.N. Wang, and P.T. Wu, *Science and Technology of Thin Film Superconductors 2* Edited by R.D. McConnell and R. Noufi, Plenum Press, New York, 1990 p. 131.

69 Y.H. Wang, L. Li, Y.Z. Zhang, Y.Y. Zhao, and P. Xu, Cryogenics 31 (1991) 439.

70 Y. Hakuraku, Y. Aridome, D. Miyagi, N.G. Suresha, and T. Ogushi, Jpn. J. Appl. Phys. 28 (1989) L819.

71 S. Kishida, H. Tokutaka, H. Higashi, K. Nishimori, and N. Ishihara, Applied Surface Science 48/49 (1991) 446.

72 M. Watamori, K. Oura, F. Shoji, T. Yotsuya, S. Ogawa, and T. Hanawa, Jpn. J. Appl. Phys. 28 (1989) L346.

73 Q. Li, O. Meyer, X.X. Xi. J. Geerk, and G. Linker, Appl. Phys. Lett. 55 (1989) 310.

74 N.G. Dhere, J.P. Goral, A.R. Mason, N.R. Parikh and B.K. Patnaik, S*cience and Technology of Thin Film Superconductors,* Plenum Press, New York, (1989) p. 407.

75 T.C. Huang, A. Segmuller, W. Lee. V. Lee, D. Bullock, and R. Karimi, IBM Research Report (1988) RJ 6411, (62529).

76 J. Sizemore, R. Barton, A. Marshall, J.C. Bravman, M. Naito, and K. Clark, IEEE Trans. Magn. MAG-25 (1989) 2245.

77 J.W. Ekin, T.M. Larson, N.F. Bergren, A.J. Nelson, A.B.B. Swartzlander, L.L. Kazmerski, A.J. Panson, and B.A. Blankenship, Appl. Phys. Lett. 52 (1988)

78 D,B. Schwartz, P.M. Mankiewich, R.E. Howard, L.D. Jackel, B.L.Straughn, E.G. Burkhardt, and A.H. Dayem, IEEE Trans. Magn. MAG-25 (1989) 1298.

79 W.K. Schomburg, M. Heidinger, G. Nother, J. Reiner, V.Windte, W. Schauer, and K. Kadel, Cryogenics 31 (1991) 366.

Table 2.1. Comparison of process characteristics [After [38]]

Process	Control of film stoichiometry	Deposition rate	Large-area coverage	Film surface quality
Sputtering (single source)	Fixed	High	Good	Good
Co-evaporation (plasma-assisted)	Variable	Very high	Very good	Good
Flash evaporation	Fixed	Medium	Good	Moderate
Molecular beam epitaxy (MBE)	Very variable	Low	Very good	Very good
Pulsed laser ablation (PLD)	Fixed	High	Moderate	Moderate
PA-CVD (single source)	Variable	Very high	Very good	Good

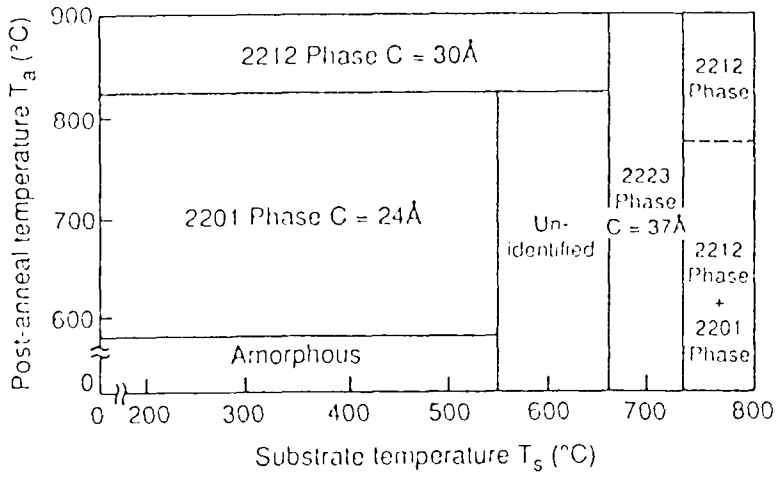

Figure 2.1. Process temperature dependence of crystallinity of BiSrCaCuO thin films (After [58]).

Table 2.2. Properties of some related substrate materials used for Bi-based high T_c superconductors

Substrate material	Crystal system (Structure)	Existence of twins	Lattice constant(A^o) *a,b*-axis	Thermal expansion coefficients(K^{-1})
$SrTiO_3$	cubic (perovskite)	no	$a = 3.905$	$9.4\text{-}10.8 \times 10^{-6}$
MgO	cubic (NaCl)	no	$a = 4.213$	$8\text{-}12.8 \times 10^{-6}$
$LaAlO_3$	rhombohedral (perovskite)	reported	$a = 5.364$ $(3.793)^*$	
$LaGaO_3$	orthorhombic (perovskite)	reported	$a = 5.496$ $b = 5.526$ $(a,b = 3.890)^*$	9.0×10^{-6}
$NdGaO_3$	orthorhombic (perovskite)	reported	$a = 5.426$ $b = 5.502$ $(a,b = 3.851)^*$	-
Al_2O_3	rhombohedral	no	$a = 4.758$	5.0×10^{-6}
$CaNdAlO_4$	tetragonal	no	$a,b = 3.690$	-

*: In the pseudocubic representation

Table 2.3. Properties of Bi-based superconductors

BSCCO phases	Crystal system (Structure)	Lattice constants(A^o)	Thermal expansion coefficients(K^{-1})
$Bi_2Sr_2Ca_{n-1}Cu_nO_{4+2n}$	orthorhombic (oxygen deficient perovskite between double Bi-oxide layers)	$a = 5.41(3.83)^*$ $b = 5.44(3.85)^*$	
n = 1		$c = 24.6$	12×10^{-6}
n = 2		$c = 30.6$	12×10^{-6}
n = 3		$c = 37.1$	12×10^{-6}

*: In the pseudocubic representation

Table 2.4. Percentage mismatch between Bi-based superconducting phases and substrates at ~850°C [80].

Superconducting material	Substrate material					
$Bi_2Sr_2Ca_{n-1}Cu_nO_{4+2n}$	$SrTiO_3$ 3.905 (A^o)	MgO 4.213 (A^o)	$LaAlO_3$ 3.793 (A^o)	$LaGaO_3$ 3.890 (A^o)	$NdGaO_3$ 3.851 (A^o)	$CaNdAlO_4$ 3.690 (A^o)
$a = 5.41(3.83)A^o$	-1.92	-9.07	0.98	-1.54	-0.54	3.79
$b = 5.44(3.85)A^o$	-1.41	-8.59	1.50	-1.03	-0.03	4.33

Table 2.5. Low temperature growth processing of Bi-based thin films

Technique and deposition rate	Substrate temperature (Ts) and thickness	Oxygenation and Heat Treatment (^oC)	Comments	Authors
RF magnetron sputtering, 500 A^o/h	680^{o}C 1000 A^o (MgO)	As-grown(760 Torr O_2 cooled) annealed(at 400^{o}C,760 Torr,for 2h %100 O_2 %0.2 O_2	Tc 82K, Jc(70K) 1x10^5 A/cm^2 Tc 68K Tc 82K	Miura et al. [49]
RF magnetron sputtering, 10^4 A^o/h	537^{o}C 2000-10000A^o (MgO)	at 26 Torr,in-situ soak for 5 min at 537^{o}C at 600^{o}C	 Tc 13K Tc >80K Jc(4K) 7x10^5 A/cm^2	Jedamzik et al. [50]
DC magnetron sputtering, 84 A^o/h	660-740^{o}C 2500 A^o (MgO)	300 Torr O_2 cooled Ts=660, 700, 720^{o}C,	Ts<660^{o}C semiconducting Tc 50K, 73K, 81K Jc(77K) 8x10^4 A/cm^2 (4.2K) 3x10^6 A/cm^2	Hakuraku et al. [47]
DC magnetron sputtering, 84 A^o/h	720^{o}C 2500 A^o (MgO)	at different PO_2 cooled PO_2=0.3, 30, 300 Torr	For thickness>2500 A^o Tc<70K Tc 25K, 55K, 81K Jc(77K) 8x10^4 A/cm^2 (4.2K) 3x10^6 A/cm^2	Hakuraku et al. [51]
DC magnetron sputtering, 2500 A^o/h	580-800^{o}C 5000 A^o (MgO)	0.5 Torr O_2 cooled Ts=625, 650, 680, 700^{o}C	Cooling rate 75 to 150^{o}C/min Tc 45K, 62K, 71K, 78K	Tsung et al. [52]
DC sputtering 1320 A^o/h	744^{o}C ($SrTiO_3$) 4000 A^o	at 2.7 hPa O_2 ,in-situ soak for 50 min at 744^{o}C	Without soak Tc is low Tc >80K, Jc(77K) 1.6x10^5 A/cm^2	Wagner et al. [53]
Reactive co-sputtering 8400 A^o/h	805^{o}C 5300A^o $SrTiO_3$, MgO	As-grown 3.5 mTorr O_3 cooled to 300^{o}C then O_2 cooled annealed 870^{o}C 30 min in Ar+%5O_2	 Tc 68K Jc(4.2K) >10^6 A/cm^2 Tc 80K Jc(4.2K) 4x10^6 A/cm^2	Kucera et al. [54]
AC sputtering	660^{o}C (MgO) 2000-10000 A^o	0.05kPa O_2 cooled Ar and O_2(7:3) cooled	Tc 74K Tc 66K	Yang et al. [55]
Ion beam sputtering 360 A^o/h	640^{o}C 600 A^o (MgO)	1.3x10^{-3} Torr atomic O cooled Oxygen plasma-on Oxygen plasma-off at 400^{o}C	 Tc 60K(500^{o}C 1h in air Tc 80K) Tc 76K	Fujita et al. [56]

Table.2.6. High temperature growth processing of Bi-based thin films

Technique and deposition rate	Substrate temperature(Ts) and thickness	Sintering conditions	Comments	Authors
DC magnetron sputtering 3600 A^o/h	150°C (MgO, $CaNdAlO_4$,) 0.7-1x10^4 A^o	at 870°C in air for 1h on MgO on $CaNdAlO_4$,	Tc 106K, Jc(<60K)>10^4 A/cm^2 Tc 104K, Jc(<60K)>10^5 A/cm^2	Kula et al. [65]
RF magnetron sputtering 5000 A^o/h	600°C (MgO) 10^4 A^o	at 857°C with sintered bulk in air for 40 h (sing. 2223)	Tc 102K, Jc(10K)>10^4 A/cm^2, below and above 40h multiphase	Marino et al. [66]
RF magnetron sputtering	Unheated (MgO) 0.6x10^4 A^o	on bulk with facing down at 845°C, 14h in air	Tc 103K, for without bulk or annealed facing up Tc lower	Chin et al. [67]
RF magnetron sputtering 9600 A^o/h	RF magnetron sputtering 2500 A^o/h	on uncalcined bulk with facing down at 840°C 20h by the bulk at 830°C 15h	facing down surface rough Tc 109K Tc>105K, Jc(77K)4x10^2 A/cm^2	Tseng et al. [68]
RF magnetron sputtering with multiple target	400°C (MgO) 10^4 A^o	at 850 in air for 10 min 60 min	contained 200 nm PbO layer Tc 94.5 Tc 106.5	Tanaka et al. [63]
RF magnetron sputtering	Unheated (MgO) 1.8-0.23x10^4 A^o	in Au capsule with calcined bulk at 850°C 3h slow heating	for fast heating Tc is lower but resistivity is better Tc 106K	Hayakawa et al. [61]
DC magnetron sputtering 12000 A^o/h	250-400°C (MgO) 0.8-1.5x10^4 A^o	in air for 3h at 840°C(slow cooled) at 860°C	Jc(77K)>2.7x10^3 A/cm^2 Tc 110K Tc 80K	Wang et al.[69]
DC magnetron sputtering 180 A^o/h	250-750°C (MgO) 10^4 A^o	at 850°C 3h deposited at Ts=250°C Ts=400°C	Pb mole fraction:2 in film Tc 105K Tc 115K	Yoshinori et al. [70]
RF magnetron sputtering 2500 A^o/h	340-500°C (MgO) 10^4 A^o	at 865°C in air for 4 h (Bi-2212)	Tc 83K (Ts=380°C, has lowest resistivity than others)	Kishida et al. [71]

CHAPTER 3

Experimental methods used for preparation and characterisation of films

3.1. Introduction

In this chapter thin film growth experiments, including target and substrate preparation and deposition by magnetron sputtering, and techniques used for studying properties of the films produced will be described. Deposition of thin films has been carried out with rf magnetron sputtering, however the principle of dc magnetron sputtering is also described to make the rf sputtering process more understandable. In section 3.5 specification of the conditions under which sputtering experiments have been performed is given. The last step in preparing films is the sintering of the film deposited at lower temperatures.

In the following sections the principles of the characterisation techniques used in the present work are given. Finally patterning of thin films into preliminary device structures, their processing, and the results obtained are presented.

3.2. Target preparation for sputtering

One advantage of RF sputtering is that an insulating target may be used. Targets of different composition have been used to reach the right stoichiometry in the thin films.

In order to prepare targets the appropriate amounts of Bi_2O_3 (99.9%), PbO (99.9%), CuO (99%), $Sr(NO_3)_2$ (99%) and $CaCO_3$ (99%) powders were intimately mixed and ground

by ball milling for 24 hours using ZrO_2 media in an appropriate amount of 2-propanol. The powder slurry was then dried on a hot plate, being constantly stirred with a magnetic stirrer to prevent segregation. Next for the heavily PbO doped Bi-2223 target the dried powder was calcined at 650^{o}C for 10 hours in air, ground with a pestle and mortar and pressed at a pressure of about 3 Tons/inch^2 in a hardened stainless steel die into a 50 mm diameter and 2 to 5 mm thick disk pellet. The disk pellet was again annealed at 675^{o}C for 4 hours in air.

Initially the dried powder had been calcined at 845^{o}C for 10 hours in air, but (due to the presence of large amount of PbO) had stuck to the combustion tray. Reduction to 790^{o}C prevented the sticking, but partial melting resulted in a very hard product, difficult to grind. Finally 650^{o}C was found suitable to get fine and soft powder which allows the target to be made easily. The targets prepared in this way were not good conductors, with a nominal room temperature resistance of 100 kΩ.

For the preparation of Bi-2212 targets the same process described above has been followed except for sintering conditions. In this case the dried powder was first sintered at 820^{o}C for 24 hours in air, ground and pressed into a disk pellet. After that, the disk pellet was sintered at 830^{o}C for 12 hours in air. The 2212 targets using nominal stoichiometric composition were not superconducting, but exhibit high conductivity with a nominal room temperature resistance of 20Ω.

Uncalcined targets have also been used, but calcination of the target was found useful to produce a more dense and strong target, which is important to provide effective cooling of the target during sputtering and to avoid the risk of sucking out powder particles under high vacuum. Kishida et al. [1] reported that the deposition rate of films prepared using a mixed powder target without sintering is approximately half the deposition rate of films prepared using sintered targets.

Some pellet targets bent and had large cracks from thermal expansion during high temperature sintering. This sort of target is not suitable when considering effective cooling and homogeneous deposition. It also gives rise to difficulty in fixing on the magnetron table. In order to prevent bending of the target a ceramic plate was put on top of the pellet during

sintering and very slow cooling down to room temperature employed. This process has produced sufficiently flat and crack free targets.

The target was fixed on the magnetron table by using silicon loaded silver paste or silver paint to get good thermal contact, or without either, and tightened to the magnetron table by the target clamp .

3.3. Cleaning and polishing of substrates

When the thickness of the thin film (less than 1μm) is considered the importance of a well polished substrate can be understood. In the present work, three kinds of single crystal, with the size 10x10 or 5x10 mm^2 (MgO) surface area and 1 or 0.5 mm thick, have mainly been used as a substrate. These are MgO, $SrTiO_3$ and $LaAlO_3$ single crystals oriented on the [001] direction. Back reflection Laue photographs of these substrates are shown in **Fig. 3.1** for MgO and $SrTiO_3$ and in **Fig. 3.9** for $LaAlO_3$. The symmetrical distribution of the spots indicates the perfection and orientation of these single crystals.

Previously used single crystal MgO substrates have been cleaned by dipping into diluted HCl acid (35%) in de-ionised water (HCl: de-ionised water = 1:5) for a few seconds. After cleaning some small cavities randomly distributed on the surface were observed under the optical microscope. The reason for this kind of surface structure could be: (1) over etching of the part where the cavity formed due to the intrinsic porosity in the film (2) impurities having different etching time than that of the BSCCO (3) very small degree of chemical reaction between substrate and BSCCO film or impurities because of the relatively soft nature of MgO substrates. This undesirable case has not been observed on hard $SrTiO_3$ and $LaAlO_3$ substrates. These latter two substrates were used as-cleaned chemically without repolishing.

MgO substrates have been polished after each cleaning off of the film. In order to polish the substrates, initially diamond pastes of 6μm, 3μm, 1μm, 0.25μm, 0.1μm grain sizes were used with texmet polishing cloths. This process was not successful in obtaining well polished scratch free smooth surfaces. Then the polishing cloth was changed to a

microsoft one for 1μm and smaller diamond paste and then a silicon-water with Si grain size of 0.05μm diluted with de-ionised water was used as a last step. A very well polished smooth surface has been obtained by this process.

The substrate was degreased with acetone, then rinsed in de-ionised water, and blown dry before loading on a copper disk using silver paint, then dried on a hot plate or in air.

3.4. Sputtering

In this study the Planar Magnetron Sputtering (PMS) technique has been used to prepare thin films. The deposition of thin films of BSCCO ceramic material was carried out in a model DS500 sputter deposition system manufactured by Oxford Applied Research. The principle of the sputtering was briefly described in chapter 2. In the case of a planar magnetron (**Fig. 3.2**), a magnetic field is imposed in such a way that the electrons are trapped in the region near the target surface. The closely confined electrons are forced to move in a path within the magnetic field and if the magnetic path is closed then the electrons will circulate freely around the enclosed magnetic field. A gas atom entering this electron cloud has a greater probability of losing an electron, since this region of high density of electrons has large ionising efficiency. This means that a lower gas pressure is required to maintain the sputtering process. The rate of removal of the material from the target is ten times faster than in the case of diode sputtering.

As the electrons are confined to a certain region then very few of them are able to go to the substrate holder which is normally at ground (+) potential and therefore there is little substrate heating in magnetron sputtering. However the target comes under fierce ion bombardment, particularly in the centre of the electron cloud, causing a very localised heating of the material in the "race track" area. This can cause target materials to shatter or melt due to the large thermal gradient and the fact that the material cannot dissipate the heat fast enough. There are two main types of magnetron sputtering; rf and dc regarding the bias voltage. In both cases the electrons and ions are produced in the above way.

3.4.1. DC Sputtering

If a potential is applied between two electrodes held in a low gas pressure, ions and free electrons are accelerated towards the relevant electrodes. Collisions between positive ions and the cathode, and electrons with neutral gas atoms, generate further electrons and ions respectively. At a certain voltage which depends on the gas pressure, the process becomes self-sustaining and a luminous glow discharge is created. The discharge is "normal" at the beginning because the current can be increased by increasing the area of the glow discharge (at constant current density). Further increase of the voltage increases the current density and in this 'abnormal discharge' condition, control of the ion energies and current densities is possible and conditions are suitable for sputtering. The separation of electrodes is relatively small for sputter deposition so that the discharge and the voltage distribution can be schematically represented as in **Fig. 3.3**. Two major regions in the sputtering discharge are the luminous region or negative glow across which the voltage is constant, and the cathode dark space or sheath across which the entire applied voltage is dropped. Further details of the processes occurring in sputtering plasmas may be found in, for example, reference [2].

The DC sputtering process requires a metallic target. In the case of an insulating target ion bombardment by positive ions can occur initially, but loss of electrons from the target surface (to neutralise the ions) causes positive charging of the surface and increases the potential towards zero. The target charges up and eventually the potential on its front surface is too small to sustain the discharge.

3.4.2. RF Sputtering

If the applied voltage is reversed before the surface of the target voltage reaches zero, electron rather than ion bombardment can occur, and hence the electrons tend to decrease the now positive voltage towards zero. This decrease will occur much more rapidly than the increase under positive ion bombardment because of the much greater speeds of the lighter electrons. A further reversal of the applied voltage will in fact make the target

potential even more negative, as shown schematically in **Fig. 3.4**. Repeated reversal of the applied voltage gives rise to the target acquiring a net, constant, negative voltage or self-bias. The effect of repeated reversal of the applied voltage is shown in **Fig. 3.4 b**. At this point the net ion and electron currents in each half cycle are equal. Thus cycling the applied voltage at high frequencies (in practice rf frequencies greater than 1 MHz) enables a continuous discharge to be sustained. Under a sinusoidal variation **Fig. 3.4 b** would approximate to **Fig. 3.4 c** and ion bombardment would be almost continuous.

The rf plasma technique is comparatively better than the dc magnetron plasma technique in producing a uniform plasma for thin film preparation [3].

3.5. Deposition of thin films

In order to produce thin films of BSCCO ceramic compound on single crystal substrates the procedure described below was adopted. The sputtering chamber was cleaned with acetone before each sputtering. Five pieces of substrate, cleaned and polished as described in section 3.3, were stuck down with silver paint on to a copper disc. After fixing the substrate holder to the anode face to face keeping 6 cm distance to the target in the sputtering chamber, the chamber was pumped down to a pressure of 1×10^{-6}mbar. At this stage the substrate was heated to the desired temperature (usually around 200^{o}C) and the turbo molecular pump turned off. Sputtering gas (usually Ar) was introduced to produce a total pressure of 10^{-2}mbar in the chamber. Then sputtering was commenced by applying rf power to the target. Powers of 50 watt were usually used and the chamber pressure monitored by Pirani gauge. When sputtering is started the chamber pressure slightly increases so it needs to be adjusted by a needle valve to the desired pressure until a steady pressure is obtained.

The deposition of films usually has been carried out at relatively low temperature as the heater system of the sputtering machine does not work properly at the high temperature needed for crystallisation in-situ (about 750^{o}C). No thickness monitor was available on the sputtering apparatus used, for direct monitoring of the thickness of the film during the

deposition process. The thickness of the films for some patterned samples has been measured in a Confocal Scanning Laser Microscope (CSLM). Deposition rate was about 0.025 nm/s for the sputtering conditions described above.

Although deposition of films was carried out on to a variety of substrates under a variety of conditions, the conditions given above were optimal and usually films were produced under these sputtering conditions. The effect of the condition parameters on the film composition and/or film properties will be discussed in the following chapters (chapters 4-5)

3.6. Sintering of films

Films as-deposited at low temperature are amorphous with a shiny smooth surface. Therefore, to grow the desired superconducting Bi-2212 and Bi-2223 phases from the as-deposited films described in section 3.5 requires ex-situ annealing. A variety of annealing cycles has been used to provide the optimum conditions for growth of each phase. As deposited films were taken from the sputtering chamber and the silver paint cleaned from the back side of the substrate with acetone before sintering. Initially Bi-2212 films were annealed in an open Al_2O_3 crucible in a tube furnace. The film was positioned in the centre of the tube furnace. Later on a Carbolite furnace was used for annealing and was found to be more suitable than the tube furnace in providing a more stable temperature environment at the sample. In both furnaces a calibrated programmable temperature controller was used to take each film through a predetermined annealing cycle. The majority of films were annealed in air. Some Bi-2223 films were annealed in partial O_2 pressure to study the oxidising effect on this phase. Precise details of the sintering conditions used will be given in the following chapters of results (Chapters 4-5).

3.7. Characterisation techniques

3.7.1. Powder X-ray diffraction

The X-ray diffraction (XRD) technique has been used extensively to characterise the phases present, the extent of structural disorder and the degree of preferred orientation in prepared thin films. For this purpose, a Philips $\theta/2\theta$ PW 1050 powder diffractometer which can scan a diffraction pattern in a computer-controlled process has been employed. Ni-filtered Cu-Kα ($\lambda = 1.5418A^{o}$) radiation was produced from a 40 kV X-ray tube.

In a powder diffractometer, an X-ray beam strikes a flat surface of a powder at an angle θ, and simultaneously the intensity of the diffracted X-ray beam at an angle 2θ is detected. When the Bragg condition $2d_{hkl}\sin\theta = \lambda$ is fulfilled, interference occurs, where d_{hkl} is the spacing between planes with Miller indices (hkl), θ is the angle between these planes and the incident monochromatic X-ray beam of wavelength λ. With this so called θ-2θ scan, the positions of diffraction peak are resolved, and from the position and the intensity of these peaks, the structure of major phases and the presence of unknown phases can be revealed. The resolution for phase detection is about 5%. Further details of powder X-ray diffraction processes may be found in reference [4].

As Bragg diffraction will only take place from planes close to the film normal, any texture in the film normal to the substrate will be shown in the XRD pattern by comparison with the standard spectrum from powdered material. The strongest powder lines will be considerably reduced in intensity, with an increase in the lines corresponding to the texture orientation. **Fig. 3.5** shows the XRD patterns of the pressed Bi-2212 powder having relatively little preferential orientation and a thin film well oriented along the c-axis produced from a target made from the same powder.

If all lattice planes lie parallel to a flat substrate surface, a theta scan peak profile with a narrow full width at half maximum (FWHM) will be produced. As lattice planes deviate from this parallel orientation, the theta scan FWHM increases. Since each grain in a polycrystalline sample contributes to the diffracted beam profile as it is rotated into the

correct Bragg geometry, the theta scan peak FWHM can be considered as a relative measure of the orientation distribution present in a sample. Powder XRD patterns corresponding to completely and partially c-axis oriented Bi-2212 films, prepared with different heat treatment processes are illustrated in **Fig. 3.6**. The higher annealing temperature (830^{o}C) has produced better alignment (narrower peaks) in (a) than the lower temperature (820^{o}C) in (b). There are three causes for broader or weaker diffraction lines: small grain size (less than 0.1μm), nonuniform strain and stacking faults [5]. Therefore, it is difficult to detect the intrinsically weaker low angle peaks and those from minor impurity phases.

3.7.2. Electron Probe Micro Analysis (EPMA)

Composition analysis of the thin films obtained is especially important for preparation of superconducting thin films. Film compositions were determined both qualitatively and mostly quantitatively by using energy dispersive X-ray spectrometry (EDS) and wavelength dispersive X-ray spectrometry (WDS), respectively.

In these techniques a flat sample is exposed to an electron beam, which penetrates a typical distance in the order of 1μm. The core electrons of the atoms of the sample are excited by the electron beam, and when they return to their ground state, X-ray radiation is emitted. These X-rays exhibit an energy characteristic of the excited atom. The energy (or equivalently, wavelength) and intensity of the emitted X-rays are detected, from which the kind and amount of elements in the sample can be determined by comparing them with spectra generated by standard samples of known composition. Detailed description of the complex calculations of the concentration of the elements present in the sample may be found in references [6,7].

Electrons in a focused beam will penetrate the sample and undergo scattering processes in the specimen. The interaction volume is found to have dimensions of several micrometers with the depth substantially greater than the width and to have a distinctive pear shape (**Fig. 3.7 a**). The origin of this shape can be understood in terms of the characteristics of elastic and inelastic scattering which generates characteristic X-rays by

collision of electrons with atoms in the sample until their energy falls below the critical excitation energy Ec for a given X-ray wavelength. This interaction volume (the depth intensity profile ϕ) is dependent in width and depth on the sample atomic number Z and density ρ. The depth of this excitation volume also affects the intensity of X-rays detected because of the higher probability of absorption by the specimen of the X-rays generated at greater depths. Therefore an absorption factor, A, dependent on density and composition of the sample must be considered in any quantitative analysis. The detected X-ray intensity is also affected by the atomic number, Z, of the elements of interest, and by fluorescence effects, F, caused by the high energy X-rays generating further X-rays of lower energy. Taking these three factors, or ZAF corrections, into account enables calculation of the concentration of elements present.

In the present work, quantitative analysis was carried out in a Cameca Camebax Microprobe equipped with computer controlled analysis and ZAF correction routines using a $\phi\rho z$ program for two wavelength dispersive spectrometers, and an energy dispersive spectrometer for qualitative work. WDS has a lower counting efficiency and requires longer analysis time than EDS. However WDS has improved resolution (10 eV cf. 150 eV), and peak-to-background ratios and mass sensitivities both an order of magnitude better than EDS, so it has the potential for improved accuracy and detection of low concentration contaminant elements.

The $Bi_{M\alpha}$, $Pb_{M\alpha}$, $Sr_{L\alpha}$, $Ca_{K\alpha}$, $Cu_{K\alpha}$ lines were analysed with a 15kV accelerating voltage, and using standards for the ZAF routine of pure Cu, Wollastonite ($CaSiO_3$), pbte (PbTe), srf (SrF), and pure Bi.

An accelerating voltage 15kV was chosen in order to minimise penetration of the electron beam. Accurate analysis of low energy $O_{K\alpha}$ X-rays is difficult, and so to calculate the film composition, the remainder of the film not accounted for by Bi, Pb, Sr, Ca, or Cu was assumed to be O. This enabled the concentrations of Bi, Pb, Sr, Ca, and Cu to be calculated directly from the intensities of their respective X-Rays, while the O concentration was calculated as the difference between the total metal concentration and 100%.

The penetration depth of the electron beam into the film has important consequences for estimating the errors involved in the analysis of the film. If a film examined is too thin, the electron beam penetrates the substrate, generating substrate X-rays and reducing the relative intensity of the characteristic X-rays from the superconducting thin film as observed by Usui [8] on 0.1μm YBCO thin films. In order to avoid e-beam substrate interaction, Usui suggests Total-Reflection-Angle X-ray spectroscopy (TRAXS) using very low glancing ($\theta_g < 5^o$) and take off angle ($\theta_t < 3^o$) (**Fig 3.7 b** and **c**). This configuration has been adopted for the Bi-2223 films which have thickness of 0.5-0.7μm. The glancing angle was kept at 5^o by tilting the film and the take off angle of $1\text{-}33^o$ scanned for an acceleration voltage of 25 kV. An EDS spectrum is illustrated in **Fig 3.8 a** and **b** for take off angles of 4^o and 33^o, respectively. The top spectra in each figure were taken from a flat sample, that is the standard configuration (untitled, $\theta_g = 90^o$ $\theta_t = 62^o$). It is clear that characteristic X-rays from the MgO substrate ($Mg_{K\alpha}$ line) are hardly detectable in intensity even for a flat sample and an acceleration voltage of 25 kV. Characteristic X-rays from the superconducting thin film ($Bi_{M\alpha}$, $Pb_{M\alpha}$, $Sr_{L\alpha}$, $Ca_{K\alpha}$, $Cu_{K\alpha}$ lines) are considerably depressed in intensity for the tilted sample. Therefore in the course of this study the standard configuration was used for composition analysis.

From each sputtering batch one sample from a certain position on the substrate holder was kept for EPMA. As these as-deposited films at relatively low temperature had a smooth shiny surfaces, routine accurate characterisation has been performed prior to high temperature annealing. Also point analysis from different grains has been carried out on sintered films.

3.7.3. Laue X-ray diffraction

Laue X-ray diffraction is especially suitable for determining crystal orientation and assessing crystal quality on the scale of the beam size. In this technique, the white X-ray beam produced by an X-ray tube with W-anode is perpendicularly focused on the crystal. The X-rays diffracted by the crystal are detected as spots at certain positions on a film,

placed behind the crystal in a forward diffraction configuration or in front of the crystal in a back scattering configuration. From the geometric arrangement of these spots, the symmetry of the crystal structure as well as the crystal orientation can be determined.

This technique has been used to assess substrate crystal perfection and also in an attempt to investigate whether the film on a single crystal substrate of interest grows epitaxially or not. For this purpose back reflection Laue photographs of a thin film (about 0.5 μm thick) and the substrate which supports the same film, have been taken for the same exposure period of 40 minutes with a X-ray tube voltage of 40 kV. These Laue photographs are illustrated for a $LaAlO_3$ single crystal substrate with and without Bi-2223 thin film on it in **Fig. 3.9**. These two pictures are the same, indicating no extra diffraction detected from the film (even for an exposure time increased up to 40 minutes) because of the small amount of film material. For an elongated exposure time above 40 minute the size of the light area in the photograph centre becomes larger so that all spots in that part disappear. Therefore, epitaxial growth could not be assessed by Laue X-ray diffraction.

3.7.4. Scanning Electron Microscopy (SEM)

The conventional SEM can be operated so that the electron beam strikes the specimen at a single location. Within the interaction volume, both elastic and inelastic scattering occur as described in section 3.5.2. producing detectable signals from backscattered electrons, secondary electrons, characteristic and continuum X-rays, etc. By measuring the magnitude of either backscattered electrons or secondary electrons with a suitable detector, a determination of local topography of the specimen can be made at the location of the electron beam impact. In order to study more than a single location, the beam can be moved from place to place by means of a scanning system. Secondary electrons are generated at very shallow depths of about 0.1 μm with energy ≤ 50 eV while backscattered electrons are scattered from atoms at depths of about 1μm with energies above 50 eV

In order to study the surface morphology of the films after annealing, a Hitachi S510 was used most and occasionally a Philips 501 SEM. The latter is equipped with an EDS detector for qualitative analysis, using principles similar to those described in section 3.5.2.

3.7.5. Measurement of electrical properties

For electrical measurements such as critical temperature and critical current density the standard four-point contact technique has been used. Four silver contact pads, above 1 mm wide strips separated from each other by 1 mm were evaporated on to the unpatterned films through a shadow mask placed on the film. Silver or copper wires, 0.15 mm in diameter, were then stuck to the pads with high conductivity silver paste. Often wires were stuck directly to the film with silver paste to save the film for other measurements such as surface resistance, optical and microwave response and SQUID properties.

The resistivity versus temperature characteristic was obtained by injecting a current of 100μA, corresponding to a current density of $2A/cm^2$ for a 0.5μm thick and 10 mm wide unpatterned film, through the outermost contacts and measuring the voltage drop between the inner contacts. To determine film resistance as a function of temperature, films were cooled in Lake Shore Cryotronics closed cycle refrigerator cryostats. The sample was heated from considerably below the critical temperature with a ramping rate of 0.25K/min to avoid any possible temperature gradient. Sometimes a self heating regime was adopted. The voltage drop was detected by an EG & G electronics 5208 lock-in amplifier. A simple computer program was used to control the heating rate and simultaneously record the temperature of the sample and voltage measured by the lock-in amplifier.

The critical current density (J_c) in liquid nitrogen (77K) and at different temperatures in the cryostat was measured by using a dc current source with the criterion of 1μV/mm.

3.8. Patterning of thin films

Fabricating devices from high T_c films requires the patterning of the films into device structures of interest without any degradation of the electrical properties. Standard

processes for fabrication of micro and nano structures employ either (a) subtractive techniques such as wet or dry etching, or (b) additive techniques such as lift-off [9].

Dry etching such as reactive ion etching [10] or argon ion milling [11] and pulsed laser evaporation [12] are promising for producing micron-sized patterns used by most groups to pattern high T_c superconducting thin films. But there is a possibility that they degrade the transition temperature [13] and damage the substrate [14]. Wet chemical etching with various acid etchants such as solutions of phosphoric acid (H_3PO_4), nitric acid (HNO_3), hydrochloric acid (HCl) [15, 16] and ethylenedamine tetra-acetic acid (EDTA) [14, 17] present a viable alternative in this respect. The EDTA, saturated with de-ionised water, provides a very low etching rate allowing control of the desired smooth-sidewalled patterns when compared with other acid etchants with very low concentrations (1:40 acid: water, removal rates larger than 0.5 μm/min) [14].

Nonoptical lithographies such as e-beam lithography, ion beam lithography and X-ray lithography are generally used to define patterns smaller than can be done by using photolithography as they have higher resolution than optical lithography.

3.8.1. The principle of lithography

Virtually all lithography techniques employ energy sensitive chemical substances called photoresists. These are applied to the surface to be etched as thin film coatings and then selectively exposed to an energy pattern i.e. light (photolithography), electrons (e-beam lithography), ion beams (ion-beam lithography) or X-rays (X-ray lithography) etc. that form exposed areas. The resist film is then subjected to a development process that selectively removes either the exposed or the unexposed resist, depending on whether the photoresist is positive or negative. The pattern produced can then be removed by using techniques such as etching, evaporation, or plating.

Positive resists are those in which the development step removes the exposed resist. Negative resists are those in which development removes the unexposed resist. Negative resists consist of a base of synthetic rubber compound containing a few percent of a light

sensitive agent which facilitates the formation of cross-linkages between the base molecules. This cross linking inhibits its dissolution. In the case of positive acting photoresists the process described above works in reverse i.e. light sensitive agents facilitate dissolution of resist.

The photoresist absorbs moisture from the atmosphere easily, thus causing it to swell. A soft-bake below 100^{o}C serves to remove most of the water from photoresist which improves its adhesion. After development, hard-bake (80-120^{o}C) is also recommended with the same purpose as the soft-bake and additionally to increase the strength of the photoresist against the etching solution.

The other crucial parameter in making photolithography is the thickness of the photoresist film which has to be within certain limits combining exposure and development time and to provide an effective barrier to the various etchants.

3.8.2. Patterning process

In the present work, in order to impose a meander-type structure, or a long narrow line track for optical and microwave response measurement, or microbridges for dc SQUID (Superconducting Quantum Interference Device) patterns on Bi-based thin films, the conventional photolithography technique has been used with wet chemical etching mainly in EDTA, HNO_3 and HCl have also been used as etchant.

In order to make a pattern the superconducting film was first degreased in acetone and blow dried. After that the whole film surface to be patterned was covered with a uniform film of positive photoresist, S1400-27, by spinning on a rotating vacuum chuck at 4000 rpm for 30 seconds in a photoresist spinner. The thickness of photoresist film was about 1.5μm. The photoresist covered film has been soft-baked on paper tissue at 90^{o}C for 3 minutes to dry the photoresist before putting the photographic mask pattern on it. The film was carefully positioned under the mask aligner, supplying mercury UV light at a wavelength of 365 nm with an intensity of 3 mW/cm^2 during exposure. Exposure time was optimised at 20 seconds after several experiments. The photoresist layer was subsequently developed for

30-120 seconds in solutions of 25-50% developer in de-ionised water. Finally the sample was immersed in a saturated solution of EDTA/H_2O for 15-25 minutes at ambient temperature without hard-bake. To eliminate concentration degradation of the etching solution with time excess EDTA crystals were kept in the solution. After the etching process, the sample was rinsed with water and immersed in acetone to strip the photoresist film.

The mask pattern which contains four dc SQUID patterns with different parameters was supplied by National Physical Laboratory (NPL). Each dc SQUID pattern consist of a round washer design with two symmetrically arranged constrictions of width 10μm, 20μm, 40μm, and 80μm. A meander-type pattern with a track 150μm wide and 1 cm long and straight line track pattern prepared on a transparency using a photographic technique was also used as a mask.

3.8.3. Results and discussion

Fig. 3.10 shows SEM photographs of a well defined meander type pattern with a track 150μm wide and 1 cm long and a SQUID pattern prepared using the process described above in EDTA. EDTA/H_2O and H_3PO_4 have a very low etching rate at room temperature when compared 9% HCl. Therefore it is easy to control the etching process to produce well defined patterns in the first two etching solutions. In the case of 9% HCl the etching rate is quite fast and a material with yellow colour (probably Bi_2O_3) remained on the substrate.

Hard-bake made at 120^oC for 5-10 min. prevented etching of the sample even in 0.9% HCl/H_2O solution for a couple of min. Therefore, instead of hard bake, after patterning all films were annealed at low temperature (600-700^oC) for several hours to evaporate any water and other chemical solvents. Annealing at 700^oC following wet chemical etching has been found very effective in reducing the room temperature resistivity of the samples, while annealing below 650^oC did not affect that room temperature resistivity.

Table 3.1 gives the room temperature resistivity of some samples after etching and after annealing for Bi-2212 films patterned into a 150μm wide and 1 cm long meander-type

structure using standard photolithography and wet chemical etching. The reduction ratio in resistivity varies from sample to sample over a range running from 86% to 3%. This effect is optimisation of the oxygen content as discussed in section 5.3. The small reduction ratio of 3% in resistivity in sample 310 suggest that the variation of reduction ratio from sample to sample with low temperature annealing can be related to the granularity or microstructure of the film. Microstructures of some of these sample are illustrated in **Fig. 3.11**. Except for sample 310 all others have pure microstructure and thus good electrical properties.

The same effect has also been observed for Bi-2223 films patterned into SQUID patterns described above. The reduction ratios in room temperature resistance (resistivity could not be calculated because of the geometry of SQUID pattern) measured on the same sample from separate patterns having different constriction width is more or less the same, supporting the idea of that the microstructure of film affects the reduction ratio (**Table 3.2**).

In order to understand whether there is any effect of the etching process on the critical temperature, the critical temperature of the same sample before and after patterning has been measured using the same bias current on a SQUID pattern which has two constrictions of 20μm in width. Temperature dependence of resistance is shown in **Fig. 3.12** for this sample. Critical temperature of the patterned sample is ≈2K lower than the unpatterned film. In fact this is not an accurate test because a drop in $T_{c\text{-}zero}$ of a few Kelvin may well correspond to a loss in critical current density by orders of magnitude. However it can give a rough idea about the depression of electrical properties of the film. The accurate test for this purpose is J_c measurement before and after etching. But, J_c measurement usually requires a patterned bridge in the first place. Muller et al. [18] used a Vibrating Sample Magnetometer to measure the Jc of BSCCO films before and after etching in EDTA, and reported that no depression was seen.

References

1 S. Kishida, H. Tokutaka, H. Higashi, K. Nishimori and N. Ishihara, Applied Surface Science 48/49 (1191) 446.

2 B.N. Chapman, *Glow Discharge Processes*, J. Wiley, New York (1980).

3 Y. Okuna, S. Yagura, and H. Fujita, J. Appl. Phys. 69 (1991) 146.

4 H.S. Peiser, H.P. Rooksby, and A.J.C. Wilson, *X-Ray Diffraction by Polycrystalline Materials* John Wright & Sons Ltd., London, 1955.

5 B.D. Cullity, *Elements of X-Ray Diffraction*, Addison-Wesley Publishing Company, 1956, chapter 9.

6 S.J.B. Reed, *Electron Microprobe Analysis*, Cambridge University Press, Cambridge 1975.

7 V.D. Scott and G. Love, *Quantitative Electron-Probe Microanalysis*, Ellis Horwood, 1983.

8 T. Usui, ISTEC Journal, 5 (1992) 13.

9 D.P. Kern, K.Y. Lee, R.B. Laibowitz, and A. Gupta, J. Vac. Sci. Technol. B 9 (1991) 2875.

10 S. Matsui, N. Takado, H. Tsuge and K. Asakawa, Appl. Phys. Lett 52 (1988) 69.

11 A. Enokihara, H. Higashino, K. Setsuna, T. Mitsuyu, and K. Wasa, Jpn J. Appl. Phys. 27 (1988) L1521.

12 A. Inam, X.D. Wu, T. Venkatesan, S.B. Ogale, C.C. Chang and D. Dijkamp, Appl. Phys. Lett 51 (1987) 1112.

13 D.W. Face, J.M. Graybeal, T.P. Orlando and D.A. Rudman, Appl. Phys. Lett 56 (1990) 1493.

14 F.K. Shokoohi, L.M. Schiavone, C.T. Rogers, A. Inam, X.D. Wu, L. Nazar, and T. Venkatesan, Appl. Phys. Lett 55 (1989) 2661.

15 I. Shih and C.X. Qiu, Appl. Phys. Lett 52 (1988) 1523.

16 Y. Yoshizako, M. Tonouchi, and T. Kobayashi, Jpn J. Appl. Phys. 26 (1987) L1533.

17 C. W. Yuan, A.B. Berezin, and A.L. de Lozanne, Appl. Phys. Lett 60 (1992) 2552.

18 F.J. Muller, J.C. Gallop, J.R. Laverty, M.A. Angadi, A.D. Caplin, S. Labdi, and H. Raffy, *Symposium on high T_c thin films at ICAM 91*, Strasbourg, France *"High T_c superconductors thin films 1992*" ch. 132, pp. 587-591

Table 3.1. The reduction in room temperature resistivity of some Bi-2212 samples wet chemical etched in EDTA/H_2O and 0.9% HCl (first three samples, 95, 98 and 132), with annealing at 700°C for 7 h in air. All these measurement were taken from 150μm wide 1cm long meander-type pattern.

Sample Number	Room temperature resistivity (Ωcm)		reduction ratio (%)
	After etching	After annealing	
95	1.05×10^{-2}	1.47×10^{-3}	86
98	6.75×10^{-3}	1.16×10^{-3}	83
132	9.00×10^{-3}	1.32×10^{-3}	85
133	1.54×10^{-3}	4.50×10^{-4}	71
253	5.07×10^{-3}	1.45×10^{-3}	71
257	1.24×10^{-3}	7.51×10^{-4}	39
291	1.11×10^{-3}	6.58×10^{-4}	41
292	2.21×10^{-3}	9.23×10^{-4}	58
297	3.41×10^{-3}	1.40×10^{-3}	59
309	8.55×10^{-4}	5.50×10^{-4}	36
310*	5.38×10^{-4}	5.22×10^{-4}	3

*This sample is on $SrTiO_3$ substrate. The others are on MgO substrates

Table 3.2. The reduction in room temperature resistance of a Bi-2223 film wet chemical etched in EDTA/H_2O with annealing at 700°C for 7 h in air. These measurement were taken from three different SQUID patterns on the same sample.

The width of constrictions	Room temperature resistance (Ω)		reduction ratio (%)
	After etching	After annealing	
20 μm	925	233	75
40 μm	485	185	62
80 μm	453	160	65

(a)

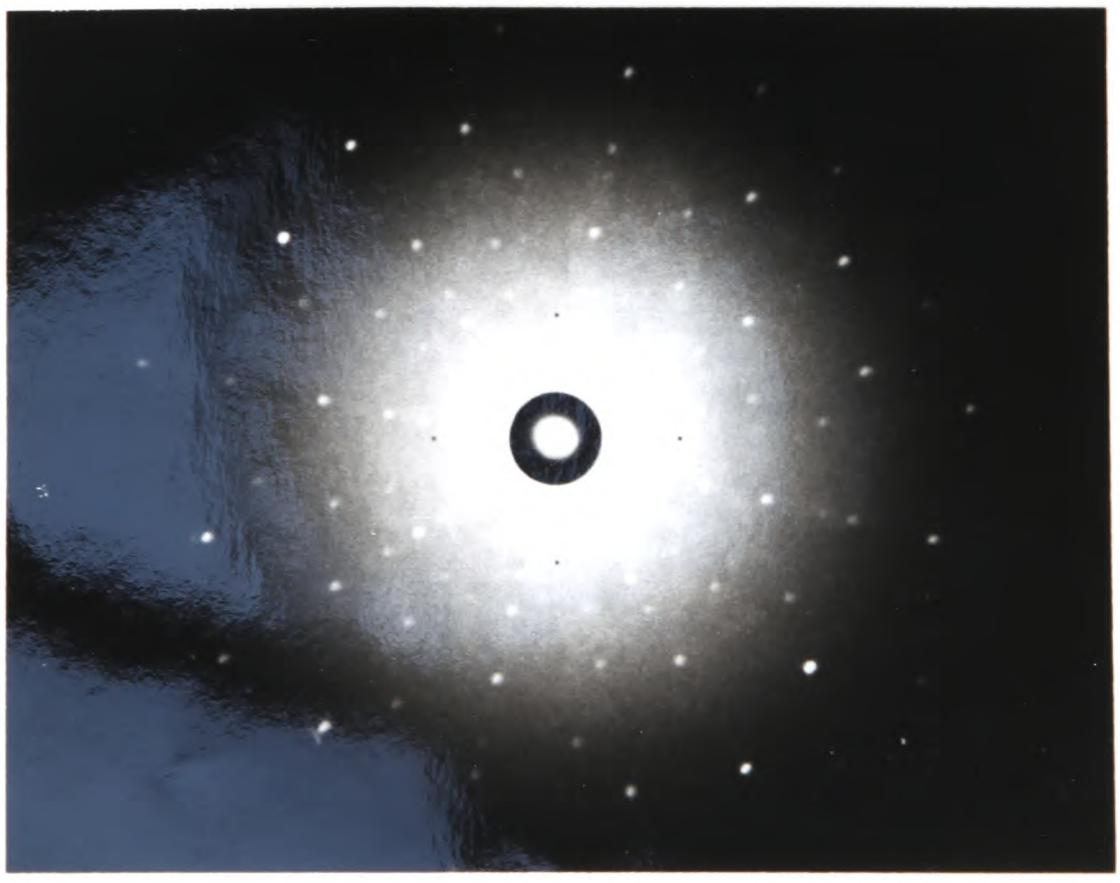

(b)

Figure 3.1 Back reflection Laue photographs of a single crystal (a) MgO [100] (b) $SrTiO_3$ [100] substrates, beam approximately along [100].

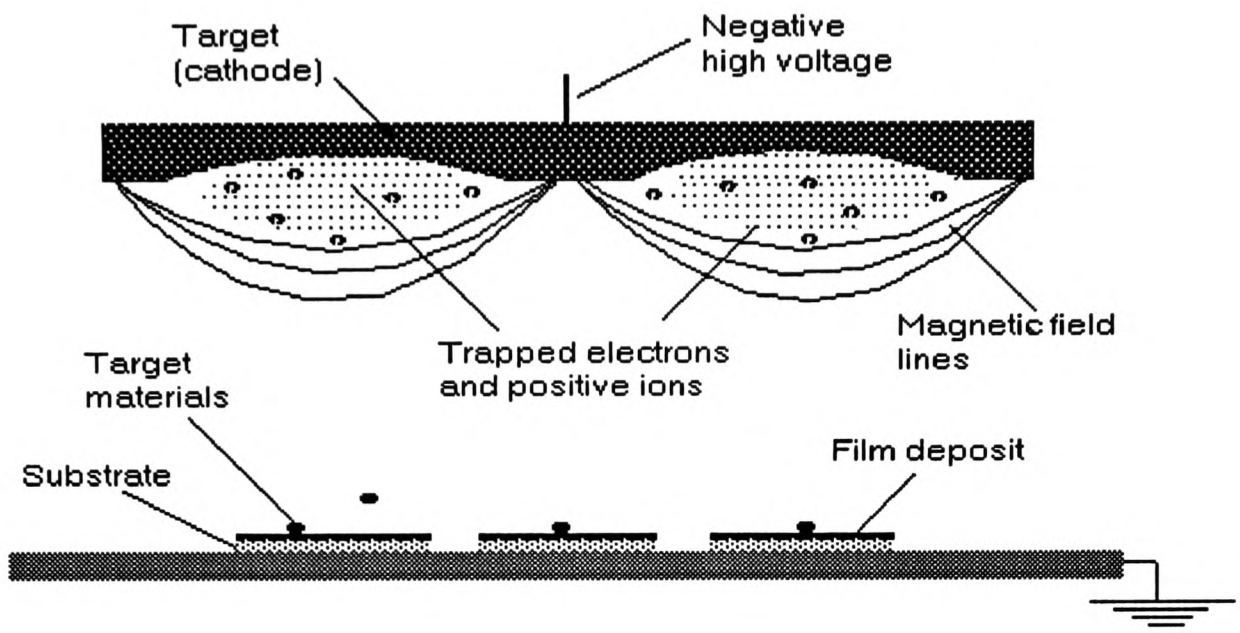

Figure 3.2 Cross section of planar magnetron

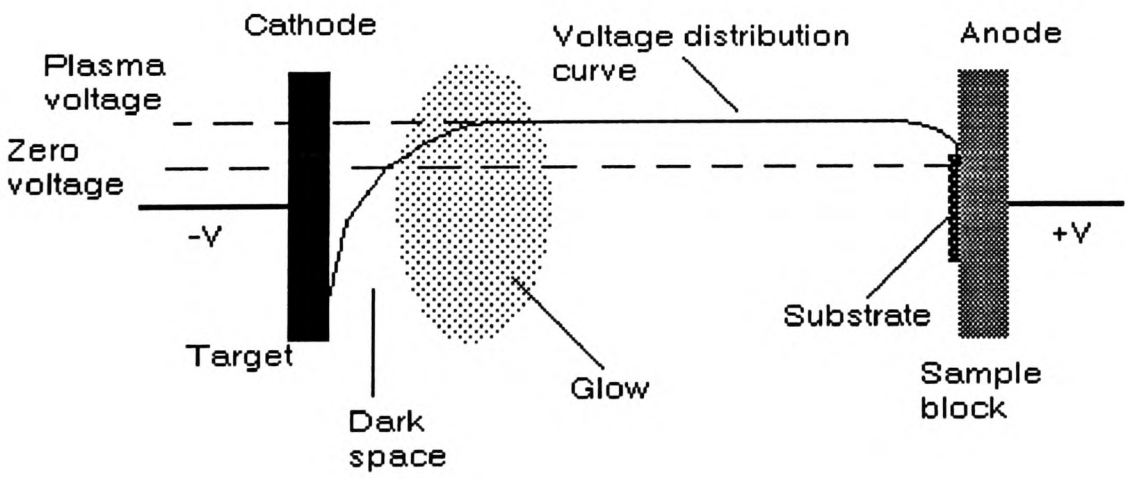

Figure 3.3 Voltage distribution in a DC discharge

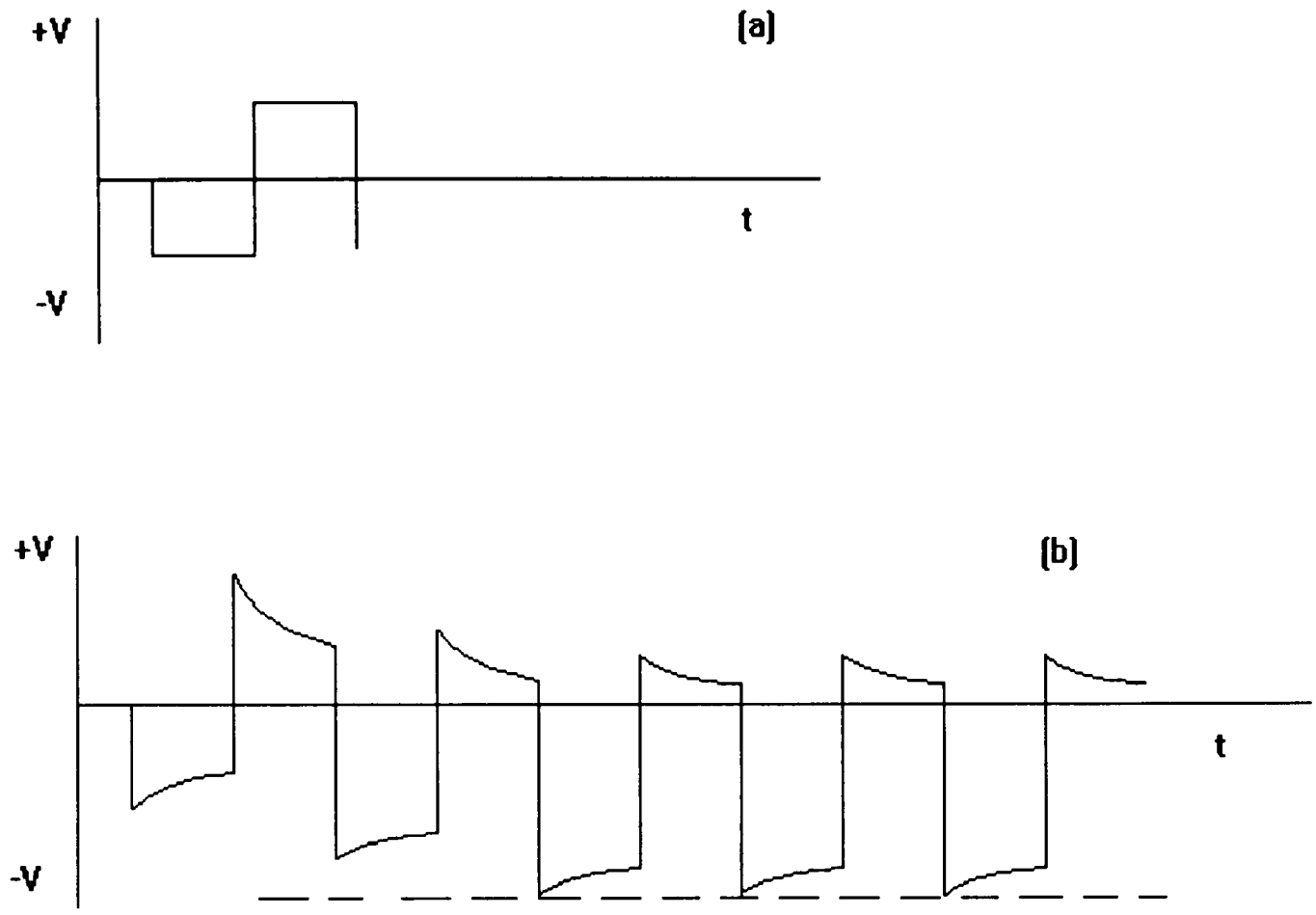

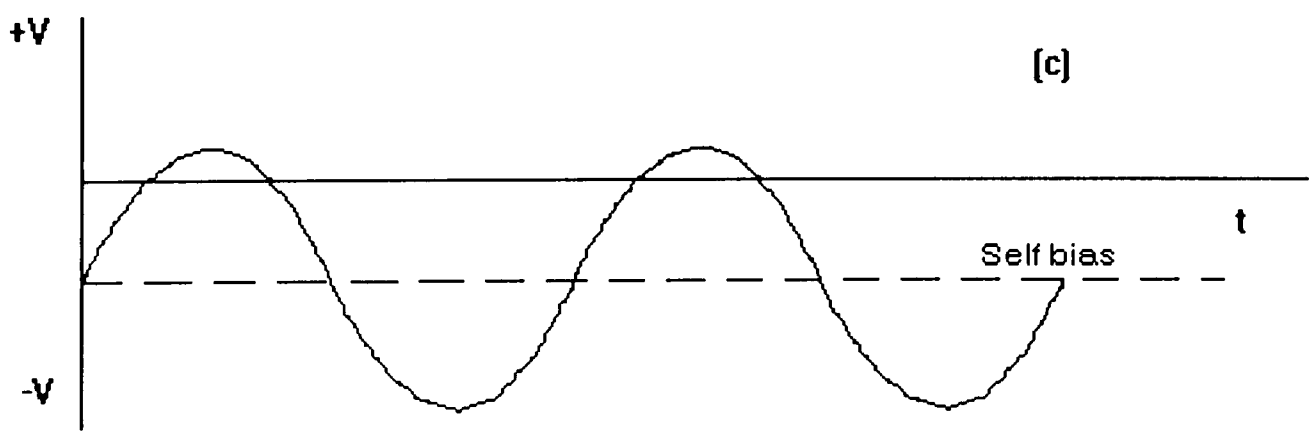

Figure 3.4 (a) Applied voltage (b) Variation of target voltage with time on application of an alternating square wave voltage (c) Actual voltage variation developed at target during the application of an oscillating voltage

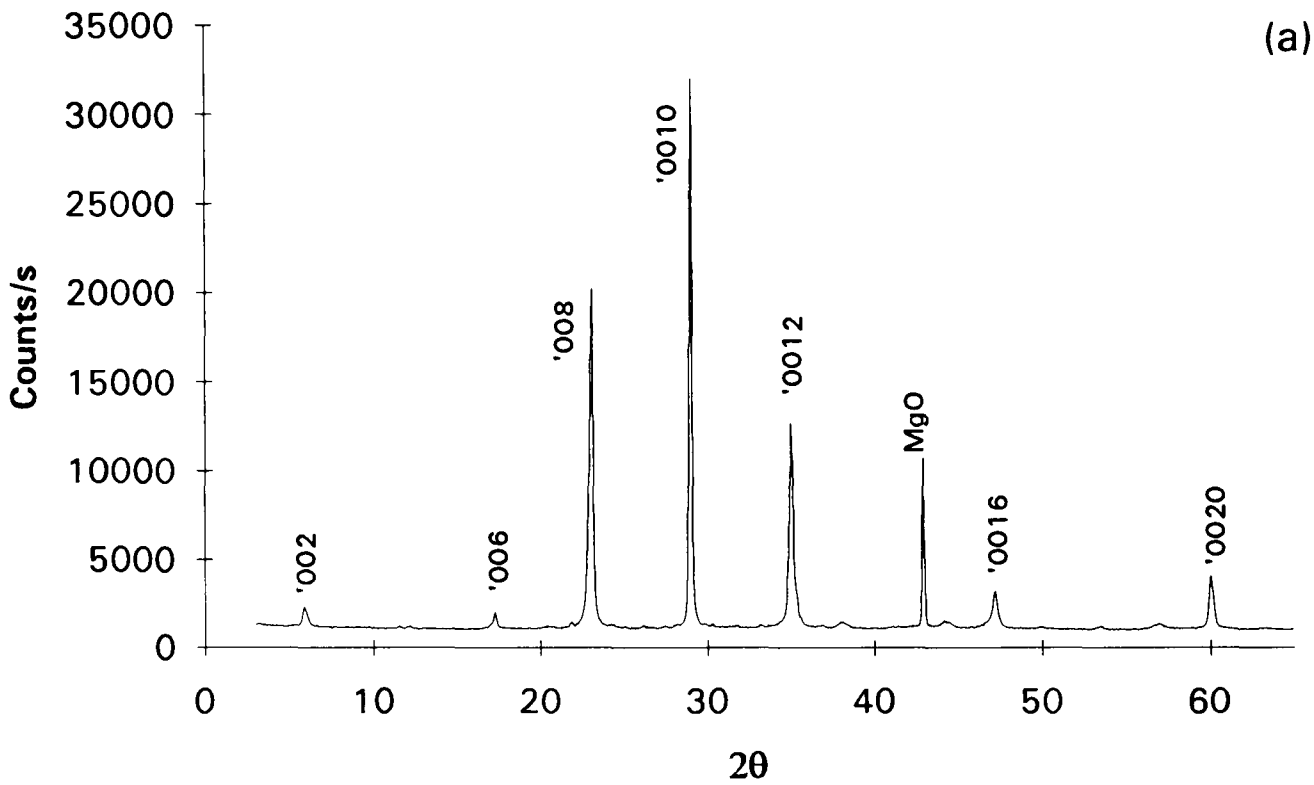

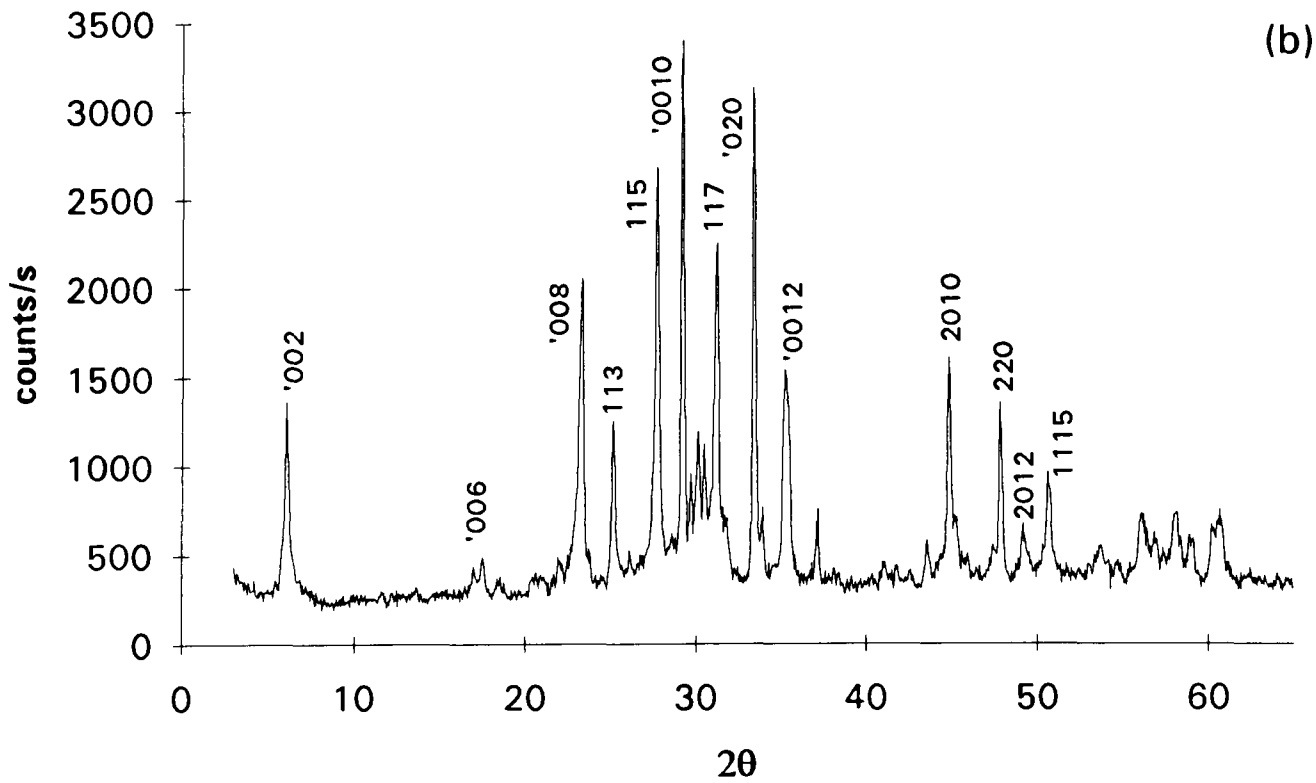

Figure 3.5 A comparison of the XRD patterns taken from: (a) completely c-axis oriented thin film and (b) pressed 2212 powder pellet which has partially preferential c-axis orientation due to the pressing process.

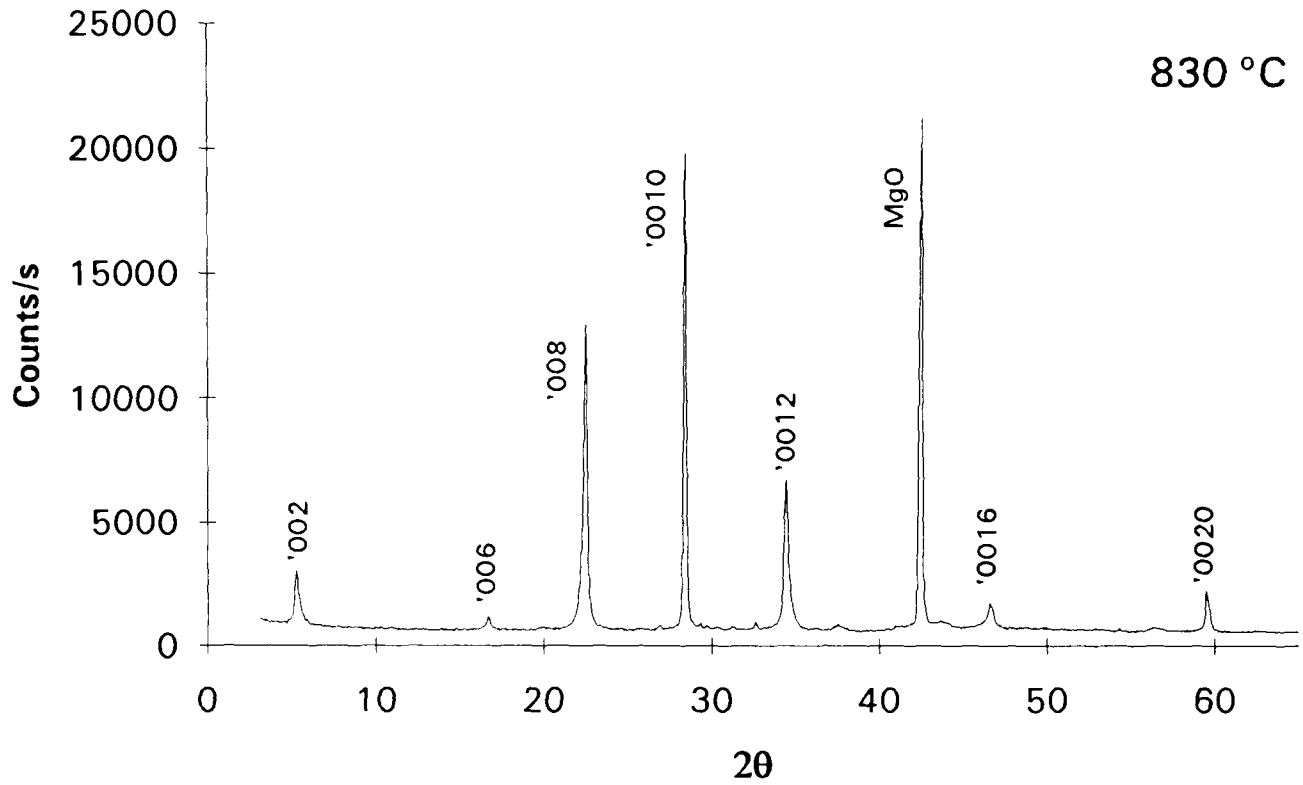

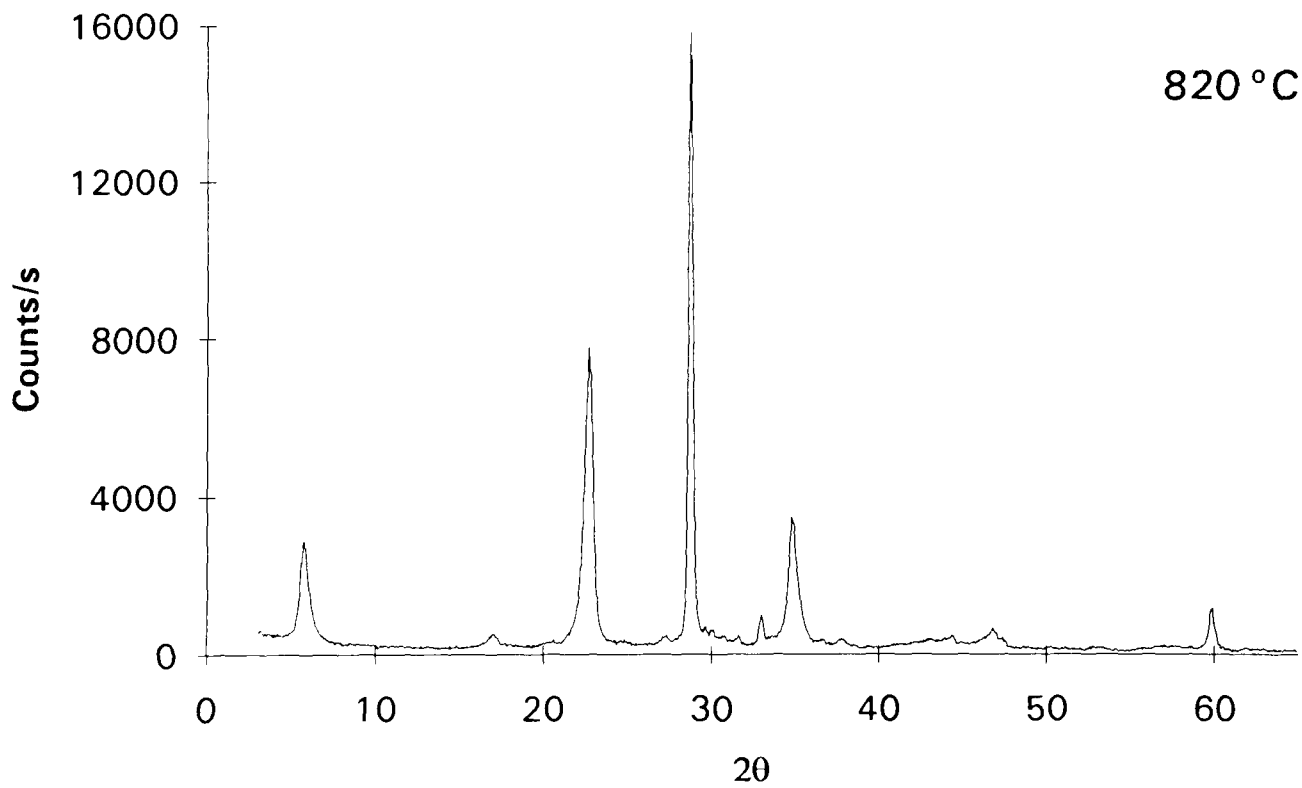

Figure 3.6 The effect of annealing temperature on line broadening of XRD patterns of Bi-2212 films annealed for 10 h at different temperatures.

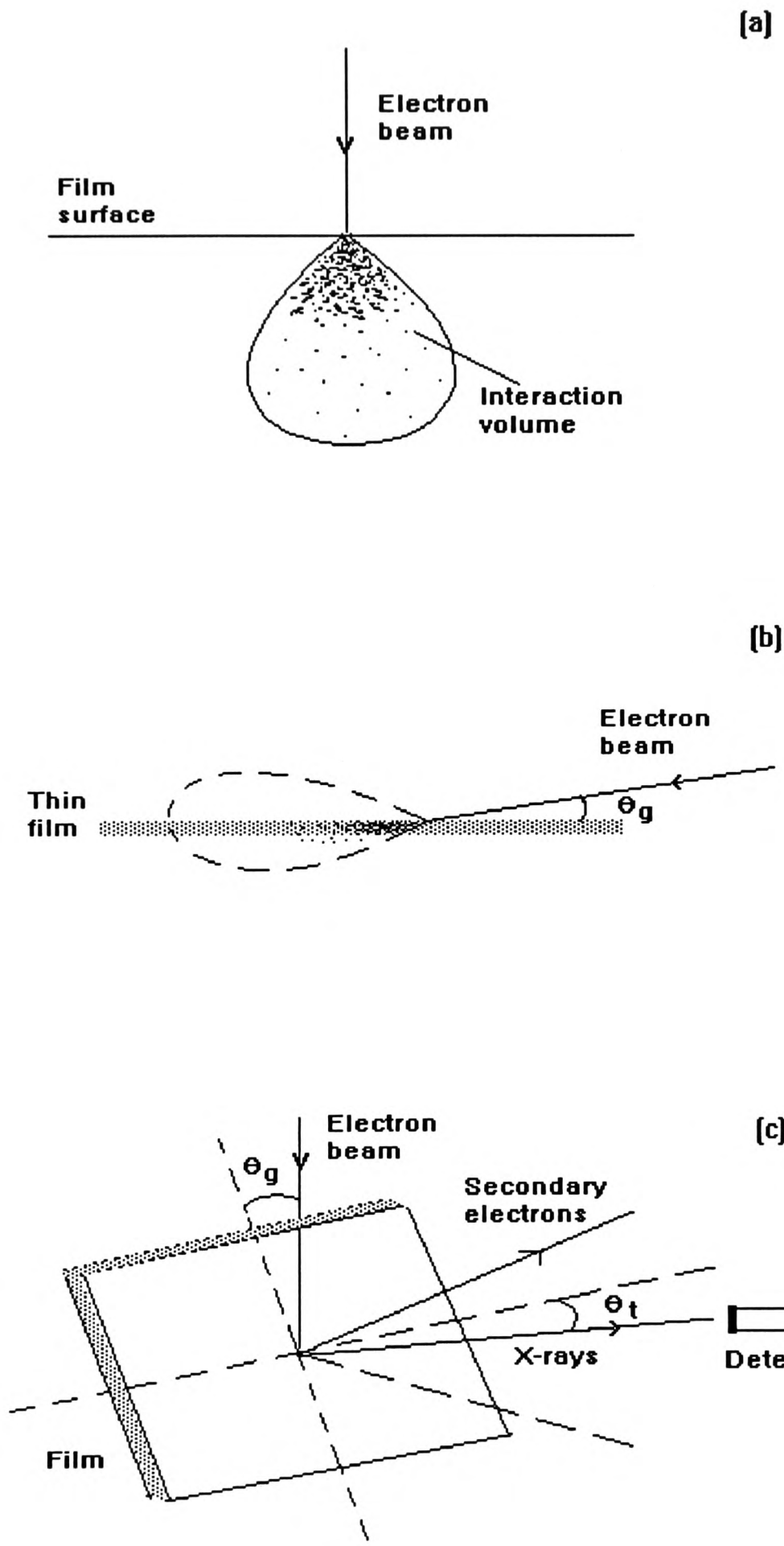

Figure 3.7 Representation of interaction volume examined by EPMA. (a) In case of flat sample (b) In case of tilted sample (c) Schematic representation for tilted configuration.

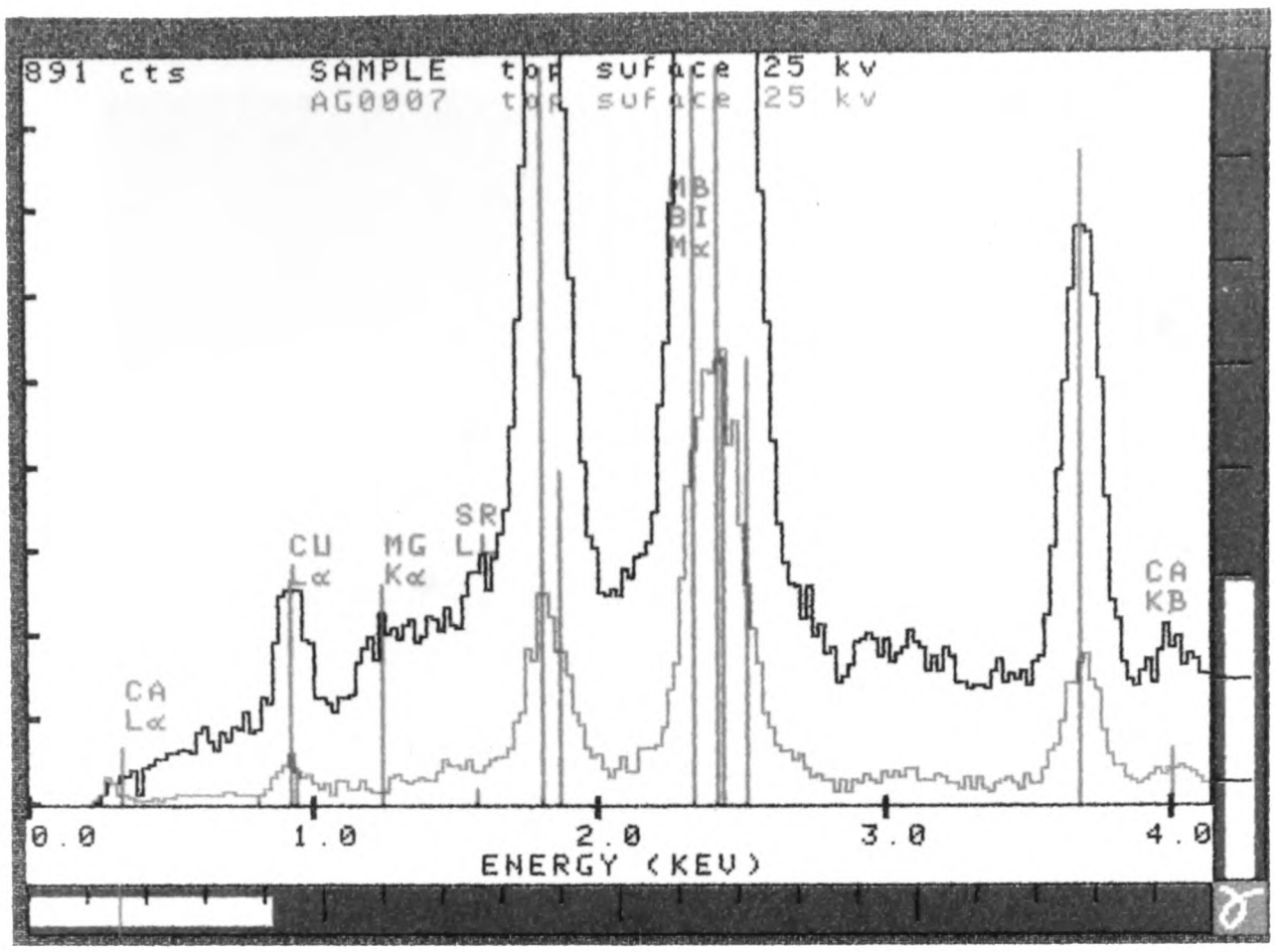

(a)

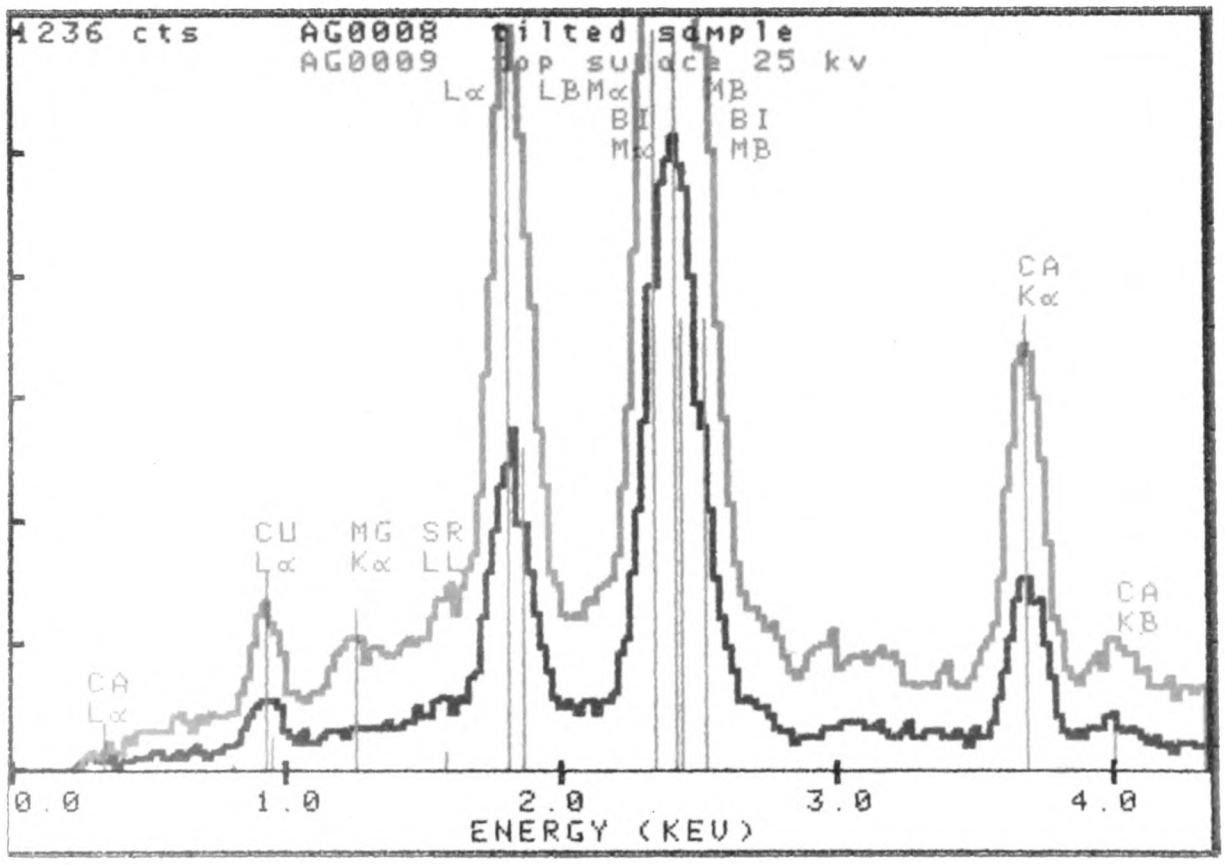

(b)

Figure 3.8 EDS spectrum of an as-deposited Bi-2223 thin film for tilted samples ($\theta = 5^{o}$). Take off angle for the lower spectrum (a) 4^{o} (b) 33^{o}. Upper spectrum in both figures was obtained from standard configuration (flat sample, $\theta_g = 90^{o}$, $\theta_t = 62^{o}$)

Figure 3.9 Back reflection Laue photographs of a (a) single crystal $LaAlO_3$ [100] substrate (b) 0.5 μm thick Bi-2223 thin film on the same $LaAlO_3$ substrate.

(a)

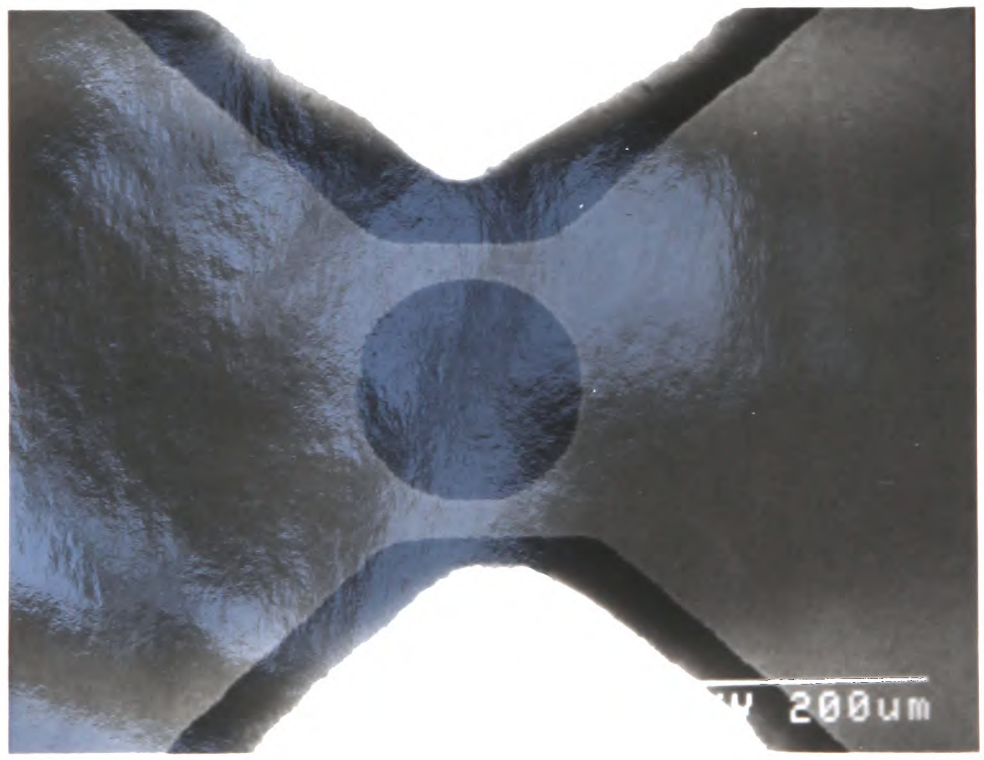

(b)

Figure 3.10 A photograph of a (a) a meander strip (b) a DC SQUID patterned using EDTA/H_2O as etchant.

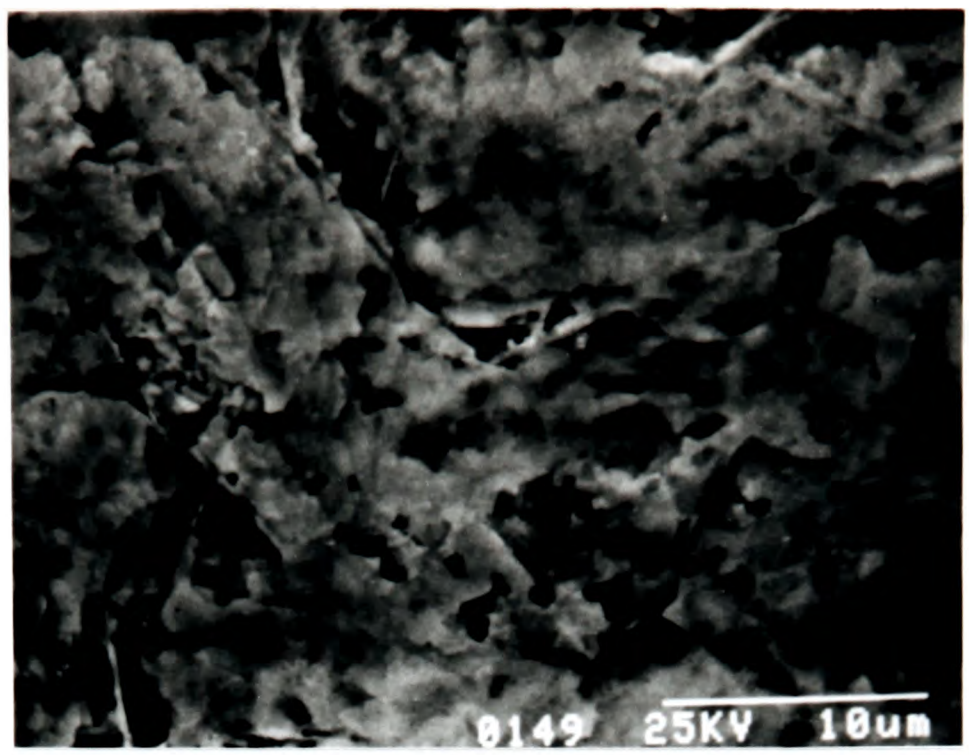

(a)

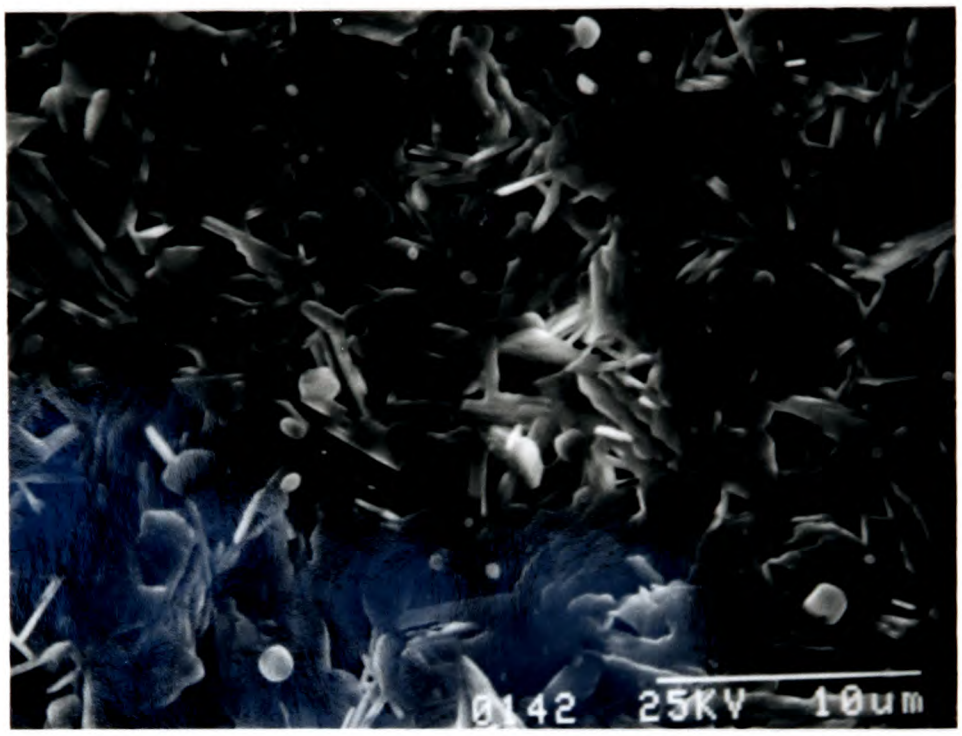

(b)

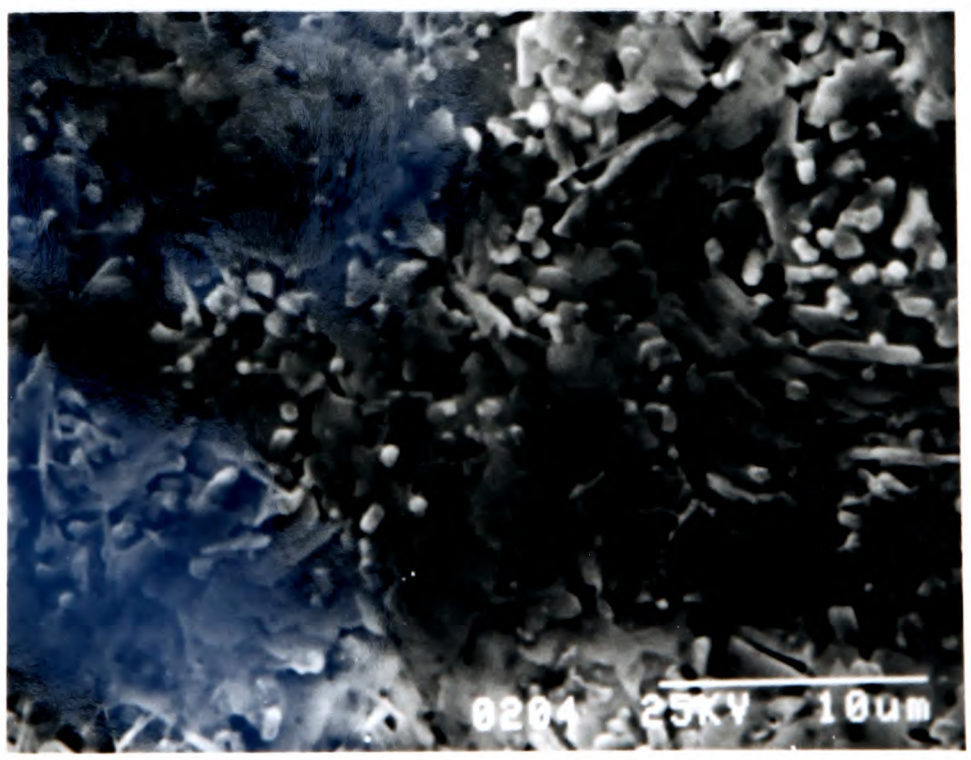

(c)

Figure 3.11 SEM micrographs of some Bi-2212 film (a) sample 133 (b) sample 291 (c) sample 310 (on $SrTiO_3$).

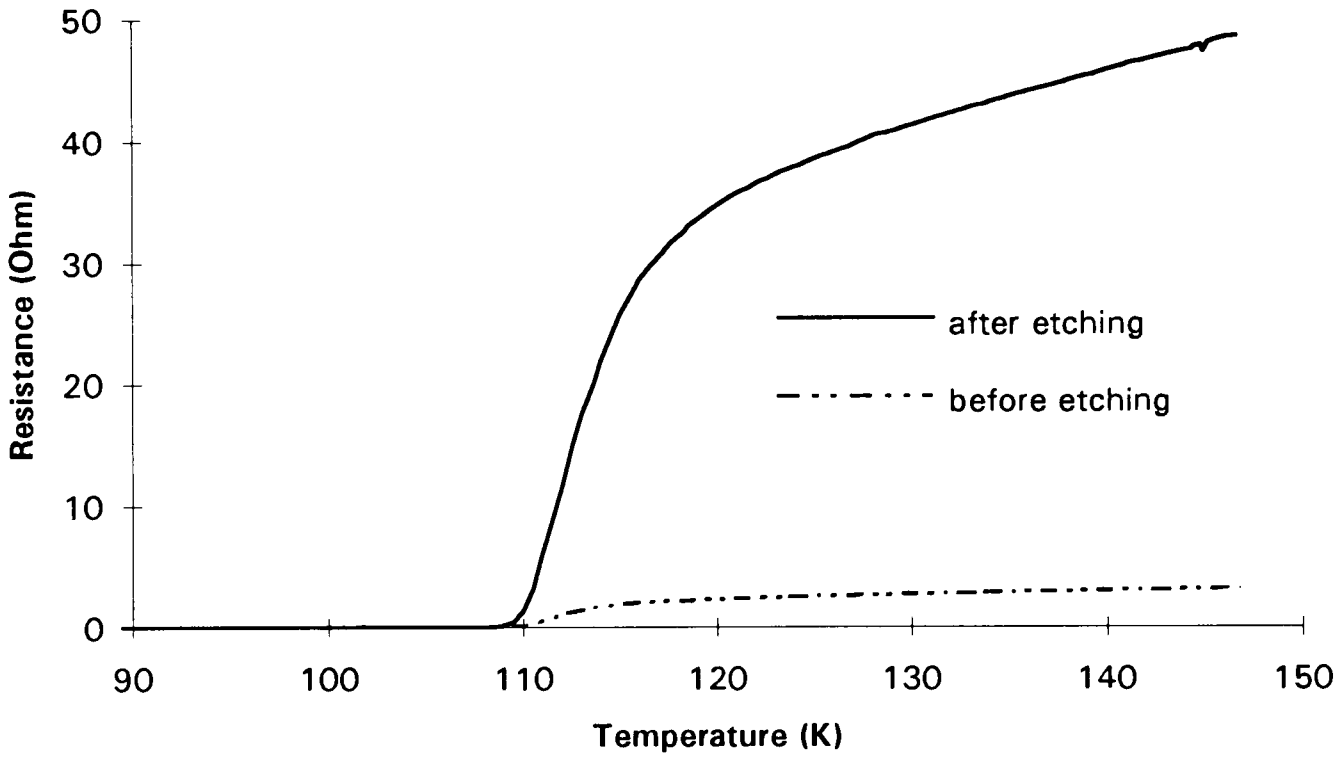

Figure 3.12 Temperature dependence of resistance of a sample before and after patterning with wet chemical etching in EDTA.

CHAPTER 4

Sputtering and process conditions for Bi-2212 thin films

4.1. Introduction

The development of reproducible and stable processes for homogeneous deposition of high quality and large area high T_c films is crucial for the fabrication of many superconducting devices. Plasma sputtering techniques have been widely pursued and proved suitable for the fabrication of high T_c thin films [1, 2]. However, the method is not completely understood, in particular, for the BSCCO system. Sputtering in a glow discharge environment is rather complicated [3]. Therefore, it is known that control of the "global" parameters alone does not lead to a stable and reproducible deposition [4]. One of the key issues concerning the proper study of film characteristics as a function of one growth variable is stoichiometrical control. An understanding of the influence of the growth variables on composition may lead to progress in overcoming these impediments to useful studies of BSCCO thin films.

This chapter will describe work performed in making superconducting thin films of Bi-2212 by a rf magnetron sputtering technique. As mentioned above there are many parameters affecting film properties, but most important is the control of film stoichiometry. It would be nonsense to discuss the effect of other parameters on film properties unless we make sure that film stoichiometry is constant. Therefore film properties were assessed together with film composition. All films described here were grown on MgO single crystal

substrates with voltage leads for electrical measurements 1 mm apart unless otherwise stated.

The work on Bi-2212 was undertaken principally as a precursor to that on Bi-2223 described in the following chapter. Many research groups had already successfully prepared 2212 by both ex-situ and in-situ techniques, but comparison with films prepared in the particular sputtering equipment available in Oxford was felt to be a worthwhile undertaking. Furthermore, as will be seen below, considerable understanding was gained on the effect of several sputtering and processing parameters.

4.2. The effect of the sputtering conditions on film composition

The composition of as-deposited Bi-2212 thin films has been investigated as a function of the rf magnetron sputtering variables, i.e. substrate to target distance, total sputtering gas pressure and aging of the target, in an on-axis configuration. The target used throughout these experiment was prepared from powder of nominal composition of Bi-2212 supplied by BDH and sputtering was conducted in Ar atmosphere. The discharge was run at a rf power level of 50 watt over the 2 in. disk target. The substrates were not intentionally heated to gain a near-unity sticking coefficient for all incoming particles. The temperature during deposition was in the range of 110-120^{o}C. These sputtering conditions, including substrate to target distance of 55 mm and gas pressure 10^{-2}mbar are called "standard deposition conditions" and used throughout these experiment unless otherwise mentioned. The as deposited film metallic compositions were analysed using wavelength dispersive X-ray spectroscopy (WDS) which was carried out on an electron probe microanalyzer (EPMA). All the analysed films were of thicknesses greater than 1μm to ensure that the primary electron beam did not penetrate the films and generate X-rays from substrates.

4.2.1. Substrate-target distance

In order to investigate the effect of substrate to target distance on film composition, this distance was changed between 35 and 95 mm by using a substrate holder with

different lengths. The substrate holder was made from 1.5 mm thick copper plate bent into a right angle for on axis configuration (**Fig. 4.1 a**). All sputtering parameters except for substrate-target distance and sputtering time have been kept constant. Sputtering time has been increased with increasing substrate-target distance to obtain approximately the same film thickness above 1μm, since the deposition rate decreases with increasing substrate-target distance. At least two spots from representative areas of each of the 5x10 mm^2 films were analysed for five samples placed on an Al disk of 40 mm diameter (**Fig. 4.1 b**) for each substrate-target distance to provide the average film composition over ten points from the large Al disk area of 9.62 cm^2. The variation of metallic composition (normalised to Cu:2) with substrate to target distance is shown in **Fig .4.2.** As can be seen from **Fig. 4.2** for distances between 35 and 55 mm the film composition is close to the target composition; Ca, Sr and Bi ratios decrease with increasing substrate-target distance above 55 mm. In this work 55 mm has been used as a near optimum substrate-target distance.

4.2.2. Ar pressure

The effect of the gas pressure on the cation ratio of metallic elements has also been investigated by changing Ar gas pressure through $10^{-2}$to 10^{-1}mbar. **Fig. 4.3** shows the dependence of Ca, Sr and Bi ratios (normalised to Cu:2) in films deposited at 55 mm substrate to target distance. It was found that the Bi ratio in the deposited films is very sensitive to sputtering gas pressure while Sr and Ca are not much affected. The Bi ratio of the deposited film is very close to that of the target for a pressure of 10^{-2}mbar, increasing with increasing Ar pressure. Therefore 10^{-2}mbar was used as an optimum pressure value providing a film composition which is very close to the target composition.

4.2.3. Target aging

The effect of time of target use on film composition was investigated over 72 hours. Before deposition a newly prepared target was presputtered for 15 minutes. For this experiment one film placed at the same position on the substrate holder for each run, was

kept for metallic composition analysis. All films used for this purpose were deposited under the same sputtering conditions. At least two spots from representative areas of each film were analysed to provide the average film composition. **Fig .4.4** shows the dependence of the metallic composition of films on the age of the target. This figure shows that over approximately 12 hours sputtering the Sr and Bi ratio in the deposited film decreases and becomes almost stable over a long period of 60 h. Therefore it is suggested that presputtering of a newly prepared target for at least 12 h is required to reach a steady state condition. Oxygen out-diffusion from the target surface, aided by ion impingement, is believed to be responsible for causing changes in the target and therefore a compositional variation of the sputtered films under the pure Ar atmosphere as the sputtering time increases. Introduction of oxygen into the vacuum chamber at a level of no less than $1.3x10^{-3}$mbar might be an alternative to long presputtering [5].

4.2.4. Deposition rate

The effective parameters on the deposition rate are substrate to target distance, rf power, sputtering gas pressure and, specially for multicomponent high T_c superconductors, the aging of the target. The effect of the first two parameters is well known, being that deposition rate increases with decreasing substrate to target distance and increasing rf power. The effect of target aging on the deposition rate over 60 h accumulated sputtering time and gas pressure for a narrow pressure range around 10^{-1} mbar were investigated in this study and it was found that with increasing gas pressure and aging of the target the deposition rate gradually decreased. The deposition rate of Bi-2212 films as a function of accumulated sputtering time and gas pressure is given in **Fig. 4.5** and **4.6**, respectively.

4.3. The variation of composition over large area

To investigate the variation of composition over large area, substrates were placed on the aluminium disk of 40 mm diameter in the positions shown in **Fig. 4.1 b**. The distance between the centre of the outer substrates and the centre of the disk is 1.5 cm. An analysis

from two points for each position was taken. The variation of the atomic concentration of metallic cations with substrate position for a substrate target distance of 55 mm is shown in **Fig. 4.7**. This result revealed that there is no significant change of film composition from position to position in the range studied.

4.4. Peeling off of thin films

The main difficulty encountered in growing thin film by this process was the peeling off of films during ex-situ annealing, even at rather low temperatures, such as below 500^{o}C. Initially several reasons for the peeling off were considered such as: (1) substrates not chemically well enough cleaned, (2) heating rate, (3) starting temperature of annealing, (4) film thickness and finally (5) thermal expansion mismatch between substrate and deposited film due to wrong composition of films.

In order to clean the polished substrates chemically they were washed first in acetone then in de-ionised (DI) water with ultrasonic vibration before loading into the furnace for high temperature annealing at above 1000^{o}C. Substrates cleaned in this way were placed in the chamber without touching their surfaces. The as-deposited film thickness was less than 1μm with a light brown colour. The annealing process was started from room temperature with a ramping rate of 1^{o}C/minute. But again films sometimes completely and sometimes partly peeled off from the substrates above 400^{o}C. Keeping this routine process the study has been focused on the thermal expansion mismatch between film and substrate due to wrong composition of the film. All films which had not peeled off, or which had partly stayed on the substrate, had the XRD pattern of the phase of interest when they were annealed at a suitable temperature.

To investigate the composition effect on the peeling off mechanism, EPMA analysis has been done for a film taken from each batch from the same position on the substrate holder. **Fig. 4.8 a** shows the ratio of atomic cations (Bi, Sr and Ca normalised to Cu:2) for the peeled off films. This figure also shows the Bi/Sr ratio. It can be seen from the figure that apart from runs 2-4, which have a Bi/Sr ratio less than 0.9, all the others have a Bi rich

composition. On the other hand, apart from runs 14-16, the Bi/Sr ratio is above 0.9 and not more than 1 for unpeeled films (**Fig. 4.8 b**). This analysis suggests that the peeling off mechanism may be related to the Bi/Sr ratio; if it is less than 0.9 or above 1 peeling off of the film during high temperature annealing may occur. However, the question of why when the Bi/Sr ratio is too high (runs 14-16, **Fig 4.8 b**) or too low (not on the figure) the film did not peel off, is still open.

4.5. The affect of sintering conditions on film properties

4.5.1. Annealing temperature

Films from the stoichiometric Bi-2212 single target under the standard sputtering condition as deposited on cold substrates were uniform, shiny and insulating. The composition of a typical as-deposited film was $Bi_{1.96}Sr_{1.96}Ca_1Cu_{2.4}$ (normalised here to Ca:1). Clearly the composition of the films differs from that of the target in that it is rich in Cu. However, this composition was not fixed, the ratio of (Ca+Sr)/Bi being changed between 1.41 and 1.56 for the films used to study the effect of annealing temperature on the as deposited films, but they were all rich in Cu. Crystallisation of the desired superconducting phase was achieved during high temperature annealing in air. Films were slowly heated a with ramping rate of 2^oC/min. from below 500^oC to the desired annealing temperature and sintered at different temperatures for more than 6 h, then slowly cooled at a rate of 2^oC/min. to 600^oC. Below 820^oC and above 845^oC Bi-2212 has formed together with Bi-2201 phase. **Fig. 3.6** (previous chapter) and **Fig. 4.9** show XRD-patterns of some films annealed at between 820^oC and 845^oC. XRD patterns of these films revealed that almost single phase Bi-2212 can be obtained in a temperature range of width at least 25^oC. However, as can be seen from XRD patterns, the best textured film was obtained for the annealing temperature regions of 830-835^oC with a c-axis lattice parameter of 30.22 A^o. The width of the reflections indicates the presence of faults in samples annealed above or below this temperature region. Nevertheless (00l) reflections of the phases Bi-2201 and Bi-

2212 are difficult to resolve in a $\theta/2\theta$-scan, e.g. the positions of (0010) for Bi-2212 and (008) for Bi-2201 differ by less than 0.1^{o}.

The effect of annealing temperature and substrate on the microstructure of the film are presented in **Fig. 4.10** for some samples taken from the same sputtering batch and annealed in air for 10 h. The as deposited compositions of these films are supposed close to each other with a (Ca + Sr)/Bi ratio of 1.47. It is clear from the microstructure of these films that the sample annealed at 820^{o}C is more granular and contains more needle type structure (**Fig. 4.10 a**) than the sample annealed at 830^{o}C (**Fig. 4.10 b**) (both on MgO substrates). Annealing at relatively high temperature increased the grain size while reducing the amount of needle type structure. However, the film grown on $SrTiO_3$ and annealed together with the latter film (at 830^{o}C) has much better microstructure with well connected plate like grains. The difference between the microstructure of these samples may be attributed to the different nature of the substrate material, indicating that the adopted annealing condition is very suitable, at least for this composition, for films grown on $SrTiO_3$.

Fig. 4.11 shows the temperature dependence of resistivity for the samples annealed at different temperatures for longer than 6 h in air. The highest temperatures of onset and zero resistance are 96K and 82K, respectively for the sample annealed at 830^{o}C which has a (Ca + Sr)/Bi ratio of 1.41 (curve b). An increase of 0.5 in the (Ca + Sr)/Bi ratio did not affect the transition temperature ($T_{c\text{-}zero} = 82$K) while it reduces the $T_{c\text{-}onset}$ by 3K (curve c). The sample annealed at 820^{o}C showed poor superconducting properties with a long transition tail of 50K ($T_{c\text{-}zero} = 44$K, curve a). Another sample, having the same (Ca + Sr)/Bi ratio of 1.55 to that of the sample annealed at 820^{o}C, showed zero resistance at 71K with a $T_{c\text{-}onset}$ of 92K when it was annealed at 835^{o}C (curve d).

The effect of annealing temperature is clear for the later two samples having similar compositions, but it is really difficult to conclude for the first sample, which has different composition than the others, whether it is a composition effect or temperature effect. However, it is clear from the resistivity curves b and c, superconducting properties have

improved with increasing (Ca + Sr)/Bi ratio to the nominal value when they were annealed at 830°C.

4.5.2. Composition effect

In order to understand the composition effect on T_c a series of samples having different (Ca + Sr)/Bi ratios between 1.4 and 1.65 were annealed at 830°C for more than 10 h. **Fig. 4.12** shows the $T_{c\text{-}zero}$ and $T_{c\text{-}onset}$ dependence on (Ca + Sr)/Bi ratio. This figure suggests that $T_{c\text{-}zero}$ of around 80K is achievable for (Ca + Sr)/Bi ratio between 1.4 and 1.65 while $T_{c\text{-}onset}$ remains above 90K. However $T_{c\text{-}zero}$ is above 80K for the ratio below 1.54 while it is below 80K for higher values of the ratio. With respect to this result, the question of the low critical temperature value for the sample annealed at 835°C can be explained as a combined effect of composition and annealing temperature.

Fig. 4.13 shows the resistivity dependence on temperature for samples having different (Ca + Sr)/Bi ratios annealed at 835°C for 3 h. The sample with a high (Ca + Sr)/Bi ratio of 1.95 showed poor superconducting properties with low $T_{c\text{-}onset}$ and $T_{c\text{-}zero}$ of 79K and 38K, respectively. The ratio of 1.59 has provided a narrow transition temperature of 10K with a $T_{c\text{-}zero}$ temperature of 74K, supporting the above conclusion. SEM micrographs of these films are illustrated in **Fig. 4.14**, indicating that high (Ca + Sr)/Bi ratio resulted in a pure microstructure which is consistent with the resistivity curve. The transition curve corresponding the (Ca + Sr)/Bi ratio of 1.55 has already been described in the previous section (**Fig. 4.11** curve d).

4.5.3. The effect of quenching temperature

Two films taken from the same batch were annealed at 835°C for 6 h in air and then one of them quenched from the annealing temperature to room temperature in air. The other was cooled to 500°C with a ramping rate of 2°C/min. then air quenched. The crystal structure of the films was found to remain uneffected by quenching temperature (**Fig. 4.15**). However there is a significant difference in the superconducting behaviours. $T_{c\text{-}zero}$ and $T_{c\text{-}}$

onset for samples quenched from 835°C and 500°C are 77K, 90K and 71K, 92K, respectively (**Fig. 4.16**). This variation of T_c is attributed to the oxygen content of the sample [6, 7]. As samples air quenched from the annealing temperature contain less oxygen than those slowly cooled to low temperature before quenching, this result suggests that critical temperature increases with decreasing oxygen content for the Bi-2212 phase [8]. However, the resistivity decreased with increasing oxygen content (the distance between voltage pick up leads was 1 cm for the low temperature quenched sample).The approximate resistivity values at T_c onset temperatures are 0.7 mΩcm and 0.2 mΩcm, respectively, for high and low temperature quenched samples. This result is consistent with that of Balestrino et al. [9], who reported that with increasing oxygen content resistivity and T_c both decrease.

4.5.4. Annealing time

The films have been annealed at 830°C for different periods of time from 10 minutes to 22 hours. **Fig. 4.17** shows the variation of $T_{c\text{-}zero}$ and $T_{c\text{-}onset}$ with annealing period for some samples having (Ca + Sr)/Bi ratio between 1.41 and 1.64. It has been found that Bi-2212 films should be annealed for at least 1 hour to convert the Bi-2201 phase, CuO, CaO (CaCuO) [10, 11] forming at relatively low temperature, into the Bi-2212 phase. **Fig. 4.18** shows XRD patterns of samples annealed at 830°C for 1 hour and 18 hours. It seems from the XRD patterns that prolonged annealing time can improve the structure of the film providing narrow and stronger peaks. SEM micrographs of these films are illustrated in **Fig. 4.19**. Microstructures of these films are similar with plate like grains, but the grain size of the 18 hours annealed sample is almost 5 times larger than that of the film annealed for 1 hour. The temperature dependences of resistivity curves for these samples are consistent with the XRD patterns and microstructure. $T_{c\text{-}onset}$ and $T_{c\text{-}zero}$ (**Fig. 4.20**) for 1 hour and 18 hours annealed films are 96K, 81K and 93K, 82K, respectively; resistivity is lower for prolonged annealing time. However, there is practically no difference between the transitions and XRD spectra of the films annealed for 10 hours and 18 hours.

4.6. Films on different substrates

While the fabrication process was optimised for deposition of films on polished (100) MgO single-crystal substrates, other substrates, such as (100) $SrTiO_3$, ZrO_2, Si single crystals, silver sheet, ZrO_2, diamond, and MgO polycrystal buffer layer on Si were also tested. Best results were obtained for $SrTiO_3$ with a 82K $T_{c\text{-}zero}$ and a narrow transition temperature of 8K (**Fig. 4.21**). Although on silver well textured Bi-2212 was obtained, the microstructure is very poor with large numbers of needle structures, probably Sr(CaCuO). All others were insulators apparently due to film-substrate interaction.

4.7. Long term stability

The long term stability of Bi-2212 films has been studied by measuring the resistive and transport properties of films grown on MgO and $SrTiO_3$ substrates, after several months storage in a plastic bag in a cupboard. **Fig. 4.21** shows the variation of resistance with temperature for the fresh and six months stored sample. The voltage pick up leads were 3 mm apart and were attached to the film without an evaporated silver pad in the fresh sample. There is no degradation in $T_{c\text{-}zero}$ or resistivity of the sample, and the same critical current density was measured in liquid nitrogen after six months.

4.8. Transport properties

The high degree of c-axis orientation is of great importance because of the highly anisotropic physical properties of high T_c materials. Critical current density, J_c, increases with an increasing degree of c-axis orientation. However, these oriented grains must also be well connected to each other to provide high current carrying capability. The critical current density dependence on temperature for the best films grown on MgO and $SrTiO_3$ single crystal substrates is presented in **Fig. 4.22**. Measurement has been carried out on unpatterned, around 1μm thick, films using a 1μV/mm voltage criterion. The values of J_c fall slowly with increasing temperature from 4.2×10^4 A/cm^2 at 20 K to 1.67×10^3 A/cm^2 at 77 K and from 4.3×10^3 A/cm^2 at 20 K to 6.6×10^2 A/cm^2 at 77 K, respectively, for samples

grown on $SrTiO_3$ and MgO. The approximate resistivity values at $T_{c\text{-}onset}$ are 0.2 mΩcm and 2.2 mΩcm, respectively, for these samples. However, J_c is very low when compared to in-situ produced films [12, 13]. Due to the accumulation and segregation of material during high temperature annealing, the effective film thickness is not homogeneous over the substrate.

4.9. Conclusion

The investigation of optimum annealing conditions for ex-situ films such as annealing temperature, annealing time, heating and cooling processes for any high T_c material needs the same composition of the material, otherwise it will not be possible to find out a precise annealing condition which is suitable for the composition of interest. But in the case of the sputtering deposition used here, it was not possible to get reproducible composition in the film due to the spatial inhomogeneities and instabilities of the plasma which lead to inhomogeneous film deposition. As indicated above, the sputtering chamber pressure affecting film composition especially in respect of Bi and Cu is an important parameter which needs very precise control. $T_{c\text{-}zero}$ of around 80K is achievable for (Ca + Sr)/Bi ratio between 1.4 and 1.65, while $T_{c\text{-}onset}$ remains above 90K, but best superconducting properties have been obtained for the (Ca + Sr)/Bi ratio of 1.47, which is quite close the nominal composition.

Substrate target distance up to 55-60 mm may provide a film composition close to the target composition. Rf power more than 50 watt reduces the life time of the target as the localised heating in the "race track" area destroys the initial composition of the target. It has been found that after 12 hours presputtering a target can have a steady state for a long subsequent period of 60 hours or over. The peeling off mechanism for ex-situ annealed thin films was investigated and it was found that the main reason is wrong composition within certain limits. Bi/Sr ratio should be kept between 0.9-1, (which is also essential for stoichiometry) to prevent the peeling off in as-deposited Bi-2212 thin films.

Annealing at 830-835^{o}C for 10-18 hours in air and slow cooling to below 700^{o}C has been found suitable as an annealing condition. It has also been found that quenching temperature affects the superconducting properties of the film. Samples slowly cooled from the annealing temperature to 500^{o}C in air had low T_c compared with samples quenched from the annealing temperature. This effect is attributed to the excess oxygen content for the slowly cooled sample. However resistivity is lower for the sample cooled slowly. It is believed that excess oxygen decreases the anisotropy in the compound [9]. On the other hand, fast quenching from the annealing temperature may induce some micro cracks in the film. Therefore, in order to optimise the oxygen content in the sample, slow cooling in reduced atmosphere can provide better microstructure. No degradation has been detected on the superconducting properties of the Bi-2212 thin film stored in ordinary laboratory conditions for six months and over. Highest critical temperature of 88 K and highest critical current density of 4.2×10^4 A/cm^2 at 20 K to 1.67×10^3 A/cm^2 at 77 K has been measured on samples grown on MgO and $SrTiO_3$ substrates, respectively. These J_c values are not comparable with typical in-situ grown thin films.

4.10. General discussion

The preparation of thin films of these compounds demands an especially precise control of all parameters independently of the employed deposition method. In particular, the composition of the cations and the correct amount of oxygen is of crucial importance for the properties of the films. Furthermore, with a view to potential applications, besides a smooth and homogeneous surface, a high critical current density should be achieved at 77K. Films able to fulfil these demands are best prepared by in-situ methods, since the J_c values of post-annealed films are usually lower by at least one order of magnitude due to a polycrystalline structure in the *ab*-plane. However there are some applications such as bolometric detectors which require polycrystalline thin films rather than epitaxial ones. These applications will be described in chapter 6.

As summarised in chapter 2 section 2.4.1. and **Table 2.5.** for sputtered films several research groups have already successfully prepared Bi-2212 thin films with by in-situ techniques T_c values in the region of 90K and J_c of $1.6x10^5 A/cm^2$ at 77K in zero magnetic field [12]. The attainable critical current density of ex-situ films prepared in the present work is lower than those reported values.

Because of the anisotropy in critical current densities of high T_c superconductors, The *c*-axis alignment is of particular importance. It was frequently reported that the FWHM value of XRD peaks correlated well with J_c values [14]. Relatively broad XRD peaks observed in briefly annealed samples can be substantially narrowed by prolonged annealing [15]. However, even well oriented films exhibit poor transport properties implying that some other factors are operating. It has been reported from the study of YBCO bicrystals that J_c across grain boundaries falls rapidly with increasing misorientation angle [16]. This has later been proven in a number of experiments on YBCO, which show the presence of weak links when some grains have their orientations in the *ab*-plane at large angles.[17, 18]. The other mechanism responsible for low J_c in these ex-situ films is rough surface structure caused by high temperature annealing leading to inhomogeneous effective film thickness. The results which have been described in this chapter are compatible with the observation of these other groups.

References

1 C.B. Eom, J.Z. Sun, K. Yanmamoto, A. F. Marshall, K.E. Luther, T.H. Geballe, and S.S. Laderman, Appl. Phys. Lett. 55 (1989) 595.

2 R.T. Kampwirth, J.M. Grace, D.J. Miller. D.B. McDonald, K.E. Gray, M. Reiten, M. Ascolese, and H. Latvakoski, IEEE Trans. Mag. 27 (1991) 1219.

3 B. Chapman, Glow Discharge Processes, Wiley, New York, 1980, p. 237.

4 U. Kruger, R. Kutzner, R. Wordenweber, G. Mank, and A. Kraemer-Flecken, Appl. Phys. Lett. 62 (1993) 1559

5 Y. Yang, J. Vac. Sci. Technol. A 10 (1992) 3288.

6 J.L. Tallon, R.G. Buckley, P.W. Gilberd, and M.R. Presland, Physica C 158 (1989) 247.

7 G. Triscone, J.-Y. Genoud, T. Graf, A. Junod, and J. Muller, Physica C 185-189 (1991) 793.

8 J. Zhao, M. Wu, W. Abdul-Razzaq,and M.S. Seehra, Physica C 165 (1990) 135.

9 G. Balestrino, M. Marinelli, E. Milani, A. Paoletti: J. Appl. Phys. 73 (1993) 3903.

10 G.R. PAZ-Pujaalt, Physica C 166, (1990) 177.

11 S. Yaegashi, H. Murakami, J. Nishino, Y. Shiohara, and S. Tanaka, Jpn. J. Appl. Phys. 30 (1991) 471.

12 P. Wagner, H. Adrian, and C. Tome-Rosa, Physica C 195 (1992) 258.

13 S. Miura, T. Yoshitake, and N. Shohata, Physica C 165 (1990) 241.

14 Q. Li, O. Meyer, X. X. Xi, J. Geerk, and G. Linker, Appl. Phys. Lett. 55 (1989) 1792

15 M. Lelental, S. Chen, S.-T. Lee, G. Braunstein, and T.N. Bloanton, Physica C 167 (1990) 614.

16 D. Dimos, P. Chaudhari, and J. Mannhart, Phys. Rev. B 41 (1990) 4038.

17 D.K. Lathrop, B.H. Moeckly, S. E. Russek, and R.A. Buhrman, Appl. Phys. Lett. 58 (1991) 1095.

18 D.H. Shin, J. Silcox, S.E. Russek, D.K. Lathrop, B. Moeckly, and R.A. Buhrman, Appl. Phys. Lett. 57 (1990) 508.

(a)

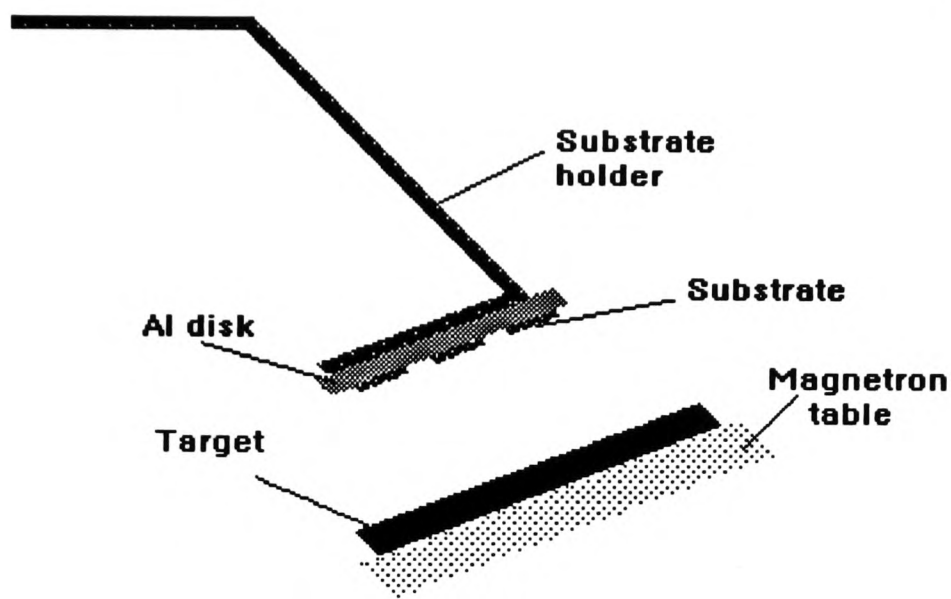

(b)

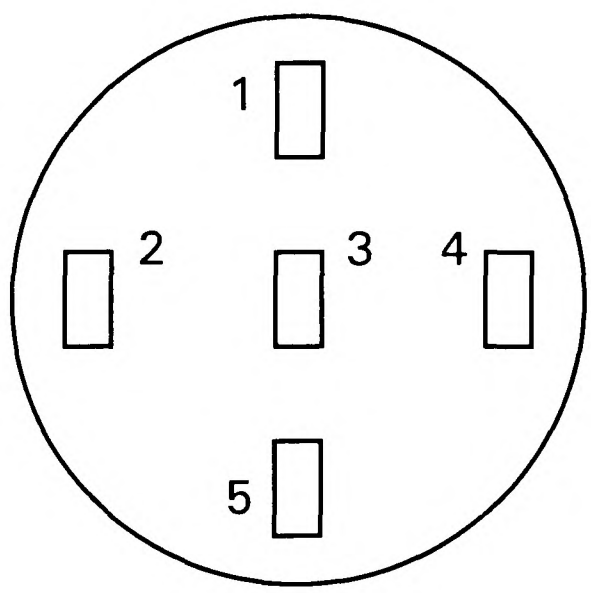

Figure 4.1 (a) On-axis position of substrates with respect to the target surface (b) The position of the substrates on the Al disk holder.

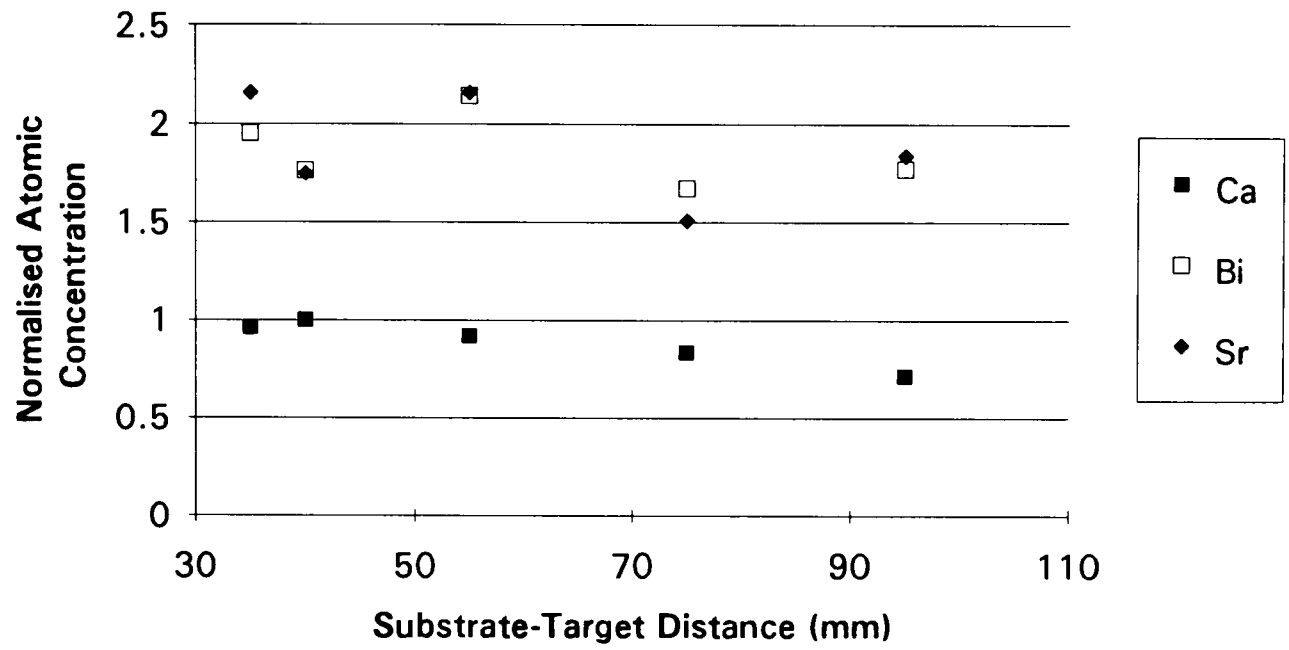

Figure 4.2 The variation of film composition deposited from the Bi-2212 target of nominal composition, with substrate to target distance.

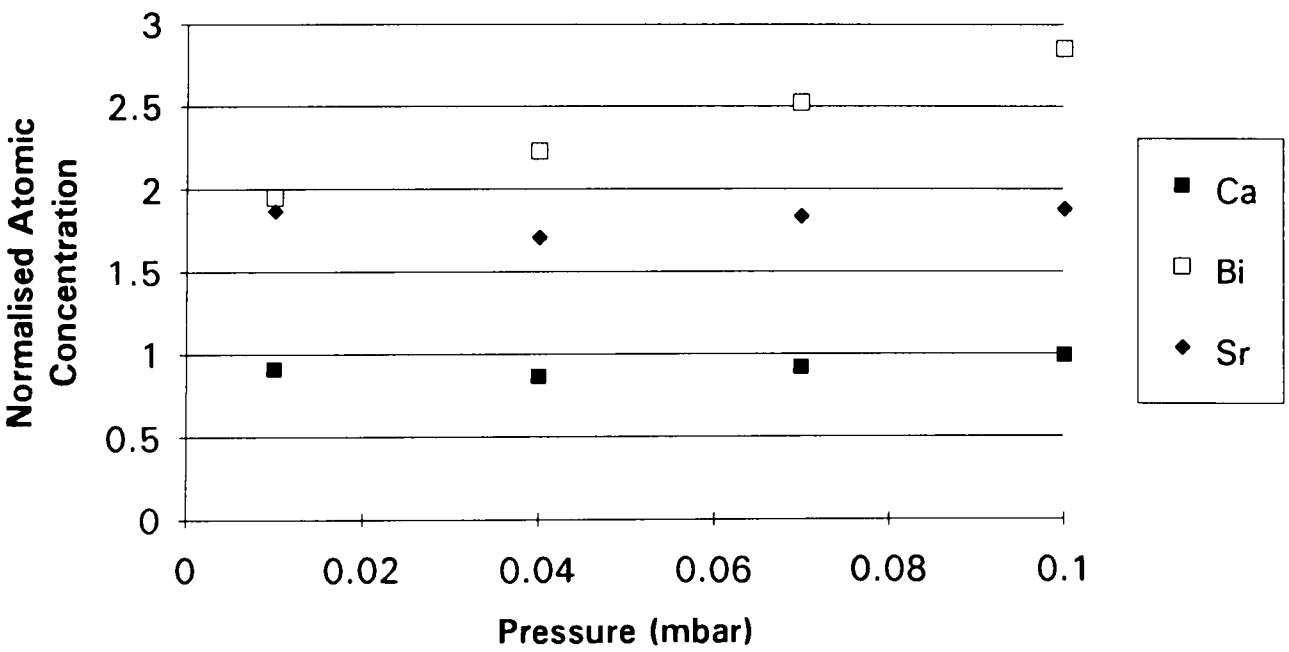

Figure 4.3 The dependence of as-deposited film composition on the sputtering chamber gas pressure for the target of nominal Bi-2212 composition

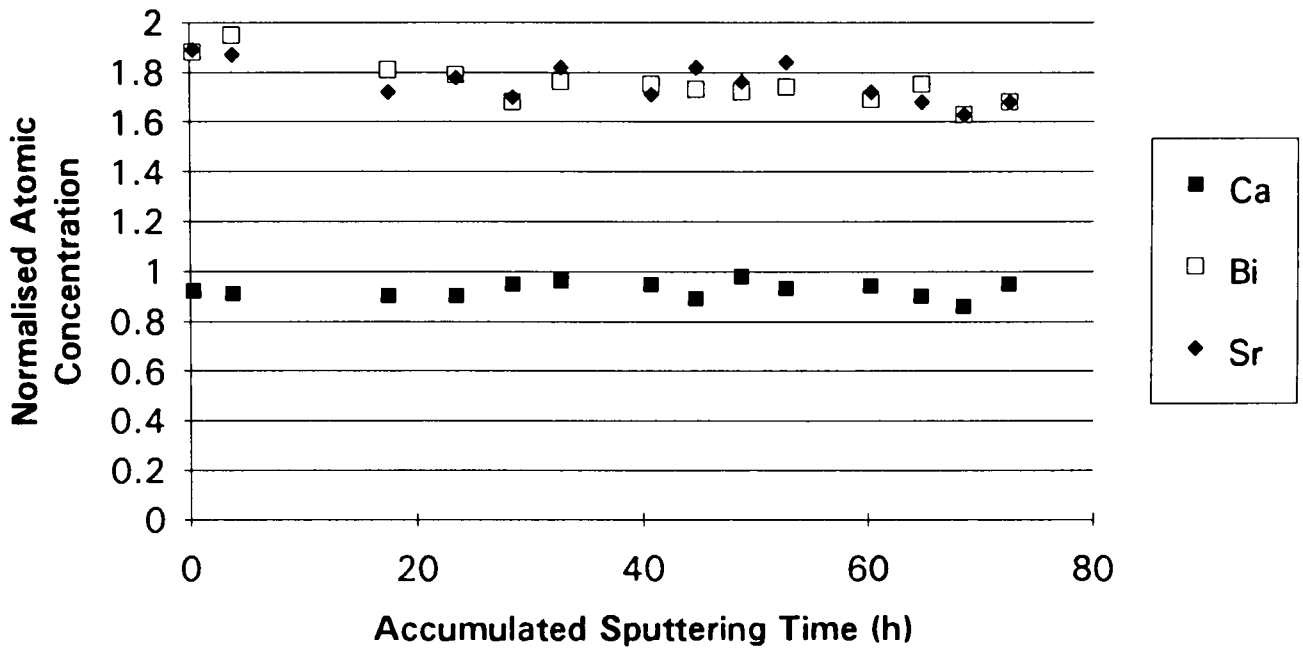

Figure 4.4 The dependence of as- deposited film composition on target aging.

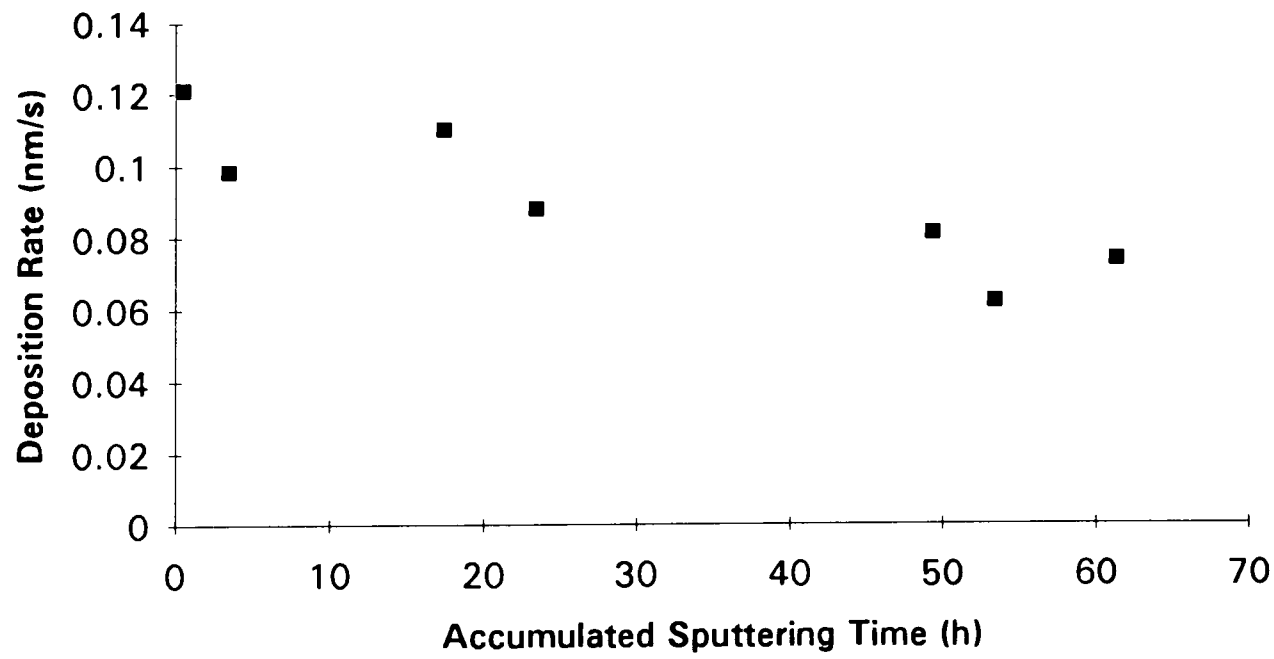

Figure 4.5 The dependence of deposition rate on accumulated sputtering time

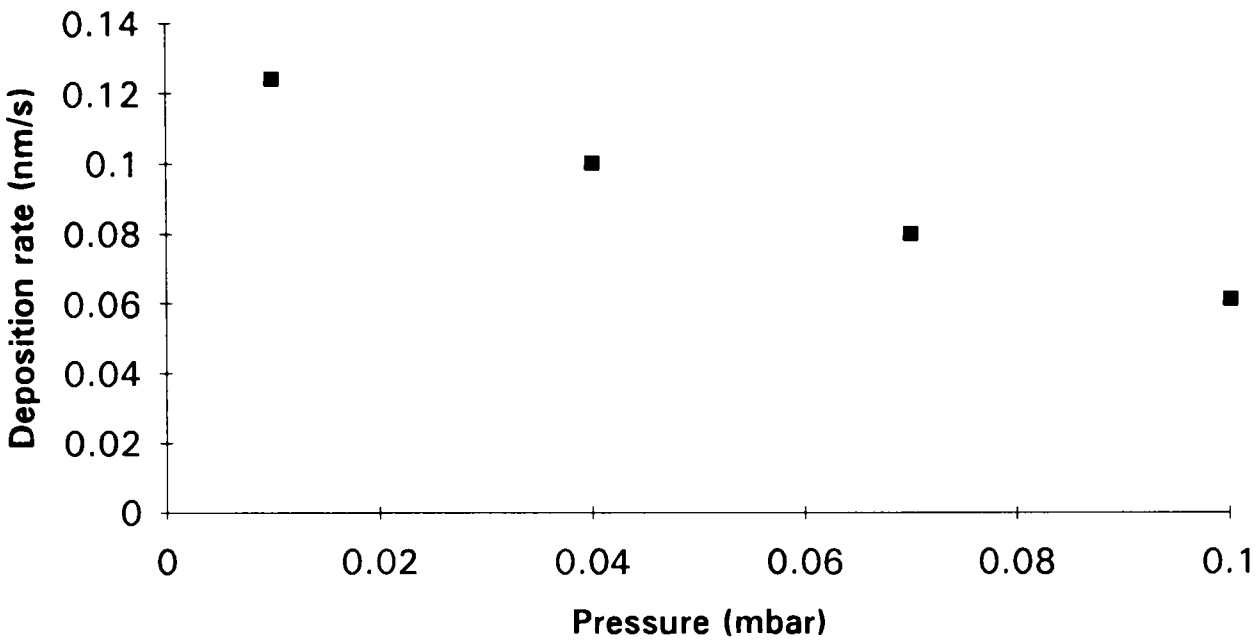

Figure 4.6 The dependence of deposition rate on sputtering chamber gas pressure.

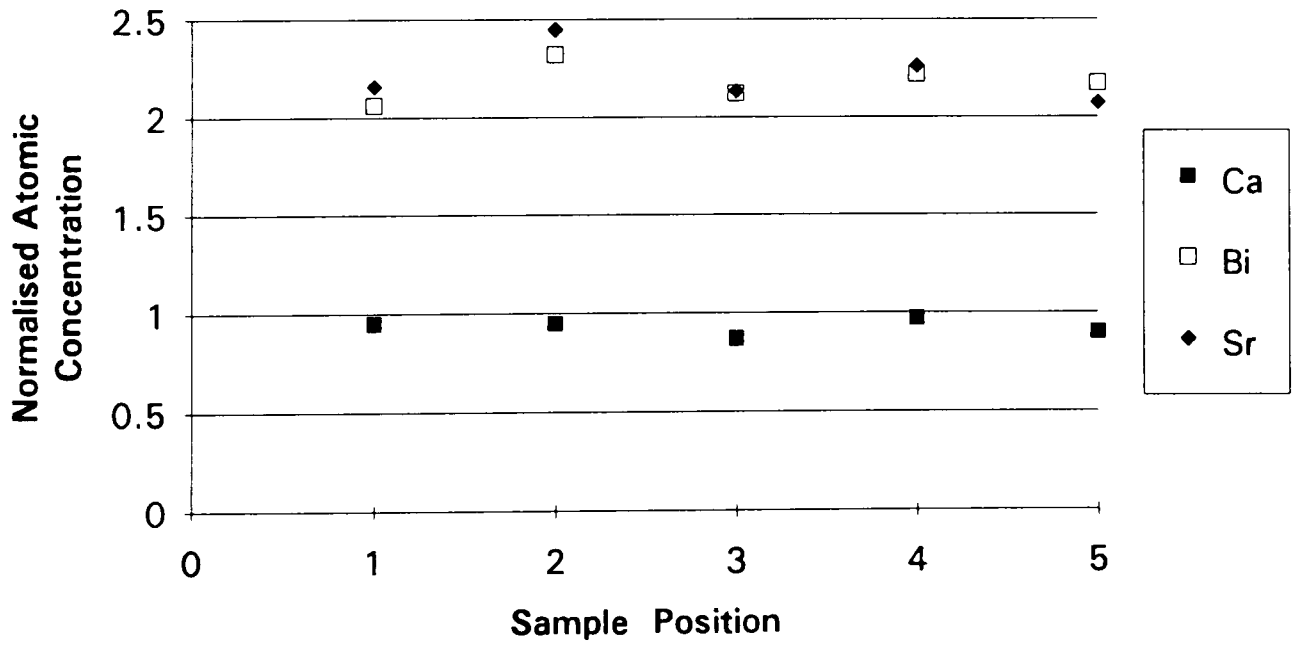

Figure 4.7 The variation of as-deposited film composition with respect to film position as shown in fig 4.1.b.

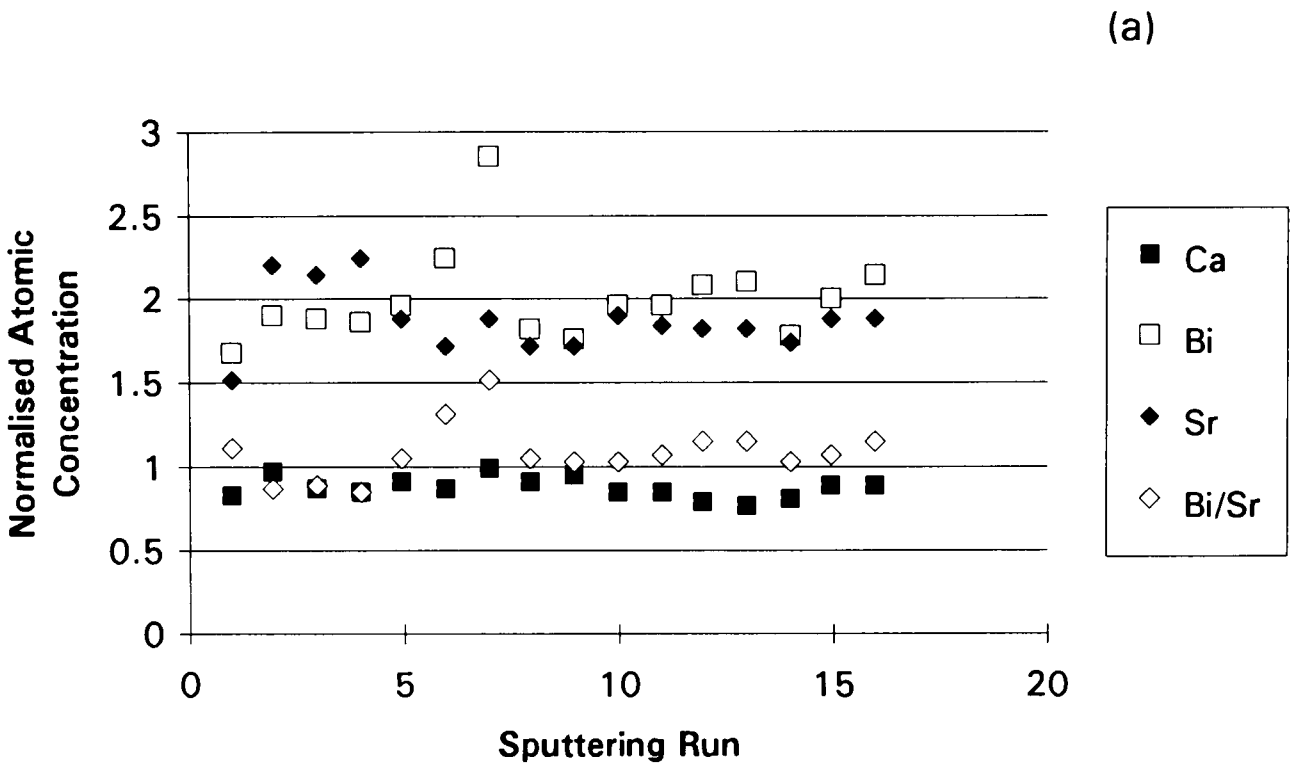

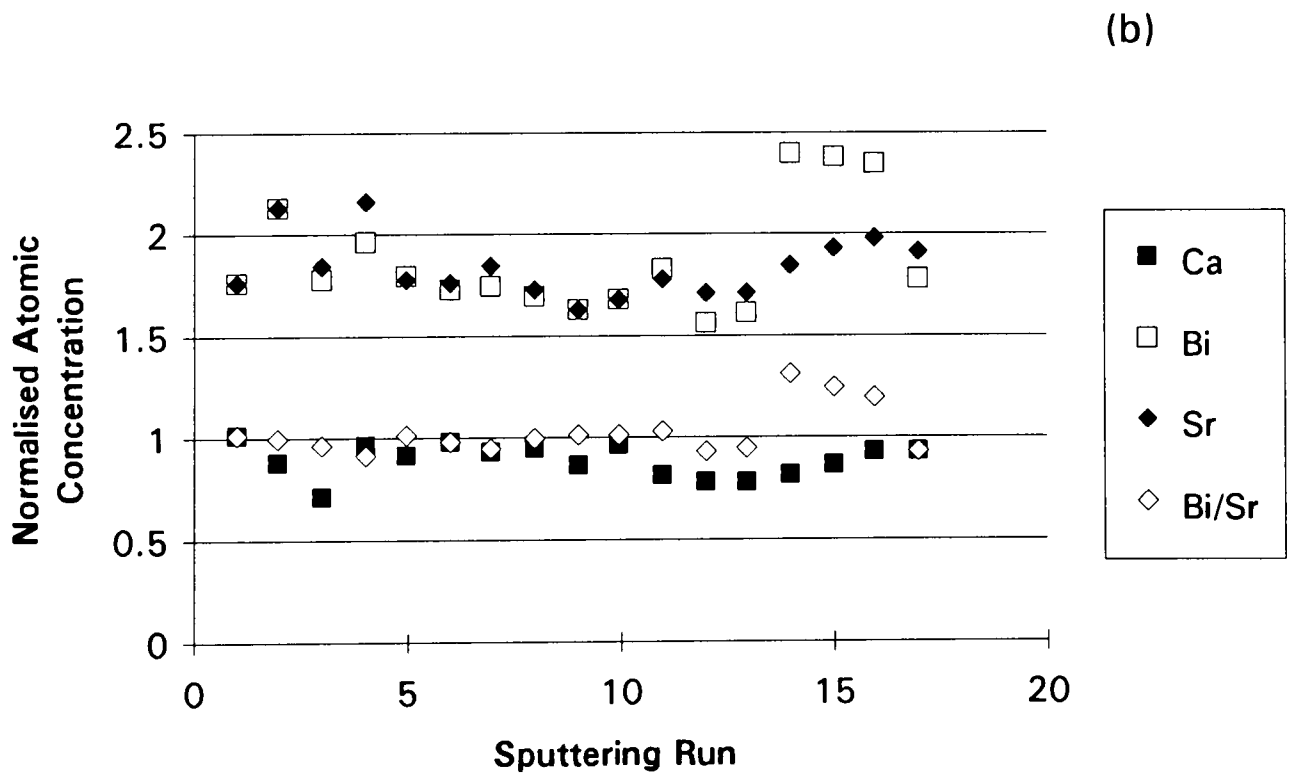

Figure 4.8 During high temperature annealing process (a) Peeled off (b) Not peeled off as-deposited film composition.

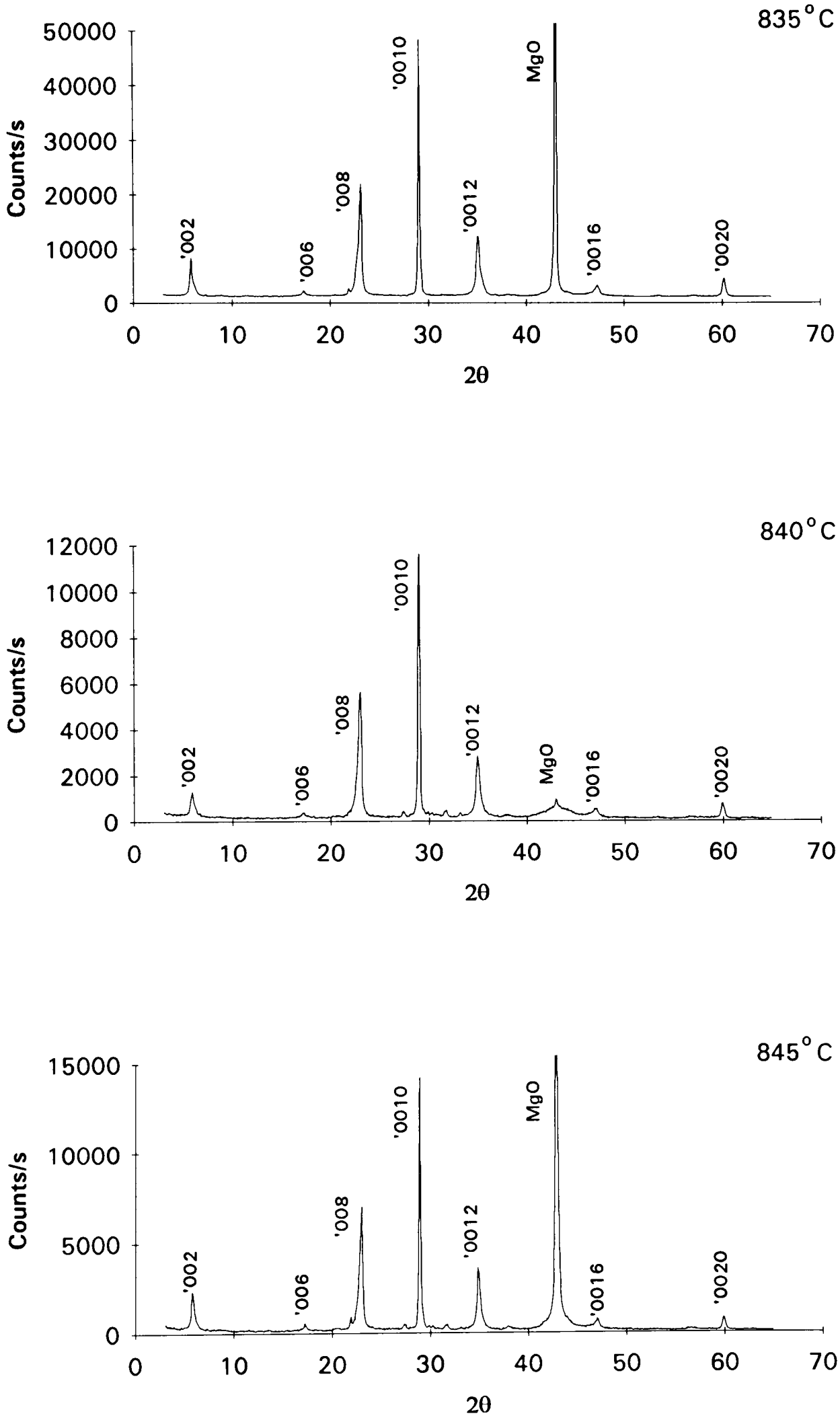

Figure 4.9 XRD pattern of the films annealed at different temperatures for 3 h in air, on MgO substrates.

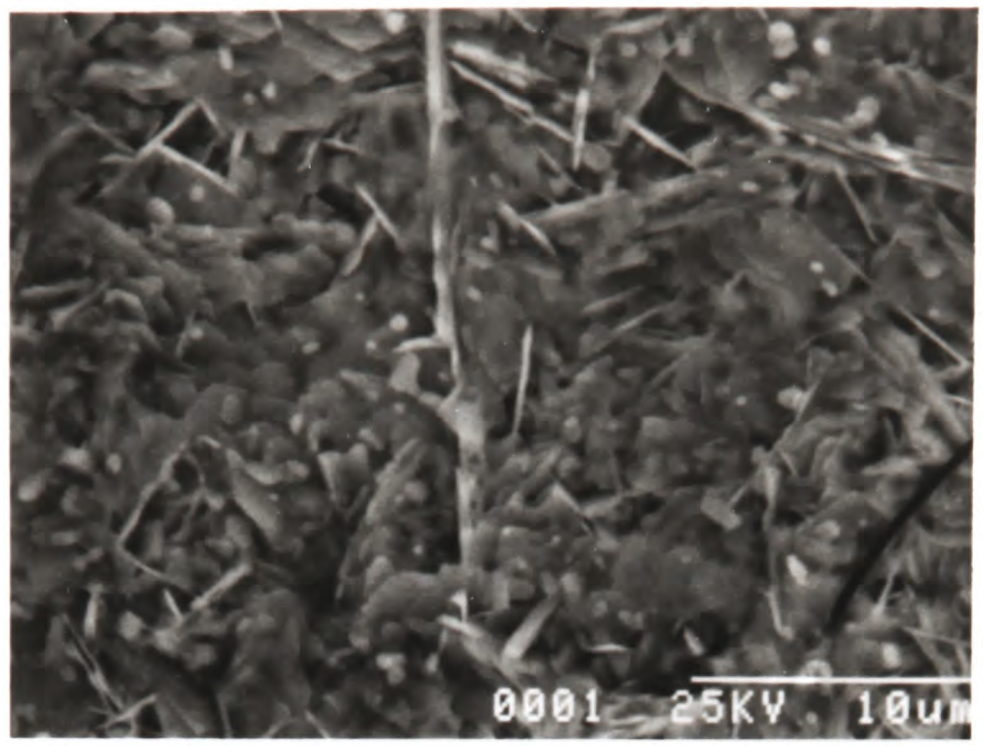

(a)

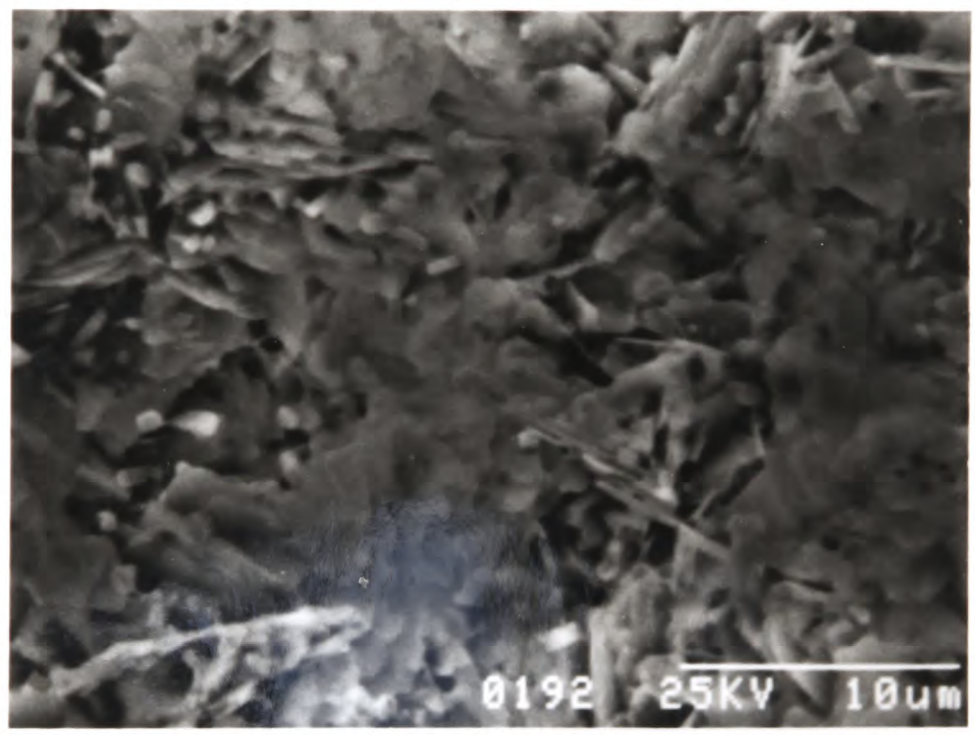

(b)

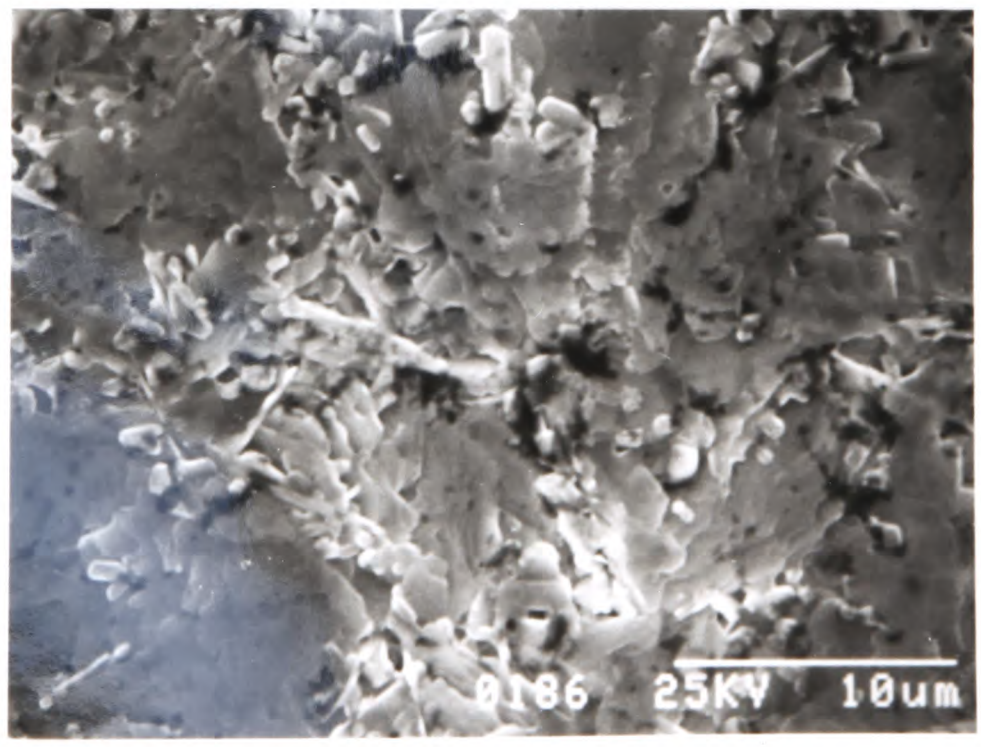

(c)

Figure 4.10 SEM micrographs of the films annealed for 10 h in air at: (a) 820°C, on MgO (b) 830°C, on MgO (c) 830°C, on $SrTiO_3$

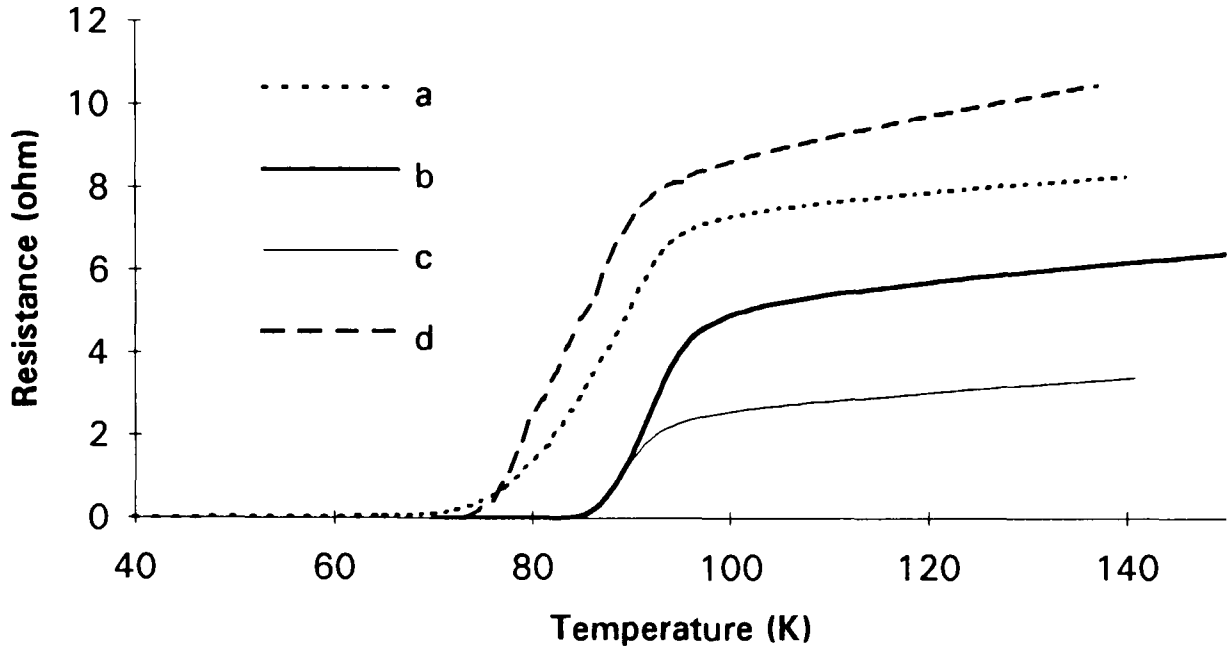

Figure 4.11 Temperature dependence of resistivity for the samples annealed at different temperatures for longer than 6 h in air having slightly different (Ca + Sr)/Bi ratio. (a) at 820°C, (Ca + Sr)/Bi = 1.56 (b) at 830°C, (Ca + Sr)/Bi = 1.41 (c) at 830°C, (Ca + Sr)/Bi = 1.46 (d) at 835°C, (Ca + Sr)/Bi = 1.55.

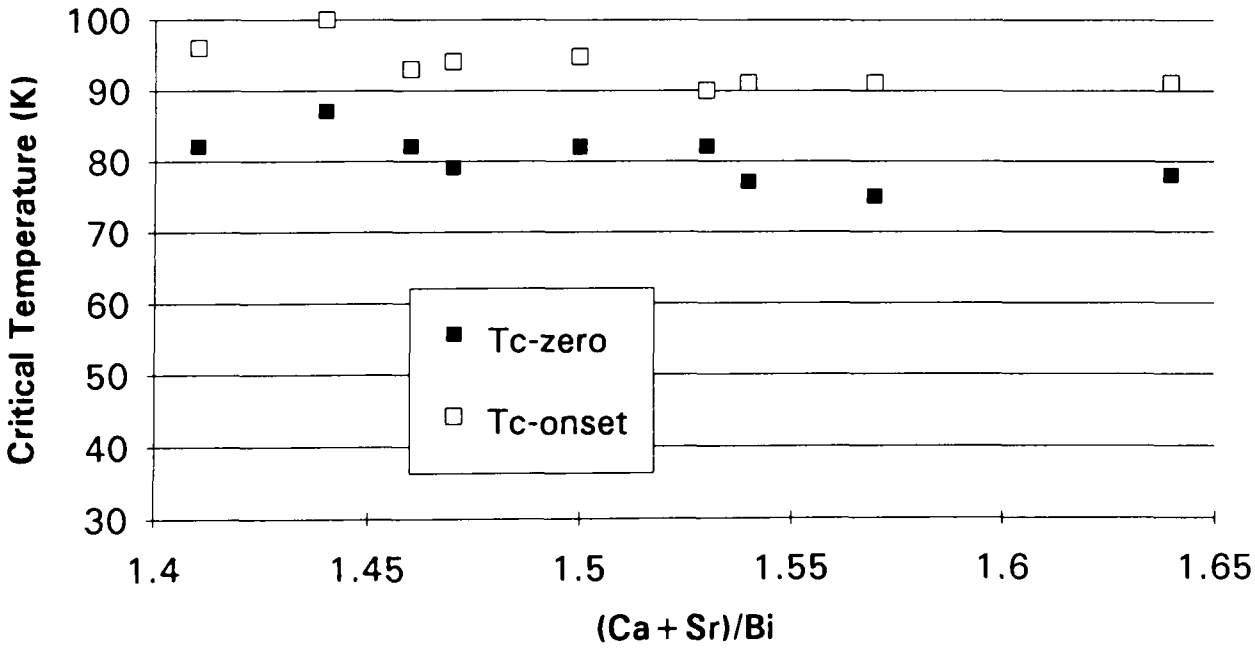

Figure 4.12 The dependence of critical temperatures on as deposited (Ca + Sr)/Bi ratio for the samples annealed at 830°C for more than 10 h.

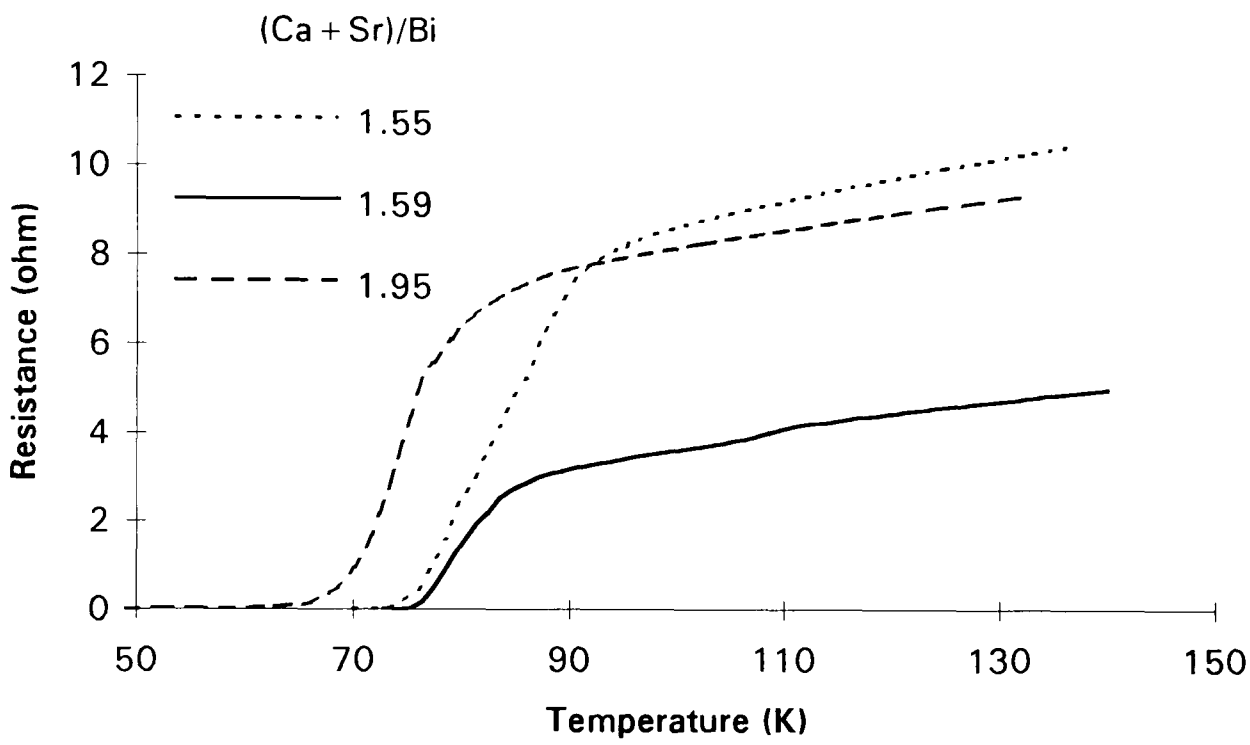

Figure 4.13 The temperature dependence of resistivity for samples having different (Ca + Sr)/Bi ratios annealed at 835^{o}C for 3-6 hours in air.

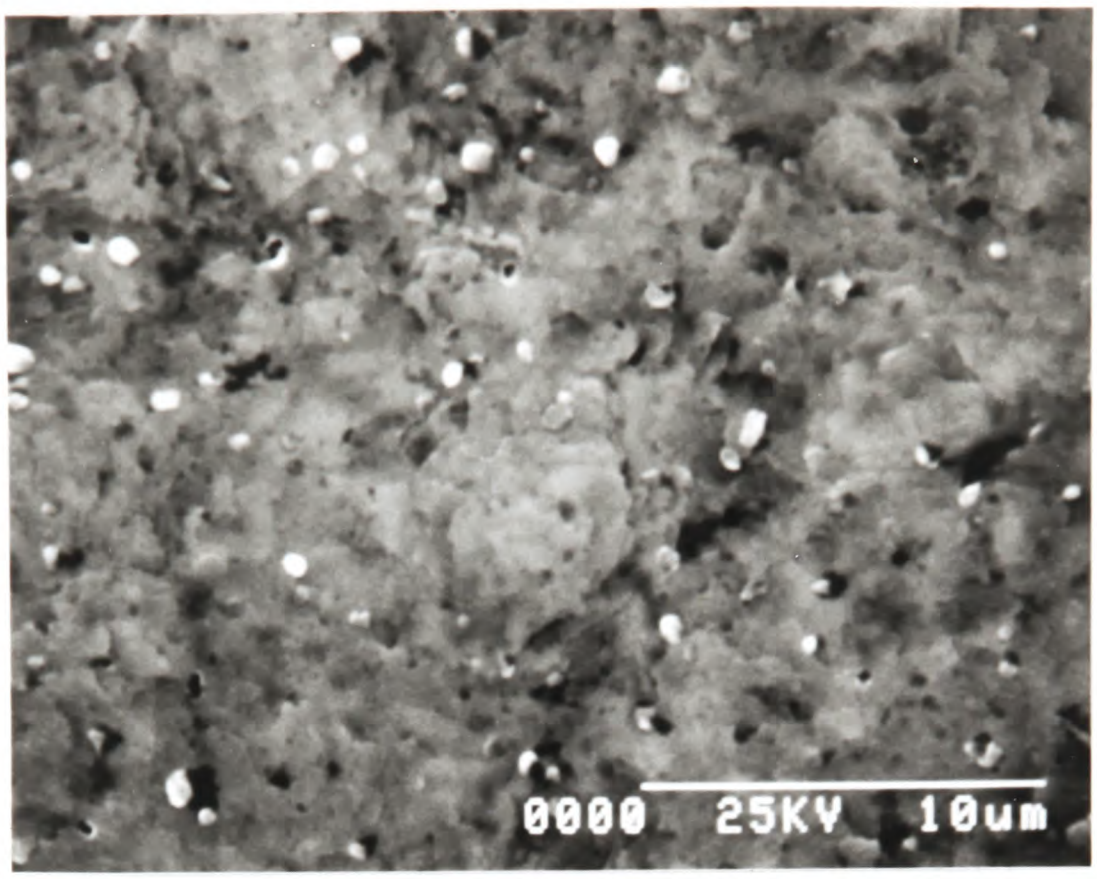

(a)

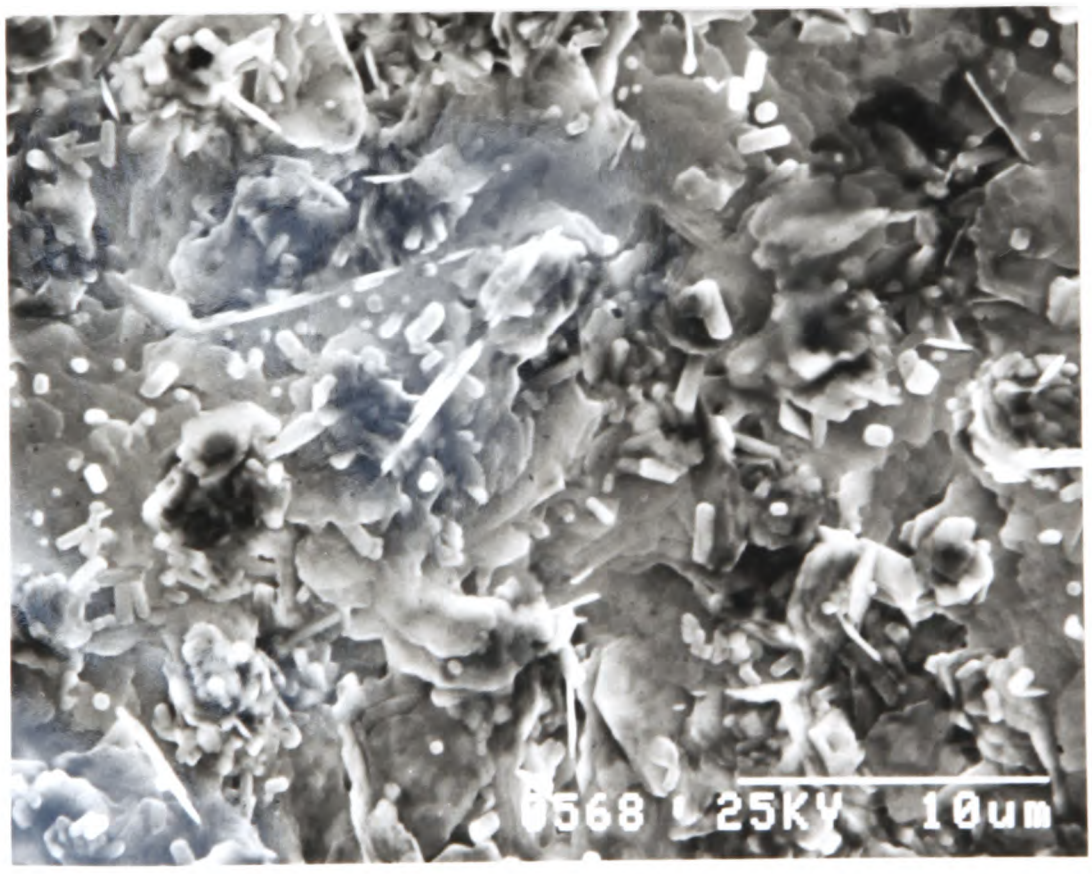

(b)

Figure 4.14 SEM micrographs of the films having different (Ca + Sr)/Bi ratio and annealed at 835^{o}C for 3 h in air (a) (Ca + Sr)/Bi = 1.59 (b) (Ca + Sr)/Bi = 1.95.

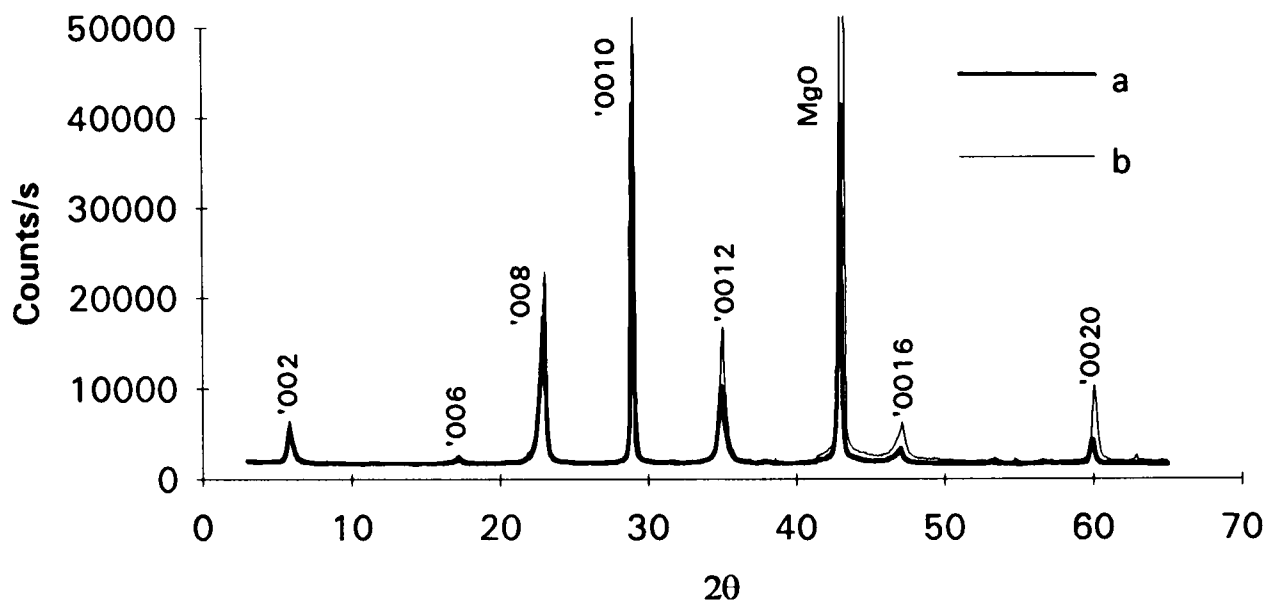

Figure 4.15 XRD pattern of samples annealed at 835^{o}C for 6 h in air and quenched from: (a) The annealing temperature (b) 500^{o}C.

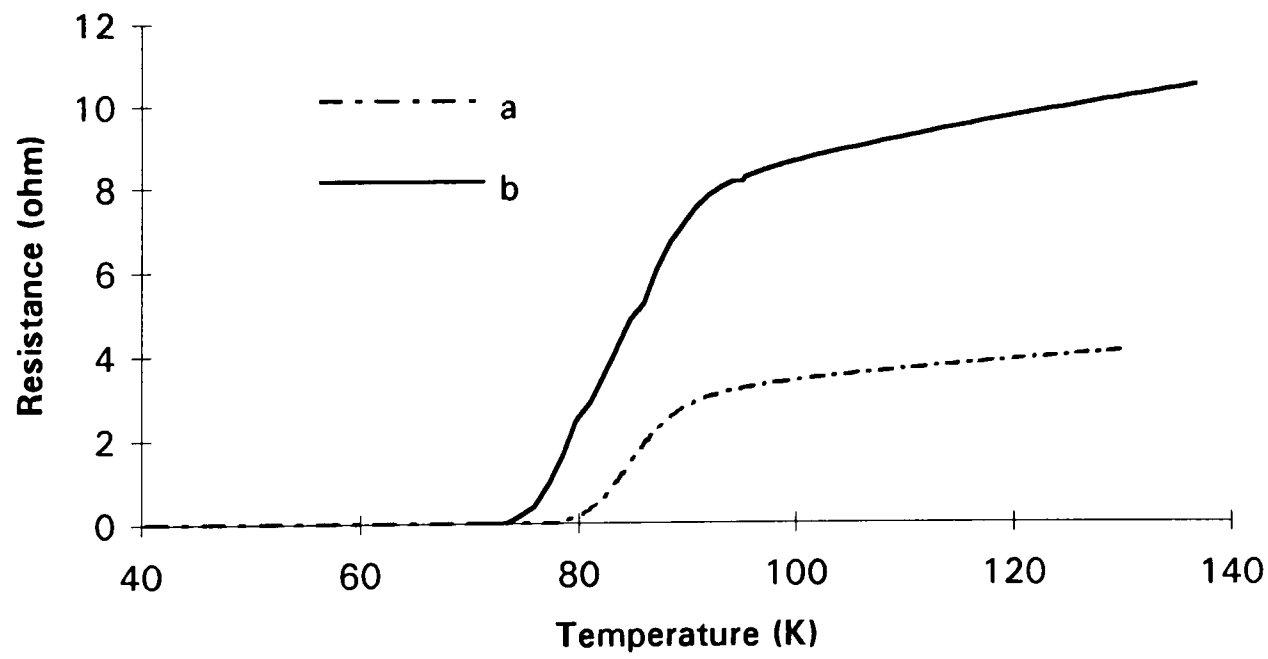

Figure 4.16 The temperature dependence of resistivity for the samples annealed at 835^{o}C for 6 h in air and quenched from: (a) The annealing temperature (b) 500^{o}C. The difference in the normal state resistance is caused principally by the different distances between the voltage contacts.

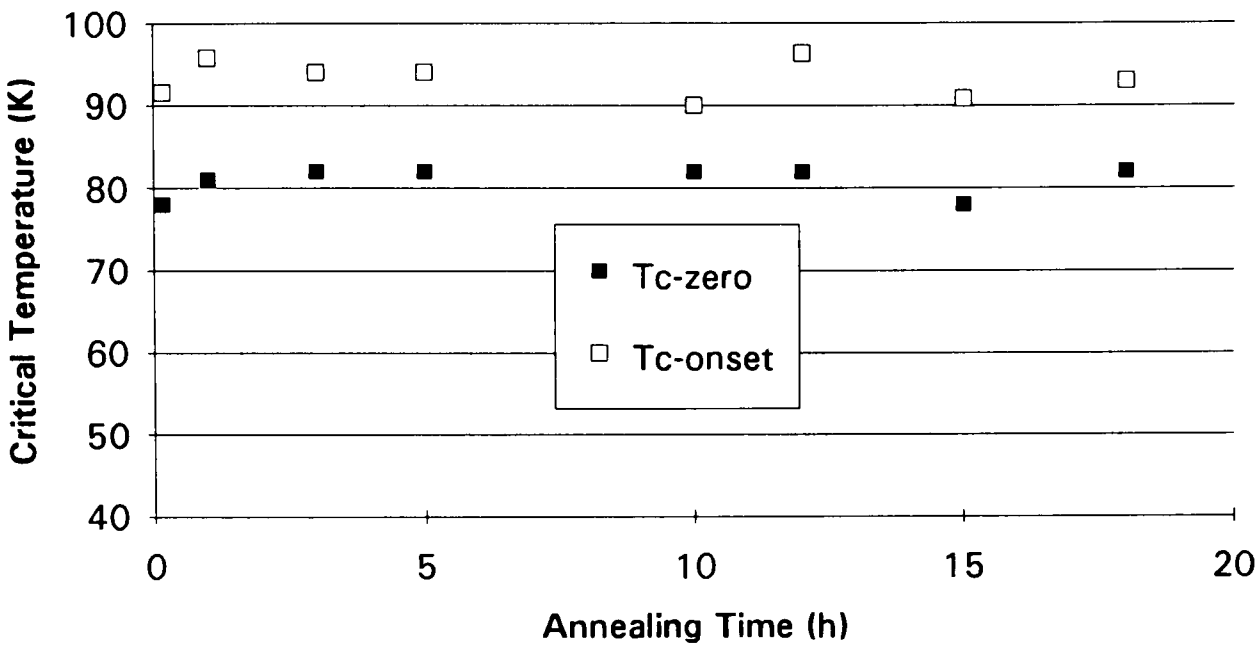

Figure 4.17 The dependence of critical temperature on annealing period for some samples annealed at 830^{o}C in air.

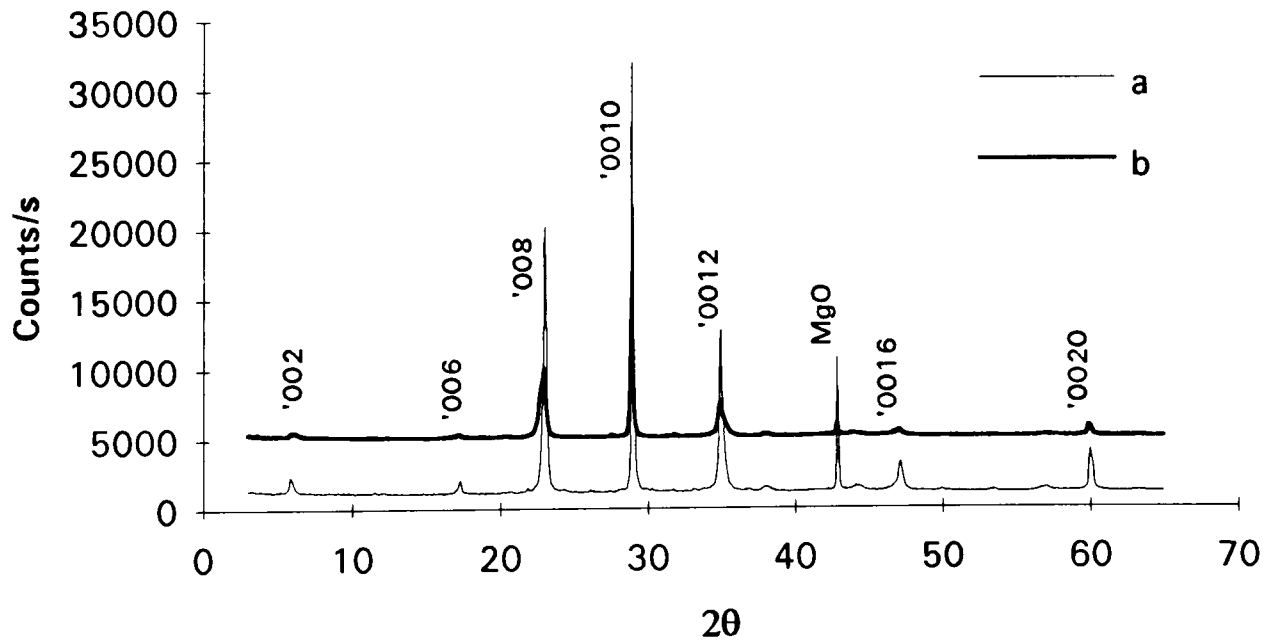

Figure 4.18 XRD pattern of the samples annealed at 830^{o}C in air (a) 18 h (b) 1 h.

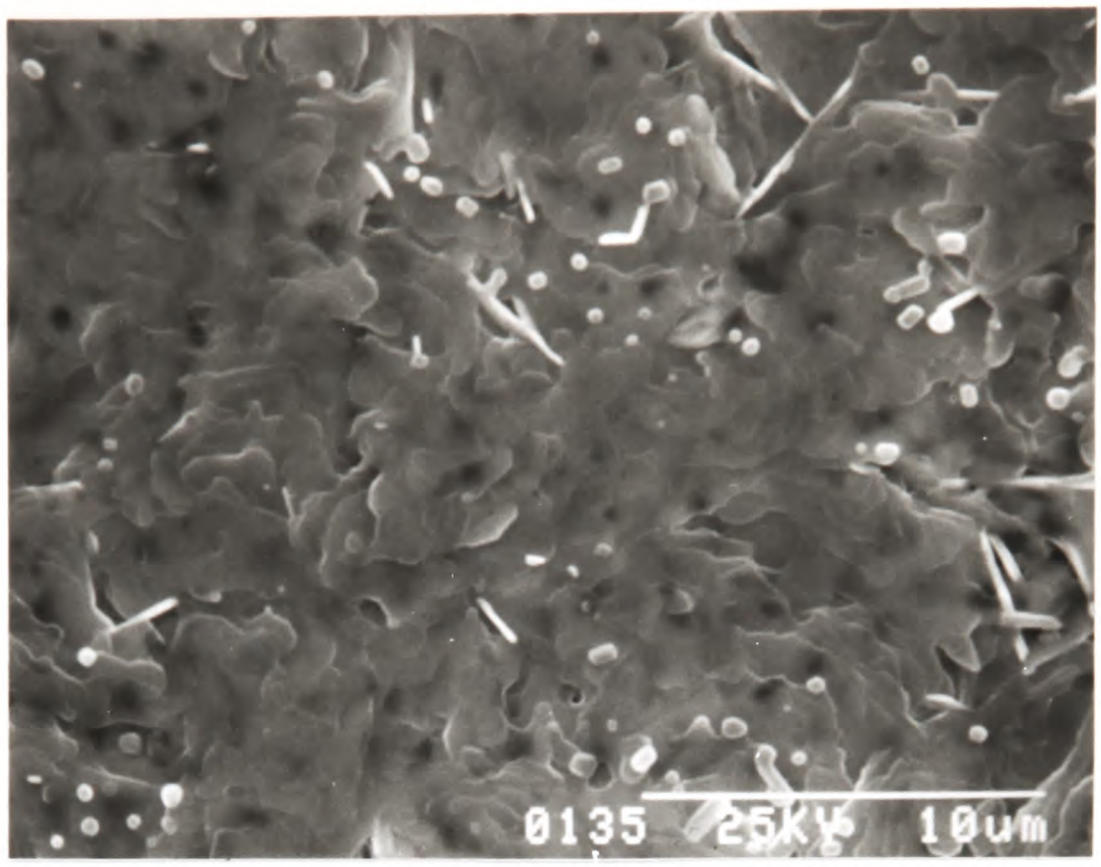

(a)

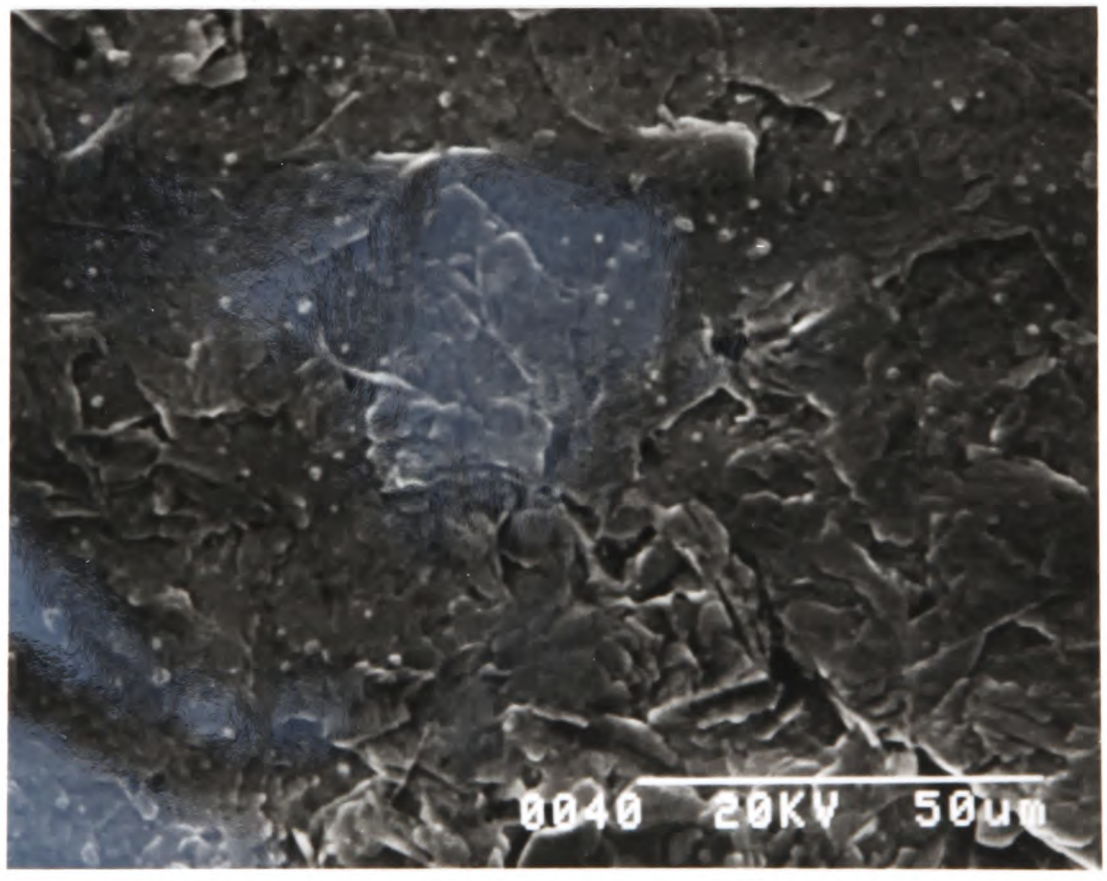

(b)

Figure 4.19 SEM micrographs of the films annealed at 830^{o}C in air for: (a) 1 h (b) 18 h

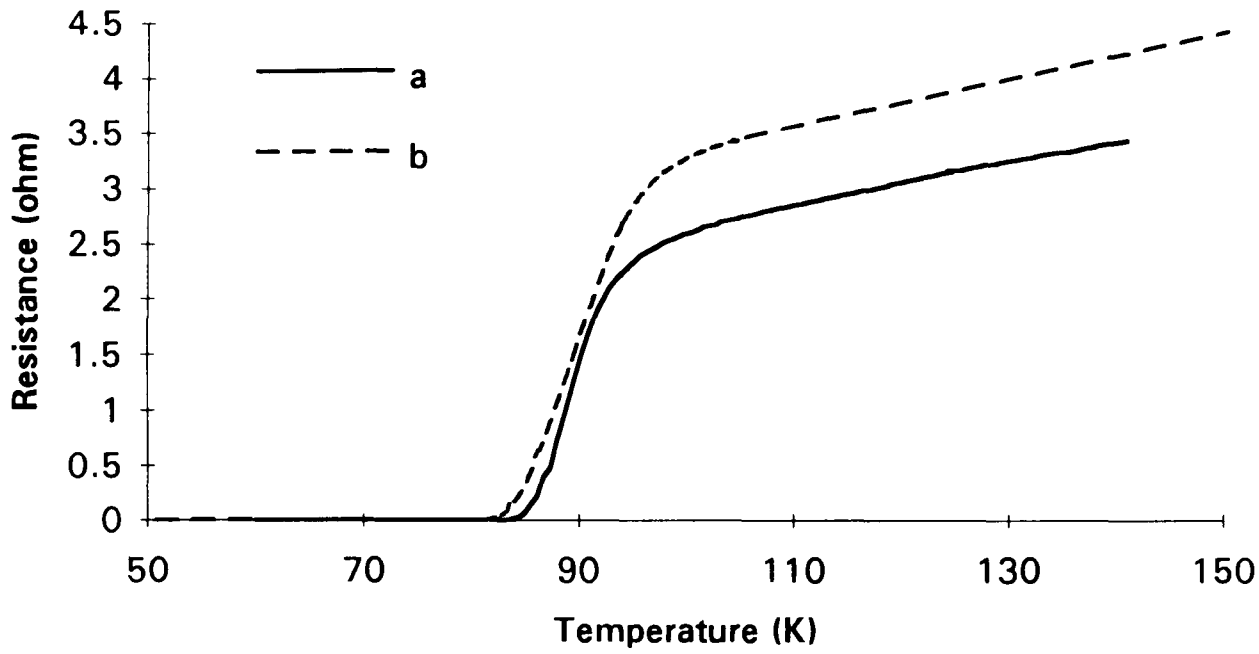

Figure 4.20 The temperature dependence of resistivity for the samples annealed at 830°C for (a) 18 h (b) 1 h.

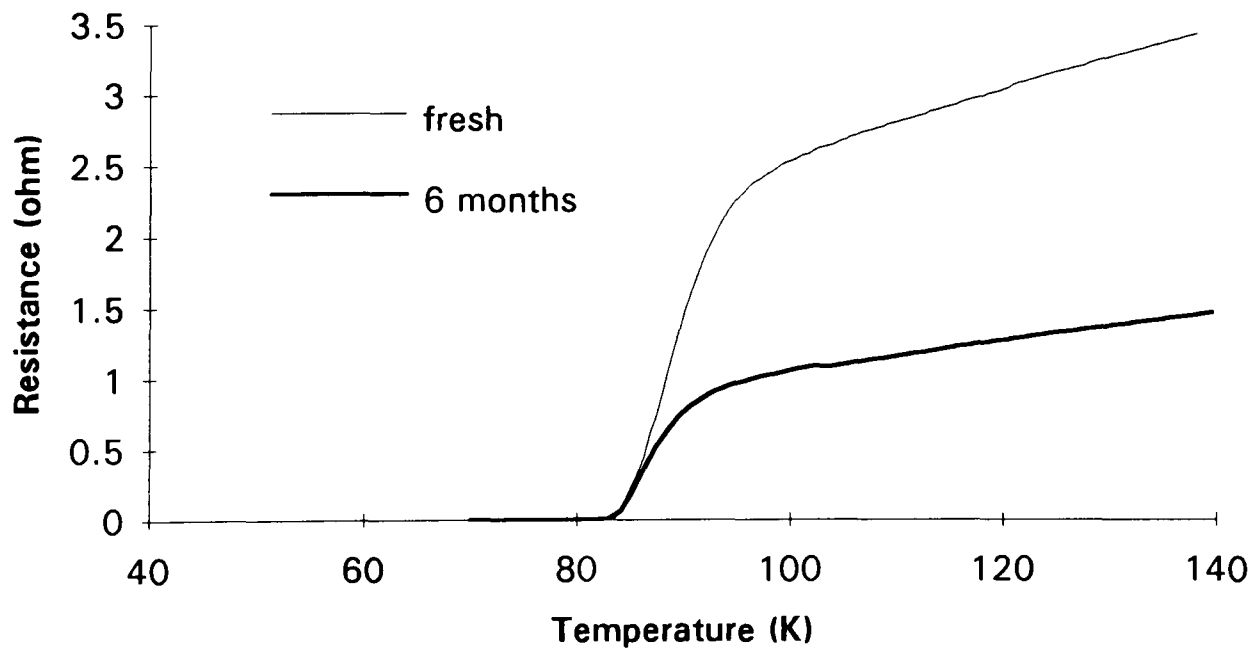

Figure 4.21 Temperature dependence of resistivity of a sample fresh and after six months storage, grown on $SrTiO_3$ substrate. The difference in the normal state resistance is caused principally by the different distances between the voltage contacts.

(a)

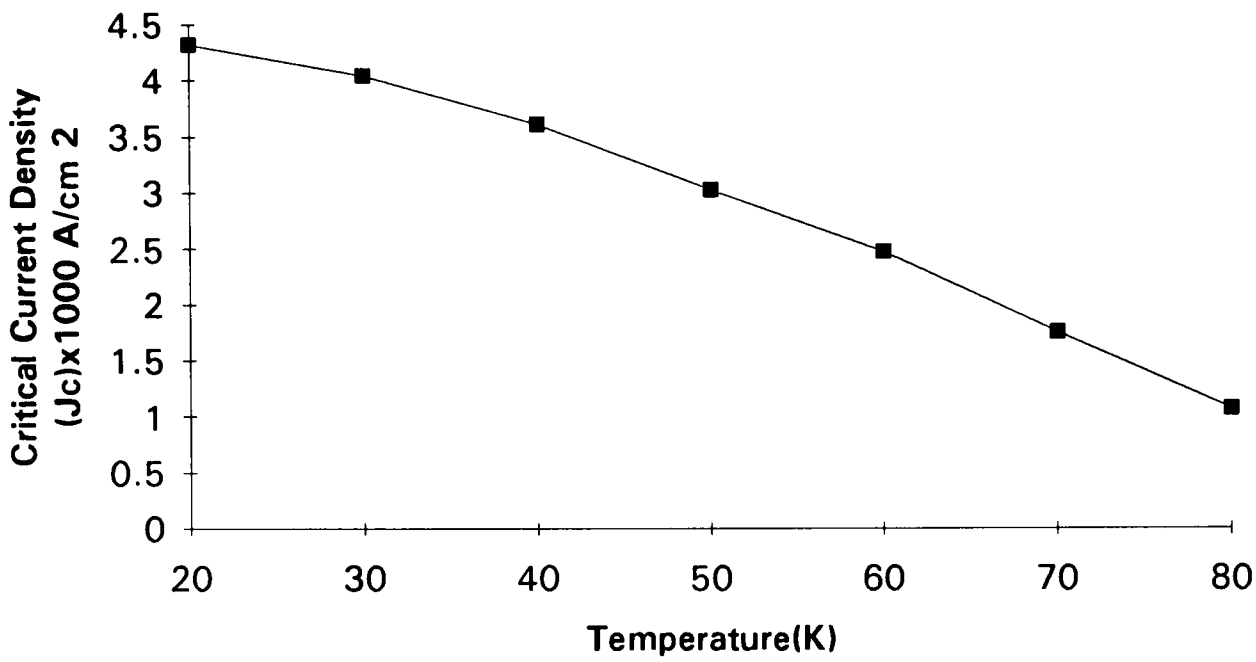

(b)

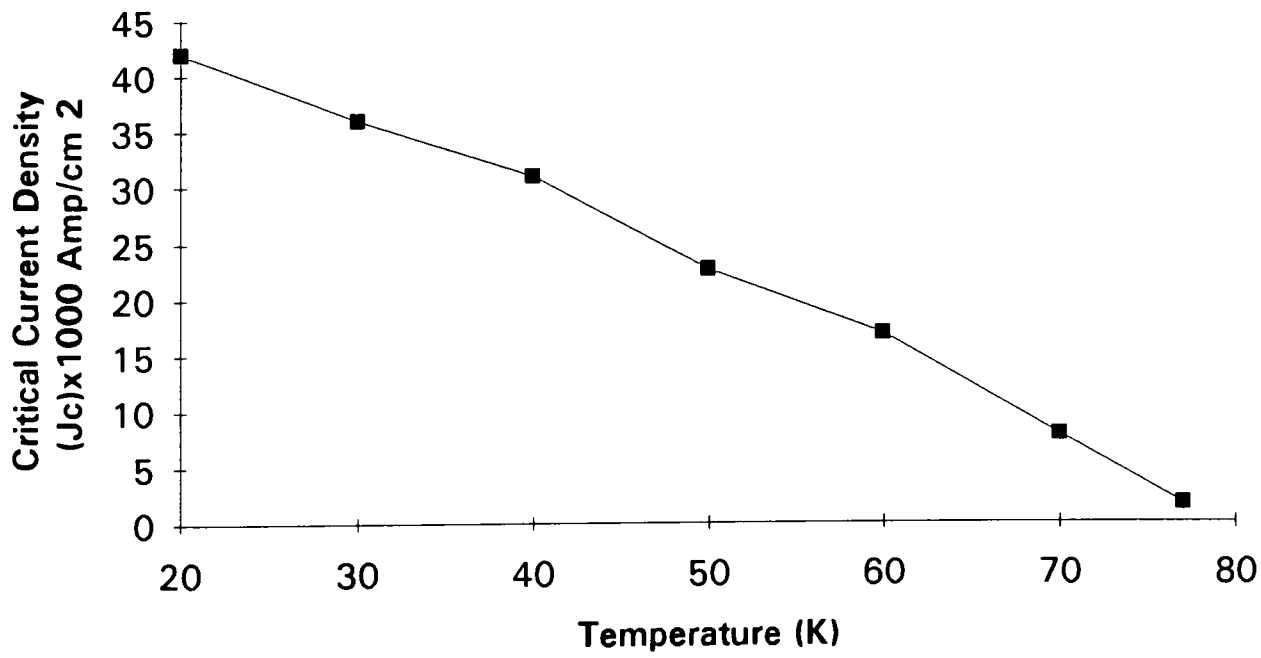

Figure 4 22 The critical current density dependence on temperature for the samples grown on MgO (a) and $SrTiO_3$ (b) substrate.

CHAPTER 5

Preparation and characterisation of Bi-2223 thin films

5.1. Introduction

It is well established that the high-T_c (110-K) phase in the $Bi_2Sr_2Ca_{n-1}Cu_nO_x$($n=1,2,3$) system with ideal composition $Bi_2Sr_2Ca_2Cu_3O_{10}$ can be promoted and stabilised by the partial substitution of Bi by Pb [1]. The effect of Pb doping is that it considerably decreases the formation temperature for the Bi-2223 phase, which is quite close to the melting point [2]. The Pb rich environment also makes it more stable which allows control of the formation of the phase in a wide temperature range. Therefore many kinds of processes for the partial substitution of Bi by Pb have been used in preparing superconducting thin films of Bi-2223 phase, including sintering at high temperatures in Pb-rich atmospheres [3, 4, 5] and use of a sputtering target containing Pb [6, 7, 8, 9]. Several reports of successful fabrication of Bi-2223 films with zero resistivity above 100K were published. Pb doping, by annealing at high temperature in Pb-rich atmosphere, usually required long annealing [10], while a heavily Pb doped film from a heavily Pb doped target can reduce the annealing time to 1 hour [8]. However Pb is more liable to be lost by evaporation during annealing in the case of thin films than from bulk material.

This chapter describes a series of experiments designed to develop reproducible fabrication conditions for reasonably good Bi-2223 thin films, about 0.5μm thick, on various single crystal substrates using heavily Pb doped single composite oxide targets, using rf

magnetron sputtering deposition and subsequent sintering at high temperatures. At the end of the chapter the effect of oxygen content on superconducting properties is discussed.

5.2. Results and discussion

5.2.1. Target composition

The films were sputtered from a heavily Pb doped single composite oxide BiPbSrCaCuO target. The nominal compositions of five targets used in this work are listed in **Table 5.1**. Targets were prepared as described in chapter 2. The chosen target stoichiometries were based on $Bi_{1.82}Pb_{2.27}Sr_{1.82}Ca_{1.95}Cu_3O_x$ as optimised by Kula et al. [8] for the DC magnetron sputtering mode. The cation ratios of Pb/Bi actually used vary between 0.8 and 1.4. Although all targets except for number 5 have allowed the production of a film having $T_{c\text{-}zero}$ of 106 K, targets numbered 1 and 2 (**Table 5.1**) have been found suitable for reproducible and reasonably good films in respect of the microstructure and also critical current density, J_c.

Table 5.1. Nominal composition of the BiPbSrCaCuO targets used for rf sputtering.

Target no.	Pb/Bi ratio	Target Composition
1	0.82	$Bi_2Pb_{1.64}Sr_{1.82}Ca_{1.95}Cu_3O_x$
2	1.00	$Bi_2Pb_2Sr_{1.82}Ca_{2.10}Cu_3O_x$
3	1.25	$Bi_{1.82}Pb_{2.27}Sr_{1.82}Ca_{1.95}Cu_3O_x$
4	1.40	$Bi_{1.82}Pb_{2.55}Sr_{1.82}Ca_{1.95}Cu_3O_x$
5	1.40	$Bi_{1.82}Pb_{2.55}Sr_{1.73}Ca_{2.20}Cu_3O_x$

The films produced from the target having Pb/Bi ratio of above 1.25 usually showed poor micro-structure with many pin holes and island-like grains. However, the assessment of film properties according to the sputtered target composition is unreliable as the deposited composition is not stoichiometric. Therefore as-deposited film compositions should be considered rather than target composition in assessment of the preparation of the films produced.

5.2.2. As-deposited film composition

EPMA measurements on as-deposited films referring to Cu content Cu = 3 are shown for some representative samples taken from different batches, which are not sequential, in **Fig.5.1**. All samples analysed were from the same position on the substrate holder. In **Fig. 5.1 a** Bi-content changes between 1.4 and 1.8 and fluctuates around 1.55 for reasonably good Bi-2223 films; below 1.4 (runs 17, 19 and 24) superconducting properties are considerably reduced, above 1.9, or higher than Sr, (**Fig.5.1 b**) the films have peeled off. Even larger Bi-content in association with large Pb-content has given rise to the formation of island like big grains. Thus the Bi-content was found crucial in the formation of the Bi-2223 phase in heavily Pb doped films. The Pb/Bi ratio runs between 0.9 and 1.5 while the Sr/Ca ratio remains around 1. All compositions having Pb/Bi ratio in this region have provided reasonably good superconducting properties when annealed at high temperature. However it has been found that films containing Pb/Bi ratios larger than 1.3 in initial composition need to be very slowly (1^{o}C/min) heated up to the desired sintering temperature to allow the escape of excess Pb. A heating rate of even 2^{o}C/min has caused the formation of separated island-like grains or inhomogeneous microstructure in those films having Pb/Bi ratio in excess of 1.3. For example, **Fig. 5.2** shows the microstructure of two such films taken from the same batch. Slightly different annealing processes have been applied to these two films. One of them was heated up from 450^{o}C to 845^{o}C then 862^{o}C with ramping rate of 2^{o}C/min. and 1^{o}C/min., respectively, and sintered at this temperature for 30 min. in air. After that furnace cooled below 500^{o}C. The other sample was annealed at the same annealing

condition except for heating and cooling rate, which were kept at $1^{o}C$/min. for both cases. The first film which was relatively fast heated and cooled with respect to the second film had large plate like grains (**Fig. 5.2 a**). However, this microstructure was not typical of the whole film surface of $1cm^2$. In the middle part of the film (a circular area of ~0.5 cm diameter) island like huge grains separated by small needle type yellow grains have formed. As the size of these yellow needles are very small, they could not be analysed accurately by EPMA, but they were rich in Ca and Pb. XRD patterns definitely showed that these small needles were Ca_2PbO_4 phase. The second film which was supposed to have similar initial composition with that of the first film had homogeneous surface structure (**Fig. 5.2 b**) through out the substrate surface and no detectable (by XRD) amount of Ca_2PbO_4 phase. However, the grain size was much smaller than the fast heated and cooled sample. **Fig 5.3** shows the temperature dependency of the resistivity curves for samples deposited on MgO substrates having lowest (0.9, **Fig. 5.1 a** run 8) and highest (1.51, **Fig. 5.1 a** run 5) Pb/Bi ratio in their initial composition (**Fig. 5.3** curve a and b, respectively). Note that the Bi ratio (Bi:1.52, 1.55) is almost the same. These two films have been sintered at $862^{o}C$ for 30 min in air with ramping rate $3^{o}C$/min and $1^{o}C$/min for low and high Pb/Bi ratio, respectively. $T_{c\text{-}zero}$ (109K) and $T_{c\text{-}onset}$ (115K) only differ by 1K with the same transition width of 6K. The difference of 1K on $T_{c\text{-}zero}$ and $T_{c\text{-}onset}$ may be attributed to the difference in oxygen content due to the slightly different cooling process, or to the initial composition considering Bi content. The other extreme composition in respect of Bi content of 1.82, with Pb/Bi ratio of ≈0.9 (**Fig 5.1 a**. run 1), sintered at the same annealing condition as above, showed $T_{c\text{-}onset}$ and $T_{c\text{-}zero}$ of 113K and 105.5K respectively (**Fig. 5.3** curve c). For this sample the cooling process is the same with the sample above having the same Pb/Bi ratio ($1^{o}C$/min down to $600^{o}C$ and subsequently air quenched). Although these three films have a current density, J_c, above 10^4 A/cm^2 in liquid nitrogen (77K), the highest J_c of $6x10^4$ A/cm^2 with the approximate normal state resistivity value of $9.5x10^{-4}$ Ωcm was measured on the sample which had Pb/Bi ratio of 1.51.

These results revealed that the initial cationic ratio of BiPbSrCaCu oxide for heavily Pb doped composition, providing reasonably good superconducting properties when they are sintered at an optimised temperature, may be around 1.55:1.65:1.87:1.83:3 (normalised to Cu). This composition is slightly Cu-rich (as compared to the nominal composition of the Bi-2223 phase), but it is necessary to compensate for film stoichiometry changes during the high temperature sintering process [8, 11]. It was found that the film quality was very sensitive to the Bi concentration rather than Pb/Bi ratio in the as deposited film. Various researchers had suggested that the nominal composition with either Ca/Sr = 1 [12], or Sr [13] or Ca [11] rich stoichiometry would lead to the formation of a high volume fraction of the Bi-2223 phase. But no significant difference was found for compositions given in **Fig 5.1 a** which contains all these compositions.

5.2.3. The formation of Bi-2223 phase

As-deposited films from target number 3 in **Table 5.1**. on MgO (001), which had a stoichiometry close to the optimised one, were sintered at different temperatures from 820°C to 875°C for 1hour in air. XRD patterns of those films revealed that the Bi-2212 phase formed together with Ca_2PbO_4 in the early stage of high temperature annealing (**Fig. 5.4 a**). Ca_2PbO_4 which forms at ≈750°C and then decomposes into CaO and a liquid phase at 822°C [14] is a highly reactive intermediate phase aiding the formation of Bi-2223 [15]. It is believed that this intermediate phase may act as an accelerator to interact with CuO and Bi-2212 to form the Bi-2223 phase [11]. The Bi-2223 phase has started to grow at 835°C when the peaks attributed to Ca_2PbO_4 were smaller (**Fig. 5.4.b**). The Bi-2223 phase became dominant against the Bi-2212 phase while Ca_2PbO_4 was hardly detected at 852°C (**Fig. 5.4 c**). The volume fraction of the Bi-2223 phase in the film increased and that of the Bi-2212 phase decreased further for annealing temperatures up to 862°C (**Fig. 5.4 d**). At 862°C the highest ratio of the Bi-2223 phase was observed (97%). Above this temperature the Bi-2212 phase started to appear again, together with some impurity phase, (Sr,Ca)CuO (not detectable by XRD), and 115 peaks of both superconducting phases indicating that the

strong c-axis orientation of grains decays (**Fig. 5.4 e**). The evolution of the respective volume fractions of the Bi-2212 and Bi-2223 phases in the film as a function of the preparation conditions have been determined mainly through the evolution of the respective intensities of the (002) reflections for these two phases. Because of their low angle positions they do not overlap with other lines in the spectrum. This variation of the Bi-2223 and Bi-2212 phase concentration with annealing temperature, estimated from the intensity ratio of the low-angle peaks of both phases, is illustrated in (**Fig. 5.5**).

Resistivity measurements made on these samples (**Fig. 5.6**) were in very good agreement with the XRD spectra. It is quite clear that $T_{c\text{-}onset}$ increases with increasing ratio of the Bi-2223 phase and remains almost constant for a wide temperature range. $T_{c\text{-}zero}$ is slightly decreased at the beginning of the Bi-2223 phase formation because of the segregation of phases. It reached 107K at 850^{o}C, in spite of the existence of a large amount of Bi-2212. If this result is considered with the result that a single step transition is observed for all samples, it can be seen that Bi-2223 is formed without intergrowth of Bi-2212, an effect of Pb doping [2]. $T_{c\text{-}zero}$ remains above 108K for sintering temperatures between 852^{o}C and 862^{o}C, then decreases remarkably with increasing sintering temperature while $T_{c\text{-}onset}$ decreases slightly from 116K to 113K. This symmetrical variation of $T_{c\text{-}zero}$ and $T_{c\text{-}onset}$ around an optimum formation temperature, and XRD data suggest that the previously formed Bi-2223 phase starts to decompose into the Bi-2212 phase and (Sr,Ca)CuO impurity phase in the shape of huge needles, rich in Ca and Cu. The microstructure and phase developments of samples annealed at various temperatures are shown in the SEM micrographs (**Fig. 5.7**).

5.2.4. Effects of Pb and its loss

Fig.5.8. shows the composition of randomly chosen plate like grains from samples annealed at different temperatures. It is seen that the composition of the grains moves closer to the nominal composition of Bi-2223 while the Pb ratio decreases with increasing sintering temperature. Further increase of sintering temperature gave rise to deviations from the

nominal composition of the grains, being quite close at the optimum sintering temperature, 862°C, while the Pb content became almost zero above 862°C. The mechanism for Pb loss is presumed to be by evaporation. The amount of Pb present in the film also quickly dropped off with increasing sintering duration. After 2 hours annealing at 862°C no detectable amount of Pb was found while the XRD pattern shows almost single-phase Bi-2223. Thus it can be concluded that permanent replacement of Bi with Pb in the crystal lattice is not the important factor in the enhancement of the Bi-2223 phase by Pb doping [9]. However, microstructures observed on films containing negligible and reasonable amount of Pb (around 0.2) suggest that Pb acts as a fluxing agent in the BSCCO system in that it decreases the density of stacking faults and increases the crystal size [16, 17, 18].

5.2.5. Effect of annealing conditions

As indicated above, high-T_c BSCCO thin films with $T_{c\text{-zero}}$ of 108K, in which Bi-2223 phase is dominant, can be obtained in a wide range of annealing temperature, at least 10°C, from a heavily Pb doped target. However 862°C was found as an optimum annealing temperature, as it provided a high fraction of Bi-2223 phase. Therefore films have been annealed at 862°C for different durations from 15 min. to 4 hours. The microstructures of some samples sintered for various lengths of time are shown in the SEM micrographs of **Fig. 5.9**. A short sintering time (15 min.) resulted in a similar microstructure to that of the sample annealed for 2 hours. A sintering time longer than 2 hours resulted in an increase in the number of huge needles of (Sr,Ca)CuO. All films to be described in this section were deposited on MgO (100) substrates from target 1 (**Table 5.1**). **Fig.5.10** presents the XRD patterns of these films annealed at 862°C for different periods of time. There is no detectable difference in the XRD patterns of 15 min. and 2 hours annealed samples, but after 3 hours annealing peaks which are forbidden for well textured grains on the c-direction of both Bi-2212 (L117) and Bi-2223 (H115) phases appeared, and the intensity of the peaks decreased indicating that the texture is getting worse. The (006) peak of the Bi-2201 phase is also detected. This long time annealing effect may be related to the lack of Pb in the

structure after prolonged annealing as discussed above. It was found that the annealing time has an effect on the film composition for heavily Pb doped as deposited films. The Pb ratio decreases while Bi, Ca and Sr slightly increase (or a corresponding decrease in the proportion of Cu) with time. Similar effects have been reported by Dew et al. [9] while they did not detect a significant deviation on the composition for film without Pb.

The temperature dependence of the resistivity for samples annealed for different periods is in agreement with the XRD data. The sample annealed for 3 hours had a long transition range with $T_{c\text{-}zero}$ 87K and $T_{c\text{-}onset}$ 114K. In fact $T_{c\text{-}onset}$ of 114K is the same for 30 min.-2 hours annealed samples. This long transition tail can be correlated with the low critical current of the sample at just below the transition temperature due to poor microstructure. Samples annealed for less than 3 hours show a sharper superconducting transition of 5-6K (**Fig. 5.11**). The short time annealing of 15 min. reduced $T_{c\text{-}onset}$ to 106K while it was above 108K for annealing periods of 30 min.-2 hours. The short time annealing effect may be explained as an effect of oxygen content, which will be discussed in section **5.3.3**, due to the excess Pb (Pb:0.26) content in the film. However, it was found that 30 min. is an optimum annealing duration, providing a sharp transition of 5K and reproducable good microstructure for the film composition described above.

5.2.6. Effects of heating and cooling rates

Heating and cooling rates have also been found to affect the film structure. Heating films very quickly (10^{o}C/min.) up to 840^{o}C then 1^{o}C/min. up to the desired annealing temperature (to avoid overshooting the set temperature) results in an increase of the ratio of Bi-2212 and Ca_2PbO_4 phase (**Fig. 5.12**). The same effect was detected for all samples heated at a constant rate of above 2^{o}C/min. from around 500^{o}C to the annealing temperature. Slow heating rate of 1^{o}C/min is necessary at least from above 700^{o}C to the desired annealing temperature for the preferential growth of Bi-2223 phase. The cooling rate is also important regarding oxygen content in the film, which will be discussed in the following section. However slow cooling (1^{o}C/min.) to 700^{o}C is essential to avoid the

undesirable micro cracks. Low temperature annealing at around 750°C, which is the formation temperature for Bi-2201 phase, for 1 hour following the cooling process resulted in an increase of the fraction of Bi-2212 phase.

5.2.7. Bi-2223 films on perovskite substrates

The films grown (under the same conditions as used for MgO substrates) on $LaAlO_3$ and $SrTiO_3$ single crystal perovskite substrates were also characterised. **Fig. 5.13** shows XRD patterns of three samples which were grown on different single crystal substrates with the same process (annealed at 862°C for 30 min. in air). The Bi-2223 film on $LaAlO_3$ was predominantly c-axis oriented, similar to the films grown on MgO, with FWHM-value 0.24° of H(0012) peak. However Bi-2212 phase was dominant rather than Bi-2223 phase on $SrTiO_3$, and FWHM-value for the H(0012) peak was slightly wider than for the previous two substrates. The microstructures of samples grown on various single crystal substrates are shown in **Fig. 5.14**.

Resistivity measurement of the films grown on $SrTiO_3$ and $LaAlO_3$ show that $T_{c\text{-}onset}$ and $T_{c\text{-}zero}$ are relatively lower than that of the film grown on MgO (**Fig. 5.15**). In the case of $LaAlO_3$ $T_{c\text{-}zero}$ was 104K with a transition range of 5K. This $T_{c\text{-}zero}$ value is the maximum critical temperature which can be achieved on $LaAlO_3$ (it varies between 102K and 104K). On the other hand the narrowest transition range of 3.5K with the same $T_{c\text{-}zero}$ of 104K (**Fig. 5.16**) was detected in another sample on $LaAlO_3$, despite the low fraction of Bi-2223 phase and existence of Ca_2PbO_4 in it (**Fig 5.12**). This sample had a slightly different annealing process as described in the previous section. It is clear from the XRD pattern of this sample that Bi-2212 phase is dominant

The same $T_{c\text{-}zero}$ value of 104K has been measured by Kula et al.[8] for Bi-2223 films, in which Bi-2212 phase was dominant, grown on twin free epitaxial perovskite $CaNdAlO_4$ substrates. They reported that the suppression of $T_{c\text{-}onset}$ may be connected either with the decreased fraction of Bi-2223 phase or detrimental inter diffusion between film and $CaNdAlO_4$ substrate during the high temperature annealing. However, in this work

it has been shown that the suppression of $T_{c\text{-onset}}$ cannot be related to the fraction of Bi-2223 phase. After cleaning of the film it was observed under the optical microscope that the substrate surface was as smooth as fresh ones, indicating no damage to the surface of the substrate. Also, no film-substrate interaction has been reported for $LaAlO_3$. Different annealing temperatures between 856°C and 862°C were scanned at 2°C intervals for samples grown on $LaAlO_3$, but no significant difference has been detected even in respect of critical current density, J_c.

The BSCCO film prepared on $SrTiO_3$ was of very low quality with a low fraction, ~25%, of Bi-2223 estimated from the ratio of low angle (002) peaks of both phases. It contains also Ca_2PbO_4 due to the uncompleted transformation of the Bi-2212 phase. The superconducting transition of this film was relatively broad with zero resistivity at 97K and onset of superconductivity at 111K. This result agrees with that reported by Kula et al. [8]. In fact, resistivity sharply drops to a low value and it seems to be zero around 104K. But the critical current at that relatively high temperature was low due to the poor microstructure, which induces the transition tail.

Although the origin of the suppression of T_c is still unclear, it may be related to the epitaxial nature of the film on $LaAlO_3$. It could not be identified, but the presumed epitaxial growth of films would account for its high J_c value of $\approx 5 \times 10^4$ A/cm^2 at 77K associated with their smooth surface relative to the rough texture of films on MgO. On the other hand the epitaxial nature of 80 nm thin films of the Bi-2212 phase deposited on $LaAlO_3$ by metalorganic deposition has been confirmed by a neutron diffraction study [19]. Especially the deposition on $LaAlO_3$ seems reasonable since the a-axis of $LaAlO_3$ (3.793 A°) has a smaller mismatch to the half diagonal-length of the base plane of BSCCO phases ($a = b = 3.828$ A°).

5.2.8. Transport properties

Most of critical current, I_c, measurements were performed at 77.3K in liquid nitrogen. Films were not patterned into microbridges for J_c measurement, because such

measurements would not represent the real film characteristic, due to the existence of long (up to 100 μm) insulator needle structures, (SrCa)CuO, as shown in **Fig. 5.14** for all substrates used. Critical current densities are calculated by dividing I_c by the cross-sectional area. Despite the existence of (SrCa)CuO needles, J_c measurement show that these films, using the above optimised process, can carry a current above 10^4 A per cm^2. The best J_c value of ~$6x10^4$ A/cm^2 was measured on both MgO and mostly on $LaAlO_3$ at 77K.

The critical current density at 77K is presented in **Fig. 5.17** as a function of magnetic fields which are applied either parallel or perpendicular to the c-axis of a modest film. The J_c value in zero field is $1.88x10^4$ A/cm^2. It decreases rapidly when a small field is applied parallel to the film surface. The decrease in J_c is more dramatic in the case of magnetic field normal to the film surface. The large difference of ~$0.6x10^4$ A/cm^2 at J_c at the zero field point shows the effect of trapped magnetic field, as the sample was not heated up above critical temperature between field cycles. After this measurement trapped field was removed by heating the sample and the same J_c value ($1.88x10^4$ A/cm^2) was measured at zero field. The dependence of J_c on the direction of magnetic field with respect to the c-axis (**Fig. 5.18**) reflects the well known anisotropic nature of the Bi-2223 phase. The maximum J_c, which appears for B perpendicular to c-axis, ($\theta = 90^o$), was used for the calibration of absolute θ value. Small deviation from $\theta = 90^o$ considerably decreases J_c and it decreases more slowly for further decreasing θ values, being minimum for $\theta = 0$. **Fig. 5.19 a** and **b** shows I-V characteristics with magnetic field as parameter at 77K for two configurations of **B** perpendicular and parallel to the c-axis of the same sample, respectively. Note that the $B = 0$ curve in **Fig. 5.19 b** contains trapped field. The non-linearity of I-V characteristics in the low magnetic field region is outstanding but becomes smaller as the magnetic field increases. The same behaviour was observed in the I-V characteristics with field orientation with respect to c-axis as parameter (**Fig. 5.20**).

5.2.9. Long term stability

The long term stability of Bi-2223 films has also been studied by measuring the resistive and transport properties of films grown on MgO and $LaAlO_3$ substrates, after several months storage in a plastic bag in a cupboard. **Fig. 5.21** shows the variation of resistance with temperature for the fresh and nine-months-stored samples on MgO and $LaAlO_3$ substrates. The current and voltage leads were attached to the film without an evaporated silver pad, and the silver paint contact was the same for both measurements. There is no degradation in $T_{c\text{-}zero}$, but the resistivity slightly increased. This may be due to aging of the silver paint. No significant degradation was detected in J_c either. The films were also thermally cycled between liquid nitrogen and ambient temperature, no degradation of J_c at 77K was observed after 10 cycles.

5.2.10. Conclusion

Bi(Pb)SrCaCuO thin films containing a high ratio of Pb ($0.9 < Pb/Bi < 1.5$) about 0.5μm thick, were deposited on $LaAlO_3$, $SrTiO_3$ and MgO substrates by using a heavily Pb ($0.8 < Pb/Bi < 1.4$) doped single composite oxide targets. As the as-deposited film composition is not stoichiometric, superconducting properties of films were assessed with respect to as-deposited film composition. A wide region for Bi ratio running from 0.9 to above 2.3 was scanned to find out its limit and effect on film properties. It was found that Bi-content of $1.4 < Bi < 1.8$ in as-deposited film may provide almost single phase Bi-2223 thin films with T_c value running from 105.5K to 109.5K (For the Bi ratio of close to 1.8 T_c is 106K), and $J_c > 10^4 A/cm^2$. It was also found that Bi-content should be below 1.9 or lower than Sr-content to prevent the peeling off of the film during the high temperature annealing process, while Sr/Ca ratio remains around 1 in this heavily Pb doped initial film composition. Although Pb/Bi ratio is not critical in the range of $0.9 < Pb/Bi < 1.5$, when it is above 1.3 slow heating and cooling rate (1^oC/min.) may prevent the retention of Ca_2PbO_4 in the film.

The effect of the sintering temperature on the formation of the Bi-2223 phase was studied, and it was found that Bi-2223 phase started to form at 835^oC. The fraction of Bi-

2223 phase increased with increasing sintering temperature at the expense of Bi-2212, CuO and Ca_2PbO_4 phases, and it reached a maximum at 862°C. Above this temperature Bi-2223 phase decomposes into Bi-2212 and Ca and Cu rich needlelike crystals, (Sr,Ca)CuO. The number of these needlelike grains increases with increasing temperature above 862°C. Similar results about the decomposition of Bi-2223 phase in bulk have been reported by Suzuki at al. [20]. Annealing time of 15-30 min. at 862°C in air has provided highly oriented films with the c-axis perpendicular to the substrate surface. For a complete transformation of the initial phases, Bi-2212, Ca_2PbO_4, and CuO formed in the early stage of the annealing process, the heating rate should be not higher than 2°C/min. for films containing Pb/Bi ratio less than 1.3.

$LaAlO_3$ and $SrTiO_3$ perovskite substrates considerably decreased T_c. Although the origin of the suppression of T_c to 104K on these perovskite substrates is not clear, it may be related to their epitaxial nature or perovskite crystal structure containing more oxygen than MgO. $LaAlO_3$ is a suitable substrate for ex-situ annealed Bi-2223 films providing the best microstructure, which allows the high critical current density of $\approx 5 \times 10^4$ A/cm^2 at 77K even in the presence of huge (longer than 100μm) needlelike structures. The microstructure is very poor on $SrTiO_3$ for these ex-situ annealed films, and the Bi-2212 phase always dominates.

No degradation has been detected in the superconducting properties of Bi-2223 thin films stored in ordinary laboratory conditions for nine months and over. The films were also thermally cycled between liquid nitrogen and ambient temperature; no degradation of J_c at 77K was observed after 10 cycles.

5.3. The effect of the oxygen content.

5.3.1. Introduction

It is well established that oxygen concentration is one of the most important parameters determining the critical temperature, T_c, of high T_c superconducting compounds.

All are oxides and the superconducting properties are closely related to the mixed-valence states of the cation species, which are controlled by the oxygen content. The dependence of the transition temperature in the BSCCO system on the hole concentration has been extensively investigated by several groups by changing oxygen content with either cation substitution [21] or annealing in various oxygen atmospheres [22, 23]. These results definitely showed that in Bi-2212 (n = 2) to reach the optimum hole concentration (about 0.2 holes per Cu atom) corresponding to the maximum T_c of about 94K required removal of oxygen from the material. It has been also shown that up to the solubility limit of Pb: 0.35 T_c decreases from 85K (Pb:0) to 76K as a result of substituting Bi^{3+} by Pb^{2+}, and thus increasing the hole concentration in n = 2 material [24] The largest variation of T_c (51.5 to 94.4K) attributed to the oxygen content has been reported by Triscone et al. [25], while no significant variation of the lattice parameters is observed.

On the other hand, there have been contrary reports on the directions and ranges of T_c variations with oxygen content for the Bi-2223 (n = 3) phase. For example, for the n = 3 phase coexisting with the 2212 phase in $Bi_{1.6}Pb_{0.4}Sr_2Ca_3Cu_4O_x$ samples, a decrease of T_c from 105K to 89K was observed as a result of ≈0.22% weight loss, whereas for the 2212 phase an increase of T_c from 67K to 89K is observed (Zhao et al.[26]). This opposing tendency is in agreement with previously reported results by Tallon [27] and Buckley [28] et al. for phase pure n = 2 and n = 3 materials quenched in liquid nitrogen from different annealing temperatures. Li and Li [29] found a small change of 2.3K in T_c for n = 3 samples air-quenched at 860°C (T_c = 106K) and O_2-annealed at 600°C for 12 hours (T_c = 108.3K). On the other hand, others [30, 31, 32] reported that T_c decreases from 110K to 106K with increasing oxygen concentration (annealed in above 100 bar of O_2 at above 600°C). Although these results concerning the oxygen content are from bulk n = 3 material, Hattori et al. [33] have reported for thin films of composition $Bi_{1.7}Pb_{0.3}Sr_{1.3}Ca_{3.3}Cu_{3.4}O_x$ that with decreasing oxygen partial pressure T_c shifts to a lower temperature (from 107K to above 90K) and the normal state resistivity increases. This result is similar to that of ref. 5 using a similar composition to that mentioned above.

In the present study the effect of cooling processes and annealing atmosphere on the superconducting properties of Bi-2223 thin films, about 0.5μm thick, were investigated. A precise determination of oxygen content was not attempted in these samples, but the characteristic variation of T_c with both cooling process and annealing atmosphere confirms the importance of oxygen stoichiometry, suggesting the existence of a critical oxygen content which determines the highest possible value of T_c of 109.5K.

5.3.2. Experimental details

The films were sputtered from a BiPbSrCaCuO target with cationic ratios of 2:1.64:1.82:1.95:3 on MgO (100). After deposition, the films were sintered at 862^{o}C for 30 minutes in air and cooled down to different low temperatures (700 to 150^{o}C) with a cooling rate of 1^{o}C/minute, and subsequently air quenched to room temperature. This slow cooling is designed to allow the oxygen content of the films to equilibrate dynamically before quenching. The films have also been sintered and cooled in different partial oxygen atmospheres (air + 25% O_2 or Ar).

5.3.3. Results and discussion

The cationic ratios of as-deposited films were around Bi:Pb:Sr:Ca:Cu = 1.6:1.5:1.95:1.85:3 (normalised to Cu) for the films investigated unless otherwise mentioned. After sintering at 862^{o}C for 30 minutes, point analysis on the plate like grains indicated that the cationic ratio was Bi:Pb:Sr:Ca:Cu = 1.82:0.23:1.97:1.86:3 for a typical film. Large amounts of Pb have evaporated during sintering, while the net Bi increases, and Sr and Ca remain almost the same.

The crystal structure of films has been found to remain unchanged with reducing and oxidising heat treatment, from characteristic XRD pattern from an almost monophasic Bi-2223 thin film. **Fig. 5.22** shows the quenching temperature dependence of T_c for films sintered at 862^{o}C for 30 minutes in air, and cooled slowly to various temperatures before a final quench in air. T_c is maximum (above 109K) for a quenching temperature of 650^{o}C and

is decreased to 105.5K for films quenched below 550°C, indicating that T_c decreases with increasing oxygen content. The transition width is 5-6K except for samples quenched at 200°C. The samples quenched above 700°C showed poor superconducting properties with T_c below 90K and long transition tails. On the other hand T_c dropped to 104.5K for the sample which was slightly Bi rich (Bi: above 1.8 in as sputtered sample) and quenched at 700°C (**Fig. 5.23** curve a). Another film from the same batch quenched at 100°C had a T_c of 106.5K i.e. this time T_c increased with increasing oxygen content. This result suggests that the direction of variation of T_c with oxidising process can be affected by both the film composition and initial oxygen content.

It was also found that an over Pb doped sample (Pb: above 0.26 in annealed sample) is not sensitive to the oxygen loading below 500°C having a T_c of 106K. Two films taken from the same batch were annealed under the same conditions (heated up from 450°C with a ramping rate of 3°C/min. to 862°C and sintered at this temperature for 30 min. in air) and subsequently quenched at 500°C and below 100°C. The resistivity curves of these samples are almost same, with T_c values of 106K and transition widths of 5K (**Fig. 5.24** curve a, b). One of these samples was reannealed at 750°C for 1 hour in a 25% Ar rich atmosphere and then air quenched at 700°C. $T_{c\text{-zero}}$ has increased by 2K while $T_{c\text{-onset}}$ increased by 6K (**Fig. 5.24** curve c). An increase of 4K in transition temperature and slightly increase in resistivity may be a combined effect of some porosity due to evaporation of the excess Pb, or impurity phases induced by reannealing at 750°C. As mentioned before (section 5.2.6) 750°C is a critical temperature for annealing causing an increase in Bi-2212 even during the cooling process. Reannealing did not cause similar situations except around 750°C. The decrease of T_c to 106K with excess Pb content is consistent with the result reported for Bi-2212 [24] where it is attributed to an increase in the hole concentration. The insensitivity of the excess Pb doped sample to the reducing and oxidising process at ambient pressure could be explained in terms of the strength of the bonding between Bi-O slabs. It has been shown on Pb-free and Pb-doped Bi-2212 single crystals that Pb induces efficient coupling between these slabs [34]. As Bi-2212 and Bi-2223 phases contain similar structural units, Pb should

also induce a similar type of bonding in the latter phase. This result reveals that the variation range of T_c with oxygen content is controlled by Pb content in the sample.

Fig. 5.23 shows the annealing atmosphere dependence of T_c for films annealed in air, 25% O_2 rich and 25% Ar rich atmospheres (both with respect to air). T_c is 105.7, 108.4, 109.5K for the O_2 rich, air and Ar rich atmospheres, respectively. This result suggests that with increasing oxygen content T_c decreases, while the resistivity of samples increases. In order to make sure that the effective parameter is oxygen content, experiments were carried out on the same sample having an initial critical current density, J_c, of 1.4×10^4 A/cm^2 at 77K. The as-prepared sample was oxygen loaded by cooling in a 25% O_2 rich atmosphere and was then annealed in an Ar rich atmosphere at 830^{o}C for 1h and quenched from 680^{o}C in air. T_c of the sample increased from 106.5K to 109.5K. T_c decreased to 108K when the same sample was reannealed at 830^{o}C for 1 hour and cooled to 280^{o}C in air, while its resistivity was not much affected (**Fig. 5.25**). This temperature (108K) is the same as that obtained for films initially annealed in air, indicating that the oxygen loading / unloading is reversible. The highest critical current density, J_c, of 2.6×10^4 A/cm^2 at 77.3K using 1 μV/mm voltage criterion has been measured on the film annealed in a reduced oxygen atmosphere (**Fig.5.23** curve b). The approximate resistivity value at $T_{c\text{-onset}}$ is 3.9×10^{-4} Ω-cm for this sample.

5.3.4. Conclusion

The effect of the annealing and cooling process in various oxygen atmospheres at ambient pressure on the superconducting properties of textured polycrystalline Bi-2223 thin films has been studied. It has been found that the optimum hole concentration corresponding to the highest possible value of T_c of above 109K can be obtained by two methods. For the as deposited film composition of $Bi_{1.6}Pb_{1.5}Sr_{1.95}Ca_{1.85}Cu_3O_x$ either quenching from between 600 and 650^{o}C following annealing at 862^{o}C for 30 min. or annealing in reduced atmosphere at ambient pressure may allow achievement of the optimum carrier concentration. It has also been shown that the direction and variation range of T_c with

oxidising process is affected by Bi and Pb content, or by the initial oxygen content of the film. In order to get the optimum hole concentration, at the above composition requires reduction of the oxygen content, whereas a slightly Bi rich (Bi: 1.82 in the above instead of 1.6) composition needs to be oxidised. The over Pb doped (Pb: over 0.26) films are not sensitive to the reducing and oxidising process used, at least at ambient pressure, but the excess Pb reduces T_c to 106K. Thus variations in the precise preparation conditions, particularly the sample composition and the sintering process, may be responsible for the contradictory results on the effect of oxygen content on the T_c values in n=3 material described in the literature.

5.4. General discussion

As indicated in the results section the use of a heavily Pb doped target is an effective way of Pb doping Bi-2223 thin films. Although heavily Pb-doped thin films form the high T_c phase rapidly, they have poor morphology unless a suitable heat treatment is applied. A large amount of Pb is necessary to synthesise the high T_c phase as the Pb dopant evaporates easily during sintering [35]. Cu content was also kept a little excess in the as-deposited films because it decreases by about of 3% during an hour of sintering [36]. The decrease of Cu content is attributed to presence of Pb in the initial composition as indicated by Dew et al. [9], where Bi content slightly increased with time. The present results in which the initial cationic ratio of BiPbSrCaCu= 1.55:1.65:1.87:1.83:3 provides nearly stoichiometric Bi-2223 thin films after sintering for 30 min. are in agreement with the above approach. Various researchers have suggested that a nominal composition with either Ca:Sr=1 [12] or Sr-rich [13] would lead to the formation of a higher volume fraction of the Bi-2223 phase. But in the present study no significant difference was found for even Ca rich compositions. However Shi et al. reported that the diffusion process is obviously enhanced by increasing initial Ca and Cu content on Pb-free bulk material [37]. Similar microstructure to that illustrated in **Fig. 5.2**, in which the Pb/Bi ratio is 1.51, was observed by Tanaka et al. [36] on nearly stoichiometric heavily Pb doped (Pb/Bi=0.93) as deposited films. This is

probably an effect of fast heating during annealing. Their optimised initial composition ($Bi_{1.83}Pb_{1.46}Sr_{1.83}Ca_{1.81}Cu_3O_x$) is quite close to our composition above except for the Pb and Bi content, and the measured T_c (106.5K) and Jc ($4.1x10^4$ A/cm^2 at 77K) values are also similar to those that we measured for the films having Bi content of 1.82 (on MgO substrates). Kula et al. [8] reported that $T_{c\text{-}zero}$ increases with increasing Pb/Bi ratio in the as-deposited film with a composition (within a few percent error) of $Bi_2Pb_xSr_2Ca_{2.15}Cu_{3.3}O_y$ (x = 0, 1, 1.5, 2, 2.5), and they explain that the best growth of the Bi-2223 phase was observed in the films with initial Pb/Bi = 1.25, with $T_{c\text{-}zero}$ and J_c values 106K, $>10^3$A/cm^2 at 77K (on MgO), respectively. This result also supports the view that excess Bi-content in the initial composition is responsible for the T_c of 106K. However, in the present work it was shown that Bi-content of $1.4<Bi<1.8$ in the as-deposited film may produce a T_c value of above 108K, and that heating and cooling rates are more important, to prevent the retention of Ca_2PbO_4 causing poor microstructure, rather than the initial Pb/Bi ratio. It was also shown that excess Pb-content (Pb: above 0.26 in the annealed sample) may reduce T_c to 106K. This effect of composition on T_c is explained in terms of substituting Bi^{3+} by Pb^{2+} and thus increasing hole concentration. Reducing and oxidising experiments revealed that hole concentration is low in the films having excess Bi, therefore they need to be oxidised to reach an optimum hole concentration. On the other hand over Pb doped samples (Pb > 0.26) are not sensitive to the reducing and oxidising process at low temperature in ambient atmosphere, but fast quenching at high temperature may help to reduce excess hole concentration.

A suppression of T_c to 104K was observed by Kula et al. [8] on twin free epitaxial perovskite $CaNdAlO_4$ substrates, where it is mainly related to the dominance of the Bi-2212 phase or detrimental inter diffusion between film and substrates. This result is similar to that detected in the work presented here on the $LaAlO_3$ and $SrTiO_3$ perovskite substrates. However the present results revealed (section 5.2.7) that there should be another mechanism responsible for the deterioration of T_c on these perovskite substrates.

References

1 S.A. Sunshine, T. Siegrist, L.F. Schneemeyer, D.W. Murphy, R.J. Cava, B. Batlogg, R.B. van Dover, R.M. Fleming, S.H. Glarum, S. Nakahara, R. Farrow, J.J. Krajewski, S.M. Zahurak, J.V. Waszczak, J.H. Marshall, P. Marsh, L.W. Rupp, Jr., and W.F. Peck, Phys. Rev. B 38 (1988) 893.

2 Y.L. Chen, and R. Stevens, J. Am. Ceram. Soc. 75 (5) (1992) 1142.

3 H. Hayakawa, K. Nakamura, S. Ikeda, K. Ogawa, and S. Takahashi, Jpn. J. Appl. Phys. 29 (1990) L943.

4 M.R. Tseng, J.J. Chu, Y.T. Huang, P.T. Wu, and W.N. Wang, J. Appl. Phys. 67 (1990) 2657.

5 S.L. Lin, C. Tien, T.S. Chin, T.W. Huang, and M.P. Hung, Jpn. J. Appl. Phys. 29 (1990) L775.

6 Y.H. Wang, L. Li, Y.Z. Zhang, Y.Y. Zhao and P. Xu, Cryogenics 31 (1991) 439.

7 Y. Hakuraku, Y. Aridome, D. Miyagi, N.G. Suresha, and T. Ogushi, Jpn. J. Appl. Phys. 28 (1989) L819.

8 W. Kula, R. Sobolewski, J. Gorecka, and S.J. Lewandowski, J. Appl. Phys. 70 (1991) 3171.

9 S.K. Dew, N.R. Osborne, P.J. Mulhern, and R.R. Parsons, Appl. Phys. Lett. 54 (1989) 1929.

10 A. Marino, T. Yasuda, E. Holguin and L. Rinderer, Physica C 210 (1993) 16.

11 Y.T. Huang, R.G. Liu, S.W. Lu, P.T. Wu, and W.N. Wang, Appl. Phys. Lett. 56 (1990) 779.

12 H. Sasakura, S. Minamigawa, K. Nakahigashi, M. Kogachi, S. Nakanishi, N. Fukuoka, M. Yoshikawa, S. Noguchi, K. Okuda, and A. Yanase, Jpn. J. Appl. Phys. 28 (1989) L1163.

13 U. Endo, S. Koyama, and T. Kawai, Jpn. J. Appl. Phys. 28 (1989) L190.

14 U. Kuxmann, and P. Fischer, Erzmetall. 27 (1974) 533.

15 T. Uzumaki, K. Yamanaka, N. Kamehara, and K. Niwa, Jpn. J. Appl. Phys. 28 (1989) 75.

16 R. Ramesh, G. Thomas, S. Green, C. Jiang, Y. Mei, M.L. Rudee, and, H.L. Luo, Phys. Rev. B 38 (1988) 7070.

17 M. Mizuno, H. Endo, J. Tsuchiya, N. Kijima, A. Sumiyama, and Y. Oguri, Jpn. J. Appl. Phys. 27 (1988) L1225.

18 T. Hatano, K. Aota, S. Ikeda, K. Nakamura, and K. Ogawa, Jpn. J. Appl. Phys. 27 (1988) L2055.

19 P. Lee, H. Graafsma, Y. Gao, H. Sheu, P. Coppens, S.J. Golden, and F.F. Lange, Acta Cryst. A 47 (1991) 57.

20 Y. Suzuki, T. Inoue, S. Hayashi, and H. Komatsu, Jpn. J. Appl. Phys. 28 (1989) L1382.

21 W.A. Groen, D.M. de Leeuw, and L.F. Feiner, Physica C 165 (1990) 55.

22 S. Miura, T. Yoshitake, and N. Shohata, Physica C 165 (1990) 241.

23 G. Balestrino, M. Marinelli, E. Milani, and A. Paoletti, J.Appl. Phys. 73 (1993) 3903.

24 M. Boekholt, D. Gotz, H. Idink, M. Fleuster, T. Hahn, E. Woermann, G. Guntherodt, Physica C 185-189 (1991) 789.

25 G. Triscone, J.-Y. Genoud, T. Graf, A. Junod, and J. Muller, Physica C 185-189 (1991) 793.

26 J. Zhao, M. Wu, W. Abdul-razzaq, and M.S. Seehra, Physica C 165 (1990) 135.

27 J.L. Tallon, R.G. Buckley, P.W. Gilberd, and M.R. Presland, Physica C 158 (1989) 247.

28 R.G. Buckley, J.L. Tallon, I.W.M. Brown, M.R. Pressland, N.E. Flower, P.W. Gilbert, M. Bowden, and N.B. Milestone, Physica C 156 (1988) 629.

29 Y.Li,and Y. Li, Journal of Superconductivity 5 (1992) 1.

30 D.E. Morris, C.T. Hultgren, A.M. Markelz, J.Y.T. Wei, N.G. Asmar, and J.H. Nickel, Physical Review B 39 (1989) 6612.

31 S.M.Green, Yu. Mei, A.E. Manzi, and H.L. Luo, J.Appl. Phys. 66 (1989) 3703.

32 C.-H. Hsu, and N.E. Gokcen, Applied Superconductuvity 1 (1993) 19.

33 H.Hattori, K. Nakamura, and K. Ogawa, Jpn. J. Appl. Phys. 29 (1990) L36.

34 L. Pierre, J. Schneck, D. Morin, J.C. Toledano, J. Primot, C. Daguet, and H. Savary, J. Appl. Phys. 68 (1990) 2296.

35 A. Tanaka, T. Machi, N. Kamehara, and K. Niwa, Appl. Phys. Lett. 54 (1989) 1362.

36 A. Tanaka, N. Kamehara, and K. Niwa, Appl. Phys. Lett. 55 (1989) 1252.

37 D. Shi, M. Tang, M.S. Boley, M. Hash, K. Vandervoor, H. Claus, and Y.N. Lwin, Physical Review B 40 (1989) 2247.

(a)

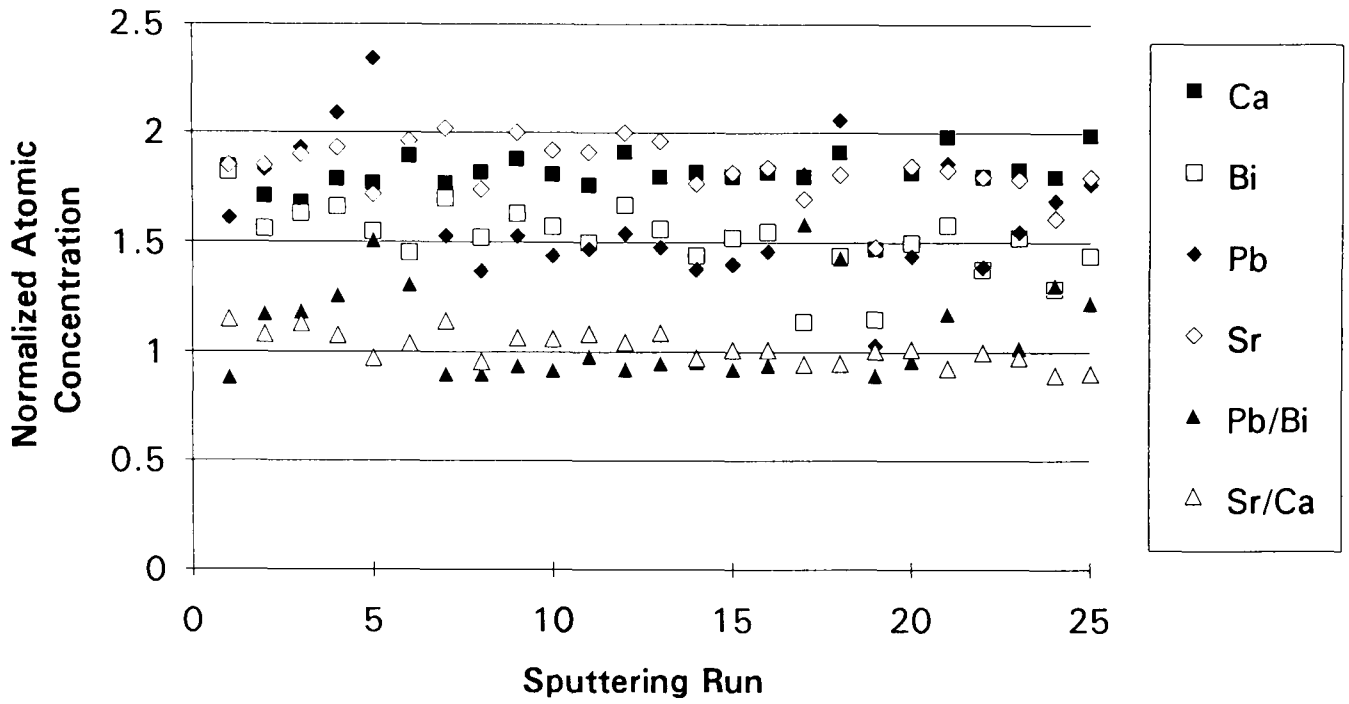

(b)

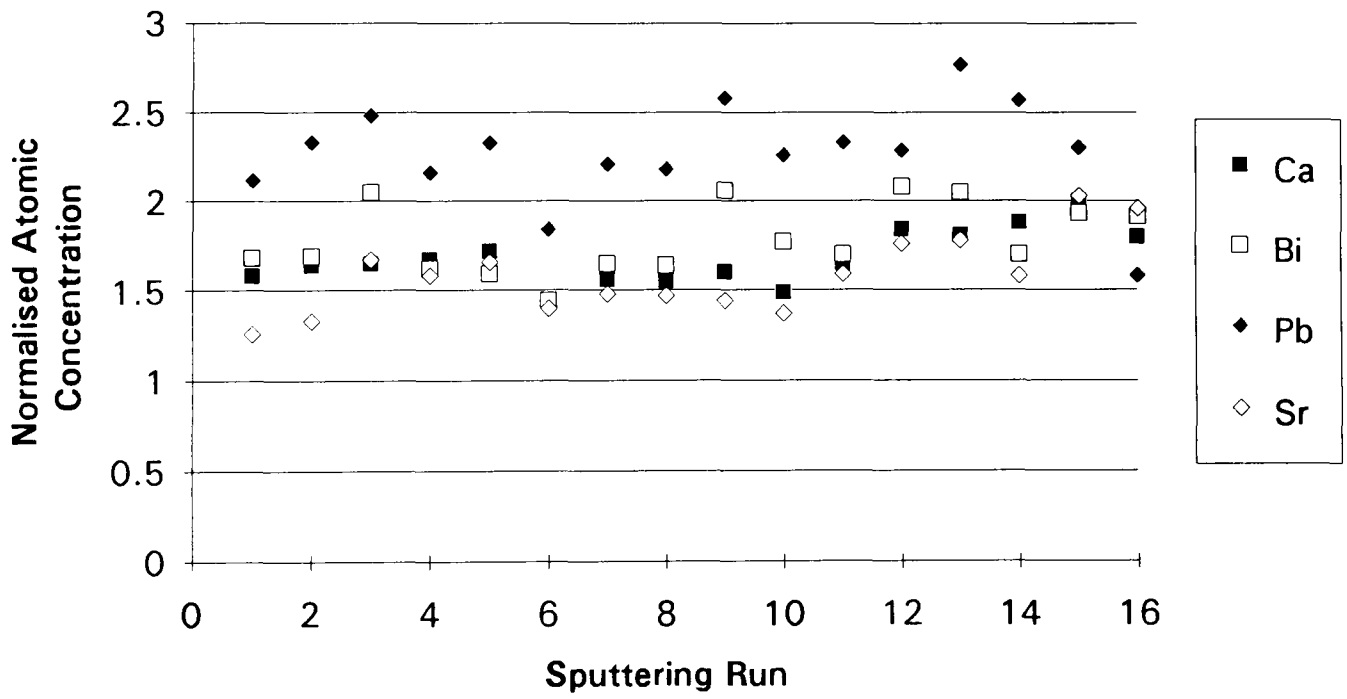

Figure 5.1 As deposited film composition for some representative samples taken from different batches. (a) Not peeled off (b) Peeled off, during high temperature annealing process

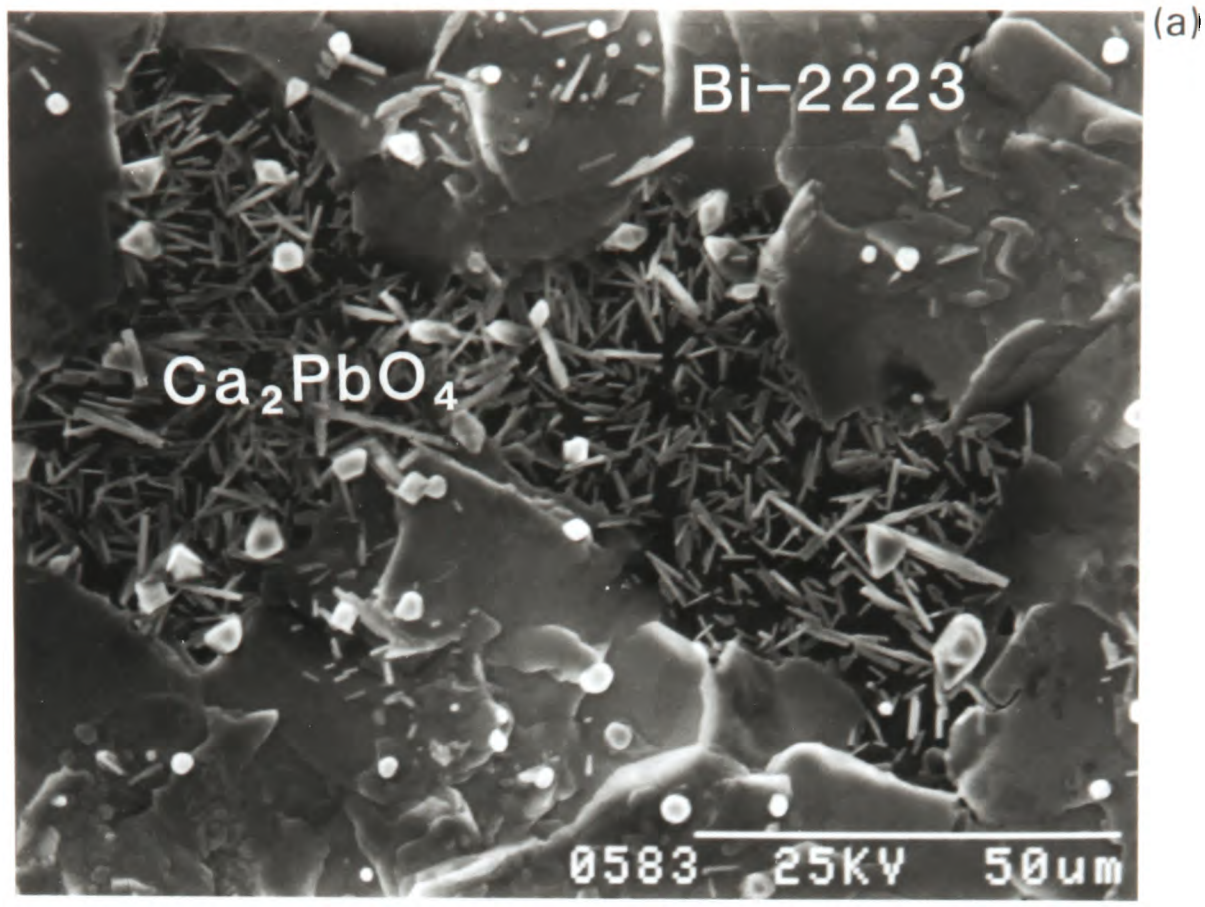

Figure 5.2 SEM micrographs of the films having Pb/Bi ratio of 1.51 in as-deposited film composition, annealed at 862^{o}C for 30min. in air. (a) Heated up with ramping rate of 2^{o}C/min. and furnace cooled. (b) Heating and cooling rates are both 1^{o}C/min.

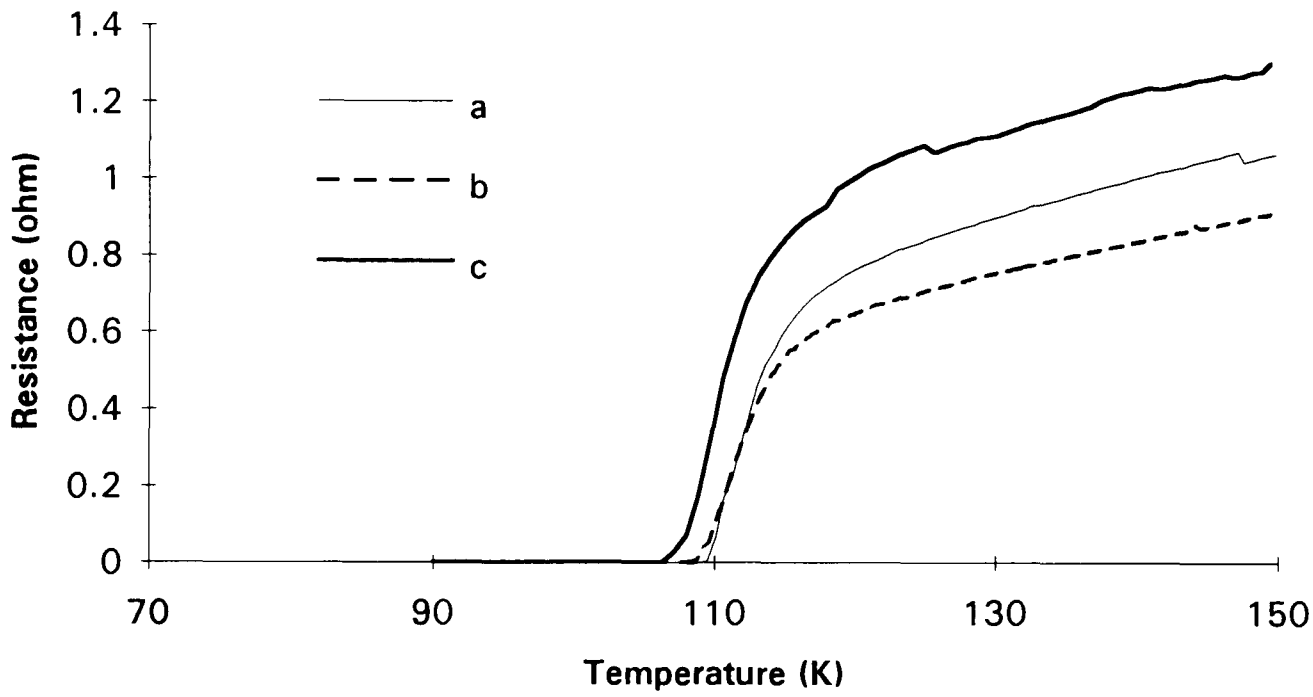

Figure 5.3 Temperature dependence of resistivity for samples annealed at 862^{o}C for 30 min. in air, on MgO, having different Bi and Pb/Bi ratio in the as deposited film. (a) Bi:1.52, Pb/Bi = 0.9 (b) Bi:1.55, Pb/Bi = 1.51 (c) Bi:1.82, Pb/Bi = 0.88.

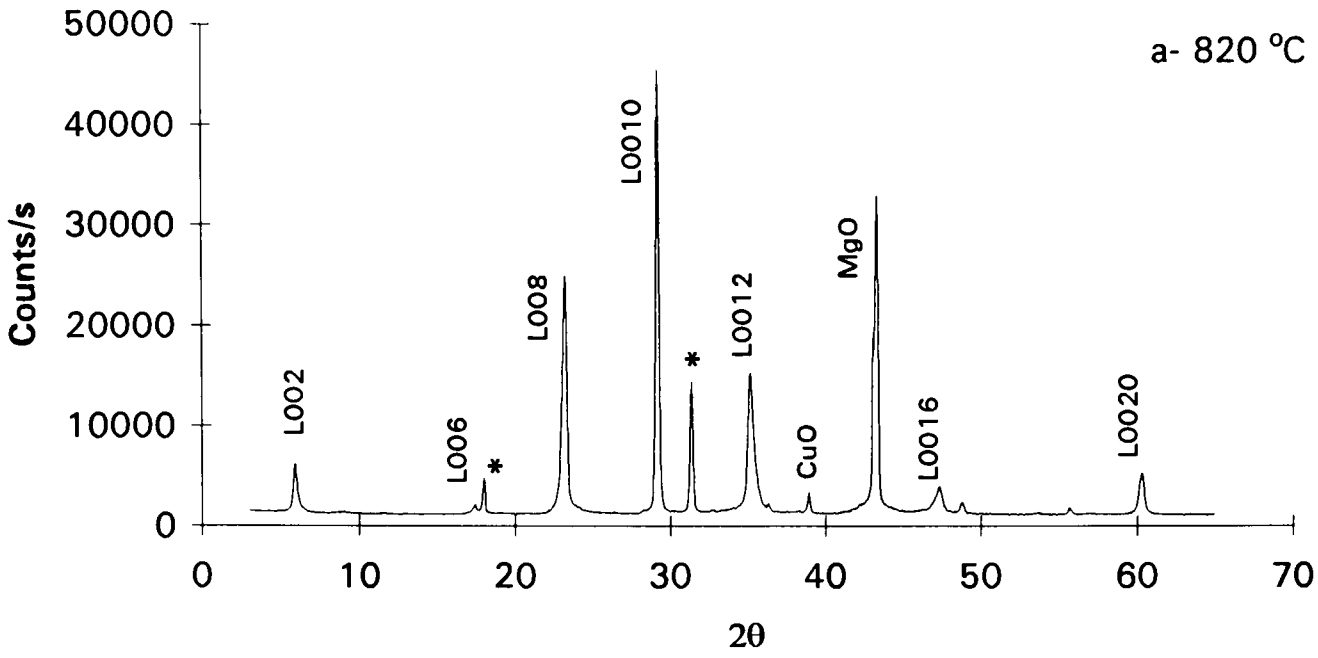
a- 820 °C
Counts/s
2θ
L002
L006
L008
L0010
L0012
CuO
MgO
L0016
L0020
*

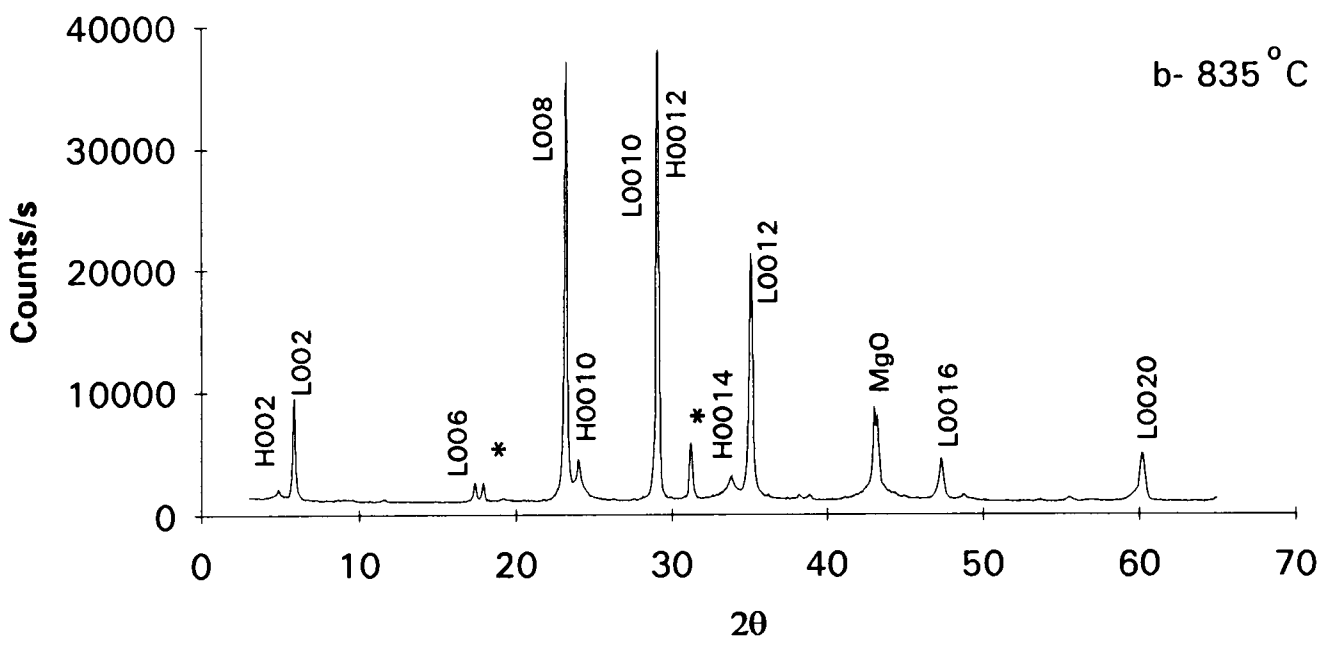
b- 835 °C
Counts/s
2θ
H002
L002
L006
L008
H0010
L0010
H0012
H0014
L0012
MgO
L0016
L0020
*

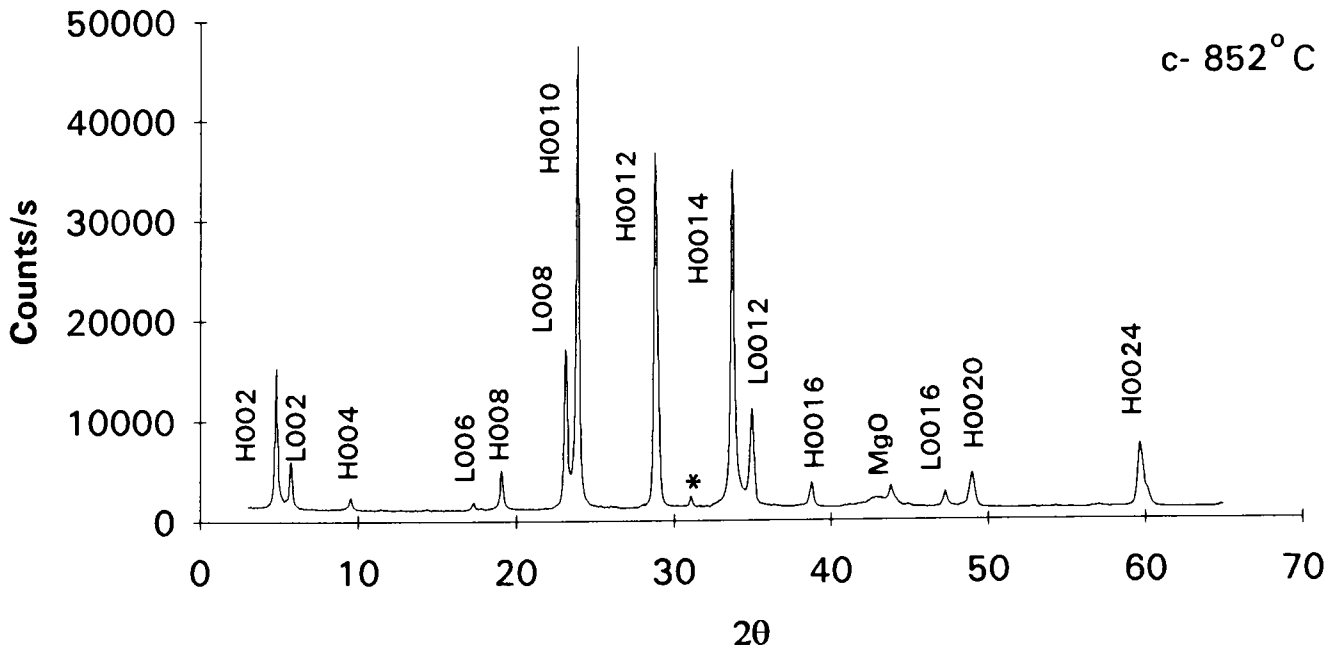
c- 852 °C
Counts/s
2θ
H002
L002
H004
L006
H008
L008
H0010
H0012
H0014
L0012
H0016
MgO
L0016
H0020
H0024
*

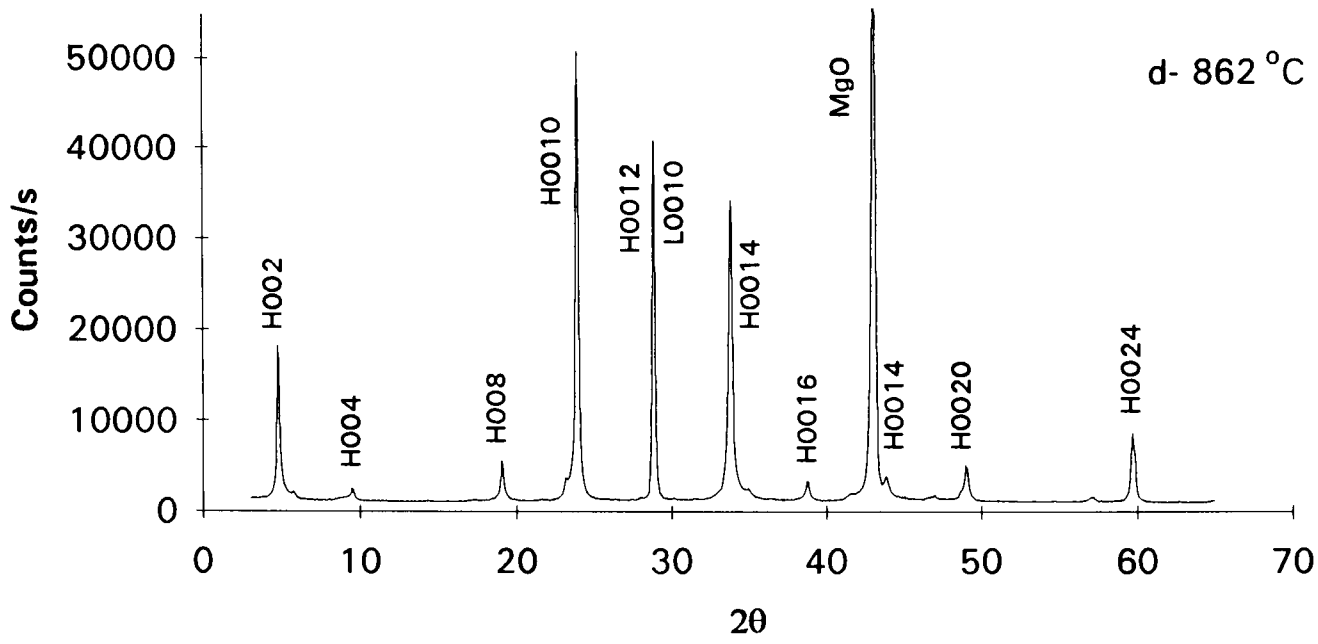

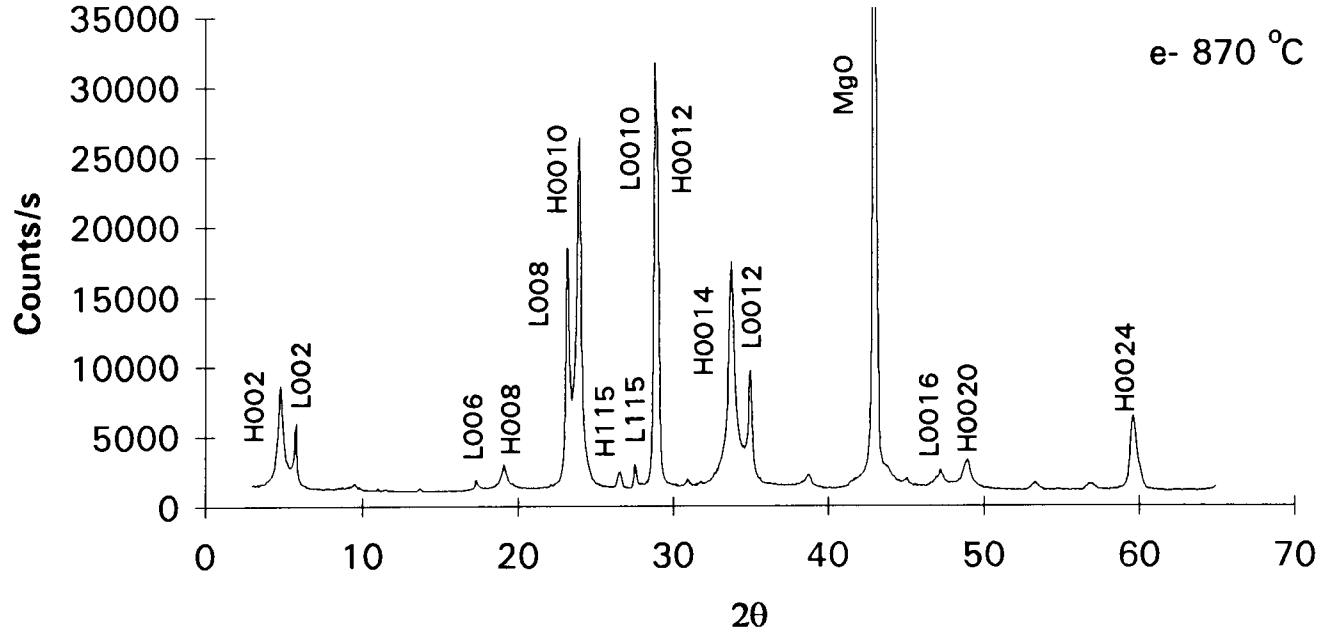

Figure 5.4 XRD pattern of the films annealed at different temperatures for 1h in air , on MgO substrates. The peaks of the Bi-2223, Bi-2212 and Ca_2PbO_4 phases are labelled by H, L and *, respectively.

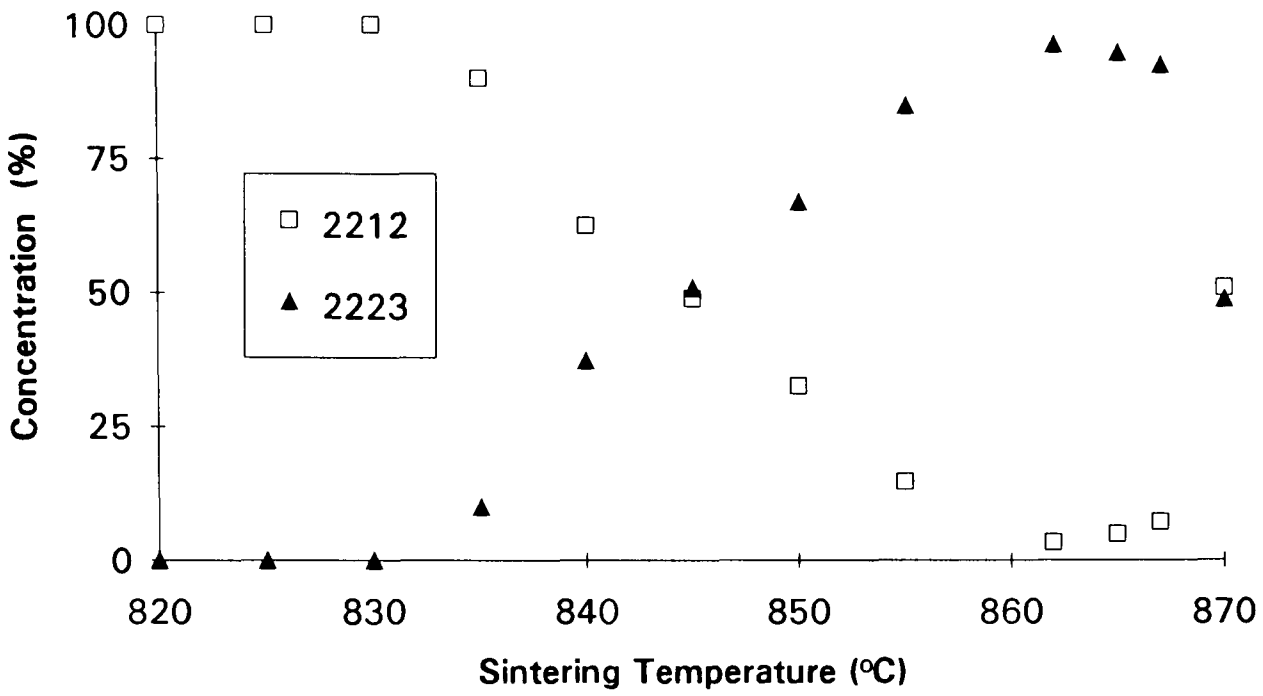

Figure 5.5 The variation of the Bi-2223 and Bi-2212 phase concentration with sintering temperature for 1 h in air

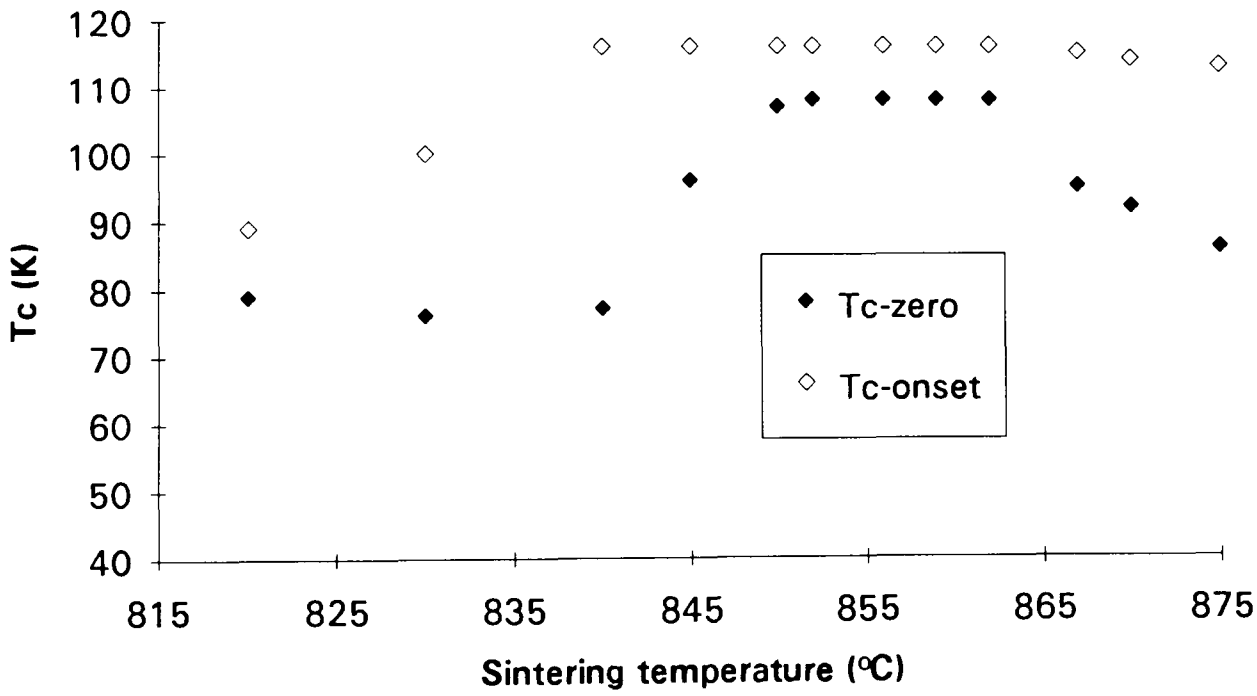

Figure 5.6 The variation of the Tc-zero and Tc-onset temperature with sintering temperature for samples sintered at different temperatures for 1 h in air.

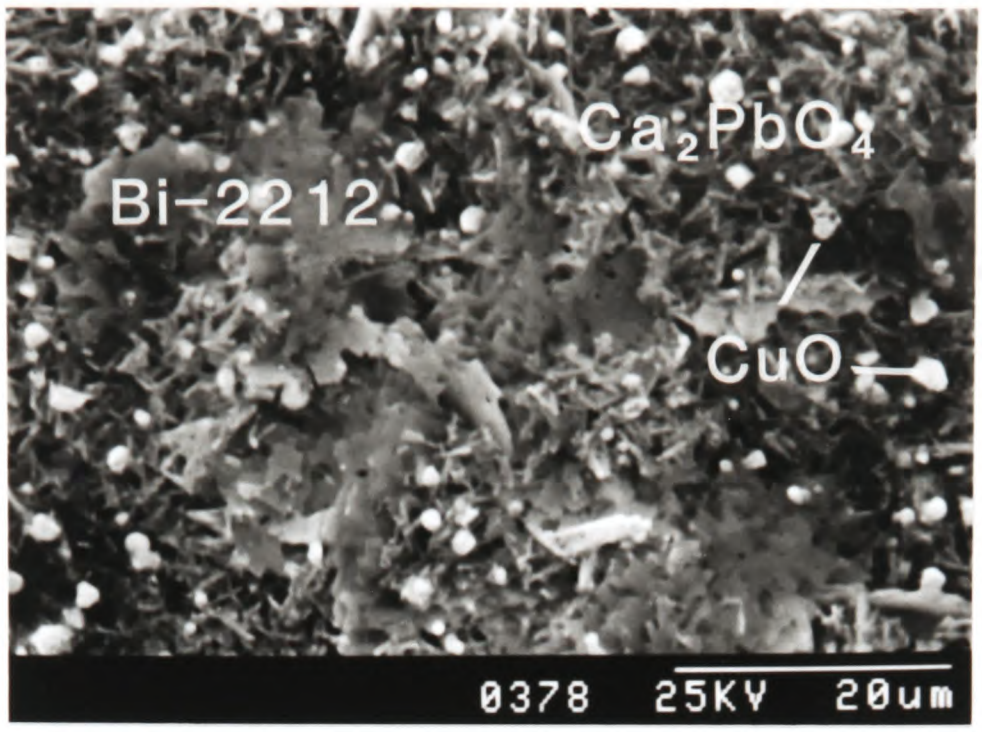

820°C

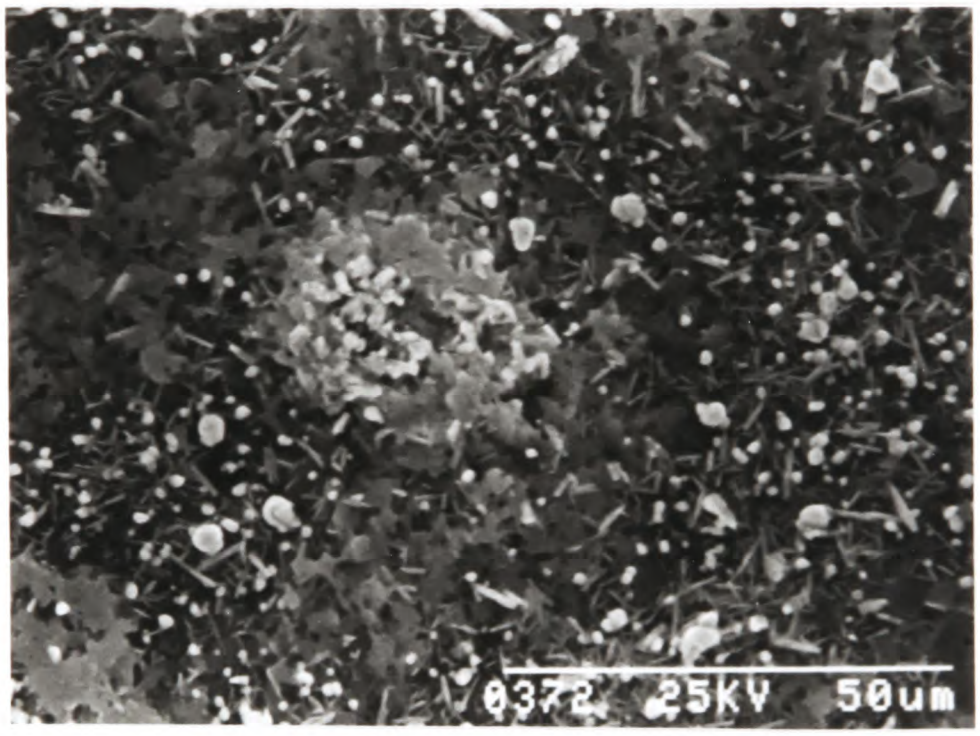

835°C

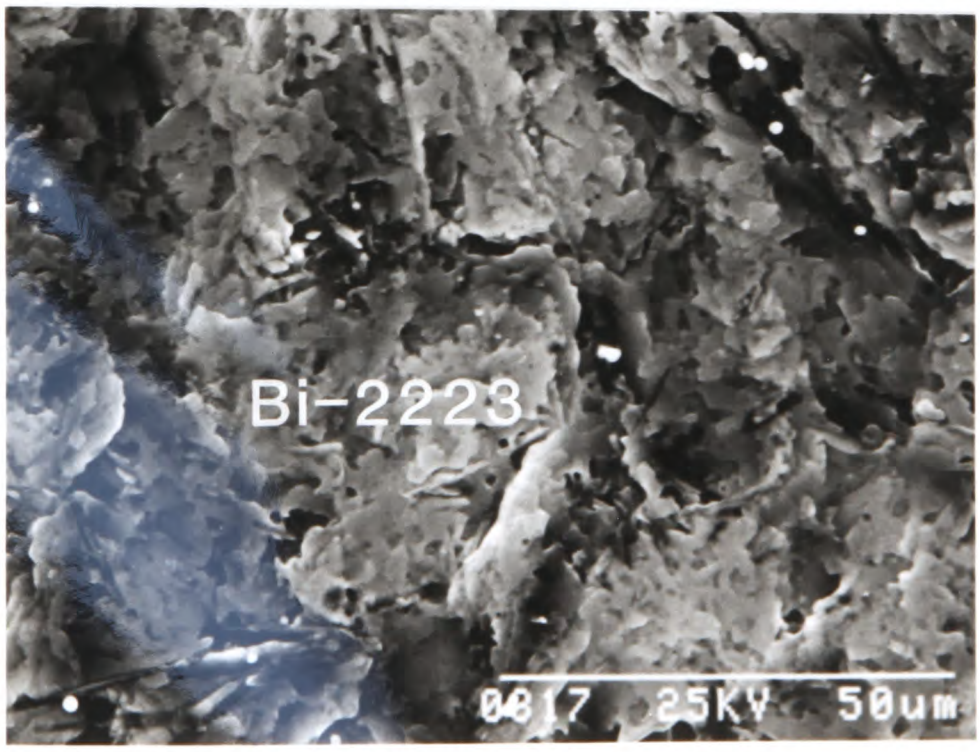

852°C

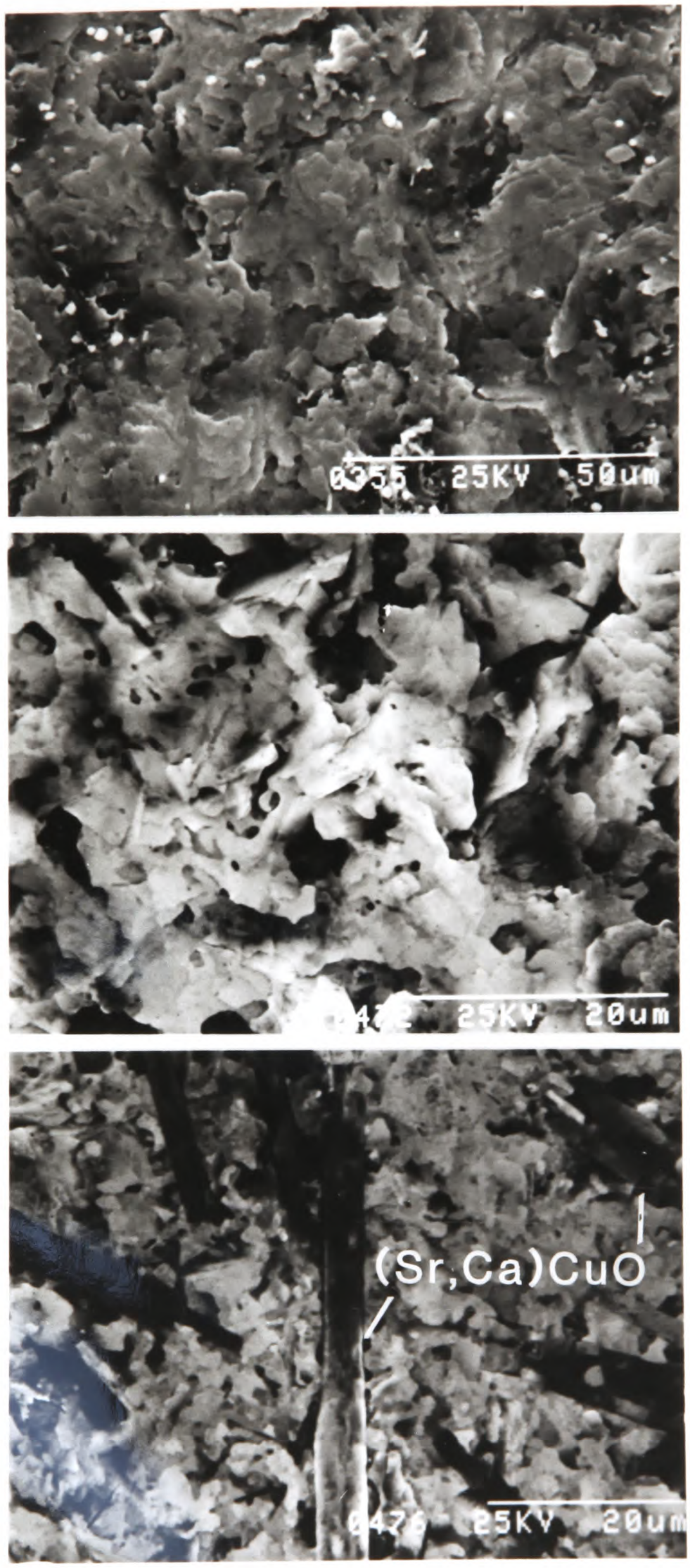

Figure 5.7 SEM micrographs of the films sintered at various temperatures for 1h in air

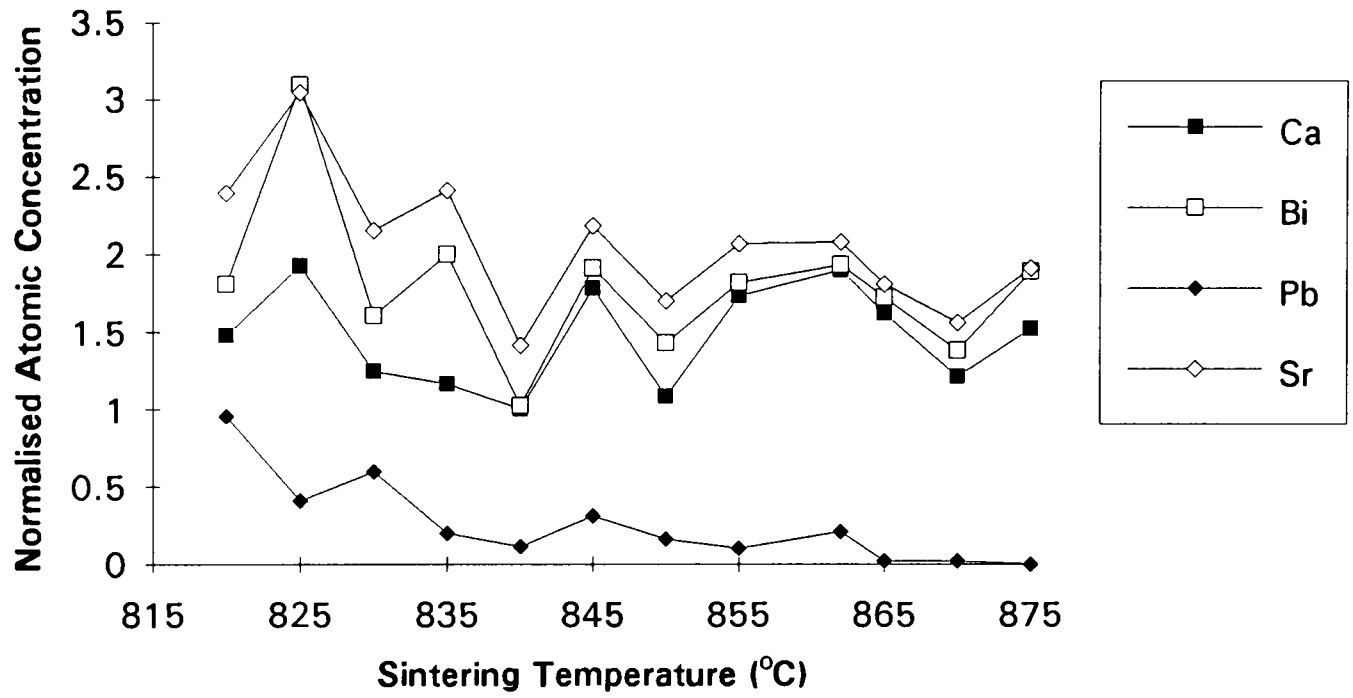

Figure 5.8 Composition of randomly chosen plate like grains from samples sintered at different temperatures.

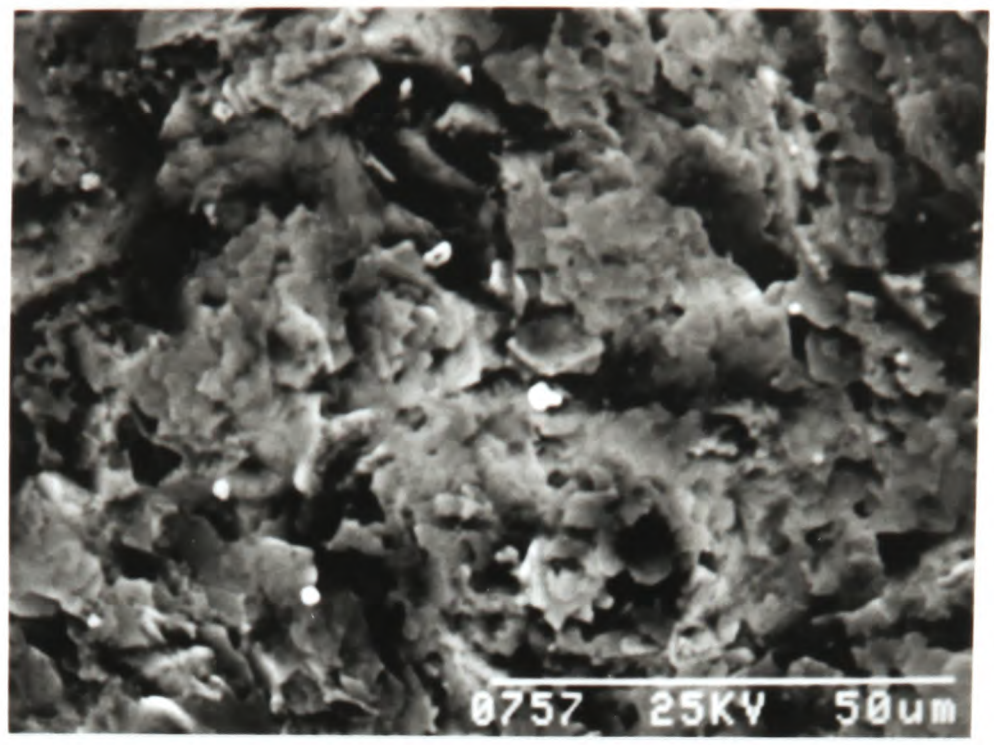

15 min.

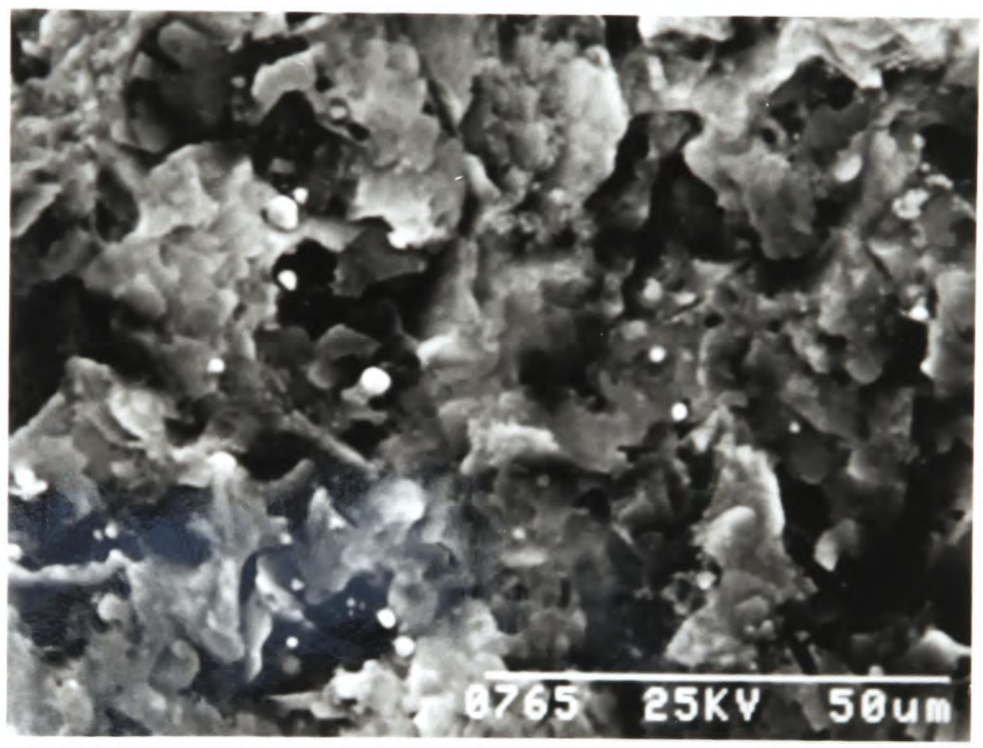

2 h

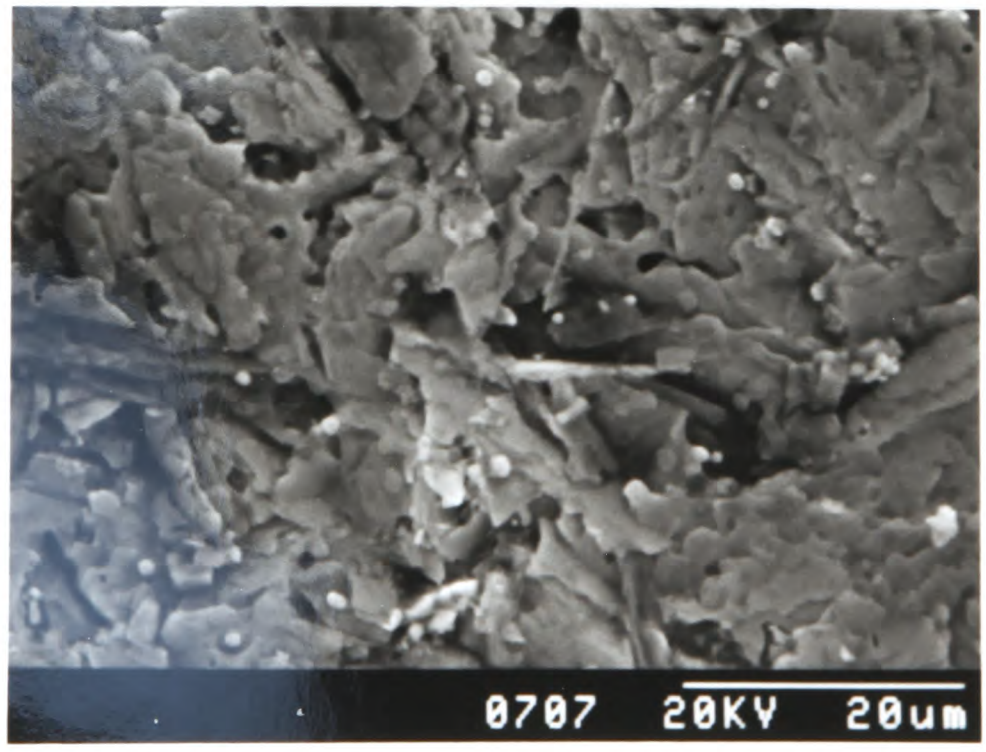

3 h

Figure 5.9 SEM micrographs of the films sintered at 862^{o}C in air for various lengths of time.

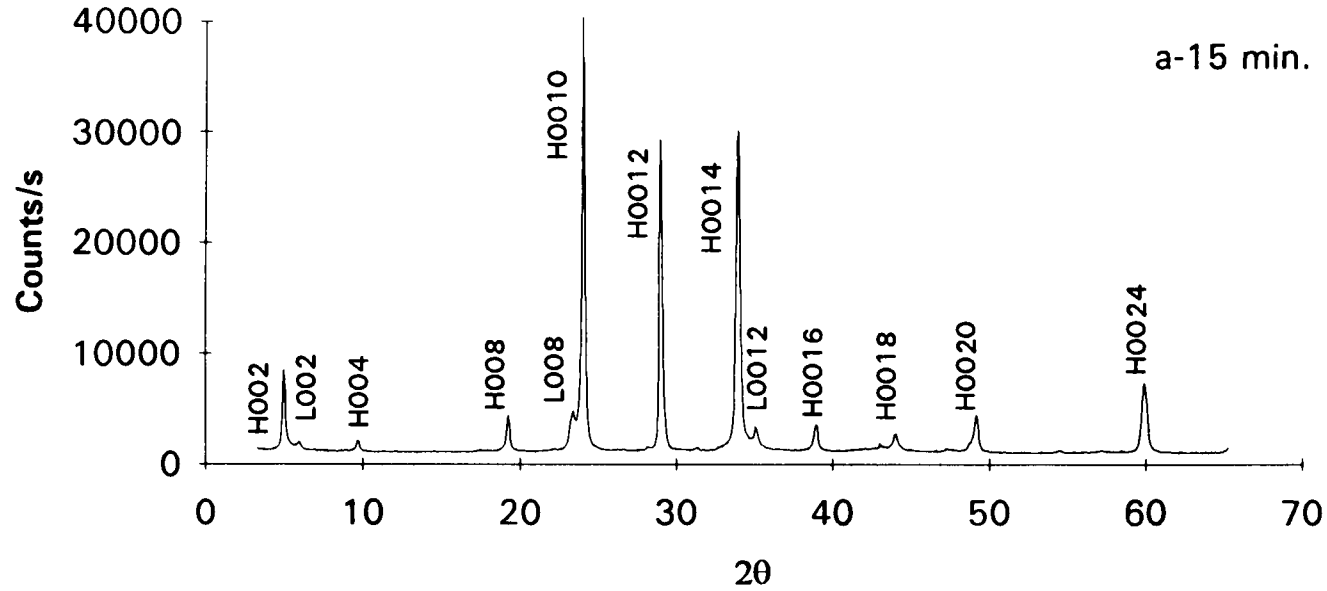

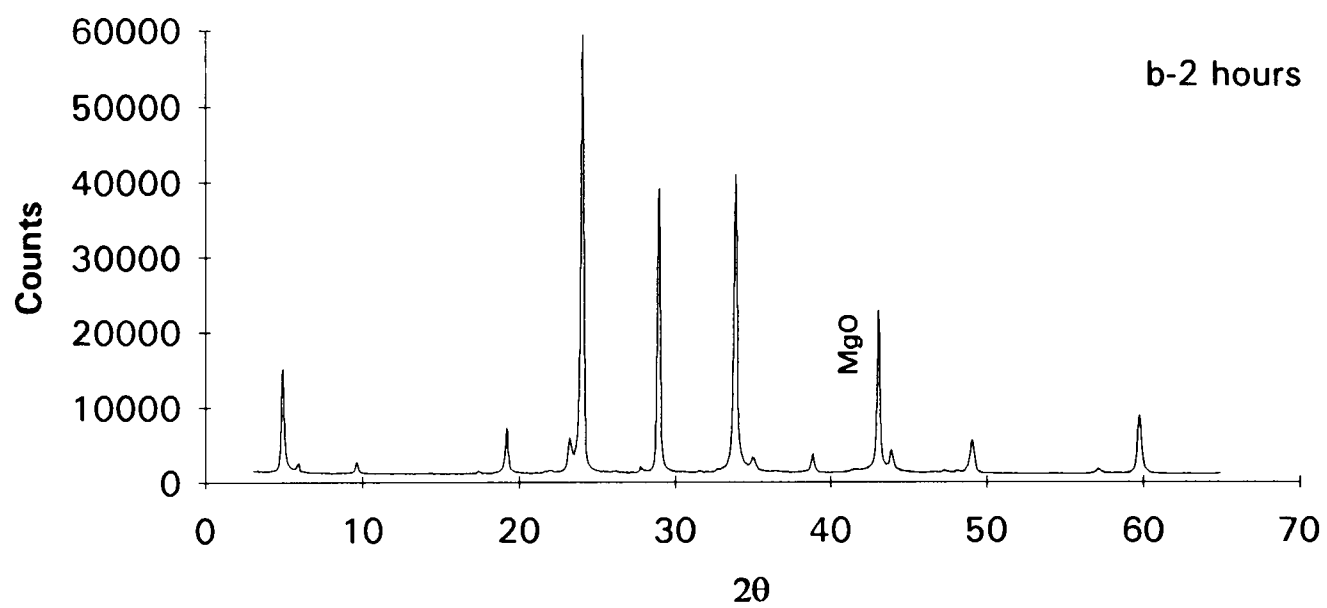

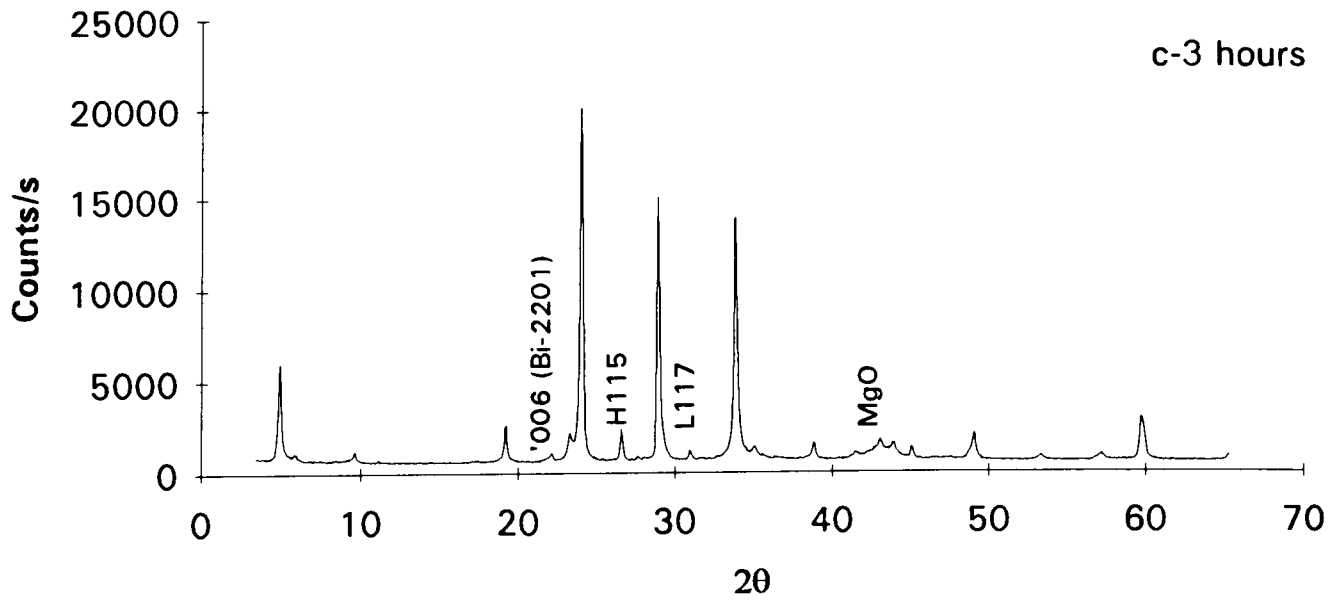

Figure 5.10 XRD pattern of some films annealed at 862^{o}C for different periods.

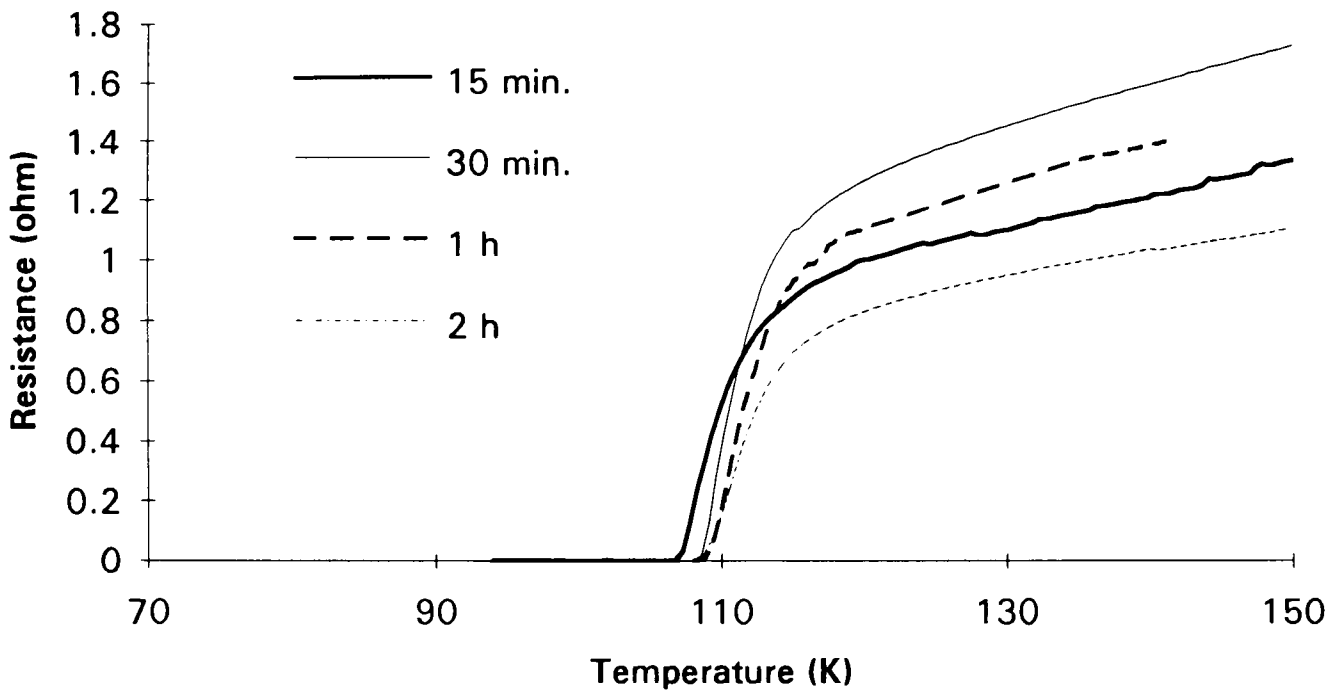

Figure 5.11 The temperature dependence of the resistivity for samples annealed at 862°C for different periods in air.

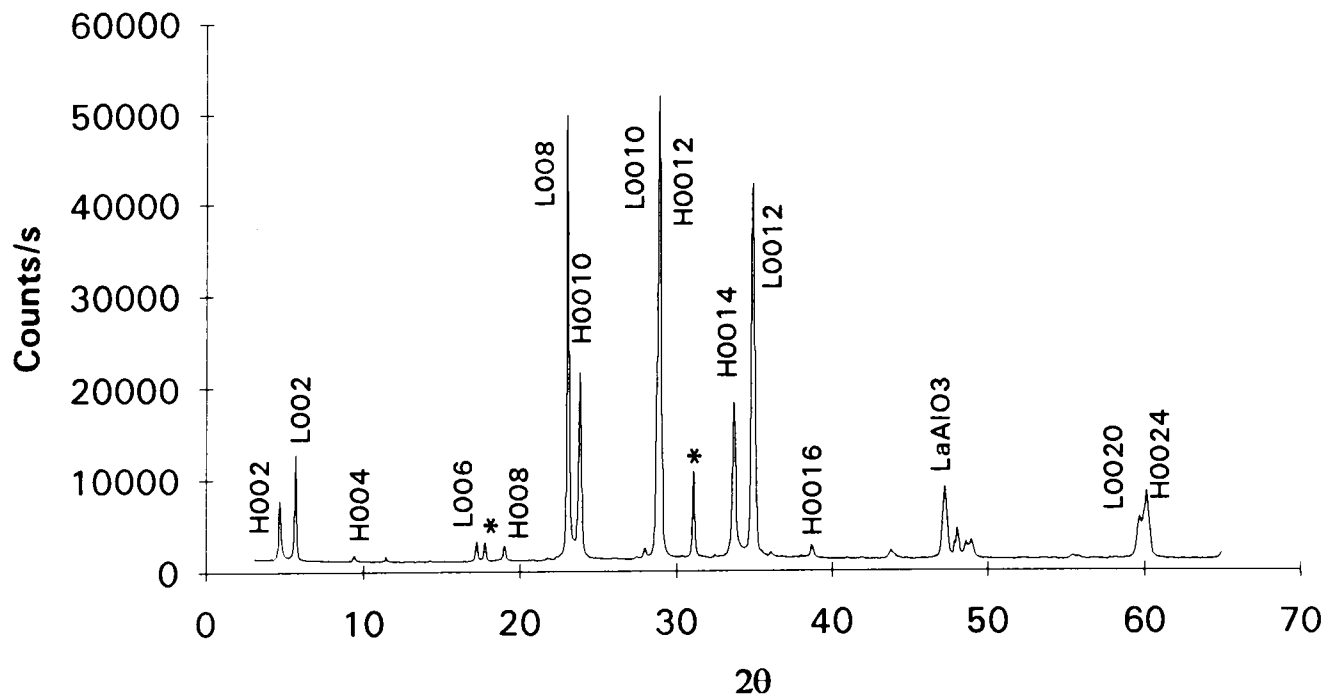

Figure 5.12 XRD pattern of the film heated up from 100°C with ramping rate of 10°C/min. up to 840°C then 1°C/min. to the annealing temperature and annealed at 862°C for 30 min., on $LaAlO_3$. The peaks of Ca_2PbO_4 are labelled by *.

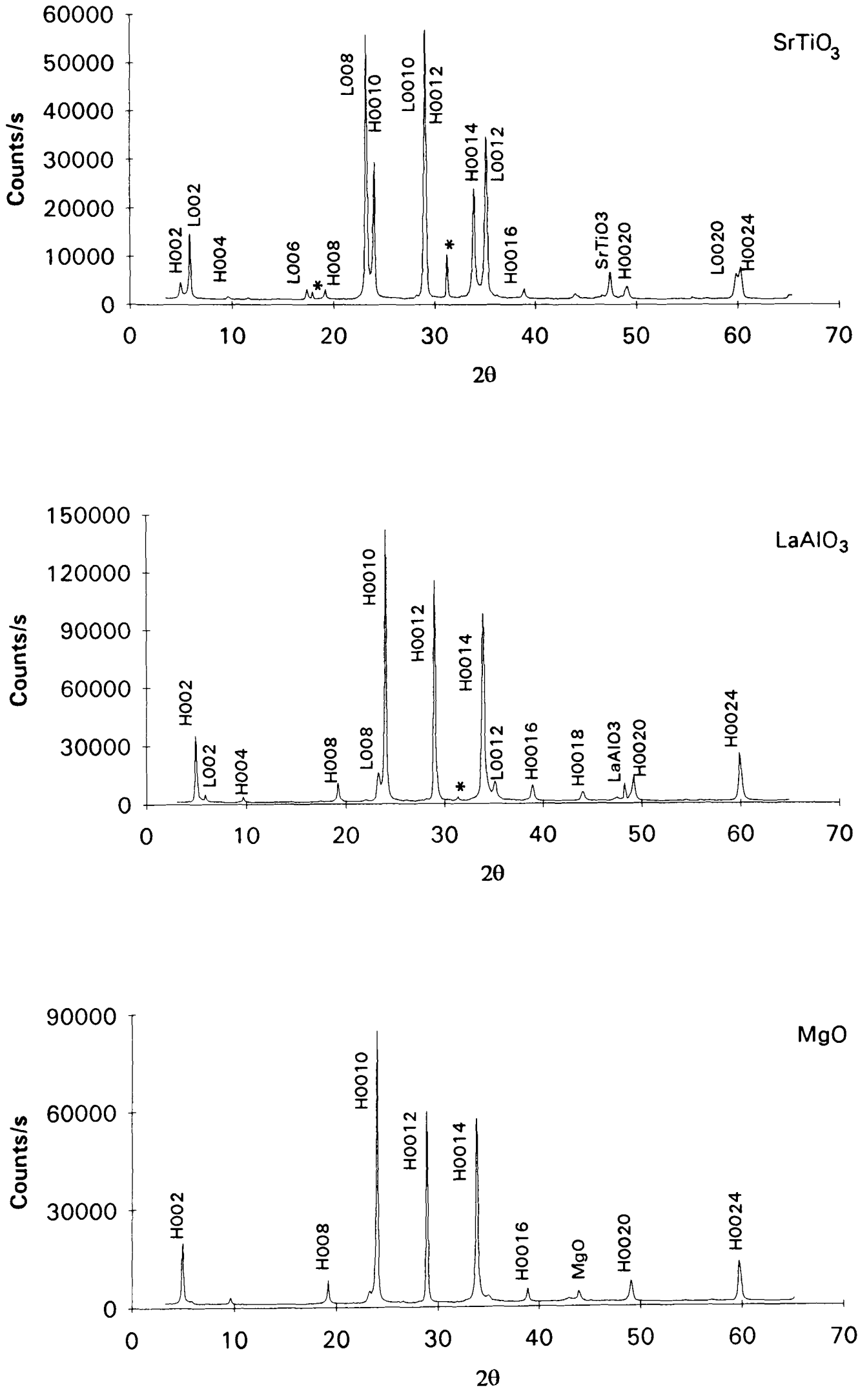

Figure 5.13 XRD patterns of the films grown on different single crystal substrates and annealed at 862°C for 30 min. in air. * indicates peaks of Ca_2PbO_4.

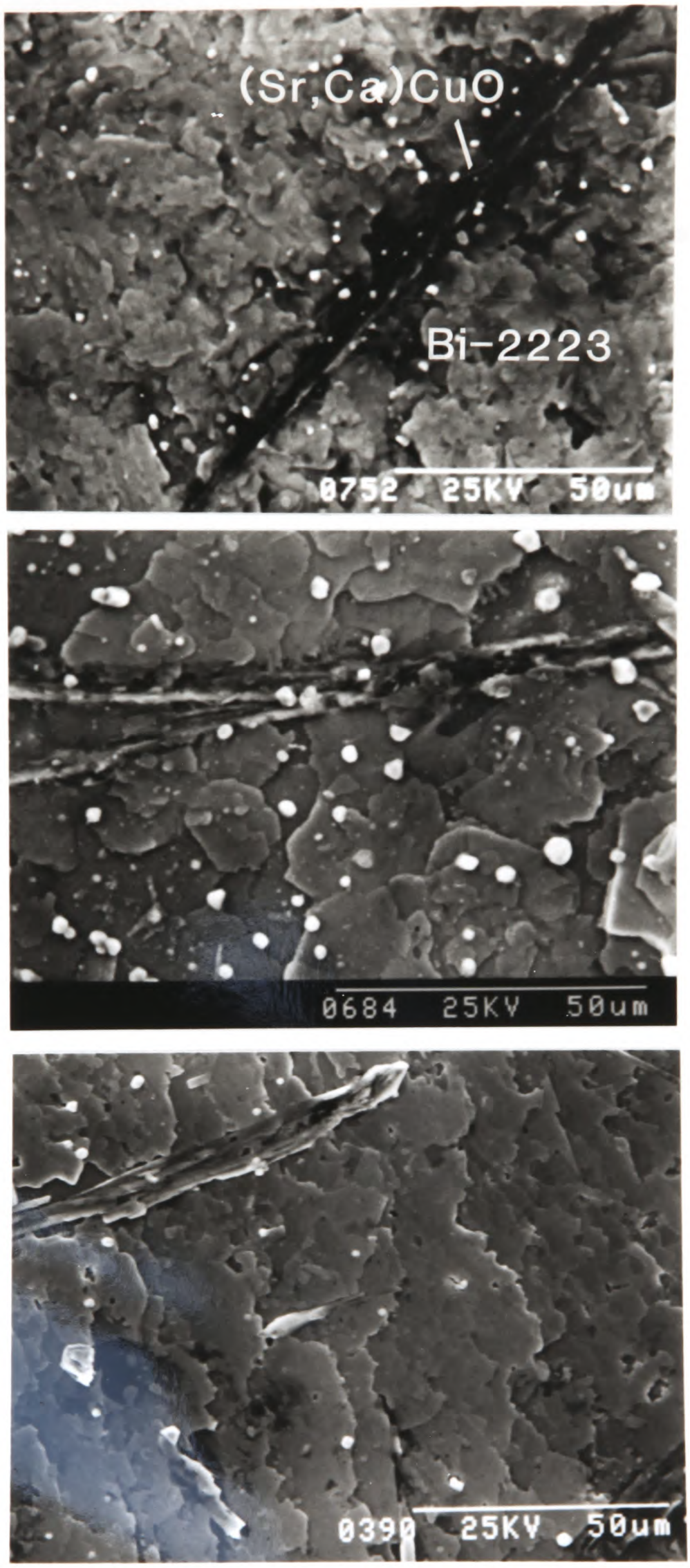

MgO

$LaAlO_3$

$SrTiO_3$

Figure 5.14 SEM micrographs of the films grown on different single crystal substrates and sintered at 862^{o}C for 30 min. in air.

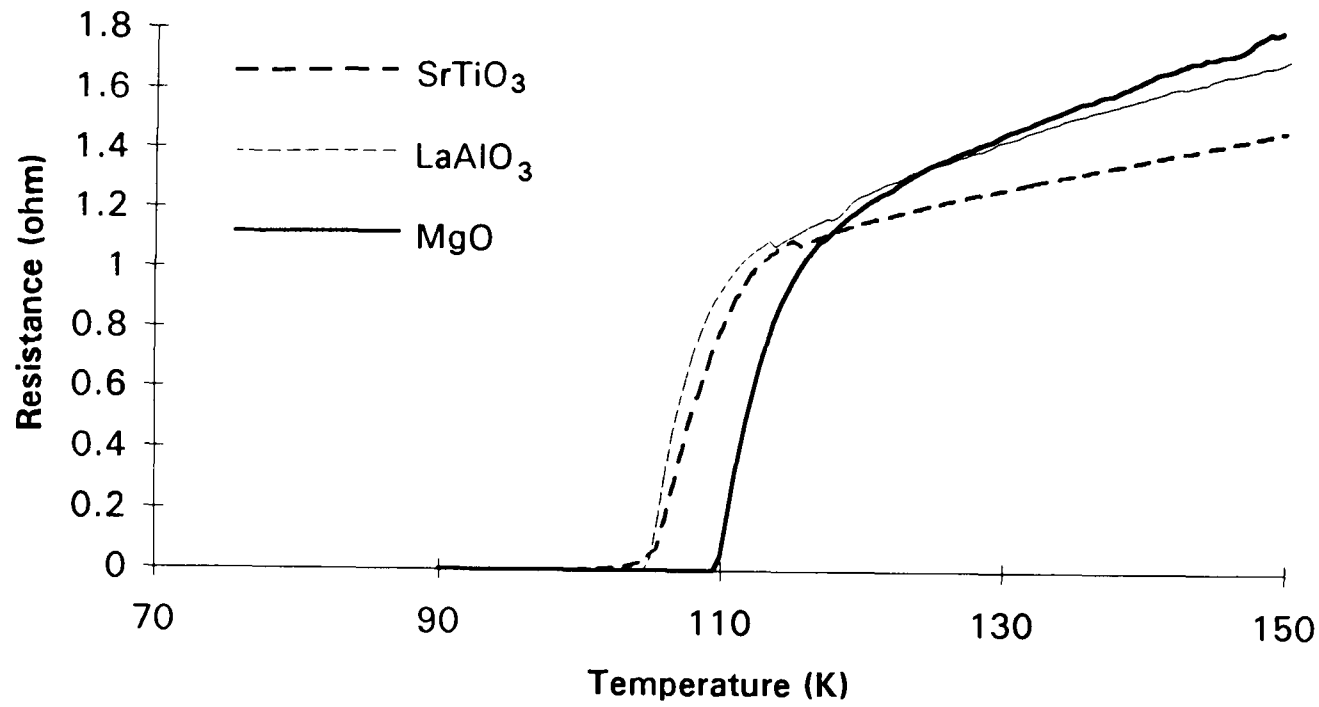

Figure 5.15 The temperature dependence of resistivity for the samples grown on different single crystal substrates and sintered at 862°C for 30 min. in air.

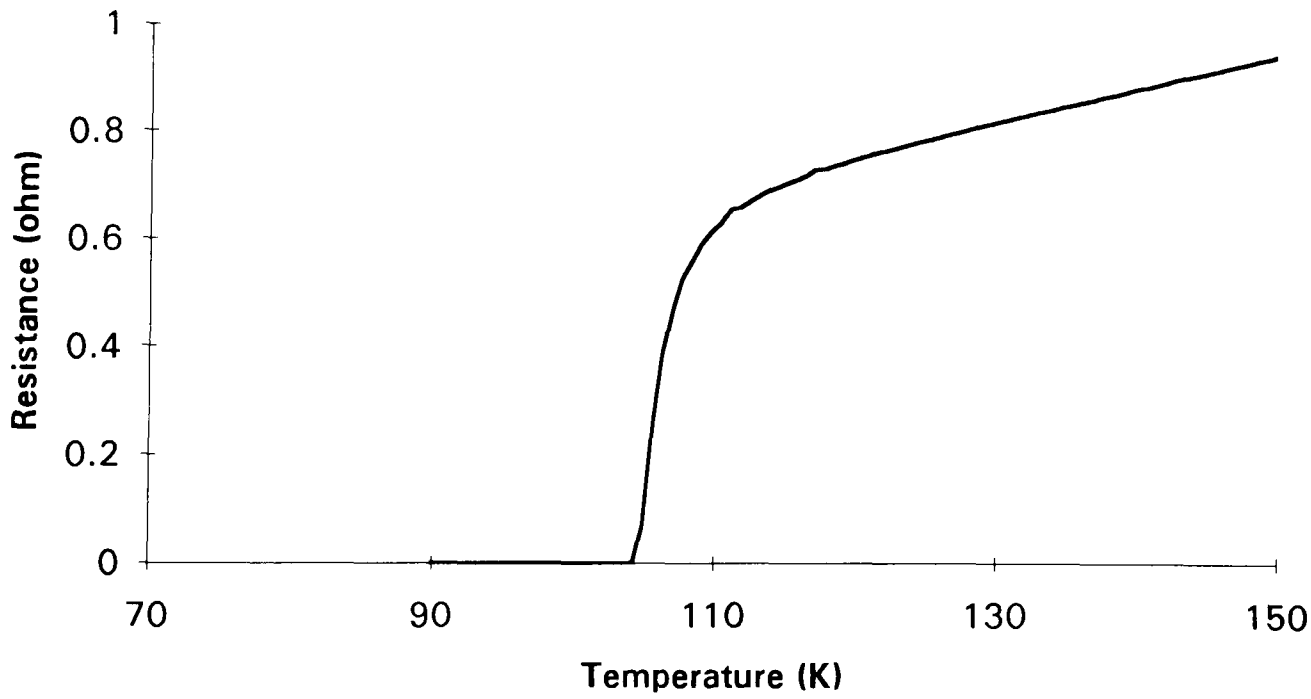

Figure 5.16 The temperature dependence of resistivity for the film grown on $LaAlO_3$ single crystal substrate and annealed at 862°C for 30 min. in air. XRD pattern of this film is shown in **Fig. 5.12** in which Bi-2212 phase is dominant.

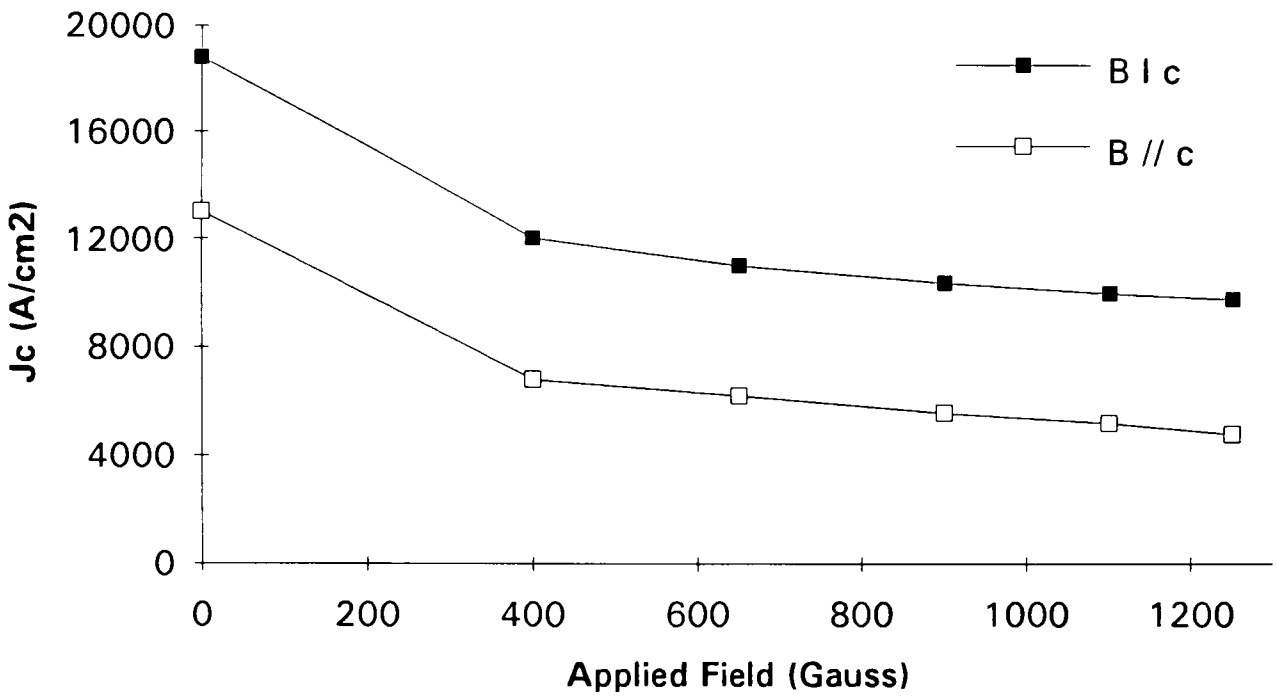

Figure 5.17 The variation of critical current density, J_C, as a function of magnetic field, which is applied either parallel or perpendicular to the c-axis of the film, at 77K.

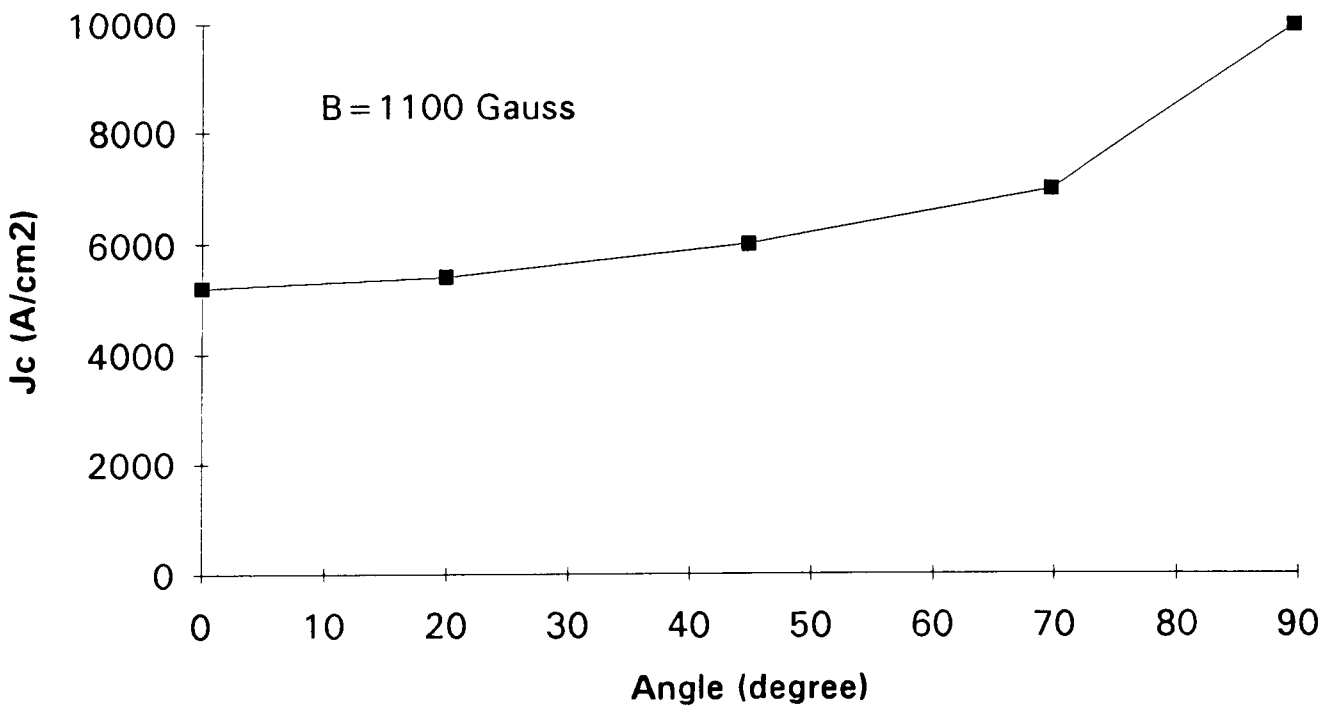

Figure 5.18 The dependence of critical current density, J_C, on the direction of applied magnetic field at 77K.

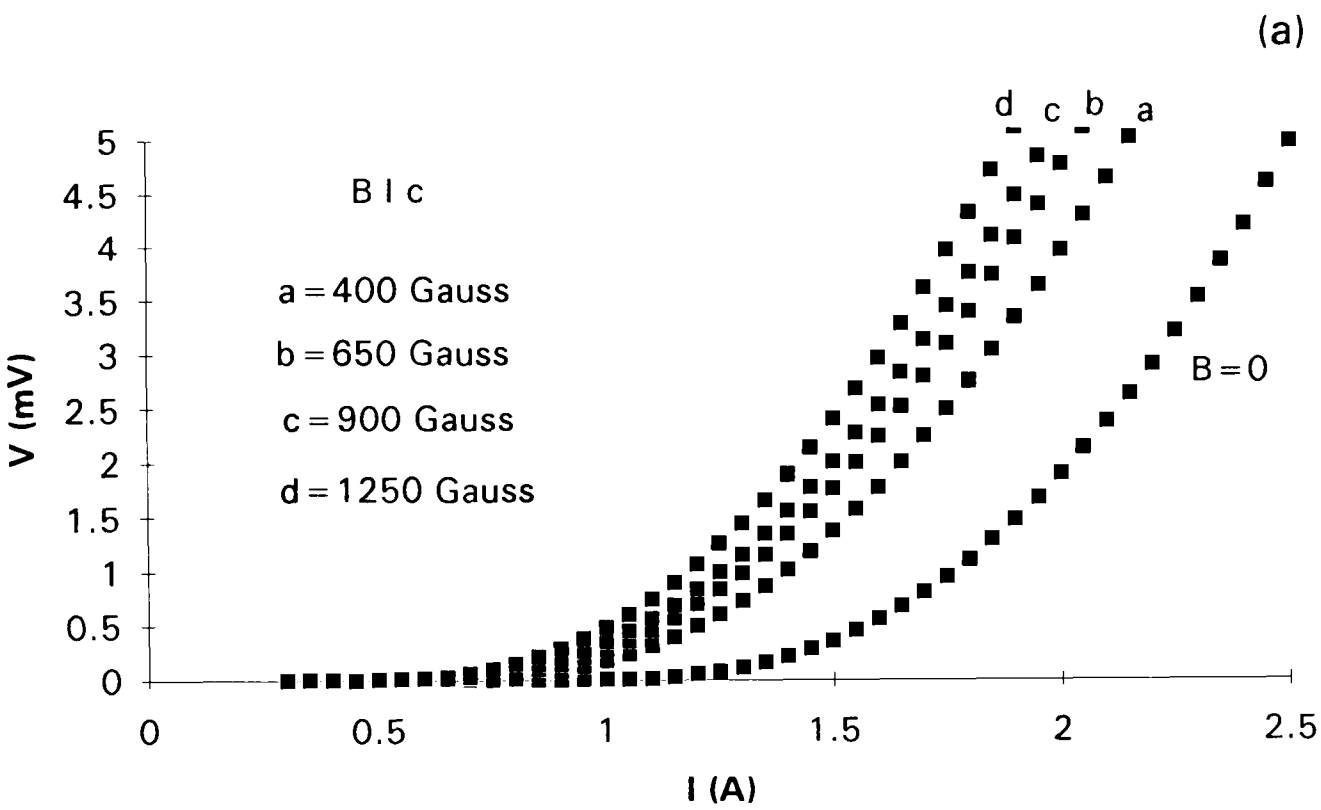

Figure 5.19 I-V characteristics as a parameter of magnetic field, B, at 77K (a) B perpendicular to the c-axis (b) B parallel to the c-axis.

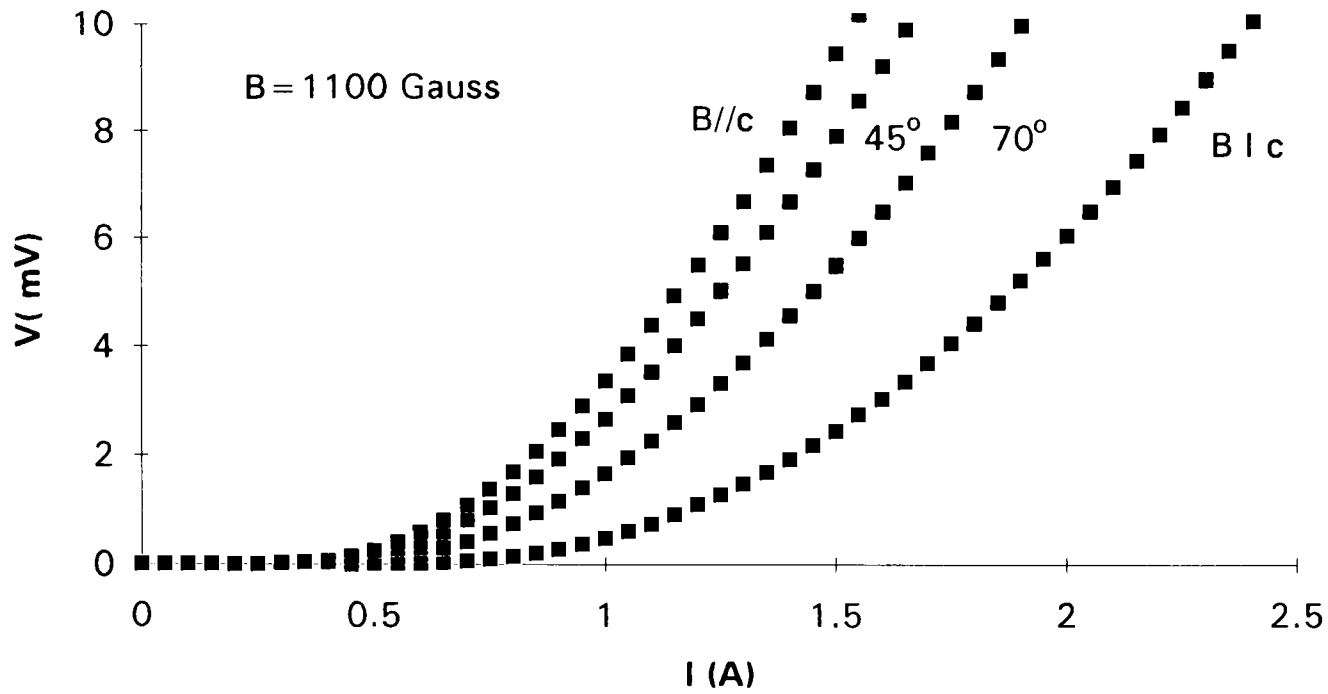

Figure 5.20 I-V characteristics as a parameter of the direction of applied magnetic field at 77K.

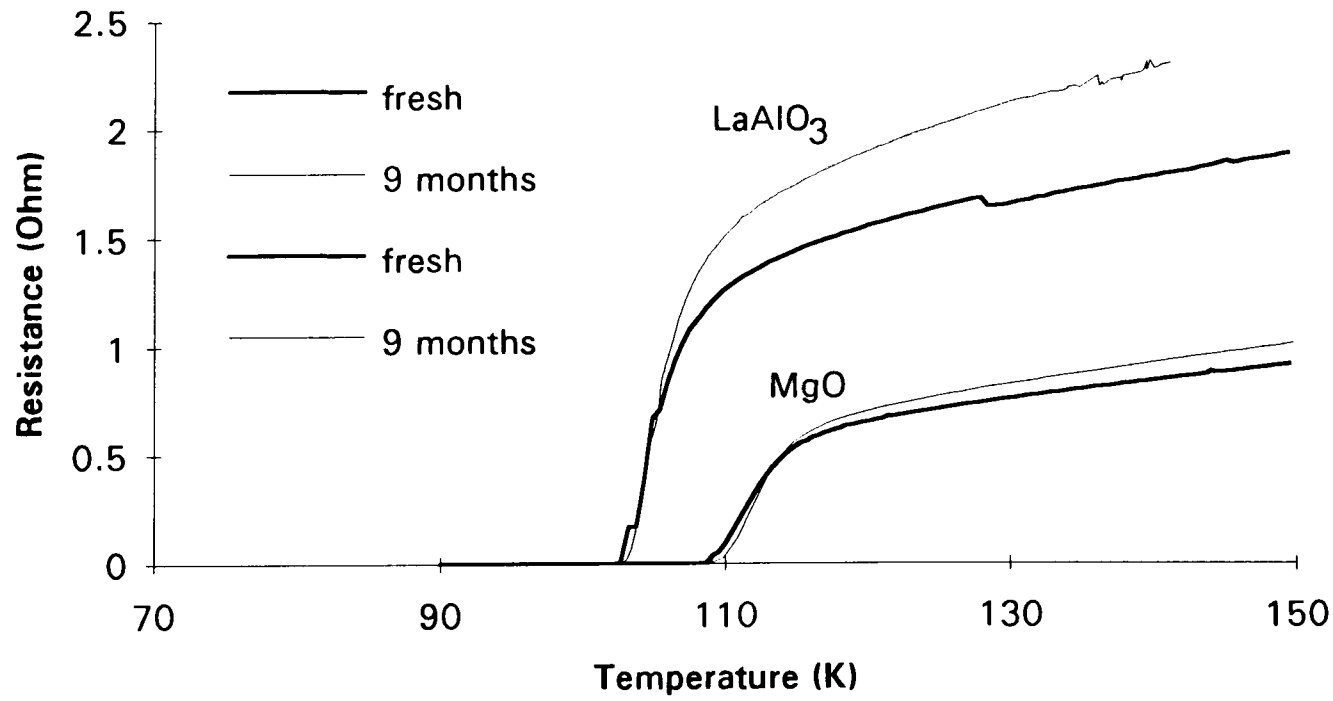

Figure 5.21 Temperature dependence of resistivity of fresh and nine months stored samples on different substrates, indicating no significant degradation of T_c.

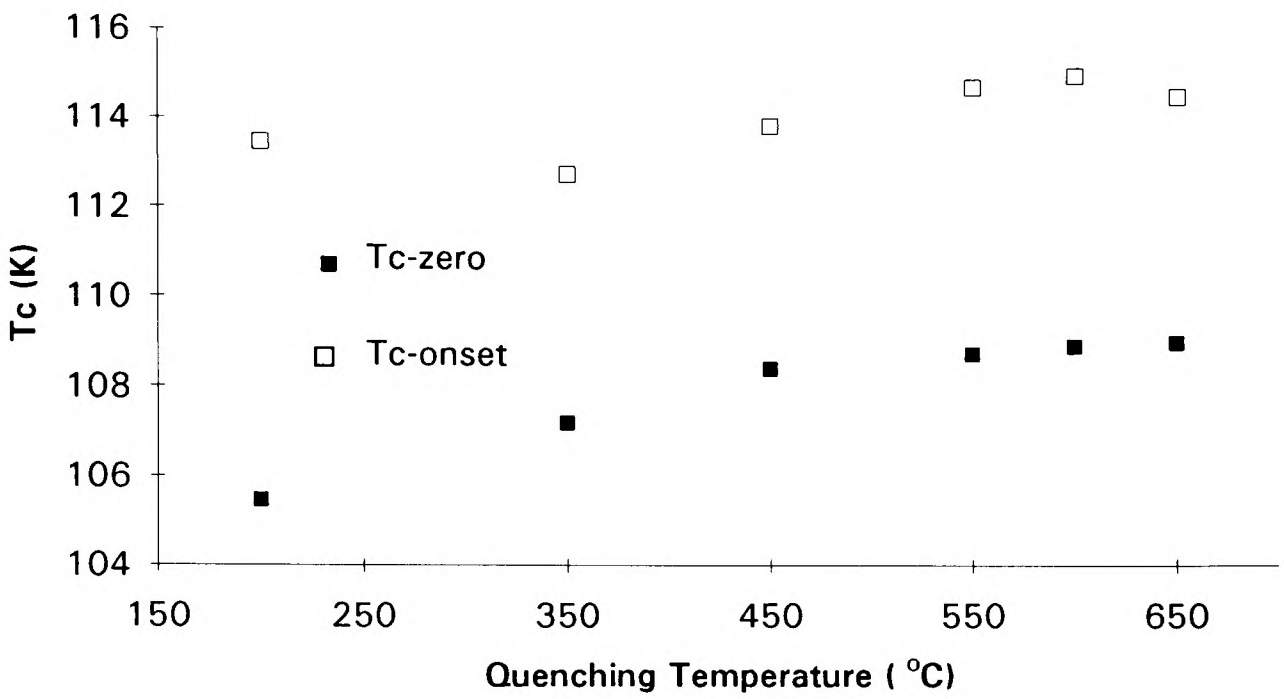

Figure 5.22 The variation of T_c with quenching temperature.

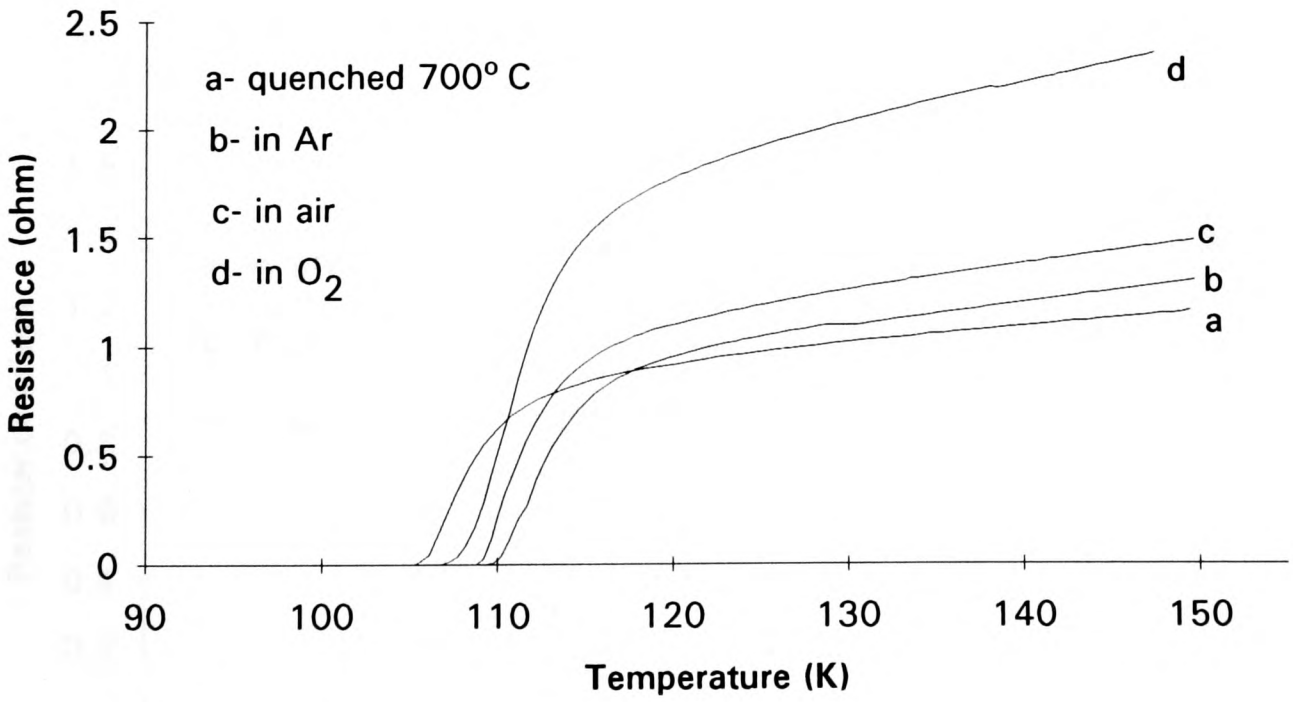

Figure 5.23 Temperature dependence of resistivity for films annealed in different atmospheres.

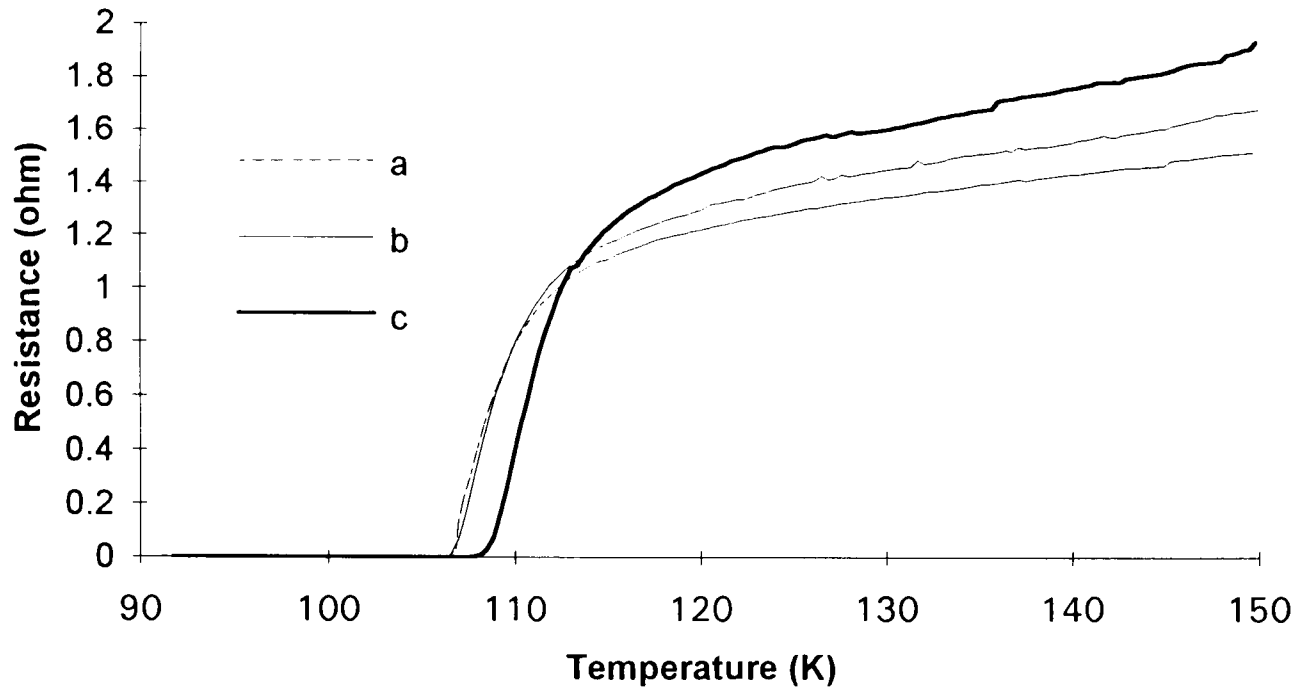

Figure 5.24 Temperature dependence of resistivity for over Pb doped films (Pb: above 0.26). (a) Annealed at 862°C for 30 min. and quenched at 500°C (b) Annealed at same condition with (a) and quenched below 100°C (c) Sample (b) reannealed at 750°C for 1 h in 25% Ar rich atmosphere.

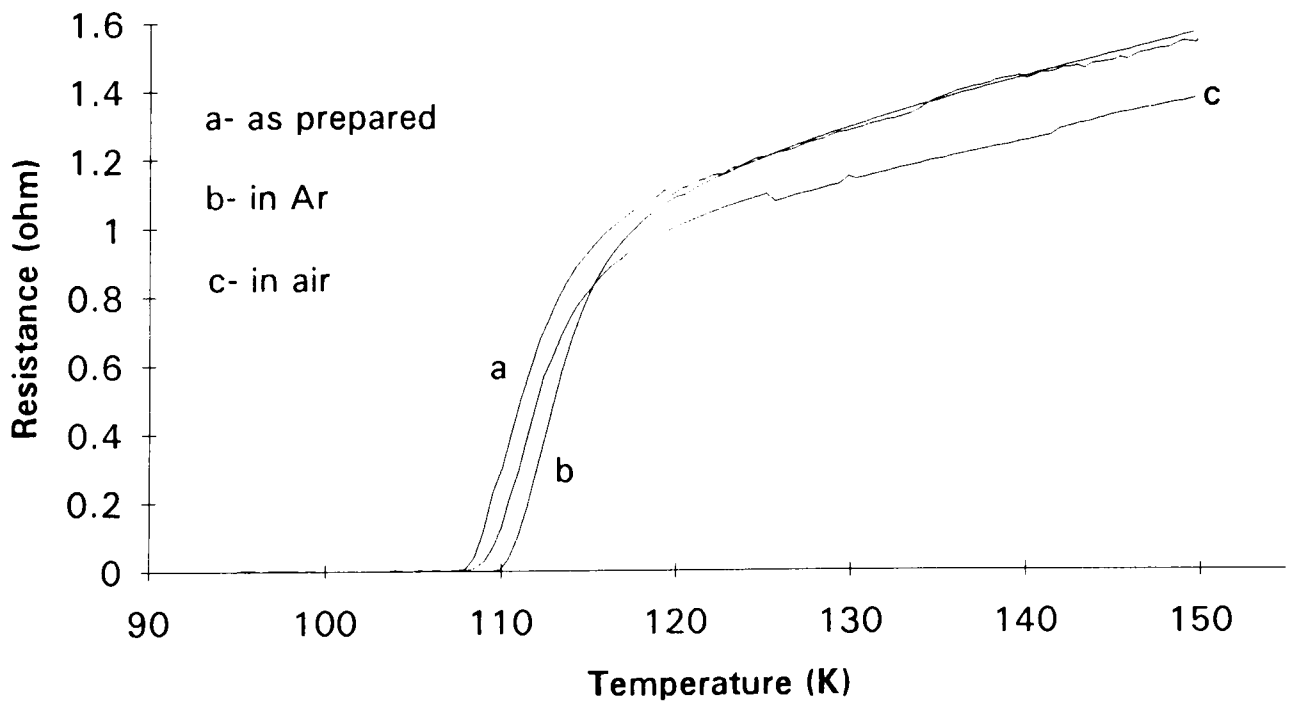

Figure 5.25 The dependence of Tc on annealing atmosphere.

CHAPTER 6

Device performance of Bi-based thin films

6.1. Response to electromagnetic radiation

6.1.1. Introduction

High T_c superconducting thin films used as broadband optical detectors have attracted a great deal of attention. They are sensitive to electromagnetic radiation in an extremely wide spectral range, from ultra-violet to millimetre waves. The response, i.e. the transient resistance change due to the absorption of electromagnetic radiation, of high T_c superconductors has been investigated by several groups [1-13]. Signals of bolometric and non-bolometric origin have been observed and the latter have been attributed to many different physical mechanisms, such as breaking of Cooper pairs by optical radiation [1] or absorption of radiation by Josephson junctions at the weak links [2] which seem to be inherent in all polycrystalline ceramic superconducting materials. However, the mechanism for the non-bolometric response is still not clear. The bolometric response, which has been carefully documented and understood [3], arises from the effect of radiation heating, followed by the resistance variation of the superconducting thin film. Boone et al. [4] reported that the non-bolometric microwave response of granular BSCCO thin films is more sensitive than the bolometric response to a He-Ne laser , which may have interesting implication for sensitive microwave detectors. A non-bolometric optical response has been reported by many groups using pulsed laser sources [5, 6, 7]. However, the identification of

the observed effects as truly non-bolometric is still debatable [8, 9]. In the case of microwave radiation it has been found that the effect is mainly non-bolometric in origin, [10, 11] as demonstrated by the variation of response with temperature and its independence of chopping frequency [12].

In this work studies aimed at distinguishing between bolometric and non-bolometric responses are presented. Preliminary results show no evidence of non-bolometric optical response using a continuous wave (cw) He-Ne laser [12], in agreement with the findings of Carr et al. [13] who used sub-nanosecond pulsed synchrotron radiation from far infrared through visible. A non-bolometric component was observed when films were irradiated with microwaves from a 34.5 GHz Gunn diode microwave generator. The radiation response of Bi-based thin films with different granularity was studied as a function of temperature, bias current, chopping frequency and presence or absence of a dc magnetic field.

6.1.2. Detection principle.

One of the simplest arrangements for radiation response measurement is shown in **Fig.6.1**, where the modulated radiation illuminates the superconducting pattern directly. In **Fig. 6.1**, a constant DC current, I, is driven through the superconducting thin film and the corresponding voltage drop, V, shows the optical response through the resistance of the film. Assuming that there is only bolometric optical response, since the film temperature is modulated by absorbing the chopped thermal energy of the cw radiation, the film resistance will also be correspondingly modulated as depicted in **Fig. 6.2**, where R is the film resistance at DC bias current, I, without the illumination. Since in the present case, the temperature variation, ΔT, in the film is relatively small as compared with the temperature range of the resistance transition, the bolometric resistance change, R_b, can be calculated by using a first-order Taylor expansion of the film resistance, R, with temperature, T, written as:

$$R_b = (dR/dT)\Delta T = \Delta V_b/I \qquad (1)$$

where ΔV_b is the bolometric optical response of the film, I is the DC bias current, and ΔT is the temperature variation caused by the chopped cw radiation.

If the film temperature is scanned from low to high temperature, the bolometric optical response can roughly be depicted as in **Fig. 6.3.**

It is also possible to have a non-bolometric optical response of the superconducting thin film, ΔV_{nb}, resulting from the modulated electromagnetic radiation, when the total optical response, R_T, is given by:

$$R_T = R_b + R_{nb} = (\Delta V_b + \Delta V_{nb})/I \qquad (2)$$

$$\Delta V_{nb} = [R_T - (dR/dT)\Delta T]\, I \qquad (3)$$

where R_{nb} is the non-bolometric optical resistance. Thus any non-bolometric contribution can be isolated by subtracting the bolometric component as defined by the temperature differential of the resistive transition from the total optical response under a rough normalization criterion in which these two curves have the same maximum value.

6.1.3. Experimental details

The c-axis aligned Bi-2212 and Bi-2223 thin films, 0.5-1 μm in thickness, prepared as described in previous chapters were photolithographically patterned into a meander-type structure with a track 150 μm wide and 1 cm long. The dimensions of the patterned films were measured by a Lasertec-1LM11 laser microscope. To investigate the radiation response of the films, different radiation sources were used, including a 1.5 mW cw He-Ne laser, a 42 mW Gunn diode microwave generator operating at 34.5 GHz and a 7mW sweep oscillator at 33.5 GHz. The experimental arrangement for radiation response measurement is schematically shown in **Fig. 6.4.** The radiation was modulated by a mechanical chopper with different numbers of slots. The specimen was sited on the cold-finger of a helium flow cryostat. The response was measured by monitoring the electrical potential across the

specimen when carrying a bias current. A lock-in amplifier with a reference frequency was used to pick up the signal of the response. A small DC magnetic field generated by a coil installed above the specimen was applied along the c-axis of the grains. The experiment was computer controlled, allowing fast and accurate acquisition of film temperature, resistance and response readings from the specimen under test. The microwave response of the film was studied as a function of several parameters such as film temperature, DC bias current, chopping frequency and DC magnetic field. The measurements of the optical and microwave responses of the films were undertaken jointly with J.D. Chern [10, 11, 12]. The particular interest of the present author is in film processing parameters and their effect on the physical properties.

6.1.4. Results and discussion

6.1.4.1. Temperature dependence of bolometric and non-bolometric responses

Fig. 6.5 shows the optical response, Vo, of a Bi-2223 film sample B383, which contains a considerable amount of 2212 phase, using the cw He-Ne laser at a bias current of 0.1 mA and 11.6 Hz, where three normalized curves are presented in the same figure: R vs. T, dR/dT vs. T and Vo vs. T. Direct comparison of the dR/dT vs. T and Vo vs. T curves shows that the optical response was proportional to dR/dT and was bolometric. Since there were two phases (2212 and 2223) in the film (identified by the X-ray diffraction measurement), two peaks were observed in the optical response. The large resistance at low temperatures was due to the increased contact resistance after several rounds of measurement. A non-bolometric component was found in the microwave response of the same sample at 0.1 mA and 382 Hz as shown in **Fig. 6.6**. Since the microwave response does not correspond to the dR/dT curve, it must include a non-bolometric component. Sample B383 was a granular film grown on a MgO (100) substrate with a resistance of 3.15

kΩ at 120K. Even when the bias current was small, the microwave response of this granular film, shown in **Fig. 6.6**, was large.

A similar non-bolometric component was found in the response of a Bi-2212 film on $SrTiO_3$, sample B310, at 0.1 mA and 232 Hz as shown in **Fig. 6.7**. Sample B310 was a single phase well-connected film with a small normal state resistance of 192Ω at 120K. The response occurred around the temperature range of the superconducting transition and peaked at 92K with a response of 5.9 μV, which is small when compared to that of another Bi-2212 film, sample B98, shown in **Fig. 6.8**. Sample B98 was a granular film on MgO with a resistance of 3030Ω. The maximum response of this film was at a temperature less than 51K and was 2.98 mV at 51K. Comparison of **Fig. 6.7** and **Fig. 6.8**. shows that the response pattern of a presumed epitaxial film (on $SrTiO_3$) and a granular film are quite distinct. The presumed epitaxial film showed a small peak near the transition edge and its low temperature ($T<<T_c$) response was almost negligible, whereas a large response was observed in the low temperature range for the granular film. The designation "epitaxial" and "granular" were assigned by comparing a number of physical properties; J_c, appearence, microstructure, c-axis texture (but see section 3.7.3 for discussion of difficulty of detecting epitaxy).

The reason for this significant difference is presumably the fact that the granular film contains many more Josephson-type weak links than the epitaxial one. As the temperature ($<T_c$) of the granular film is decreased, some of the non-superconductive inter-grain boundaries turn into weak links; since the total density or reaction intensity (with the microwave radiation) of weak links is increased, the response increases until it reaches the point where the weak links start to become superconductive. The advantages of the fast and large response of the non-bolometric microwave component in granular films make it suitable for use in sensitive microwave detectors [4]. Since it is a non-bolometric response, the thermal capacitance and the thickness of the substrate are not as critical as they would be in a bolometric application such as a far infra-red detector. For the most granular film, sample B132 of Bi-2212 with resistance 31.6 kΩ at 120K, the maximum microwave response using

the Gunn diode generator was found to be four orders of magnitude larger than the peak response to the He-Ne laser at a bias current of 5 μA. Since the microwave response of a granular film remains quite large at small bias currents, while the optical response decreases as the bias current decreases, the microwave response can be much larger than the optical response.

6.1.4.2. Chopping frequency dependence of the bolometric and non-bolometric responses

Fig. 6.9 and **Fig. 6.10** show the chopping frequency dependency of bolometric optical and non-bolometric microwave responses of a Bi-2223 film using a mechanical chopper with chopping discs with different numbers of slots. The peak optical response decreases on increasing the chopping frequency, whereas the peak microwave response was almost independent of the chopping frequency. These indicate that the optical response had a bolometric component and the microwave response was non bolometric. Since the bolometric response is caused by a thermal effect, the temperature rise as well as the temperature-modulated resistance change of the film should be smaller at larger chopping frequencies. Therefore from **Fig. 6.5** and **Fig. 6.9** the optical response is mainly due to the bolometric effect. On the other hand, the non-bolometric response is not due to a thermal effect and is presumed to be a fast response. Boone et al. [4] estimated the response time of the microwave response of a granular BSCCO film as of the order of 100 ns, which is much faster than the response time with the chopped cw He-Ne laser. Therefore, the non-bolometric response is presumed to be independent of the chopping frequency provided that the response time is less than the period of time for which the film is exposed during one chopping cycle. Thus, from **Fig. 6.6** and **Fig. 6.10** the microwave response is predominantly non-bolometric.

The frequency dependence of the optical response appeared to be independent of the number of chopping slots at a given frequency, whereas the microwave response was dependent on the number of slots. The reason is the different relative dimension of the

chopping slot and the spot diameter of the radiation. The greater the number of slots in the chopping disc, the smaller the individual slot size. The spot diameter of the He-Ne laser is about 2 mm which is much smaller than the dimension of the chopping slot. Therefore, no significant dependence of the optical response on the number of slots would be expected. However, the size of the wave guide of the 26.5 GHz-40GHz Gunn diode generator is of the same order as the dimension of the chopping slot. Therefore, less microwave energy can go through the chopping disc and the microwave response decreased as the number of slots is increased and their size decreases.

6.1.4.3. Magnetic field and bias current dependence of the microwave response

Figures. 6.11 and **Fig. 6.12** show R, dR/dT and microwave response, V_{mr}, at the same bias current, 0.01 mA, versus temperature, in zero magnetic field and in the presence of a small DC magnetic field of 30 Gauss, respectively. The general features of the curves are similar. The effect of magnetic field can best be demonstrated by plotting the two response peaks on the same graph, **Fig. 6.13**, where it may be seen that the field has both depressed the response and shifted the maximum to a slightly lower temperature.

The major component of the magnetic field is normal to the surface of the c-axis oriented film. As it penetrates the intergranular regions, it is expected to switch-off some of the weak links. A similar effect is seen at the considerably higher levels of bias currents, 1 mA and 1.5 mA, shown in **Fig.6.14 and Fig.6.15** respectively. A new feature in these curves is that at the position of the previous peak there is now a shoulder, of magnitude some five times greater than the previous peak, and that an even stronger signal is found down to much lower temperatures. With a bias current of 1 mA V_{mr} shows a maximum at about 70K, but with 1.5mA this becomes a shoulder, and V_{mr} continues to increase as the temperature falls to 50K. The effect of the bias current is much greater than that of the externally applied magnetic field. This is not surprising, as a current of 1.5 mA in a film of

thickness 0.5 μm and width 150 μm gives a current density of $2x10^3$ A/cm^2, an appreciable fraction of the critical current density of the film.

The magnitudes of V_{mr}, with a bias current of 1 mA at temperatures of 70K, corresponding to the maximum value, and 89K, corresponding to the high temperature shoulder, are plotted as a function of increasing magnetic field in **Fig. 6.16**. At both temperatures the effect of increasing the field is to decrease the response.

Finally, the effect of level of bias current on V_{mr}, at the fixed temperatures of 50K, 70K, 90K and 110K is shown in **Fig. 6.17**. At the three lower temperatures, V_{mr}, initially rises with increasing bias current, passes through a maximum and than falls. The value of bias current corresponding to the maximum signal increases from 0.38 mA to 0.93 mA to 1.3 mA as the temperature falls from 90K to 70K to 50K. At 110K the magnitude of V_{mr}, was much smaller and no maximum was observed for bias currents up to 1 mA.

It is presumed that there is a distribution of both intergranular coupling strengths, and of the number density of links, in a granular superconductor. The average coupling strength will be expected to increase as the temperature is reduced from the transition temperature T_c. The number density distribution will also be a function of temperature. At a given temperature and level of bias current, the weak links in a slice of this distribution become active. Weaker links have been turned off; stronger links have yet to be turned on. As the bias current is increased, the distribution of links is sampled. The bias current producing a maximum microwave response is that which activates the links at the maximum in the distribution. A larger current will be required to do this at a lower temperature, where the average coupling strength is greater. A temperature of 110K is insufficiently below T_c (115K) for the density of active weak links to be high, and at this temperature the Bi-2212 phase is still in the normal state.

Fig. 6.18 shows the current dependence of the microwave response of presumed epitaxial Bi-2212 film, sample B310, at 80K and 93K. The response was small at small bias currents, but as the bias current was increased, the response initially increased in a non-linear manner until some maximum point was reached; subsequently it decreased very

slowly with further increase in bias current up to 20 mA. The comparison of **Fig. 6.17** and **Fig. 6.18** also agrees with the proposed weak link model. In the case of a less granular film, the microwave response is no longer sensitive to the increasing bias current once it reaches a saturation value. However, a novel effect was found in a few samples in that a negative signal was observed in the microwave response in certain ranges of bias current and temperature as shown in **Fig. 6.19** and **Fig. 6.20**. The reason for this effect is still unclear.

6.1.4.4. The bolometric component in microwave response

For a granular film, the microwave response of the film is much larger than that for an epitaxial film [4] and it is difficult to observe the bolometric component using a granular film. Therefore, a presumed epitaxial Bi-2212 film, sample B310, was chosen to study the bolometric component of the microwave response. **Fig. 6.7** shows the comparison of the temperature dependence of R, dR/dT, and V_{mr}. The results show that there was response peak around the transition edge of the film. Since the response is not proportional to dR/dT, there was a non-bolometric component in the response. However, a small response was observed at the peak position of the dR/dT curve, indicating a possible bolometric component. To investigate this effect, the chopping frequency dependence of the response was measured using the 34.5 GHz Gunn diode microwave generator at different temperatures as shown in **Fig. 6.21**. At 80K, the response was almost independent of chopping frequency and is predominantly non-bolometric. However, at 93K the response was decreased by increasing the chopping frequency, and therefore included a bolometric component. The bolometric component of the microwave response was actually quite small at small bias currents and large chopping frequencies and was almost negligible at temperatures below 80K.

6.1.4.5. The cut-off temperature

In the region of the critical temperature, with rising temperature the microwave response falls steeply to a minimum value at a cut-off temperature Tb, which may be

associated with T_c for the sample, then rises to a small but finite value in the normal state, **Fig. 6.22**. Increasing the bias current from 0.1mA to 1.5mA raises Tb by 2.5K from just under 115K to just over 117K, a behaviour which is contrary to expectation. No explanation can yet be offered for this unusual behaviour.

6.1.4.6. The co-existence of different phases in the film

Fig. 6.23 and **Fig. 6.24.** show the microwave response of a Bi-2223 film, sample B390, at bias currents of 0.01 mA and 0.1 mA respectively using the 33.5 GHz sweep oscillator. Two peaks were observed in the transition ranges of Bi-2212 and Bi-2223 phases, whereas only the transition of Bi-2223 was observed in the resistivity curve. The results of these two figures indicate that the narrow sharp peak around 110K corresponds to the higher T_c phase Bi-2223, and the broadened peak at about 85K to the lower T_c Bi-2212 phase.

The X-ray diffraction pattern of this sample (B390) shows that it contains both phases well aligned and is consistent with the assumption that the two peaks observed in the microwave response imply the co-existence of Bi-2212 and Bi-2223 phases in the film. The two phases of sample B390 are presumably well mixed and well aligned in this homogenous film. With increasing temperature from 40K at small bias currents, the minor 2212 phase, embedded in the grain boundaries of 2223 phase, first became normal and generated many intergranular weak links in the film, while the 2223 phase still remained superconducting. As the temperature increased to around 100K, all the 2212 grains became normal and the 2212 weak links decreased because of the increased regions of 2212 in the normal state. Then 2223 weak links gradually appeared as the temperature continued to increase and the response peaked at around 110K.

6.1.5. Conclusions

Two criteria are proposed to identify the bolometric and non-bolometric components of the radiation response of superconducting films. Firstly the bolometric component should

be proportional to dR/dT, whereas the non bolometric component is not. Secondly, the bolometric component should decrease as the chopping frequency is increased while the non-bolometric component should not depend on the chopping frequency. Using these criteria, it is found that both components can be observed in the microwave response of a presumed epitaxial film. In conclusion, the optical response of a cw He-Ne laser is mainly due to the bolometric effect, whereas the microwave response using a 34.5 GHz Gunn diode microwave generator is predominantly non-bolometric.

Most of the experimental results, which measured the influence of film temperature, bias current and external magnetic field on microwave response, are qualitatively consistent with a proposed picture that the non-bolometric microwave response of a superconducting film reflects the interaction between microwave radiation and the Josephson-type weak links in the sample. The onset of the response may be used to define the critical temperature, though its increase with bias current is puzzling. This response is proposed as an alternative method for the detection of different phases in the film. Thus the effect is valuable in assisting sample characterization. Granular high T_c films may have interesting applications as sensitive microwave detectors. The detector could be tuned for maximum sensitivity by matching the bias current to the operating temperature.

6.2. Microwave properties

6.2.1. Introduction

A likely application of High T_c technology is in the fabrication of passive microwave devices. Such devices need the low surface resistance, Rs, representing ohmic losses, of high T_c thin films deposited on to low loss dielectric substrates to offer high performance and compact size. Their low loss and dispersion as compared with conventional conductors, such as copper and gold, provide the potential for microwave application. Therefore a large number of measurements, especially of Rs at microwave frequencies, on high T_c thin films

have been reported using different techniques [14]. An excellent summary of this early work was given recently in review paper by Piel and Muller [15].

Most of the techniques employed to determine surface resistance make use of some form of resonant structure. Rs can then be determined by measuring the Q of the resonance and equating this to the ratio of stored to dissipated energy in the system. In spite of the number of studies on BSCCO thin films, data on Rs at microwave frequencies are still scarce [16, 17] as compared with YBCO [18, 19] and TBCCO [20, 21] thin films. The best results by far have been obtained on epitaxial YBCO and TBCCO [22] thin films grown on $LaAlO_3$ and $SrTiO_3$ substrates.

6.2.2. Surface resistance measurements

In order to characterise the microwave properties, surface resistance, Rs, measurement of some Bi-2212 and Bi-2223 samples prepared by the author has been carried out by different groups using different measurement techniques. All samples characterised using surface resistance measurement were on MgO substrates. As surface cleanliness is essential for this sort of measurement the samples were sent to the measurement laboratory before doing any electrical test on them locally. Thus films were chosen only on the basis of XRD-patterns

Two of the Bi-2212 samples were measured by Dr. J.C. Gallop's group in The National Physical Laboratory (NPL) at 16 GHz in a Niobium cavity system in the temperature range 10-100K. They reported that these films did not have low Rs even at the lowest temperature, with a value of 600 mΩ which rose to ~2000 mΩ at 77K. They also found that there is a temperature dependence of Rs at the lowest temperature which is easily measurable (unlike the best epitaxial in-situ YBCO films) and this is almost certainly associated with grain boundary junctions. The ratio of Rs(77)/Rs(100) (i.e. normalised to a convenient normal state value at 100K) was around 0.2 for these samples whereas for the best films this ratio would be ~0.01.

Another Bi-2212 film has been analysed by Rs measurement at 50GHz in a TE_{01} mode cavity at GEC Research, Baddow. An end-wall replacement technique was used. The surface resistance of this film can be seen to increase rapidly at about 85K as the film approaches its transition temperature (**Fig. 6.25**). Measurements stop here as Rs becomes too large to measure (for this particular cavity). Although superconducting, the film exhibits an extremely high residual surface resistance(~2.5 Ω). For comparison, copper exhibits a surface resistance of 28 mΩ at 50GHz and 77K.

The Rs of a pair of Bi-2223 sample was measured (by A. Jenkins in Oxford) at 4.32GHz using a parallel plate resonator technique [23]. These two samples had been tested by measuring T_c (109K) and J_c (above 1.4×10^4 A/cm^2 at 77K) before the Rs mesurement. The measurement system is essentially the same as suggested by Taber [22], see **Fig. 6.26**. The two films under test are placed either side of a dielectric spacer, with the film side against the spacer. The assembly is then clamped together using PTFE supports in an aluminium housing. Microwave power is coupled into the structure via SMA connectors and coupling probes that are arranged so as to be close to the films (but not touching). The quality factor, Q, indicating losses is then measured using a Vector Network Analyser as a function of temperature and Rs of the film calculated using the equation (after Taber):

$$Rs = \pi \mu_0 f S/Q$$

where f is resonant frequency (4.32GHz), S is the dielectric spacer thickness (0.51×10^{-3} m) and μ_0 is permeability of free space ($4\pi \times 10^{-7}$Hm^{-1}). Measurement was carried out during warm-up after being cooled in liquid nitrogen (hence base temperature of 77K). The spacer dielectric was $LaAlO_3$ which allowed a network analyser to be used.

The results are shown in **Fig. 6.27 a, b, c**, with Rs, resonator centre frequency and resonator Q, respectively as a function of temperature. Rs at 4.32 GHz and 77K is 46 mΩ. The extrapolated value to 10GHz (assuming an f^2 dependence) is 247mΩ. This Rs value is quite large compared with the copper surface resistance of 12 mΩ and the reported result by

Miranda et al.[24] for Bi-2212 film grown on $SrTiO_3$ and $LaAlO_3$ of 40 mΩ at 10GHz and 77K. The results are at the top of the sensitivity limit for this system (i.e. the Q's are very low) and therefore the results probably have a large error (±10%), but this is difficult to quantify.

6.2.3. Conclusion

It is clear that these polycrystalline films are not particularly good for microwave applications. Highly anisotropic and granular features of high T_c superconductors play an important role in the observed microwave properties. The misalignment of grains and presence of phase impurities, especially at grain boundaries, limit the microwave performance to a large extent. Therefore we believe that an in-situ grown epitaxial film is highly desirable for microwave applications.

References

1 Y. Enomoto, and T. Murakami, J. Appl. Phys. 59 (1986) 3807.

2 K. Chang, G. Yong, L.E. Wenger, and J.T. Chen, J. Appl. Phys. 69 (1991) 7316.

3 J. Clarke, G.I. Hoffer, P.L. Richards, and N.H. Yeh, J. Appl. Phys. 48 (1977) 4865.

4 B.G. Boone, R.M. Sova, K. Moorjani, W.J. Grreen, and B.E. Grabow, J. Appl. Phys. 69 (1991) 2676.

5 A Frenkel, M.A. Saifi, T. Venkatesan, P. England, X.D. Wu, and A. Inam, J. Appl. Phys. 67 (1990) 3054.

6 S.G. Han, Z.V. Vardeny, K.S. Wong, O.G. Symko, and G. Koren, Phys. Rev. Lett. 65 (1990) 2708.

7 M. Johnson, Appl. Phys. Lett. 59 (1991) 1371.

8 M.I. Flik, P.E. Phelan, and C.L. Tien, Cryogenics 30 (1990) 1118.

9 P.H. Ballentina, A.M. Kadin, and W.R. Donaldson, *Superconductivity and Applications*, Edited by H.S. Kowk et al., Plenum Press, (1990).

10 J.D. Chern, A. Guldeste, H.C. Lai, S. Aslam, D.H.T. Wu, D. Dew-Hughes, M.J. Goringe,C.R.M. Grovenor, and B. Minakovic, IEEE Trans. on Appl. Superconductivity, 3 (1993) 1757.

11 J.D. Chern, A. Guldeste, D. Dew-Hughes, M.J. Goringe,C.R.M. Grovenor, and B. Minakovic, Journal of Alloys and Compounds, 195 (1993) 567.

12 J.D. Chern, H.C. Lai, A. Guldeste, S. Aslam, D.H.T. Wu, D. Dew-Hughes, C.R.M. Grovenor, M.J. Goringe, and B. Minakovic, IEEE Trans. on Appl. Superconductivity, 3 (1993) 2128.

13 G.L. Carr, M. Quijada, D.B. Tanner, C.J. Hirschmugl, G.P. Williams, S. Etemad, B. Dutta, F. DeRosa, A. Inam, T. Venkatesan, and X. Xi, Appl. Phys. Lett. 57 (1990) 2725.

14 J.C. Gallop and W.J. Radcliffe, Supercond. Sci. Technol. 4 (1991) 568.

15 H. Piel and G. Muller, IEEE Trans. Magn., 27 (1991) 854.

16 J. Talvacchio, G.R. Wagner and S.H. Talisa Microwave J. 34 (1991) 105.

17 F.A. Miranda, K.B. Bhasin, V.O. Heinen, R. Kwor, and T.S. Kalkur, Physica C 168 (1990) 91.

18 N. Klein, H. Chaloupka, G. Muller, S. Orbach, H. Piel, B. Roas, L. Schultz, U. Klein, and M. Peiniger, J. Appl. Phys. 67 (1990) 6940.

19 N. Klein, G. Muller, and H. Piel, B. Roas, L. Schultz, U. Klein, and M. Peiniger, Appl. Phys. Lett. 54 (1989) 757.

20 G.V. Negrete, L.C. Bourne, R.B. Hammond, D.D. Strother, A.H. Caronda, M.M. Eddy, Appl. Phys. Lett. 57 (1990) 825.

21 W.L. Holstein, R.C. Taber, IEEE Trans. Mags. 27 (1991) 1568.

22 A. Lauder, C. Wilker, D.J. Kountz, W.L. Holstein, and D.W. Face, IEEE Trans. on Appl. Superconductivity, 3 (1993) 1683.

23 R.C. Taber, Rev. Sci. Instrum. 61 (1990) 2200.

24 F.A. Miranda, C.M. Chorey, M.A. Stan, C.E. Nordgren R.Y. Kwor, and T.S. Kalkur, Supercond. Sci. Technol. 5 (1992) 453.

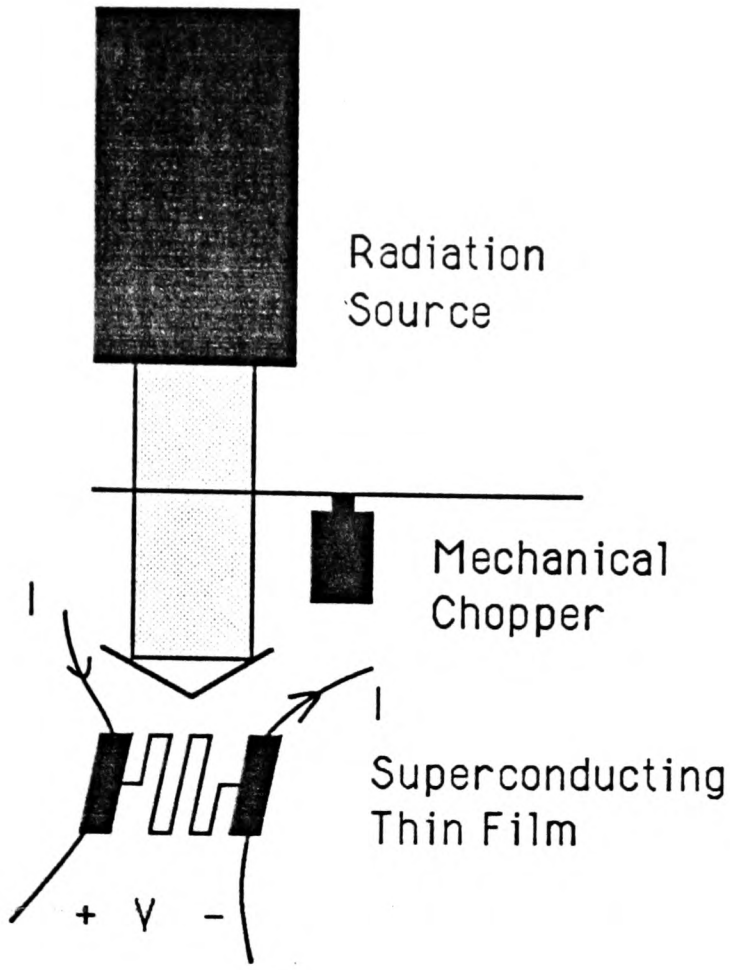

Figure 6.1 A simple arrangement for the radiation response measurement.

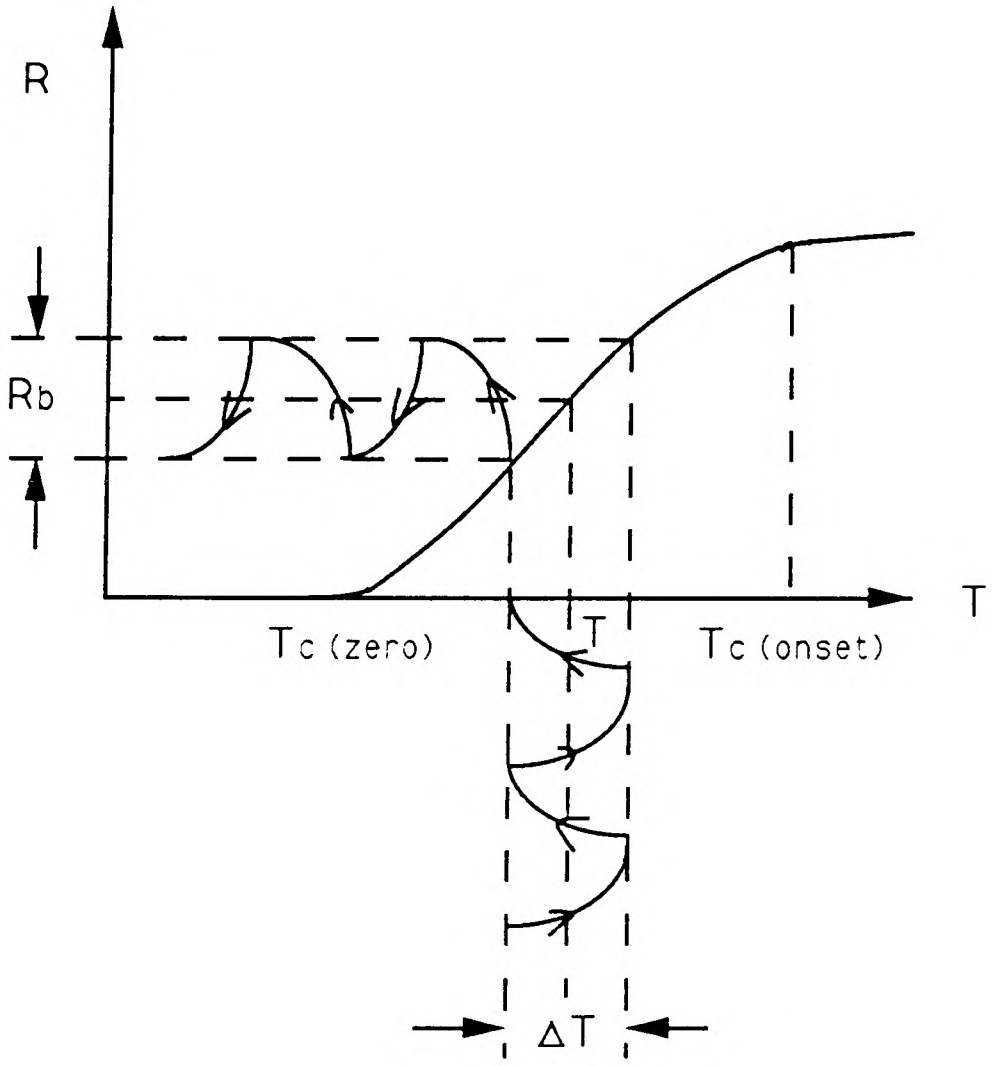

Figure 6.2 The resistance change caused by an exaggerated temperature modulation of the superconducting pattern.

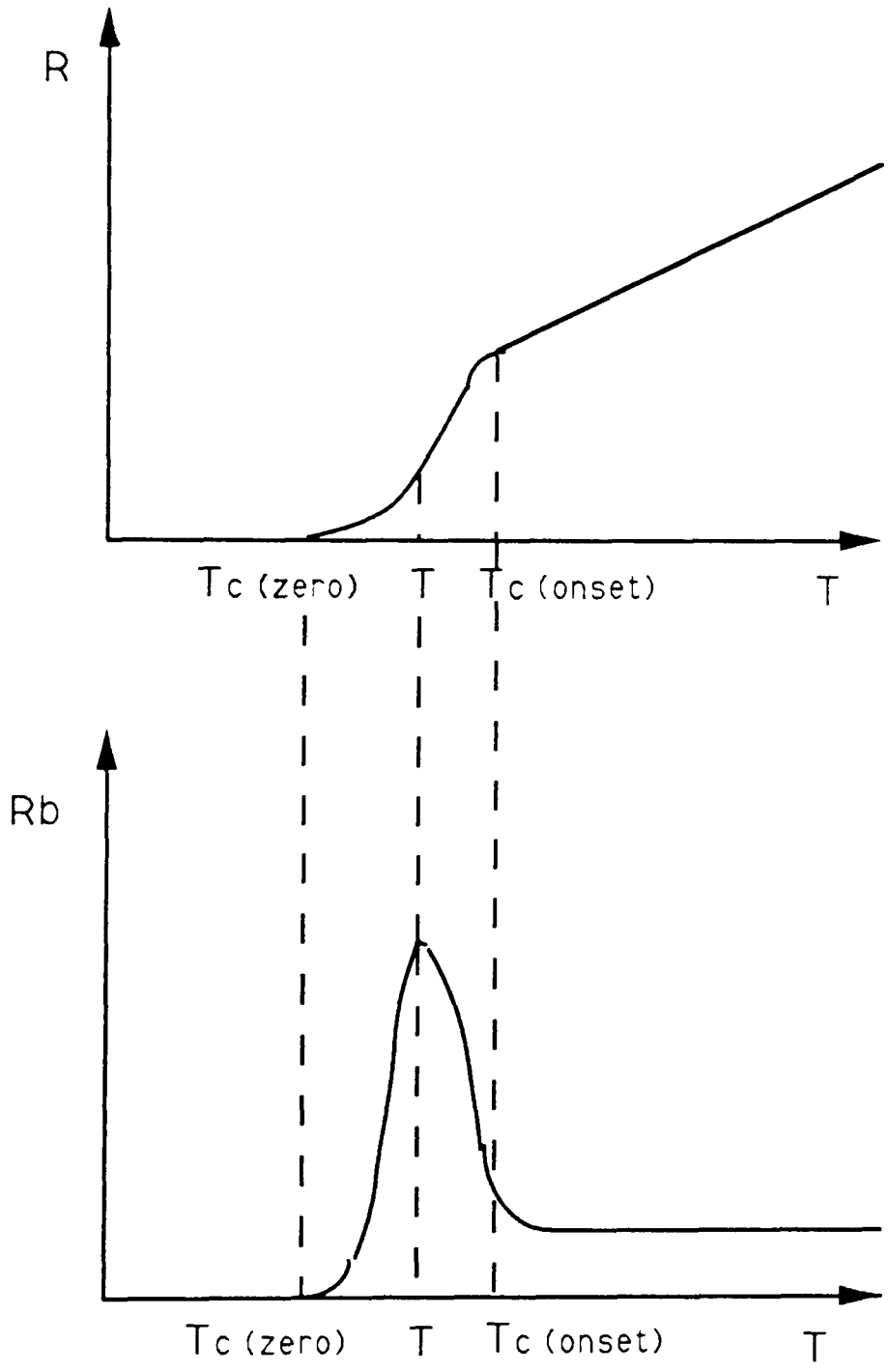

Figure 6.3 A rough comparison of the R Vs T and the bolometric optical resistance, Rb, Vs T.

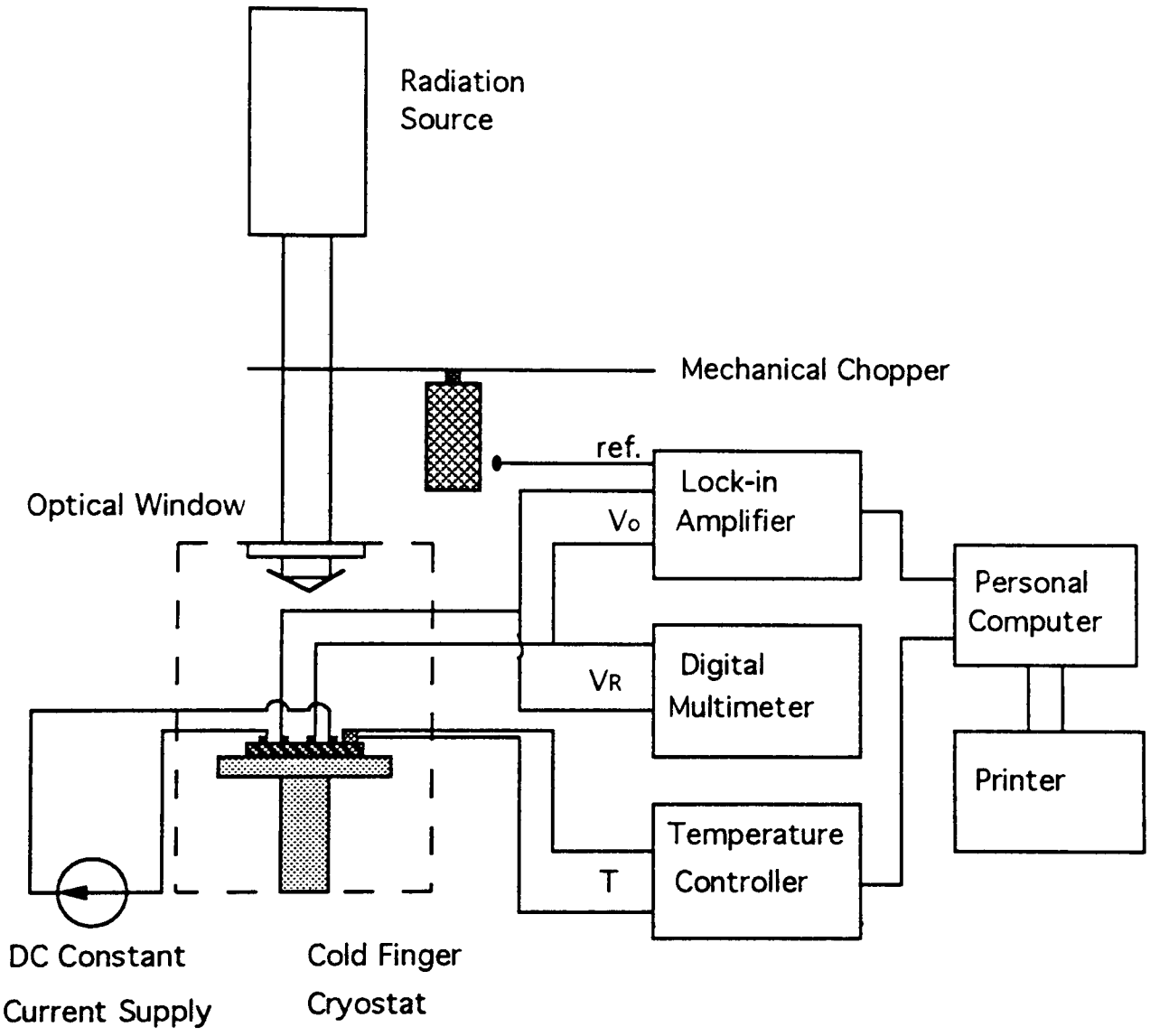

Figure 6.4 Schematic of experimental arrangement for radiation response measurement in four point configuration.

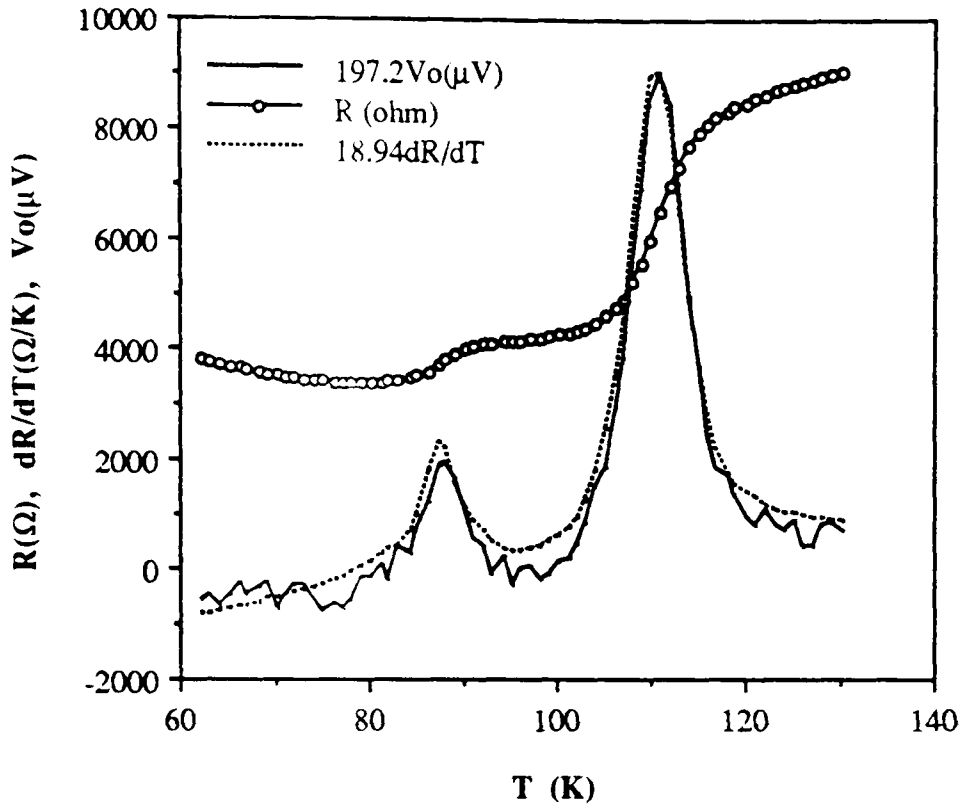

Figure 6.5 The optical response of a granular Bi-2223 film, sample B383, at bias current 0.1 mA and radiation chopping frequency 11.6 Hz, bolometric.

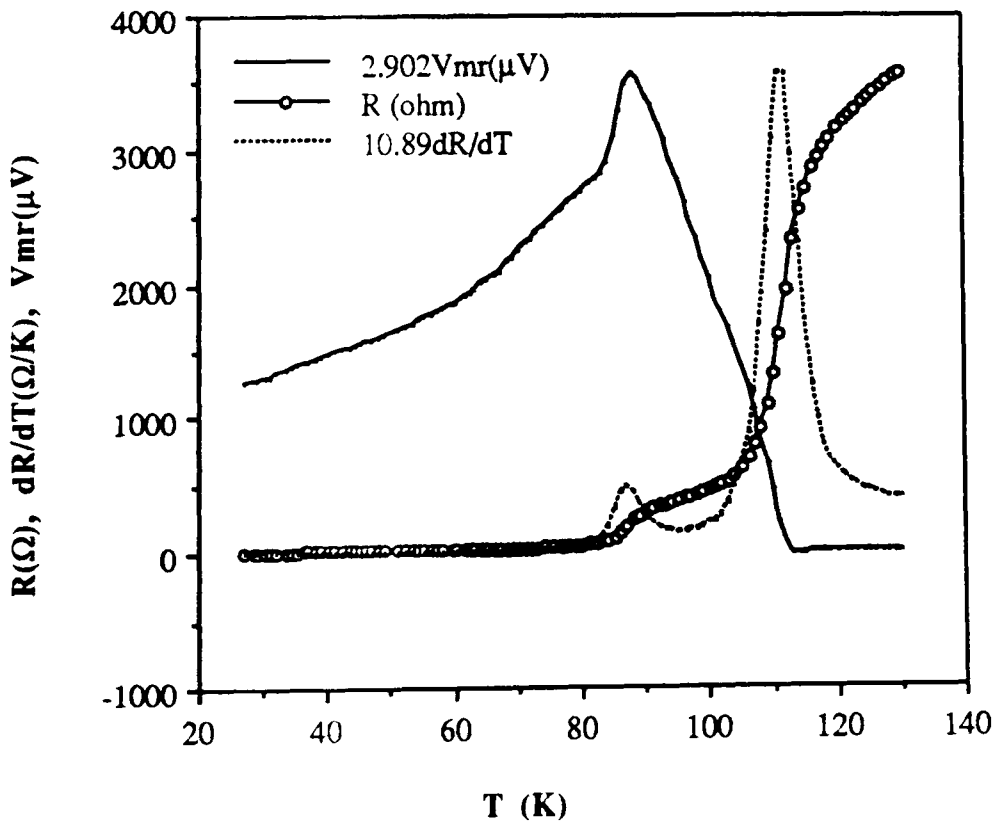

Figure 6.6 The microwave response of a granular Bi-2223 film, sample B383, at bias current 0.1 mA and radiation chopping frequency 382Hz, non-bolometric.

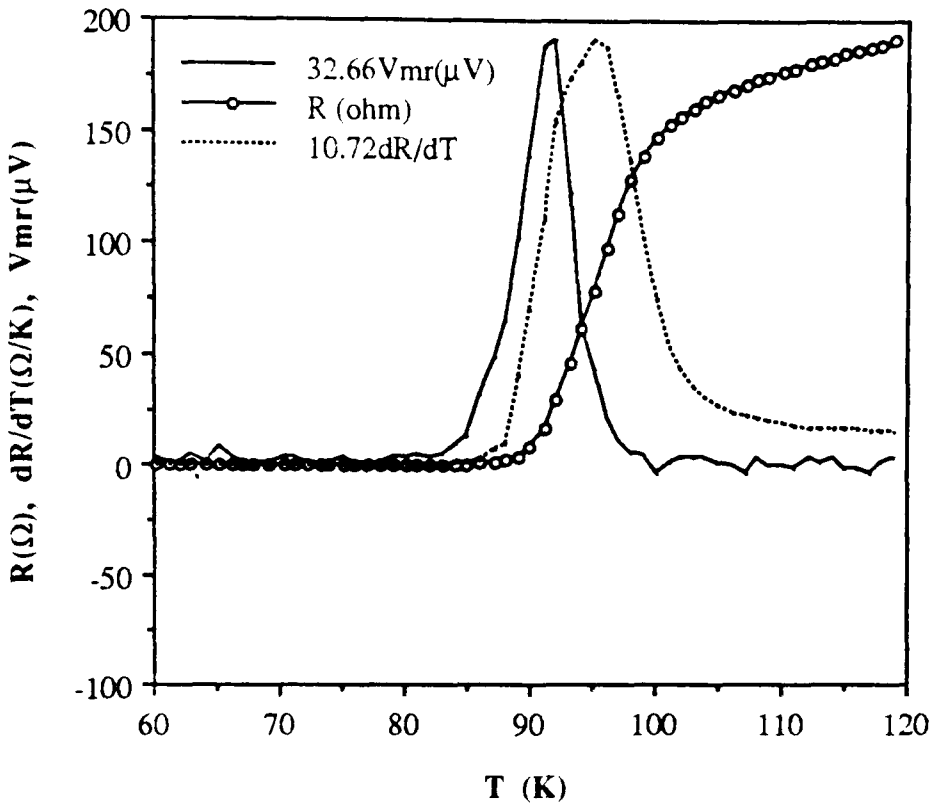

Figure 6.7 Microwave response of a less granular Bi-2212 film on $SrTiO_3$, sample B310, $R_{120K} = 192\Omega$. Bias current 0.1 mA; radiation chopping frequency 232Hz.

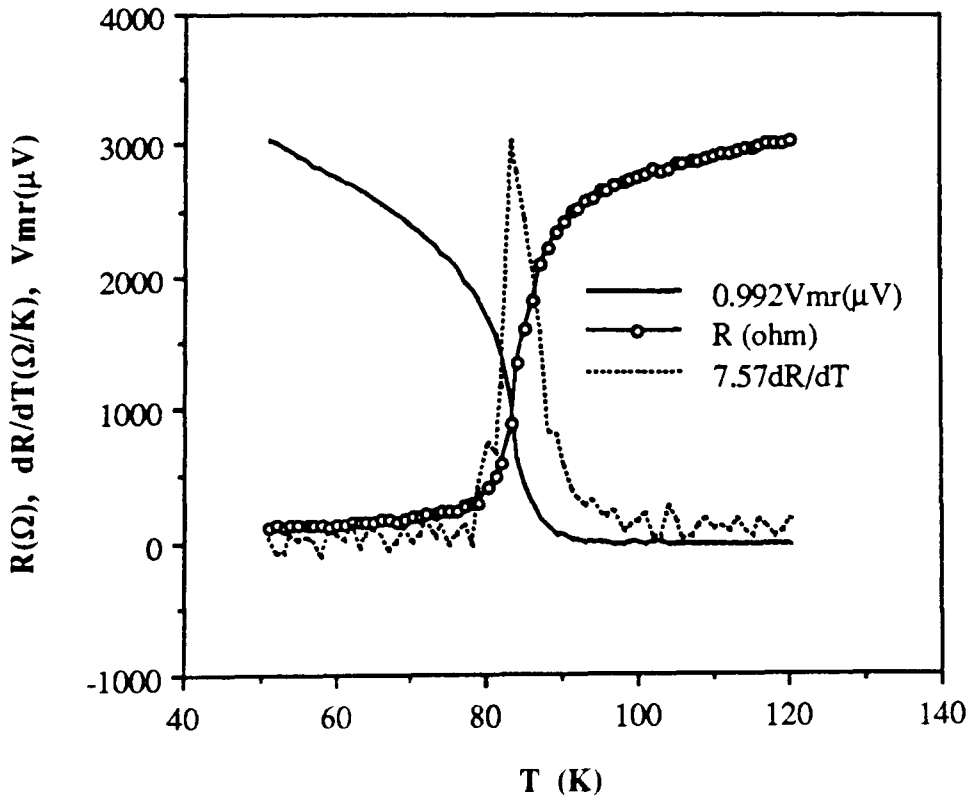

Figure 6.8 Microwave response of a more granular Bi-2212 film on MgO, sample B98, $R_{120K} = 3030\Omega$. Bias current 0.1 mA; radiation chopping frequency 333Hz.

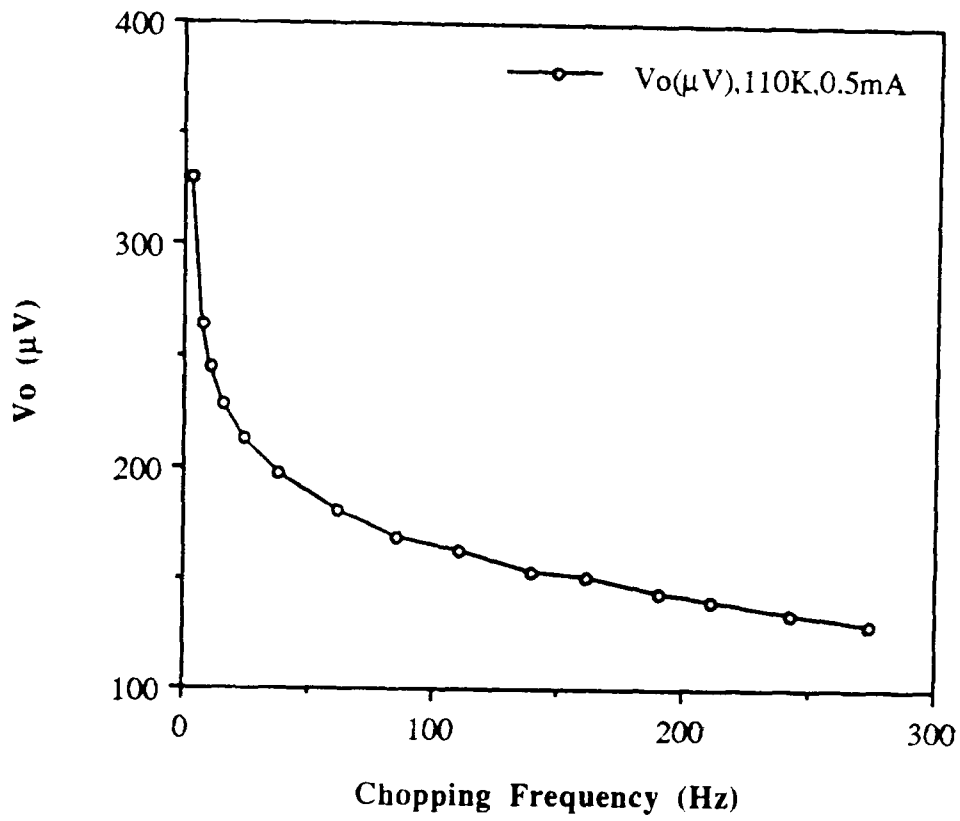

Figure 6.9 The chopping frequency dependence of the optical response of a Bi-2223 film, sample B383.

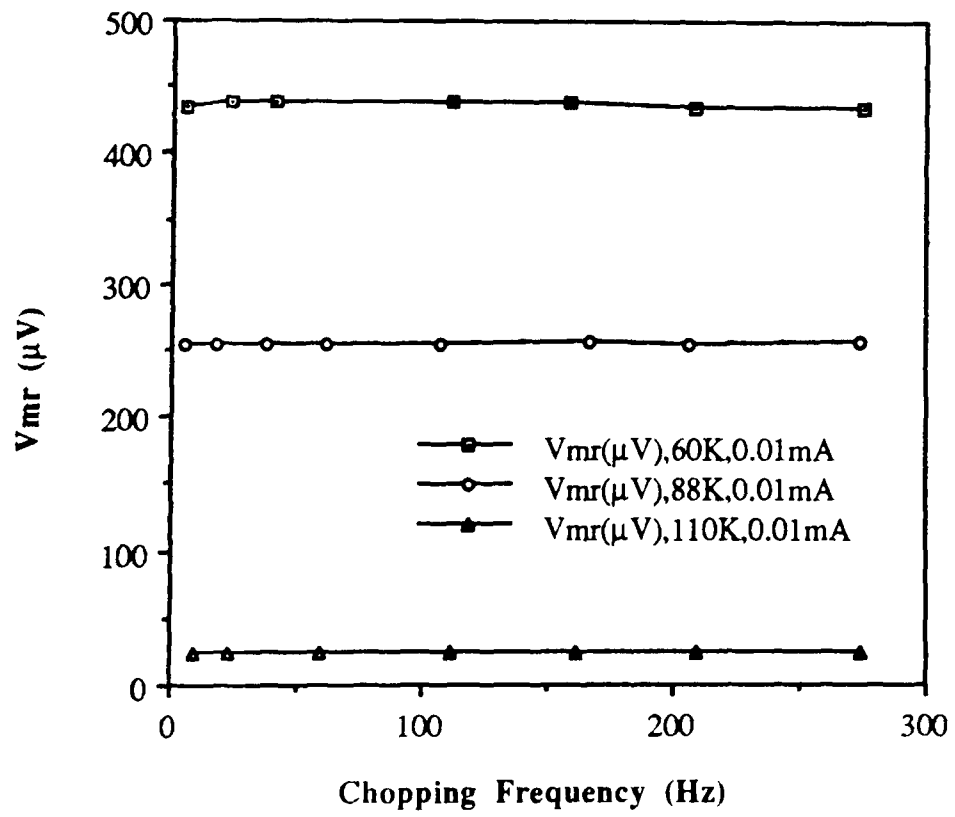

Figure 6.10 The chopping frequency dependence of the microwave response of a Bi-2223 film, sample B383.

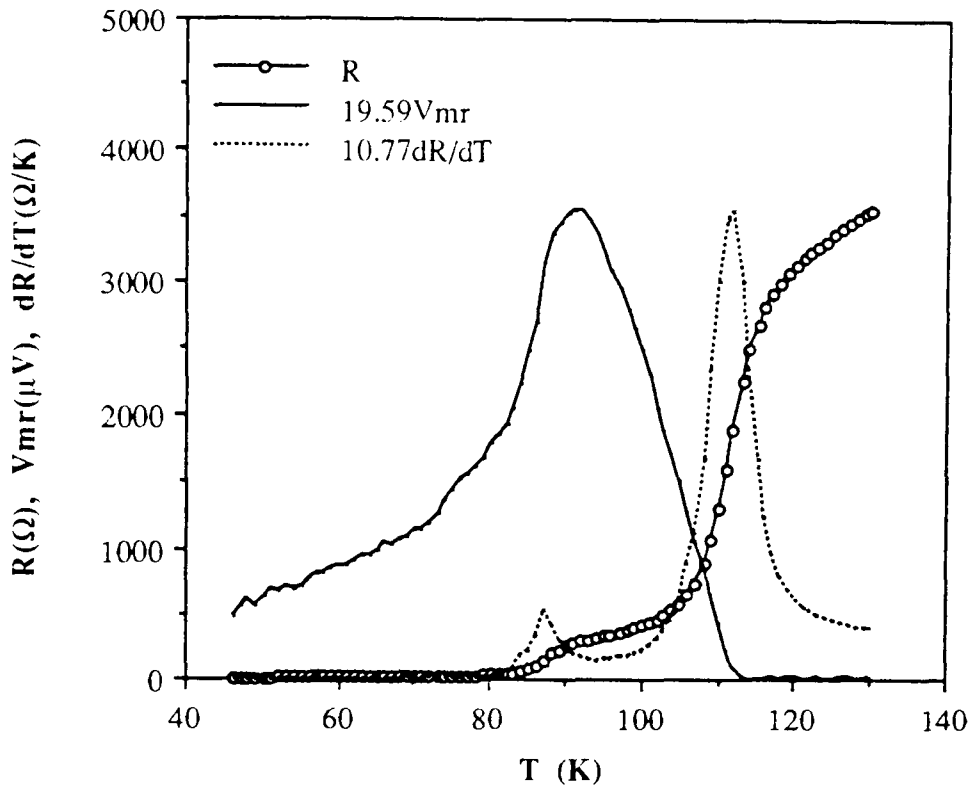

Figure 6.11 Film resistance, R, dR/dT and microwave response V_{mr} of the superconducting film as a function of temperature. Bias current 0.01 mA, radiation chopping frequency 382Hz.

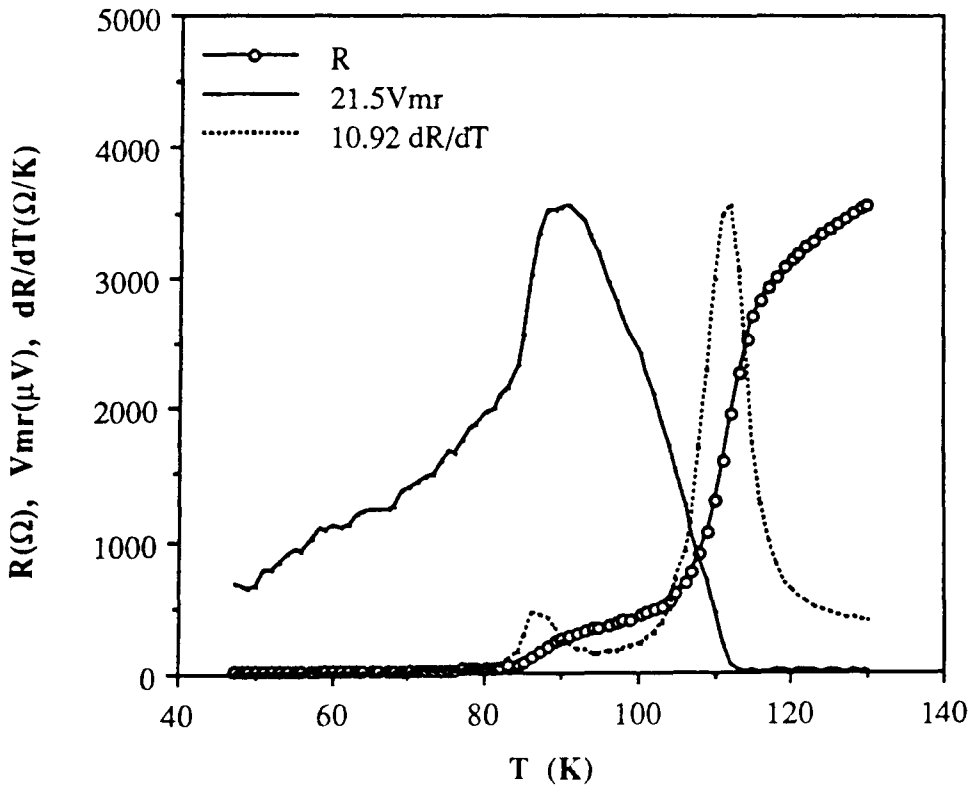

Figure 6.12 R, dR/dT and V_{mr} Vs T in a magnetic field of 30 Gauss. Bias current 0.01 mA, radiation chopping frequency 382Hz.

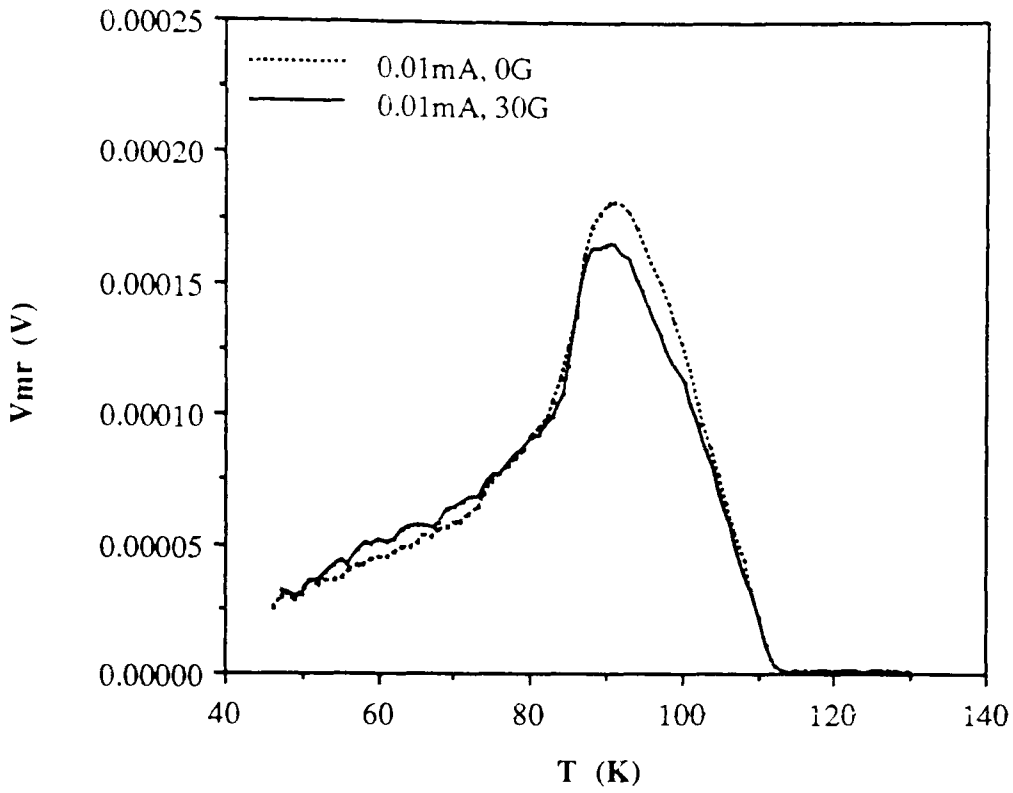

Figure 6.13 Microwave response, with and without the 30 Gauss applied magnetic field, replotted from figure 6.11 and 6.12.

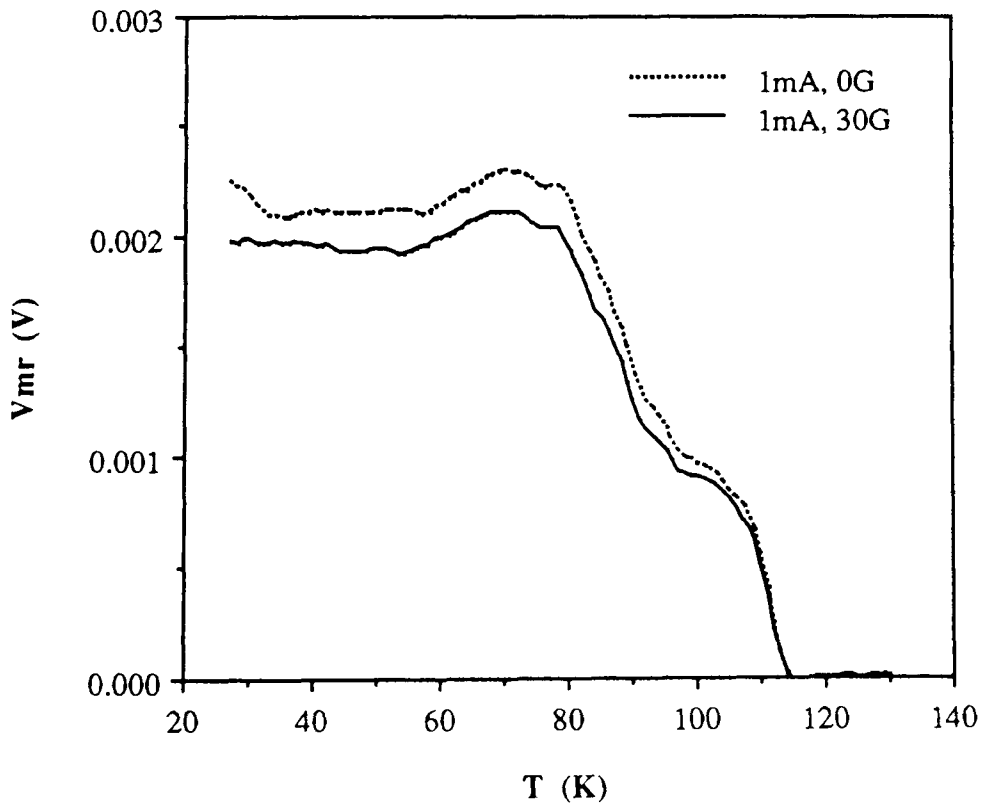

Figure 6.14 Microwave response, with and without the 30 Gauss applied magnetic field, with 1 mA bias current.

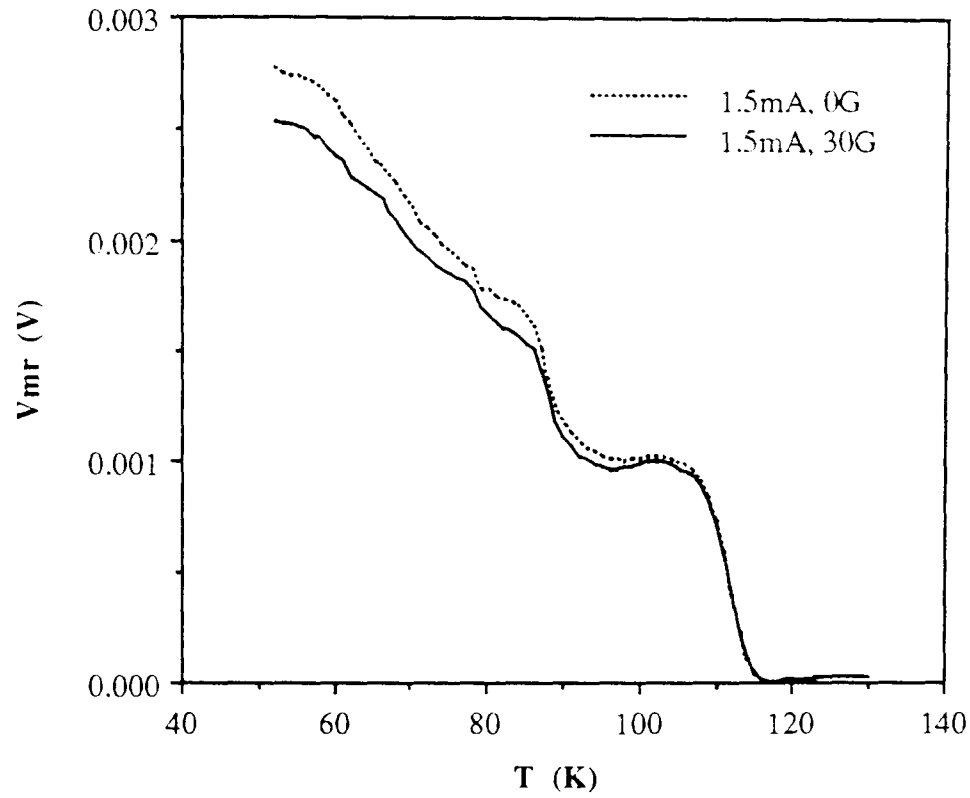

Figure 6.15 Microwave response, with and without the 30 Gauss applied magnetic field, with 1.5 mA bias current.

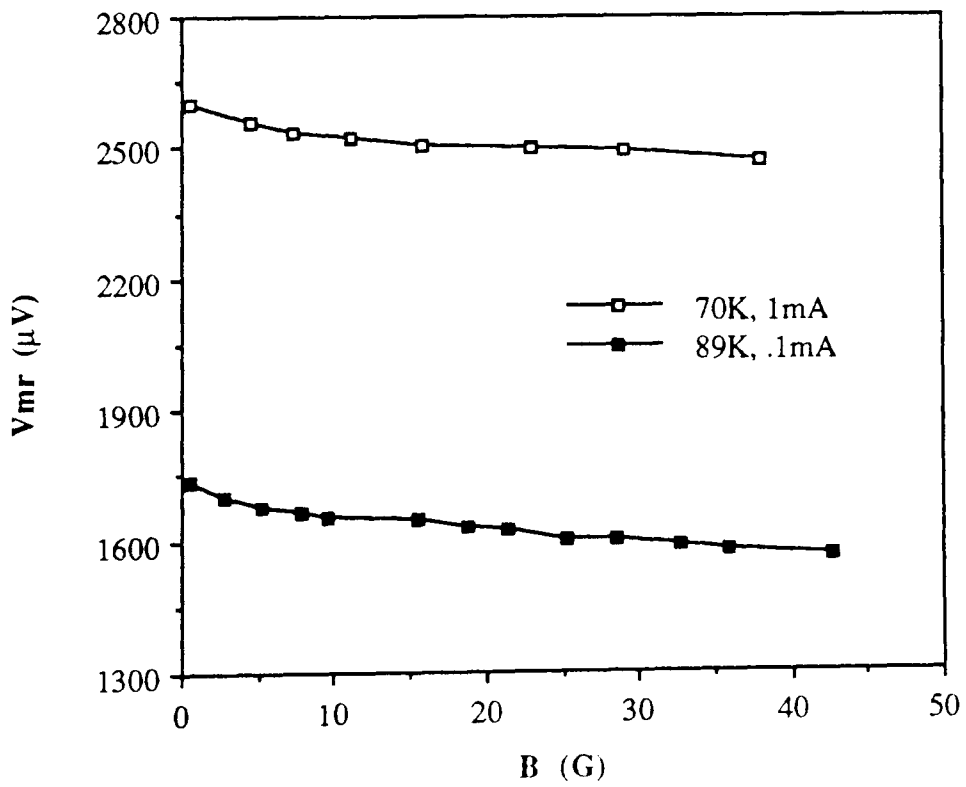

Figure 6.16 Effect of applied magnetic field on microwave response at 70K and 89K. Bias current 1 mA.

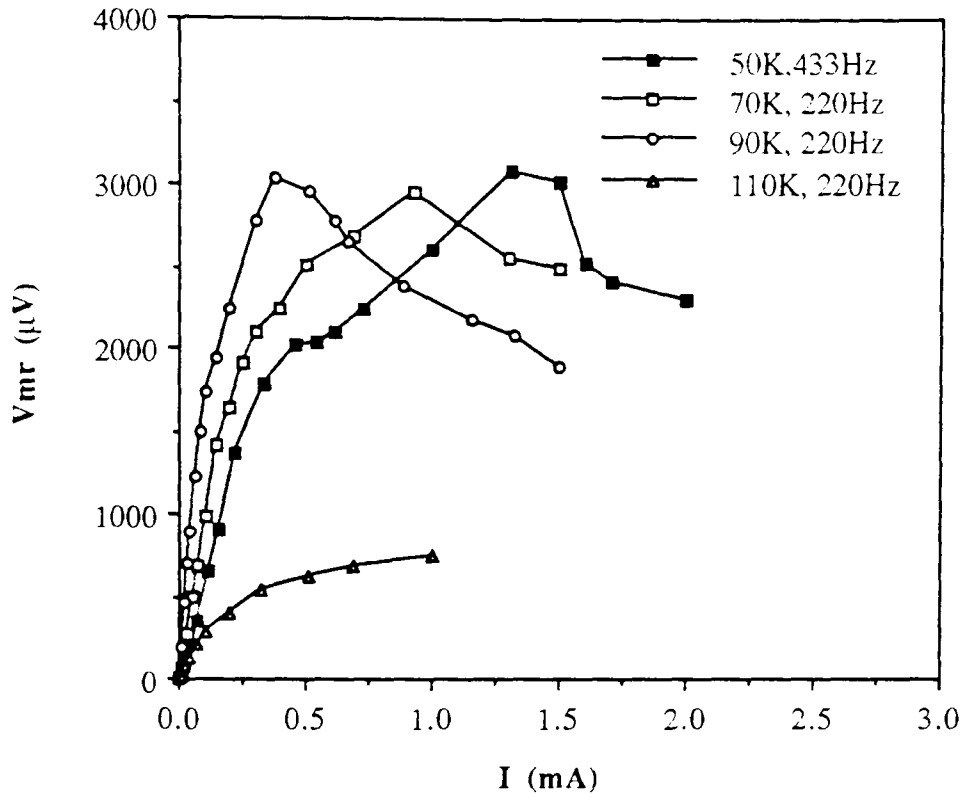

Figure 6.17 Microwave response versus bias current, at 50K, 70K, 90K, and 110K. Chopping frequency as indicated.

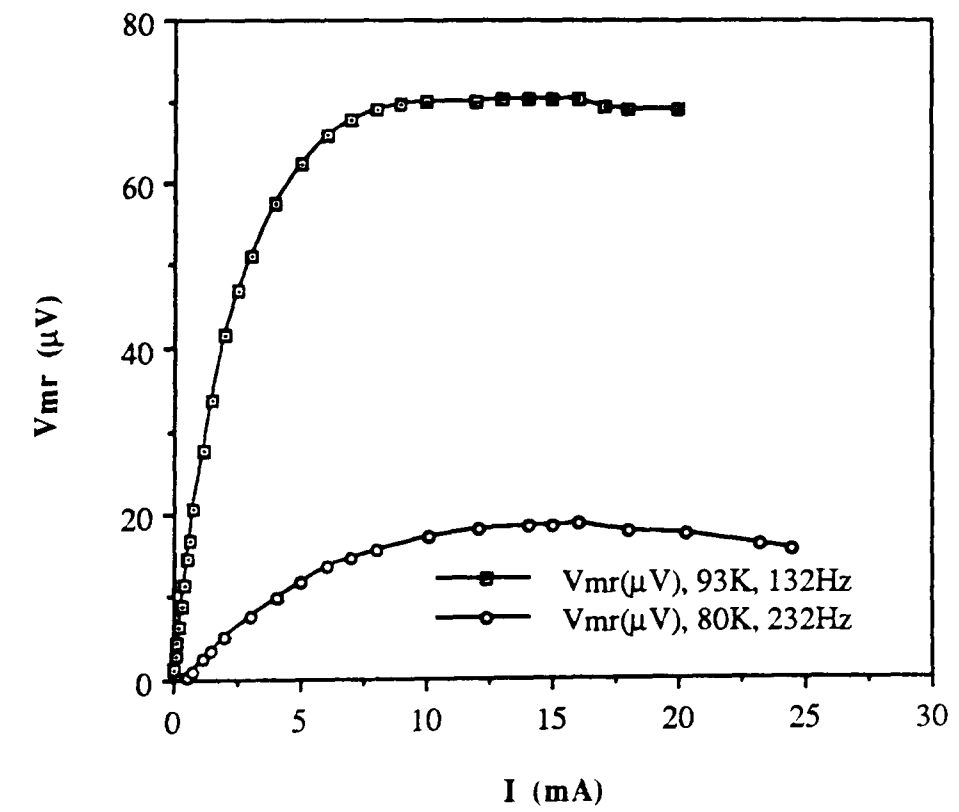

Figure 6.18 The dependence of the microwave response on the dc bias current of a Bi-2212 film, sample B310.

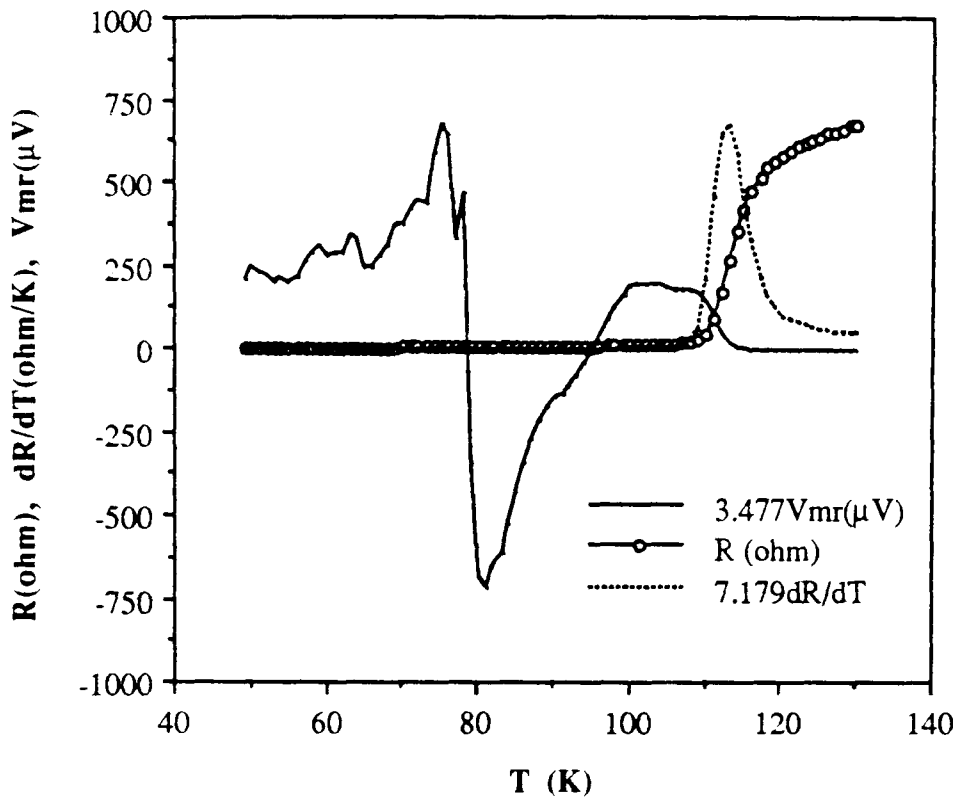

Figure 6.19 The microwave response of a Bi-2223 film, sample B390, at a bias current of 0.5 mA.

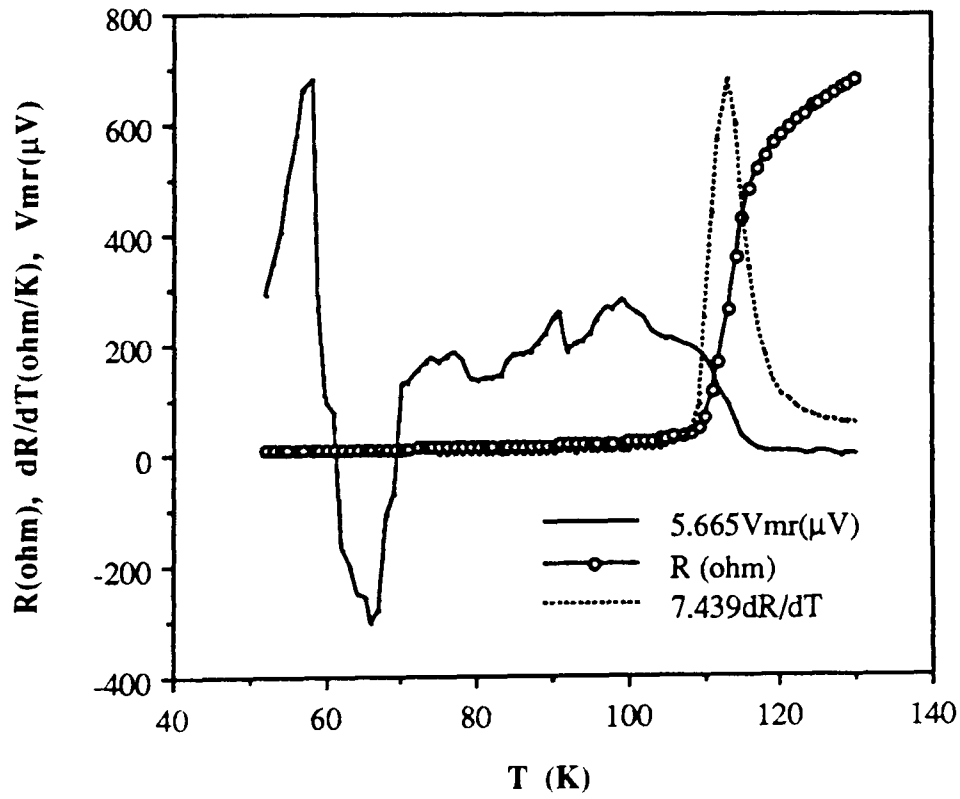

Figure 6.20 The microwave response of a Bi-2223 film, sample B390, at a bias current of 3 mA.

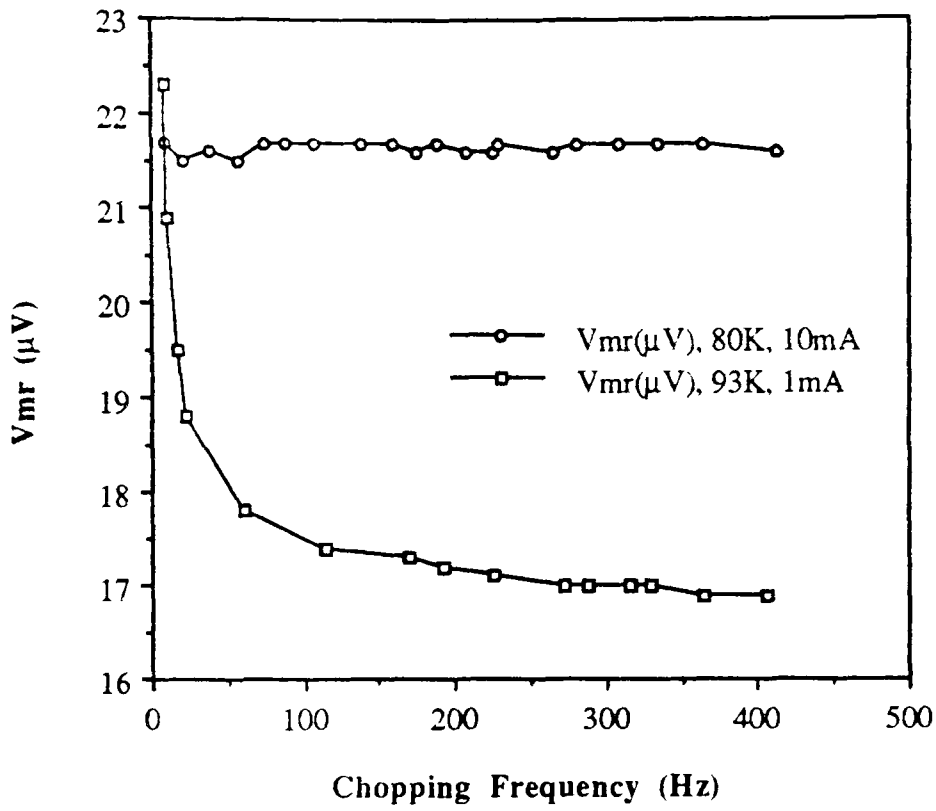

Figure 6.21 The chopping frequency dependence of the microwave response of a Bi-2212 film, sample B310, at 80K and 93K.

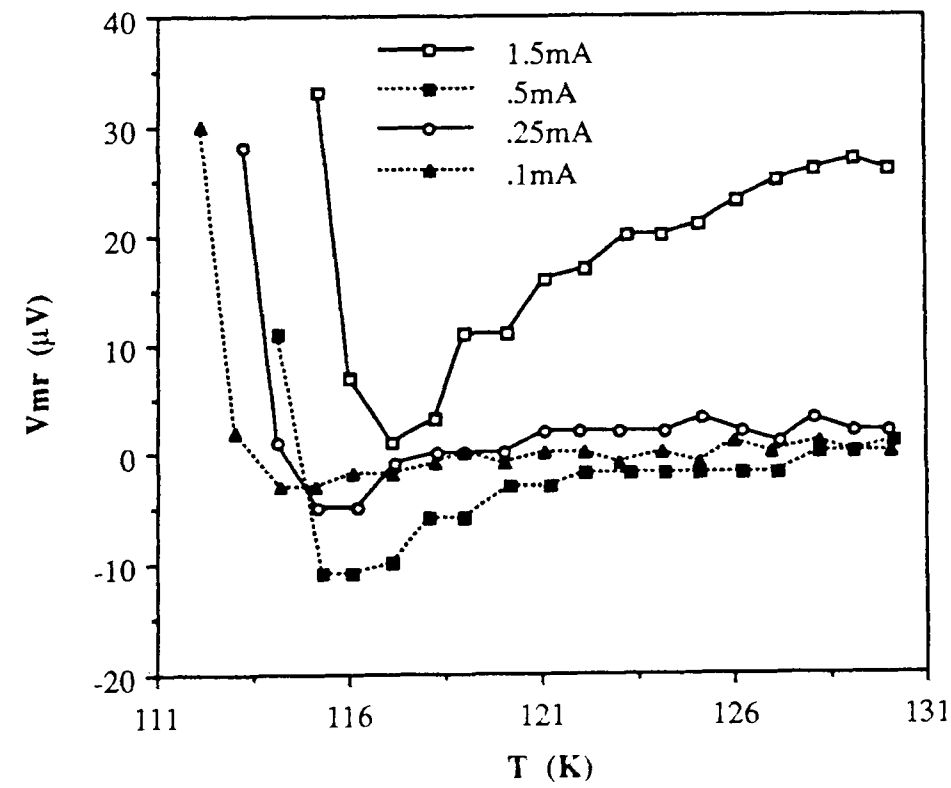

Figure 6.22 Magnified plot of V_{mr} versus T close to T_c, for different values of bias current.

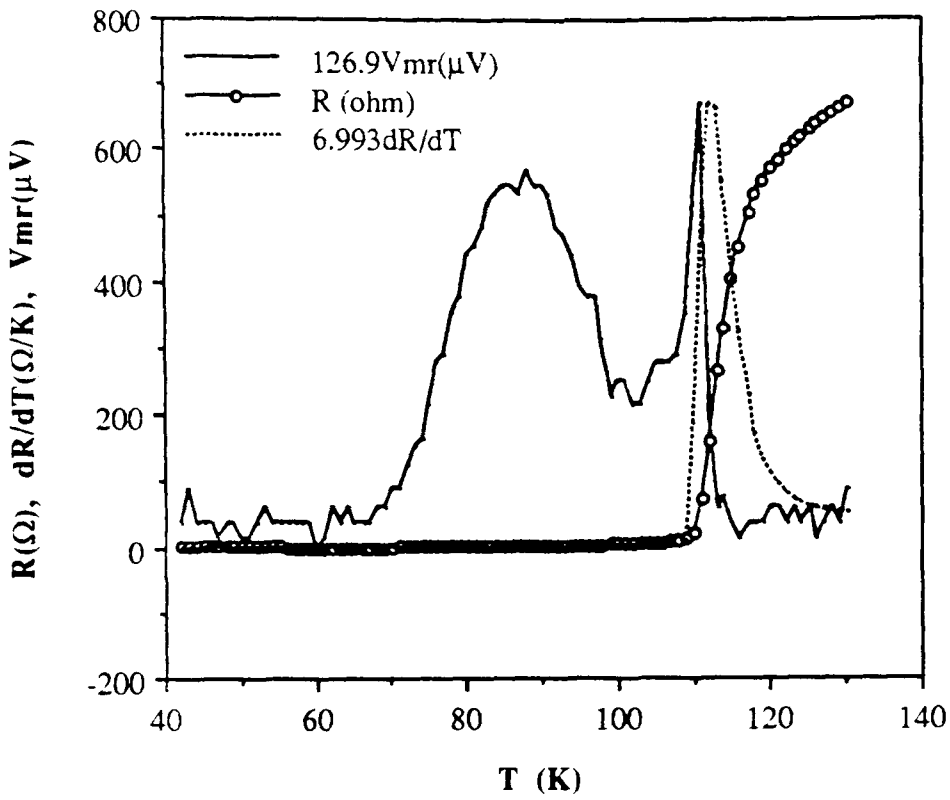

Figure 6.23 The microwave response of a Bi-2223 film, sample B390, at a bias current of 0.01 mA.

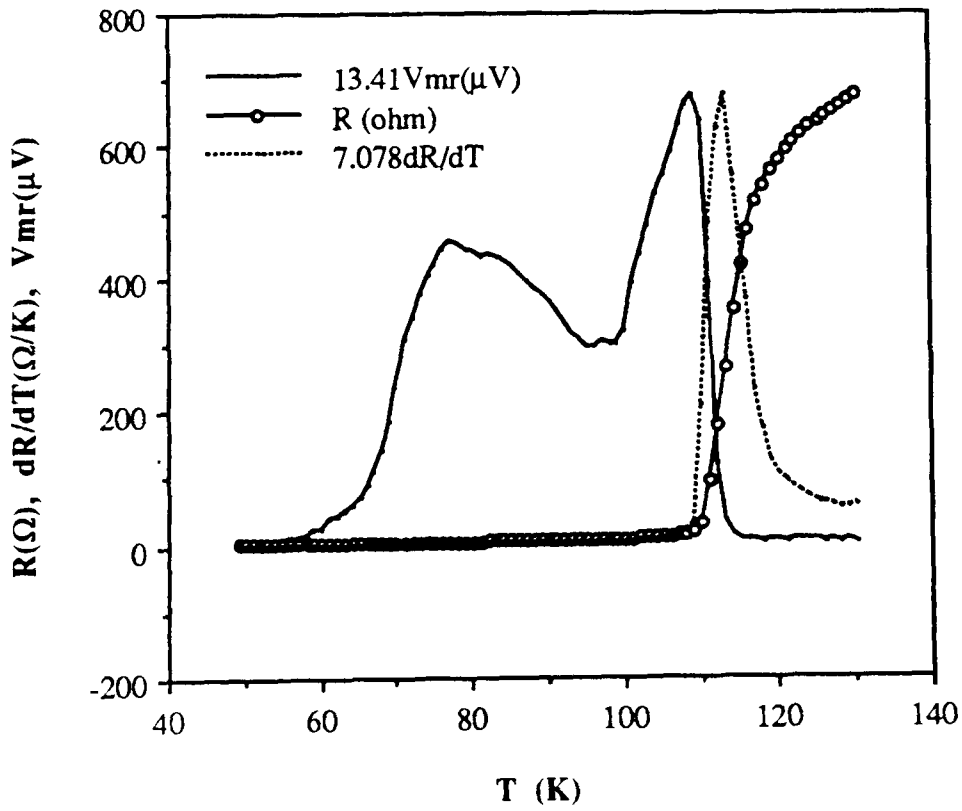

Figure 6.24 The microwave response of a Bi-2223 film, sample B390, at a bias current of 0.1 mA.

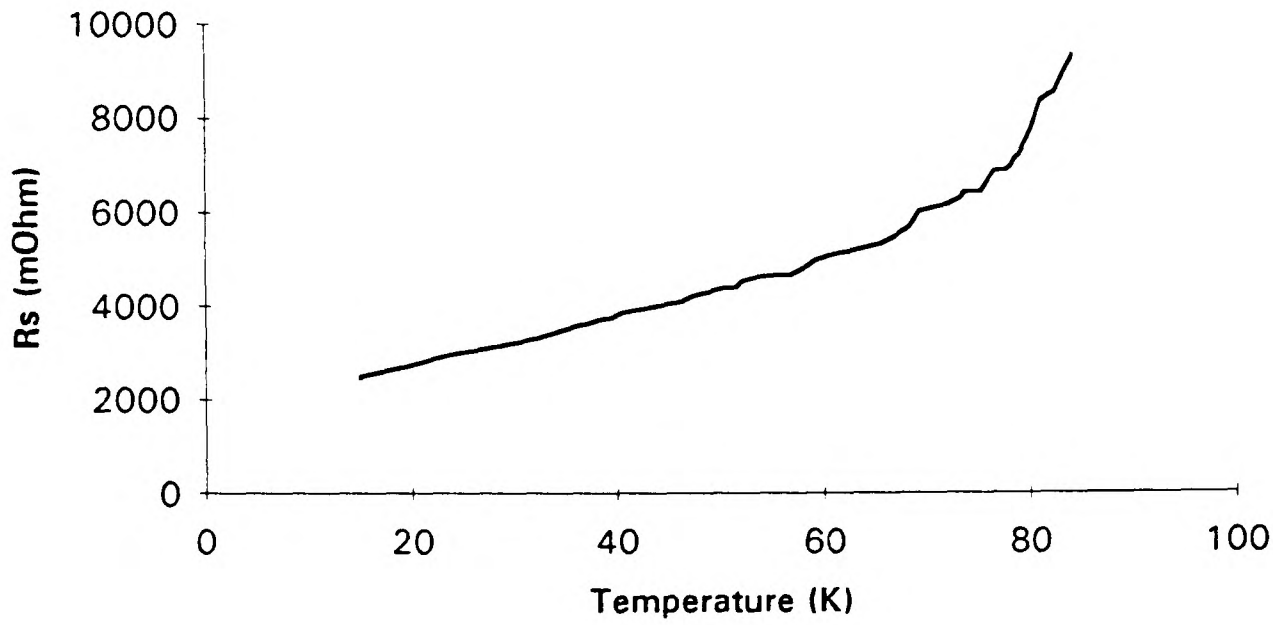

Figure 6.25 Surface resistance of a Bi-2212 thin film at 50Ghz.

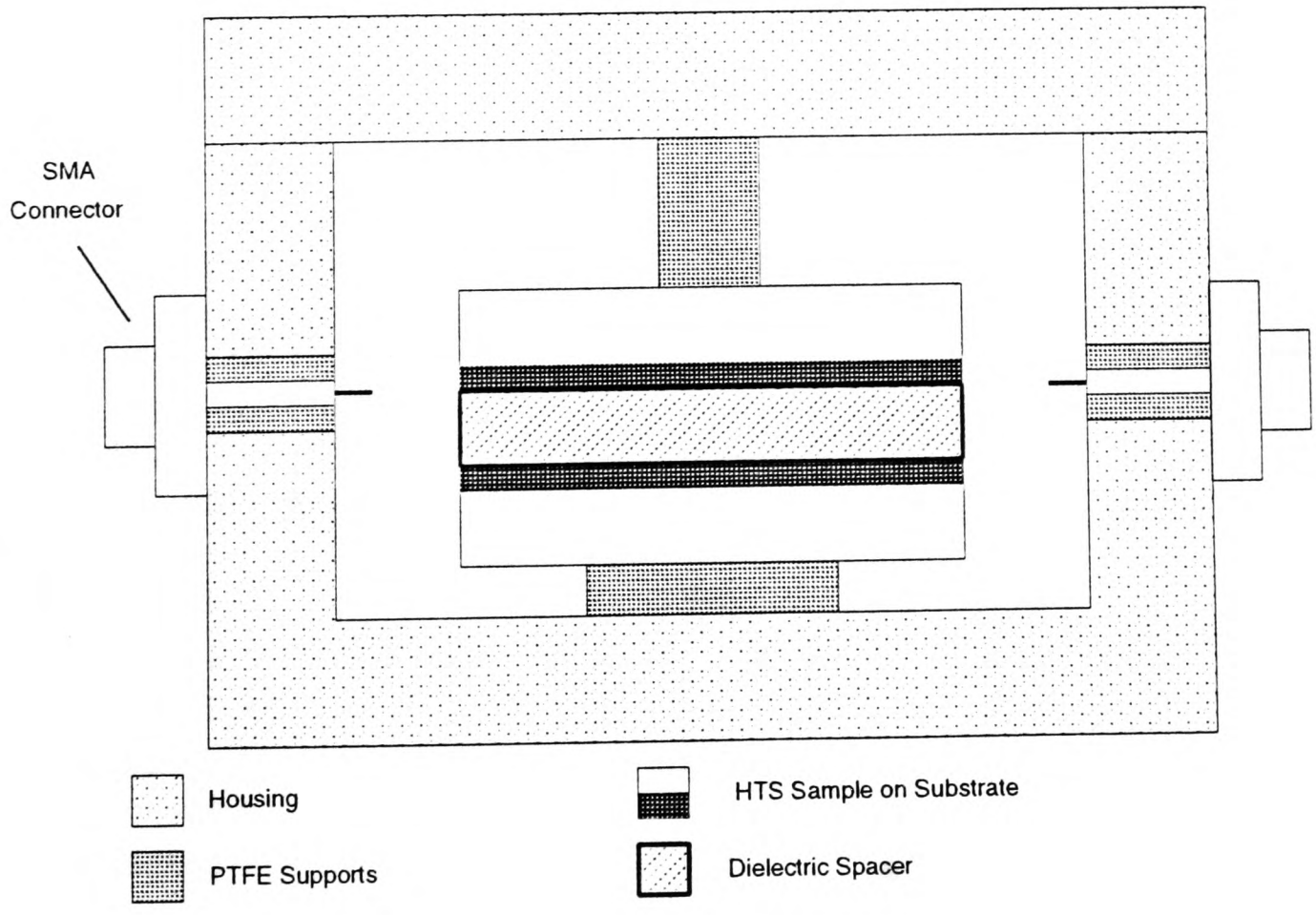

Figure 6.26 A cross section view of the measurement configuration for surface resistance (parallel plate resonator).

(a)

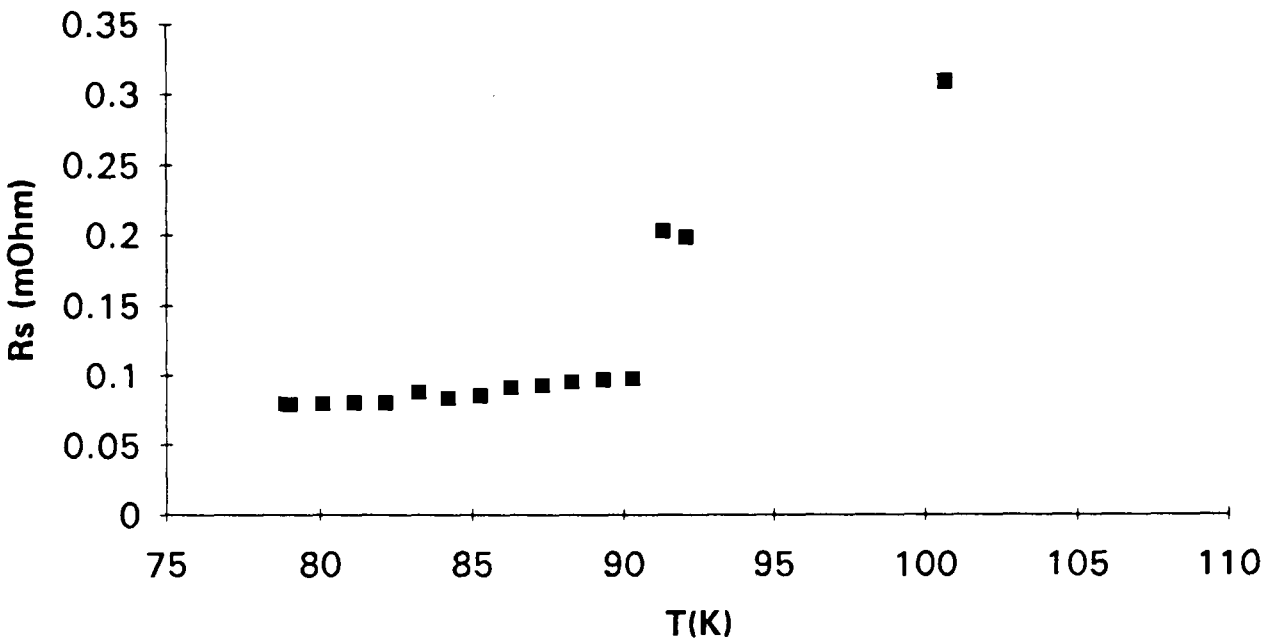
0.35
0.3
0.25
0.2
0.15
0.1
0.05
0
Rs (mOhm)
75
80
85
90
95
100
105
110
T(K)

(b)

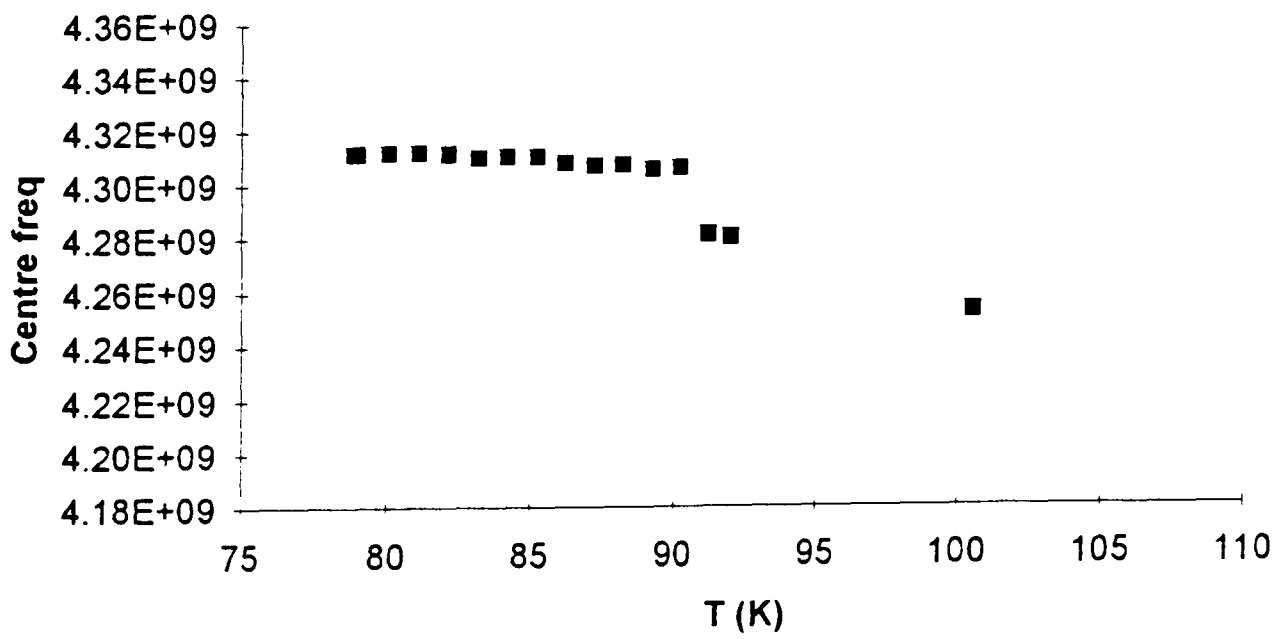
4.36E+09
4.34E+09
4.32E+09
4.30E+09
4.28E+09
4.26E+09
4.24E+09
4.22E+09
4.20E+09
4.18E+09
Centre freq
75
80
85
90
95
100
105
110
T (K)

(c)

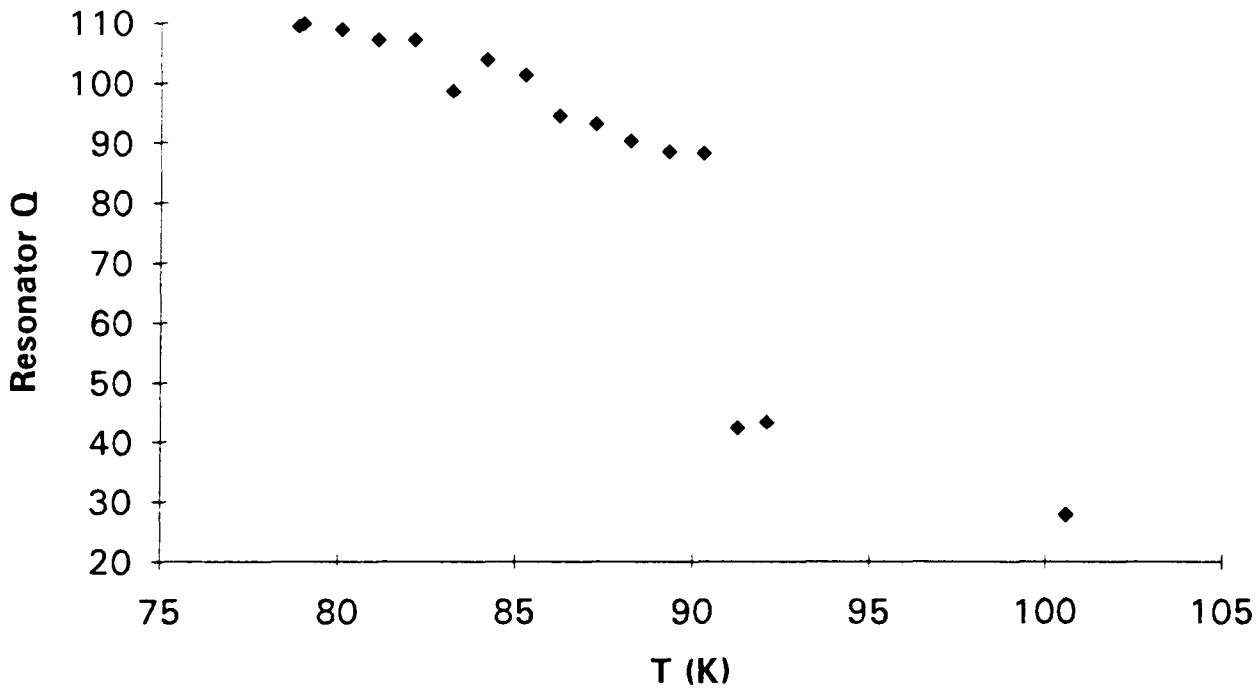

Figure 6.27 (a) Surface resistance of a Bi-2223 thin film at 4.32GHz using a parallel plate resonator technique. (b) Resonator centre frequency (c) resonator Q of the same sample as a function of temperature.

CHAPTER 7

Conclusions and suggestions for further work

7.1. Sputtering process conditions

The effect of rf magnetron sputtering conditions on the as-deposited film composition using a stoichiometric Bi-2212 target was investigated in an on-axis configuration, as the stoichiometrical control of the film is the most important parameter for the proper study of film characteristics. The following conclusions can be drawn from the result of this study:

(1) Substrate-target distance greater than 60 mm resulted in a film composition considerably deviated from the target composition. However, it is not critical between 35 and 55 mm, giving a film composition close to target composition.

(2) Rf power of more than 50 watt reduces the life time of the target as the localised heating in the "race track" area destroys the initial composition of the target, which affects the film composition.

(3) After 12 hours presputtering a target can have a steady state for a long subsequent period of 60 hours or over for an rf power of 50 watt.

(4) Sputtering chamber Ar-gas pressure has a strong effect on the Bi ratio of the as-deposited film composition, while other metallic cations, Sr and Ca, are not much affected by chamber pressure. Bi ratio in the as deposited film composition increases with increasing gas pressure in the chamber. Ar gas pressure of around 10^{-2}mbar was found suitable in our

system, but it is difficult to control precisely due to the spatial inhomogeneities and instabilities of the plasma.

(5) Target aging and increasing chamber pressure reduce the deposition rate of the film.

(6) An homogeneous film composition at least over an area of ~4cm diameter circle, which is the maximum area studied in this study, can be obtained.

7.2. Process conditions for Bi-2212 thin films

Bi-2212 thin films have been assessed by considering their initial composition in terms of Bi/Sr and (Sr + Ca)/Bi ratios with their atomic concentration normalised to Cu:2. The following conclusions can be drawn from the result of this assessment:

(1) In as-deposited films Bi/Sr ratio can be extended to between $0.9 < Bi/Sr < 1$ for films not to peel off during the high temperature annealing process. For some extreme values of Bi/Sr ratio (too high or too low) the film may stay on the substrate. However as expected, this unstoichiometric composition does not allow good superconducting properties.

(2) $T_{c\text{-}zero}$ of around 80K is achievable for (Ca + Sr)/Bi ratio between 1.4 and 1.65, while $T_{c\text{-}onset}$ remains above 90K, However, best superconducting properties can be obtained for the (Ca + Sr)/Bi ratio of 1.47, which is quite close to the nominal composition.

(3) An annealing temperature of 830-835^{o}C may provide highly oriented Bi-2212 films with the c-axis perpendicular to the substrate surface.

(4) Annealing time of 1 hour may be adequate to reach a $T_{c\text{-}zero}$ of above 80K, However, prolonged annealing for more than 10 hours may improve the microstructure of Bi-2212 superconducting thin film.

(5) Quenching temperature affects the superconducting properties as it changes the oxygen content in the sample. Quenching from high temperature increases $T_{c\text{-}zero}$, but it may result in a deterioration in J_c ,due to micro cracks induced by the thermal stress. Therefore slow cooling at least to below 700^{o}C in reduced atmosphere may help to improve the film superconducting properties.

(6) There is no degradation in $T_{c\text{-}zero}$ or resistivity of Bi-2212 thin films aged for more than six months, and films can be stored in ordinary laboratory conditions.

7.3. Process conditions for Bi-2223 thin films

Bi(Pb)SrCaCuO thin films containing a high ratio of Pb ($0.9 < Pb/Bi < 1.5$) about 0.5μm thick, were deposited on $LaAlO_3$, $SrTiO_3$ and MgO substrates by using heavily Pb ($0.8 < Pb/Bi < 1.4$) doped single composite oxide targets. These films were characterised regarding their initial composition and its effects on the superconducting properties. The following conclusions can be drawn from the result of this present work:

(1) The use of a heavily Pb doped target is an effective way of Pb doping the Bi-2223 thin films, as Pb is more liable to be lost of evaporation than other cations.

(2) Bi-content of $1.4 < Bi < 1.8$ in as-deposited films may provide almost single phase Bi-2223 thin films with T_c values running from 105.5K to 109.5K (For Bi ratio of close to 1.8 T_c is 106K), and $J_c > 10^4 A/cm^2$.

(3) Bi-content should be below 1.9 or lower than Sr-content to prevent the peeling off of the film during high temperature annealing, while Sr/Ca ratio remains around 1 in this heavily Pb deposited initial film composition.

(4) Although Pb/Bi ratio is not critical in the range $0.9 < Pb/Bi < 1.5$, when it is above 1.3 slow heating and cooling rate (1^oC/min.) may prevent the retention of excess Ca_2PbO_4 in the film. For a complete transformation of the initial phases, Bi-2212, Ca_2PbO_4, and CuO formed in the early stages of the annealing process, the heating rate should not be higher than 2^oC/min. for the films with Pb/Bi ratio less than 1.3.

(5) Bi-2223 phase starts to form at 835^oC through the initial phases (Bi-2212, CuO and Ca_2PbO_4) formed below 835^oC and the fraction of the Bi-2223 phase increases with increasing sintering temperature, while the fraction of Bi-2212, CuO and Ca_2PbO_4 phases decreases. It reaches a maximum at 862^oC. Above this temperature Bi-2223 phase starts to decompose into Bi-2212 and Ca and Cu rich needlelike crystals, (Sr,Ca)CuO. The number of these needlelike grains increases with increasing temperature above 862^oC.

(6) A single step sharp transition (around 5K) above 108 K can be obtained in a sintering temperature range (852-862^{o}C) as wide as 10^{o}C.

(7) The heavily Pb doped as-deposited film composition can considerably reduce the sintering time to 30 min. providing highly oriented films with the c-axis perpendicular to the substrate surface.

(8) On $LaAlO_3$ and $SrTiO_3$ perovskite substrates, T_c is at least 5K lower than in the case of MgO. However, $LaAlO_3$ can provide good microstructure with a critical current density, J_c, of $5x10^4 A/cm^2$ at 77K.

(9) The applied field dependence at 77K shows a fast decrease in J_c in small fields as is usual at this high temperature. The dependence of J_c on the direction of magnetic field with respect to the c-axis reflects the well known anisotropic nature of the Bi-2223 phase.

(10) There is no degradation in superconducting properties of Bi-2223 thin films stored in ordinary laboratory conditions for nine months, and thermally cycled for 10 times between liquid nitrogen and ambient temperature.

(11) For the film composition used in this study quenching from between 600 and 650^{o}C or annealing in reduced atmosphere can achieve the optimum carrier concentration. The direction of variation of T_c with oxidising process can be related to the film composition (especially Bi and Pb content) or initial oxygen content of the film. The variation range of T_c with oxygen content is controlled by the Pb content. Thus precise preparation conditions and particularly the sintering process may be responsible for the contradictory results on the Bi-2223 material described in the literature.

7.4. Device performance of Bi-based granular thin films

The radiation response of a Bi-based thin films with different granularity was studied as a function of temperature, bias current, chopping frequency and presence or absence of a dc magnetic field. The following conclusion can be drawn from the results of the present study:

(1) Optical response using a continuous wave (cw) He-Ne laser is bolometric, while microwave response using a 34.5 GHz Gunn diode microwave generator contains a non-bolometric component. The bolometric component of the microwave response is quite small at small bias current and high chopping frequency

(2) The response increases with increasing granularity of the film. The maximum microwave response using the Gunn diode generator was found to be four orders of magnitude larger than the peak response of the He-Ne laser at a bias current of 5 μA.

(3) The microwave response of a granular film remains quite large at small bias current, while the optical response decreases as the bias current is decreased.

(4) An increasing external magnetic field decreases the response. The microwave response initially rises with increasing bias current, passes through a maximum and then falls for more granular films, while it is not sensitive to increasing bias current once it reaches a saturation value for less granular films.

(5) The peak optical response decreases on increasing the chopping frequency, whereas the peak microwave response was almost independent of the chopping frequency.

(6) Most of the experimental results, involving the influence of film temperature, bias current and external magnetic field on microwave response, are qualitatively consistent with a proposed picture that the non-bolometric microwave response of a superconducting film reflects the reaction intensity of the interaction between microwave radiation and the Josephson-type weak links in the sample.

(7) Granular high T_c films may have interesting applications as sensitive microwave detectors, but they are not particularly good for microwave applications with their high Rs at microwave frequencies.

7.5. Suggestion for further work

Further studies of the thin film growth technique by magnetron sputtering should concentrate on the control of the stoichiometry of the as deposited film. The control of the film stoichiometry is very closely related to a precise control of the pressure.

In order to eliminate the formation of huge needlelike grains, (Sr,Ca)CuO, in the microstructure, which considerably decreases J_c, the correct Cu and Ca ratios in the initial composition should be investigated.

The substrate surface on which the film will be deposited is also an important parameter in controlling microstructure especially for $<5\mu m$ thick films. It needs to be polished very well. The polishing process used in this work providing scratch free surface may be recommended.

Wet chemical etching using EDTA etching solution (saturated with water) can be successful for the pattern size up to $10\mu m$. Below $10\mu m$ dry etching process should be used.

Finally, for microwave applications and to build artificial grain boundaries for SQUID applications the study should be concentrated on in-situ processing which provides high surface quality and microstructure.